Multiaxial Testing of Fibre Reinforced Composite Materials.

Thesis submitted in accordance with the requirements of the University of Liverpool for the degree of Doctor of Philosophy by

Vincent Ki Seng CHOO

June 1982

Department of Metallurgy &
Materials Science

ACKNOWLEDGEMENTS

I am very grateful to Dr. S. Hull for her vital help.

I am indebted to my supervisor Professor D. Hull for securing the financial support that made this study a reality. Thanks are also due to him for his invaluable advice, patience and above all friendship.

My thanks to Professor B. L. Eyre for use of Departmental facilities and Professor J. Alty for use of facilities in the Computer Laboratory.

I am also indebted to Dr. S. J. Neil for proof-reading and helping to put this thesis together. I would like to thank her for her patience and support too.

I would like to express my gratitude to Dr. C. Lawrence, Mr. F. Marris and Mr. R. Potter for designing and constructing the mechanical test-bed for the multiaxial servo-hydraulic feedback controlled test rig.

Thanks are due to Mr. K. T. Lim for his continuous assistance in the design and construction of the Interface Unit. I am also grateful for his advice on the electronics.

My thanks to the following friends for their help in the design and construction of the above-mentioned test rig:

(1) Dr. M. J. Legg.
(2) Dr. B. Spencer.
(3) Mr. M. Lissenburg.
(4) Mr. D. Tayor.
(5) Mr. D. Whitehurst and his staff.
(6) Dr. D. Stoten.
(7) Mr. P. M. Weston.
(8) Mr. P. Garrett
(9) Dr. M. J. Tayor
(10) Dr. M. Beer
(11) Dr. J. Lucas.
(12) Dr. A. Prinn
(13) Mr. F. Ormesher
(14) Mr. G. S. . Bal.

I thank Mr. L. Trask for proof-reading Chapter 5. Thanks are also due to Dr. F. Marsh for proof-reading Chapter 2 and his advice on the development of the data processing programs. I would also like to thank Miss M. Thorp for her advice on the development of the text processing program.

I would like to express my gratitude to all my friends in the Department, particularly those in Laboratory No. 1.

My thanks to Mr. R. Hughes and Mr. J. Gillies for their assistance in the photography

I thank all my dear friends for their support.

The financial support of Science Research Council is acknowledged.

List of Notations.

$\hat{e}_i$	Limit tensile strains for i = 1.....3.
	Limit positive shear strains for i = 6.
$\hat{e}'_i$	Limit compressive strains for i = 1...3
	Limit negative shear strains for i= 6.
S_{ij}	Compliance.
X_i	Tensile strengths for i = 1....3
	Positive shear strength for i = 6
X'_i	Compressive strengths for i = 1...3
	Negative shear strength for i = 6
$\sigma_{(ult)}$	Ultimate uniaxial strength.
E_f	Filament Young's Modulus
υ_f	Filament Poisson's ratio
υ_m	Matrix Poisson's ratio
s_f	Filament specific gravity
s_m	Matrix specific gravity.
E_m	Matrix Young's Modulus
$\sigma_{1(ult)}$	Ultimate strength in the 1 -direction
$\sigma_{2(ult)}$	Ultimate strength in the 2 - direction
$\sigma_{6(ult)}$	Ultimat shear strength in the 1 – 2 plane.
F	Strength Parameters.
G	
H	
L	
M	
N	

R	% of resin content by weight
c	Contiguity factor.
K	Filament misalignment factor
θ	Orientation of unidirectional filaments.
$[k]$	Curvature of the plate.
σ	Stress
$\sigma_{\perp c}^{*}$	Transverse compressive strength
$\sigma_{\perp T}^{*}$	Transverse tensile strength

Subscript:

$\parallel$	perpendicular to the fibre
$\perp$	parallel to the fibre
T	tension
C	compression

Superscript:

$*$	is the yield or ultimate strength

SUMMARY

The primary aim of this project was to conduct an experimental study on the failure behaviour of fibre reinforced composite materials under states of complex stress. For this purpose a feedback controlled multiaxial test rig was constructed.

The control system of the test rig is based on an eight-bit microcomputer. Control programs can be written in either the 8080-ASSEMBLER or PASCAL language. A P-code interpreter is available to provide facilities for executing the control programs written in the PASCAL language. The test rig can apply axial force, internal pressure and torsion in any required combination to a tubular specimen.

Glass fibre reinforced polyester hoop wound tubular specimens were used in the experimental work. The failure behaviour of these specimens in the following conditions was examined:

(i) combined transverse tensile and in-plane shear stresses (σ_2 — σ_6),

(ii) combined parallel tensile and transverse compressive stresses(σ_1 —(- σ_2)),

(iii) combined transverse compressive and in-plane shear stresses ((-σ_2)— σ_6).

Three highly simplified models were proposed to explain the experimental data obtained from tests carried out in the (σ_1—(- σ_2)) stress space. There was tentative agreement between the experimental data and the theoretical predictions based on these models. The loading dependency of the specimens under conditions (ii) and (iii) were investigated. In the (σ_1—(- σ_2)) stress space the transverse compressive strengths of the hoop wound specimens increased with the radial stress which was generated by the internal pressure. Apparently this radial stress also made the failure conditions independent of loading path for a given stress ratio. On the contrary, the reverse was true in

the $(-\sigma_2)$—σ_6 stress space. In this case the viscous-plastic effect due to the transverse compression was not suppressed by the introduction of the in-plane shear stress, σ_6 . In fact, the application of the in-plane shear stress tended to encourage further plastic shear deformation in the matrix. The experimental data suggest that the effect of the radial stress is significant even if its magnitude is small when compared to the other applied stresses.

CONTENTS

Chapter 4

Chapter 5

Chapter 6

Chapter 7

Appendix

Chapter 1: INTRODUCTION

More and more composite materials are finding their way into engineering fields. Many are being used to fabricate load-bearing structures. Before these materials can be used with confidence their characteristics must be studied extensively. In general, composite materials are anisotropic in nature. Inevitably it is more difficult to analyse such materials than isotropic ones.

Structural materials in service are generally subjected to complex stresses. Therefore, one important aspect of the stress analysis is to find out the conditions of failure of composite materials under complex stresses, which are normally referred to as 'failure criteria' or 'failure theories'. It would be useful for the engineering designer to be able to predict the failure of a composite material under a state of complex stresses based on these criteria. In recent years, numerous failure criteria have been proposed. Many of these are extensions of work based on isotropic materials.

It must be pointed out that no one criterion has been accepted universally as giving an accurate prediction of the conditions of failure. More experimental data will be required to substantiate these theoretical models. Unfortunately, it is not a trivial exercise to exert controlled complex stresses on test specimens under laboratory conditions. Special testing equipment is needed. Puck(1969) has used a mechanical testing apparatus that provided

axial force and torsion on a tubular specimen. Owen and Griffiths (1978) & Owen and Rice (1981) evaluated the behaviour of glass-reinforced plastics under biaxial stresses. Their machine could supply axial force and internal pressure to a tubular specimen. A comprehensive description of this machine has been given by Found (1972). Protasov and Kopnov (1965) have carried out a study on the strength of glass-reinforced plastics (grp) in a state of plane stress. They utilised an apparatus that could subject a tubular specimen to hydrostatic pressure (internal or external), axial force and torsion. The axial force and torsion were exerted by two independent hydraulic actuators. The hydraulic fluid for the hydrostatic pressure and that for the two actuators were from the same pump. Therefore, a proportional loading condition was generated. The ratio $\sigma_H : \sigma_A : \tau_{AH}$ could be varied by using interchangeable actuators of different diameter (σ_H is the Hoop stress, σ_A is the axial stress and τ_{AH} is the shear stress). Hütter, Schelling and Krauss (1974) using composite tubular specimens examined the strength of grp in multiaxial loading conditions. An electronic load-proportional control unit with a simple feedback system was used to maintain a preselected load vector and ensure a uniform increase of all loads. Wu and Jerina (1972) have developed a testing system using a small real-time control computer to characterize the mechanical properties of composites. This testing system could provide axial force, torsion and internal pressure. The testing equipment mentioned above cannot, in general, be bought 'off the shelf'. It has to be tailor-made.

The objective of the present work is to carry out an experimental study on the failure criteria of composite materials subjected to states of complex stress and on the loading path dependency of these materials. In connection with this work a multiaxial loading test rig with feedback control has been constructed. It can exert internal pressure, axial force (tensile or compressive) and torque on a tubular specimen. External pressure can be incorporated into the system at a later stage. Essentially, the test rig consists of an actuator which supplies axial force and a pressure intensifier which pressurises the tubular specimen. The torque is provided by a stepping motor coupled to a gear train. A microcomputer is used to control the test rig. The hardware and software of the control system were developed by the author. They will be described in detail in Chapters 3 and 4. The detailed design and construction of the mechanical part of the test rig were carried out by Dr. Lawrence of North-East London Polytechnic. However, the overall design specification was worked out by the author and his colleagues together with Dr. Lawrence and his staff. This consisted of determining the maximum pressure, torque and axial force required, the sizes of specimens to be accommodated, the maximum loading frequency for fatigue tests and the decision on the type of hydraulic system needed.

Optical and scanning microscopy have also been carried out on specimens tested in various test modes. It was hoped that this hybrid approach, micro and macro levels, would provide a more comprehensive understanding of the failure conditions of composite materials. The

experimental work involved subjecting hoop wound specimens to various complex states of stress along different loading paths. This is equivalent to the examination of the failure behaviours of lamina under complex stresses.

The published literature on the theoretical and experimental work on failure criteria of composite materials and their constituents will be reviewed in Chapter 2.

Chapter 2:

LITERATURE REVIEW

2.1 Introduction

Failure characterization of composite materials can be divided into two categories, viz:-

(i) Phenomenological Approach and

(ii) Micromechanics Approach.

It is the aim of this chapter to review some of the theoretical and experimental works pursued using the Phenomenological Approach. Attention will be focused on the assumptions made by the theoretical models. These assumptions directly affect the performance of the theoretical models.

2.2 Phenomenological Approach

Wu (1974) pointed out that it is possible to establish a phenomenological failure criterion for a given material by carrying out extensive experimental work on the material. The resulting criterion will be applicable to that particular material only. Therefore, for each material a failure criterion must be found by performing a set of experiments. Such a pure empirical technique is both costly and inflexible. Consequently, a mathematical model can be used to complement the failure characterization process, by providing guidance to the design of experiments and by giving a basis on which one can compare the performance among different materials. It also simplifies data reduction and documentation for the ease of retrieval

at a later stage (Wu et al., 1973). However, it can neither be used to extrapolate the response of a given material under a given state of complex stresses, which is outside the range tested, nor can it be used to interpret the mechanisms of failure.

2.2.1. The Tsai & Wu (1971) Theoretical Requirement:

Tsai and Wu (1971) drew out a list of theoretical requirements which must be satisfied by a mathematical form of failure criterion viz:-

(i) It should be invariant to the definition of the coordinate axis. Though the state of stress is a function of the coordinate axis, the condition for failure depends on the intrinsic nature of the material only. Therefore, the failure criterion must not be affected by the coordinate transformation.

(ii) It should be flexible so that it can be used to model any failure envelope irrespective of the assumptions made about the mechanisms of failure. The failure envelope is defined as the surface formed when the failure criterion is plotted, for instance, in a three-dimensional stress space.

(iii) It should have only one root for a given radial loading path, i.e. the point of failure must be unique.

OP is the Radial Loading Path

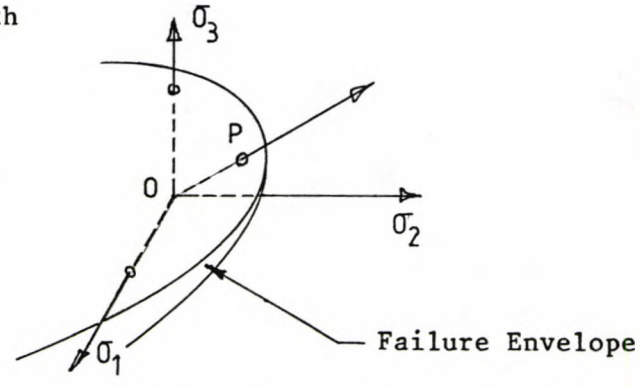

Fig 2.2.1 Graphical Representation of a Failure Criterion.

Fig 2.2.1 illustrates partially a failure criterion in graphical form. Vector OP represents a radial loading path. Point P contains the root for that particular loading path.

(iv) It should be simplified readily to provide characterization to the required degree of accuracy.

(v) It should be mathematically operational, provide unique mapping between the stress and strain spaces, and be adaptable for structural analysis.

(vi) It should permit clear definition of the principal direction of strength.

As expected, different anisotropic materials possess failure surfaces with different shapes and sizes. Such differences are a reflection of different failure mechanisms. Therefore, it is important for the mathematical model to have sufficient flexibility to allow for these differences.

It is a common practice in engineering structural analyses to choose a set of coordinate axes which simplifies the boundary conditions. The final solution may be expressed in terms of stress or strain. Hence requirement number (v) must be fulfilled. Such a constraint also implies that the failure criterion must obey the law of transformation.

2.2.2 The Theoretical Requirements of Gol'denblat and Kopnov:

Gol'denblat and Kopnov (1965) also made a list of conditions which a phenomenological mathematical model must satisfy. They

limited their argument to brittle materials only. The conditions were:-

(i) The theory of strength formulated must be able to predict the failure strength of brittle materials in a state of complex stress.

(ii) The mathematical expression must include both the stress tensor which characterizes the stress state and certain scalar or tensor quantities that characterize the strength properties of the material.

(iii) The criterion of strength must be such that the strength tensor mentioned in (ii) obeys the rules of transformation.

(iv) The criterion must be in an invariant form, which must be a function of the stress and strength tensors.

(v) The criterion should be valid for all coordinate systems.

(vi) For simple loading, only one parameter should be needed in the material characterization.

(vii) The criterion must take into account the following features:-

(a) The difference between the ultimate tensile and compressive strengths.

(b) The dependence of the ultimate shear strength on the direction of the shear stresses.

2.2.3 Gol'denblat and Kopnov's criterion of Strength for Brittle Anisotropic Materials:

Based on the theoretical requirements given in Section 2.2.2, Gol'denblat and Kopnov (1965) proposed the following strength criterion for brittle anisotropic materials, viz:-

$$(\Pi_{ik}\,\sigma_{ik})^{\alpha} + (\Pi_{pqnm}\,\sigma_{pq}\,\sigma_{nm})^{\beta} + (\Pi_{retlnm}\,\sigma_{re}\,\sigma_{tl}\,\sigma_{nm})^{\gamma} + \ldots\ldots \leq 1$$

.....(2.2.3.1)

Here repeated indices indicate summation; and i,k,p,q,m,n,r,s,t each take the numerical values of 1,2,3,...6. Π_{ik}, Π_{pqnm} etc., are strength tensors of the second and fourth rank respectively.

Gol'denblat and Kopnov (1965) examined the case where $\alpha=1$ and $\beta=1/2$. They limited their analysis to linear and quadratic terms of stress tensor components for a 2-dimensional situation. The strength tensors were assumed to be symmetrical, i.e. :

$$\Pi_{ik} = \Pi_{ki}$$

$$\Pi_{pqrs} = \Pi_{qprs}$$

$$\Pi_{pqrs} = \Pi_{pqsr}$$

$$\Pi_{pqrs} = \Pi_{rspq}$$

Applying the above-mentioned assumptions to equation (2.2.3.1), they obtained the following

$$\Pi_{ik}\,\sigma_{ik} + (\Pi_{pqrs}\,\sigma_{pq}\,\sigma_{rs})^{1/2} \leq 1 \qquad \ldots.(2.2.3.2)$$

where i,k,p,q,r,s=1,2.

Gol'denblat and Kopnov (1965) illustrated the method of determining the Π_{ik} and Π_{pqrs} for a 2-dimensional case. For the ease of discussion the following coordinate system has been chosen.

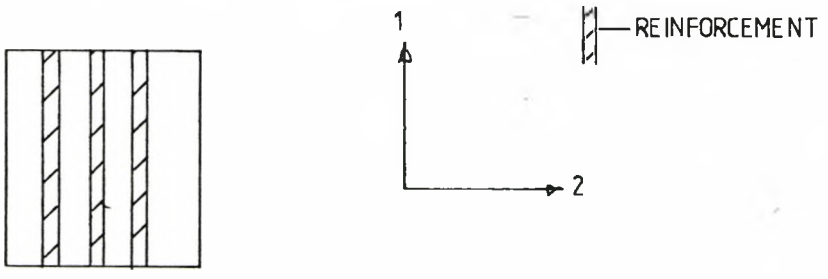

Fig 2.2.3.1. Lamina with Unidirectional Reinforcement.

These strength tensors can be determined experimentally using simple tests as shown below.

(a) For pure tension along the 1-direction, viz:-

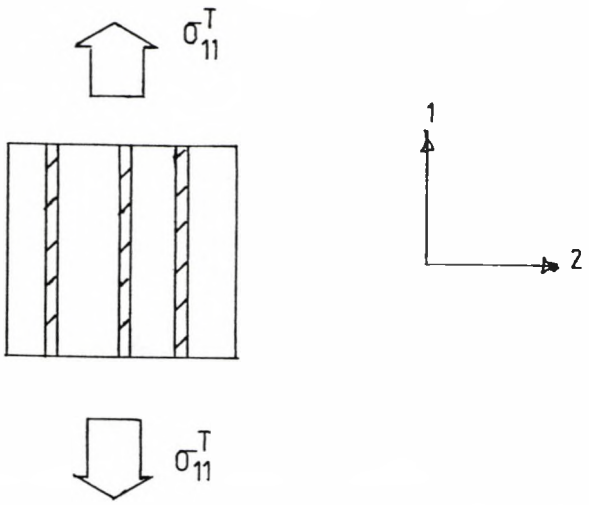

Fig 2.2.3.2. Lamina under Pure Tension acting along the 1-direction.

$$\Pi_{11}\,\sigma^T_{11} + (\Pi_{1111}\,(\sigma^T_{11})^2)^{1/2} = 1 \qquad \text{.....(2.2.3.3)}$$

(b) For pure compression along the 1-direction,

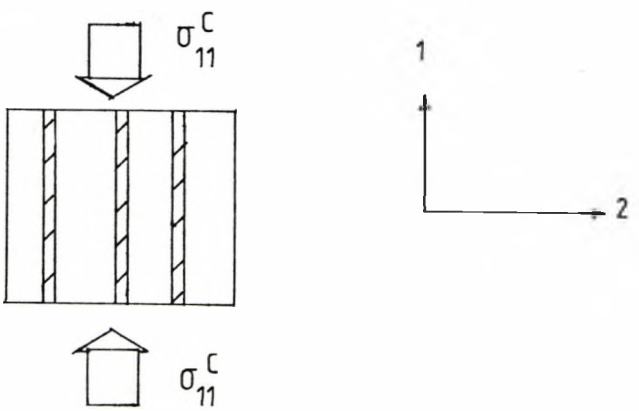

Fig 2.2.3.3. Lamina under Pure Compression along the 1-direction.

$$-\Pi_{11}\,\sigma^C_{11} + (\Pi_{1111}\,(\sigma^C_{11})^2)^{1/2} = 1 \qquad \text{.....(2.2.3.4)}$$

Similarly for pure tension and compression along the 2-direction the following relations are obtained:

$$\Pi_{22}\,\sigma^{T}_{22} + (\Pi_{2222}\,(\sigma^{T}_{22})^{2})^{1/2} = 1 \qquad .....(2.2.3.5)$$

and

$$-\Pi_{22}\,\sigma^{C}_{22} + (\Pi_{2222}\,(\sigma^{C}_{22})^{2})^{1/2} = 1 \qquad .....(2.2.3.6)$$

From equations (2.2.3.3) to (2.2.3.6) it is obvious that

$$\Pi_{11} = (1/2) \times ((1/\sigma^{T}_{11}) - (1/\sigma^{C}_{11}))$$

$$\Pi_{1111} = (1/4) \times ((1/\sigma^{T}_{11}) + (1/\sigma^{C}_{11}))^{2}$$

$$\Pi_{22} = (1/2) \times ((1/\sigma^{T}_{22}) - (1/\sigma^{C}_{22}))$$

$$\Pi_{2222} = (1/4) \times ((1/\sigma^{T}_{22}) + (1/\sigma^{C}_{22}))^{2} \qquad .....(2.2.3.7)$$

σ^{T}_{11}, σ^{T}_{22}, σ^{C}_{11} and σ^{C}_{22} are the failure stresses obtained from the experiments. In order to satisfy requirement [(vii)(b)] given in Section 2.2.2 Gol'denblat and Kopnov (1965) chose two loading cases for the determination of Π_{1122}. Π_{1122} is the interaction strength coefficient between σ_{11} and σ_{22}. They defined the direction of the shear loading according to the diagrams below:

(c) Positive shear :-

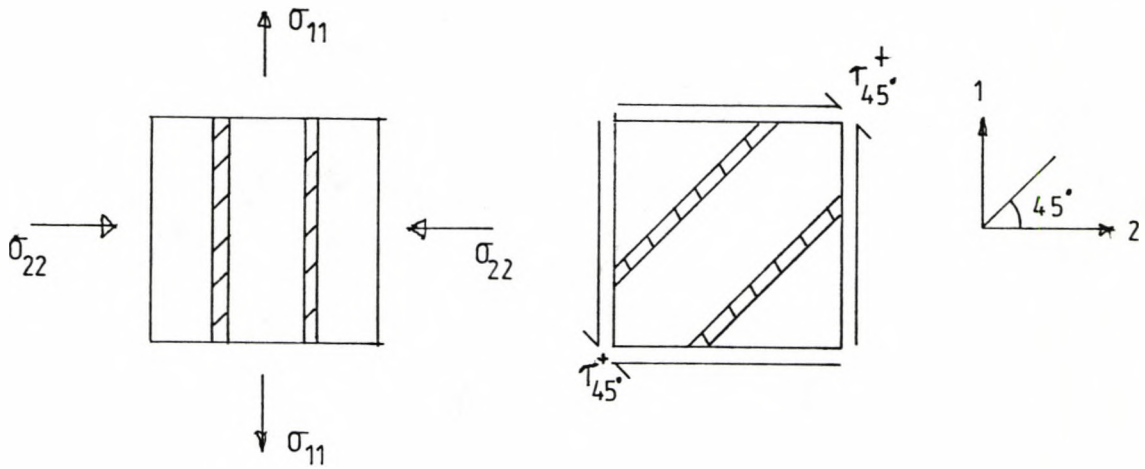

Fig 2.2.3.4. Lamina under Positive Shear Stress at 45 deg. to the 1-direction.

From fig.2.2.3.4. it can be said that

$$\sigma_{11} = + \left| \tau^{+}_{45^\circ} \right|$$

and

$$\sigma_{22} = - \left| \tau^{+}_{45^\circ} \right|$$

.....(2.2.3.8)

(d) Negative shear :-

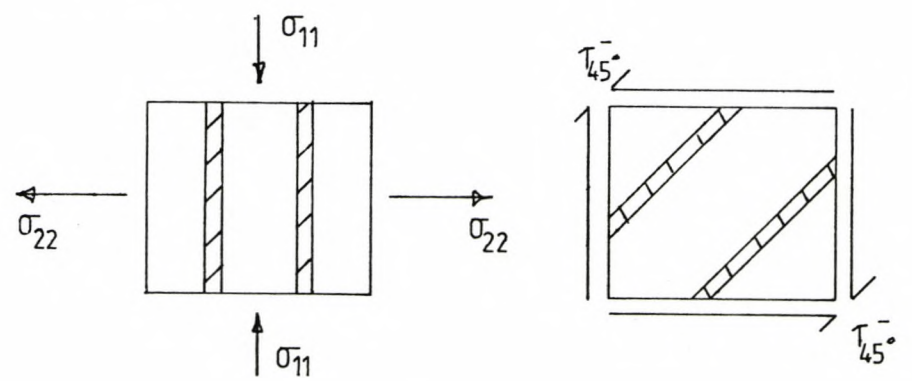

Fig 2.2.3.5. Lamina under Negative Shear Stress at 45 deg. to the 1-direction.

similarly

$$|\sigma_{11}| = |\sigma_{22}|$$

$$\sigma_{11} = -|\tau^{-}_{45'}|$$

$$\sigma_{22} = +|\tau^{-}_{45'}|$$

.....(2.2.3.9)

Substituting equations (2.2.3.8) and (2.2.3.9) into equation (2.2.3.2) one obtains:

$$((\Pi_{11} - \Pi_{22}) + (\Pi_{1111} + \Pi_{2222} - 2\,\Pi_{1122})^{1/2})\,|\tau^{+}_{45'}| = 1$$

.....(2.2.3.10)

and

$$((\Pi_{22} - \Pi_{11}) + (\Pi_{1111} + \Pi_{2222} - 2\,\Pi_{1122})^{1/2})\,|\tau^{-}_{45'}| = 1$$

.....(2.2.3.11)

Gol'denblat and Kopnov (1965) pointed out that for equations (2.2.3.10) and (2.2.3.11) to be compatible it was necessary that

$$2(\Pi_{11} - \Pi_{22}) = |(1/\tau^{+}_{45'})| - |(1/\tau^{-}_{45'})|$$

.....(2.2.3.12)

Combining equations (2.2.3.7) and (2.2.3.12) the following relation can be obtained:

$$(1/\sigma^{T}_{11}) - (1/\sigma^{C}_{11}) - (1/\sigma^{T}_{22}) + (1/\sigma^{C}_{22}) = |(1/\tau^{+}_{45'})| - |(1/\tau^{-}_{45'})|$$

.....(2.2.3.13)

and hence

$$\Pi_{1122} = (1/8) \times ((\sigma^{-T}_{11} + \sigma^{-C}_{11})^{2} + (\sigma^{-T}_{22} + \sigma^{-C}_{22})^{2} - (|(1/\tau^{+}_{45'})| + |(1/\tau^{-}_{45'})|)^{2})$$

.....(2.2.3.14)

Two pure shear states illustrated in figures 2.2.3.6 & 2.2.3.7 were also used to determine Π_{12} and Π_{1212}.

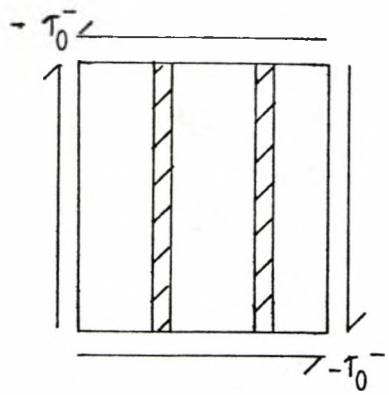

Fig 2.2.3.6. Unidirectional Lamina under -ve Pure Shear τ_0^-.

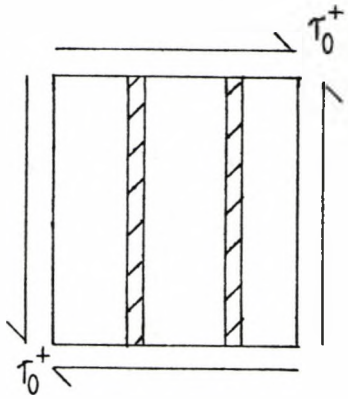

Fig 2.2.3.7. Unidirectional Lamina under +ve Pure Shear τ_0^+.

Consequently, the following equations can be obtained:

$$2\,(\Pi_{12} + (\Pi_{1212})^{1/2})\ \tau^+_0 = 1$$

$$2\,(-\Pi_{12} + (\Pi_{1212})^{1/2})\ \tau^-_0 = 1$$

.....(2.2.3.15)

which give

$$\Pi_{12} = (1/4) \times ((1/\tau^+_0) - (1/\tau^-_0))$$

$$\Pi_{1212} = (1/16) \times ((1/\tau^+_0) + (1/\tau^-_0))^2$$

.....(2.2.3.16)

However, from figures 2.2.3.6. and 2.2.3.7. it can be seen that the two systems of shear stress would have the same effect on the laminae, except opposite in sign.

$$\therefore \quad |-\tau^{-}_{0}| = |\tau^{+}_{0}| = \tau_0 \quad ; \quad \therefore \quad \Pi_{12} = 0$$

and

$$\Pi_{1212} = (1/4) \times (1/\tau_0)^2 \qquad .....(2.2.3.17)$$

Since axes 1 and 2 are the principal axes, Π_{1112} and Π_{2221} equal zero.

Gol'denblat and Kopnov (1965) noted that experimental results of textolite and bumagolite pipes in complex states of stress obtained by Zakharov (1961) agreed satisfactorily with their proposed theory.

2.2.4. Strength Tensor Criterion for Anisotropic Materials subjected to Uniaxial normal or Pure Shear Stress:

Ashkenazi (1965) introduced the idea of using 4th rank strength tensor to represent the strength characteristics of composite materials .

However, due to ambiguous translation the derivation of Ashkenazi's (1965) criterion will not be pursued further.

2.2.5. Tsai and Wu's General Theory of Strength for Anisotropic Materials:

Tsai and Wu (1971) introduced a simpler strength criterion using the same concept of strength tensor mentioned in the previous two sections. This criterion is in a scalar form:

$$f(\sigma_m) = F_{ij}\,\sigma_{ij} + F_{ijlk}\,\sigma_{ij}\,\sigma_{lk} + F_{ijlkst}\,\sigma_{ij}\,\sigma_{lk}\sigma_{st} + \cdots = 1$$

.....(2.2.5.1)

For simplicity consider only the linear and quadratic terms, then, equation (2.2.5.1) becomes:

$$f(\sigma_m) = F_{ij}\,\sigma_{ij} + F_{ijlk}\,\sigma_{ij}\,\sigma_{lk} = 1$$

.....(2.2.5.2)

F_{ij} and F_{ijlk} are strength tensors of 2nd and 4th rank respectively. By contracting equation (2.2.5.2) it changes into the form:

$$f(\sigma_m) = F_i\,\sigma_i + F_{ij}\,\sigma_i\,\sigma_j = 1$$

.....(2.2.5.3)

Here i,j,m=1,2,.....6.

by expanding equation (2.2.5.3), the following is obtained

$$F_1\,\sigma_1 + F_2\,\sigma_2 + F_3\,\sigma_3 + F_4\,\sigma_4 + F_5\,\sigma_5 + F_6\,\sigma_6 + F_{11}\,\sigma_1^2 + F_{22}\,\sigma_2^2 + F_{33}\,\sigma_3^2 + F_{44}\,\sigma_4^2 + F_{55}\,\sigma_5^2 + F_{66}\,\sigma_6^2 + 2F_{12}\,\sigma_1\,\sigma_2 + 2F_{13}\,\sigma_1\,\sigma_3 + 2F_{14}\,\sigma_1\,\sigma_4 + 2F_{15}\,\sigma_1\,\sigma_5 + 2F_{16}\,\sigma_1\,\sigma_6 + 2F_{23}\,\sigma_2\,\sigma_3 + 2F_{24}\,\sigma_2\,\sigma_4 + 2F_{25}\,\sigma_2\,\sigma_5 + 2F_{26}\,\sigma_2\,\sigma_6 + 2F_{34}\,\sigma_3\,\sigma_4 + 2F_{35}\,\sigma_3\,\sigma_5 + 2F_{36}\,\sigma_3\,\sigma_6 + 2F_{45}\,\sigma_4\,\sigma_5 + 2F_{46}\,\sigma_4\,\sigma_6 + 2F_{56}\,\sigma_5\,\sigma_6 = 1$$

.....(2.2.5.4)

This strength criterion satisfies the theoretical requirements outlined in Section 2.2.1. Tsai and Wu (1971) pointed out that the linear terms σ_i take into account internal stresses. Consequently, the criterion can describe the different failures due to tensile and compressive stresses. The quadratic terms $\sigma_i\,\sigma_j$ give an ellipsoidal form to the failure surface in the stress-space.

For a plane stress state, equation (2.2.5.4) can be simplified to:

$$F_1\,\sigma_1 + F_2\,\sigma_2 + F_6\,\sigma_6 + 2F_{12}\,\sigma_1\,\sigma_2 + 2F_{16}\,\sigma_1\,\sigma_6 + 2F_{26}\,\sigma_2\,\sigma_6 + F_{11}\,\sigma_1^2 + F_{22}\,\sigma_2^2 + F_{66}\,\sigma_6^2 = 1$$

.....(2.2.5.5)

The strength criterion given by equation (2.2.5.5) can only characterize the failure surface of any anisotropic materials expressible in an ellipsoidal or a parabolic form. However, there might be many anisotropic materials which possess failure surfaces that cannot be described accurately by the quadratic terms in equation (2.2.5.1). For such cases, terms with strength tensor coefficients of higher rank must be used. Wu (1974) examined a third order tensor polynomial failure strength criterion:

$$F_i \sigma_i + F_{ij} \sigma_i \sigma_j + F_{ijk} \sigma_i \sigma_j \sigma_k = 1 \qquad .....(2.2.5.6)$$

He established the constraints to which the strength tensor of third rank must be subjected in order to satisfy the fundamental requirements listed in Section 2.2.1. By considering a planar orthotropic case Wu (1974) came to the following conclusions about the strength tensor components.

(i) F_i : determines the origin of the failure surface or envelope along the σ_i-axis.

(ii) F_{ii} : determines the intercept of the failure envelope with the σ_i-axis.

(iii) F_{ij} : determines the orientation of the failure envelope in the $\sigma_i\sigma_j$ plane.

(iv) F_{iii} : redundant and not admissable.

(v) F_{ijk} : determines the inclination of failure envelope in the $\sigma_i\ \sigma_j\ \sigma_k$ space.

(vi) F_{ijj} : distorts the failure envelope from an ellipsoid in the $\sigma_i\ \sigma_j$ plane.

This list could be extended by examining the strength tensor components of higher order.

In the process of deriving the strength tensor polynomial criterion Tsai and Wu (1971) assumed that a failure potential exists i.e. the failure of anisotropic materials is loading path-independent. The means of determining strength tensors F_{ii}, F_{ij} and F_i have been explained by Tsai and Wu (1971). These quantities are related to the strengths of the material concerned in the following ways:

$$F_i = \frac{1}{X_i} - \frac{1}{X_i'} \qquad .....(2.2.5.10)$$

$$F_{ii} = \frac{1}{X_i X_i'} \qquad .....(2.2.5.11)$$

where $i=1,2,3.....6.$

X_i represents the tensile strength in the i-direction for i=1,2,3.

and X_i' represents the compressive strength in the i-direction for i=1,2,3.

similarly X_i represents the positive shear strength in the i-direction for i=4,5,6.

and X_i' represents the negative shear strength in the i-direction for i=4,5,6.

X_4 , X_4' are the positive and negative shear strengths respectively along the 2-3 plane.

X_5 , X_5' are those along the 3-1 plane and

X_6 , X_6' are those that act along the 1-2 plane.

The relation between F_{ij} and the strength properties of the material concerned varies with the method used for the determination of F_{ij}. Tsai and Wu (1971) illustrated several methods of determining the F_{12} component. Only one of these examples will be cited here as follows.

The determination of F_{12} using 45-degree off-axis unidirectional specimens:

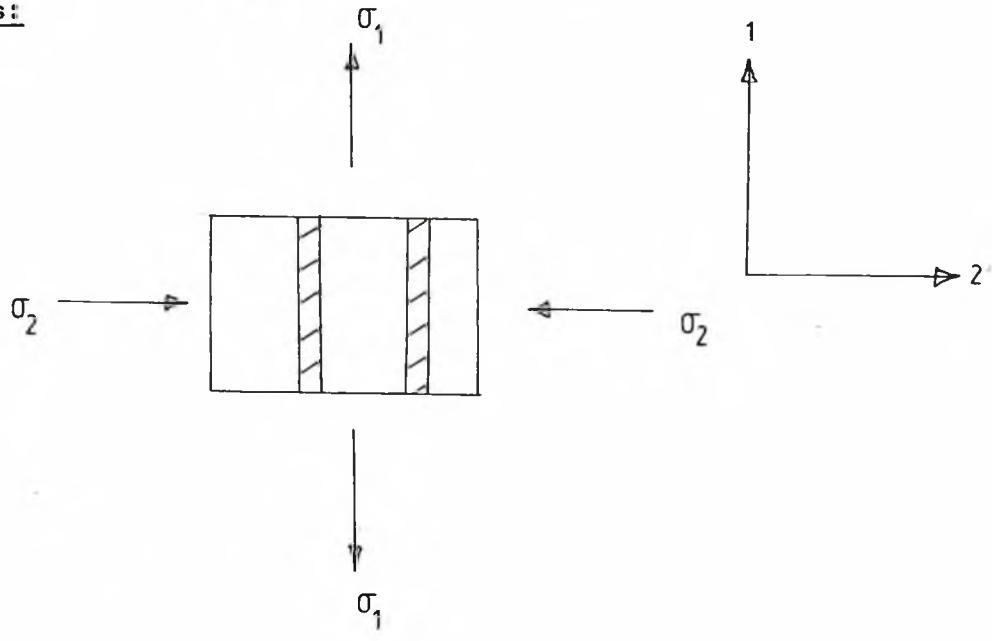

Fig 2.2.5.1 A Lamina under Pure Shear.

Let

$$\sigma_1 = V$$

and

$$\sigma_2 = -V \qquad \text{.....(2.2.5.12a)}$$

where V is the positive shear strength of a 45 degree off-axis unidirectional lamina.

$$\sigma_3 = \sigma_4 = \sigma_5 = \sigma_6 = 0 \qquad .....(2.2.5.12b)$$

By substituting (2.2.5.12a) & (2.2.5.12b) into equation (2.2.5.2) the following is obtained.

$$V^2 (F_{11} + F_{22} - 2 F_{12}) + V (F_1 - F_2) = 1 \qquad .....(2.2.5.13)$$

Rearranging equation (2.2.5.13) it can be established that

$$F_{12} = (-1/2 V^2) (1 - V((1/X_1) - (1/X'_1) - (1/X_2) + (1/X'_2)) - V^2 ((1/X_1X'_1) + (1/X_2X'_2)) \qquad .....(2.2.5.14)$$

Therefore, by performing pure shear experiments using 45-degree off-axis unidirection specimens F_{12} could be determined for a given system of composite material.

As has been pointed out by Tsai and Wu (1971) F_{12} is a very sensitive and critical quantity in their proposed polynomial strength tensor failure criterion (equation 2.2.5.1). A small variation in the value of F_{12} could have a significant effect on the failure envelope in the σ_1–σ_2 plane. This is because F_{12} determines the inclination of the failure envelope in this plane.

A detailed account of the methods of evaluating F_{12} , F_{16} , F_{26} and other interaction terms has been given by Wu (1972).

In general, it is accepted that the failure envelope cannot be open-ended, for example like a hyperboloid. In order to ensure that

the failure envelope will be always closed Tsai and Wu (1971) introduced the following stability conditions into their polynomial strength tensor failure criterion.

$$
\begin{aligned}
&F_{11}\,F_{22} - F_{12}^2 > 0\\
&F_{22}\,F_{66} - F_{26}^2 > 0\\
&F_{11}\,F_{66} - F_{16}^2 > 0\\
&F_{11}\,F_{33} - F_{13}^2 > 0\\
&F_{22}\,F_{33} - F_{23}^2 > 0\\
&F_{33}\,F_{66} - F_{36}^2 > 0\\
&\quad\vdots\\
&\text{etc}
\end{aligned}
\qquad \text{.....(2.2.5.15)}
$$

The general features of the Tsai and Wu's (1971) polynomial strength tensor failure criterion can be summarised as follows:

(i) The criterion is a scalar equation. Consequently, it is also invariant.

(ii) The rules of transformation can be applied to the strength tensors.

(iii) The strength tensors are symmetric in nature, i.e. $F_{ij} = F_{ji}$. It can be reduced to any number of spatial dimensions and multiaxial stresses by using the appropriate range of the indices, from 1 to 6.

(iv) With the transformation relation one can use the criterion to study the off-axis strength properties of a given anisotropic material.

(v) Since the criterion is invariant, it is valid for all coordinate systems when it has been proven to be valid for one.

(vi) It always ensures that the failure envelope is closed.

(vii) It is operationally simpler when compared to other, general theories based on strength tensors.

The Tsai and Wu (1971) strength criterion has been discussed at the lamina level. Nevertheless, it can be applied directly to characterize the failure behaviour of the laminate. In this case the laminate is treated as a complete entity. Unfortunately, as such the criterion has a major drawback. As explained by Wu (1972), in order to evaluated the interaction coefficients, e.g. F_{12}, the biaxial measurement must be tested at the optimal ratio $B_{12} = \sigma_1 / \sigma_2$. For a quadratic case this optimal ratio depends not only on the magnitude of F_1, F_{11}, F_2, F_{22} but also on the magnitude of F_{12}. Consequently, a series of experimental iterations must be carried out in order to determine accurately the value of F_{12}. When the cubic terms in equation (2.2.5.1) are added in the analysis, the optimal ratio depends also on the magnitude of F_{112}, F_{122}. The procedure of experimental iteration thus becomes a tremendous problem as was pointed out by Wu and Scheublein (1974). They proposed a hybrid approach. The new approach uses the Tsai and Wu (1971) strength criterion at the lamina level. The Laminated Plate Theory, which will be discussed in the following section, is then used to estimate the laminate failure surface. The number of experimental iterations can be reduced by utilizing the estimated laminate failure surface to identify the optimal ratio at which the biaxial experiment must be performed in order to determine the interaction coefficients such as F_{12}. The strength tensors F_i, F_{ij} and F_{ijk} thus determined are substituted into equation (2.2.5.1) to reevaluate a more reliable laminate failure surface. Wu and Scheublein (1974) concluded that the weakest link in the hybrid approach was the Classical Laminate Theory. They suggested that the effect of non-linearity and interlamina stresses be included in the analysis of the Laminate Theory.

Tsai and Wu (1971), using the framework and notation of their approach, made a comparison between the Hill criterion (1948) and their proposed polynomial strength criterion. Later, using the same technique Wu (1974) carried out a detailed analysis on a number of criteria that are currently available.

2.2.6. A critical examination of other Anisotropic Failure Criteria:

There are many other phenomenological failure criteria for anisotropic materials. Some of these will be examined in the light of the discussion given by Wu (1974).

Two criteria were proposed by Norris (1946 & 1950) when he was working with wood. These criteria have been reviewed by Kaminski and Lantz (1969). However, they will be viewed here from another angle.

Norris's (1946) proposed criterion has the following form:

$$(\sigma_1/\sigma_{1\,(ult)})^2 + (\sigma_2/\sigma_{2\,(ult)})^2 + (\sigma_6/\sigma_{6\,(ult)})^2 = 1$$

.....(2.2.6.1)

When equation (2.2.6.1) is expressed in the form of

$$F_i\ \sigma_i + F_{ij}\ \sigma_i\ \sigma_j = 1$$

.....(2.2.5.3)

the coefficients F_i and F_{ij} are obtained as

$$F_i = \begin{bmatrix} 0 \\ 0 \\ 0 \\ 0 \\ 0 \\ 0 \end{bmatrix} \; ; \quad F_{ij} = \begin{bmatrix} 1/\sigma^2_{1\,(ult)} & 0 & 0 & 0 & 0 & 0 \\ 0 & 1/\sigma^2_{2\,(ult)} & 0 & 0 & 0 & 0 \\ 0 & 0 & 0 & 0 & 0 & 0 \\ 0 & 0 & 0 & 0 & 0 & 0 \\ 0 & 0 & 0 & 0 & 0 & 0 \\ 0 & 0 & 0 & 0 & 0 & 1/\sigma^2_{6\,(ult)} \end{bmatrix} \quad .....(2.2.6.2)$$

From equation (2.2.6.2) it is obvious that equation (2.2.6.1) is valid only for the specially orthotropic case because F_{16} and F_{26} have been assumed to be zero. Furthermore, by equating F_{12} to zero it implies that there is no interacting effect between σ_1 and σ_2 . $\sigma_{1(ult)}$ and $\sigma_{2(ult)}$ are defined as tensile or compressive strengths in the 1 and 2 - directions.

Later Norris (1950) put forward another criterion of the form

$$(\sigma_1/X_1)^2 + (\sigma_2/X_2)^2 - ((\sigma_1\ \sigma_2)/(X_1\ X_2)) + (\sigma_6/X_6)^2 = 1$$

$$(\sigma_2/X_2)^2 + (\sigma_3/X_3)^2 - ((\sigma_2\sigma_3)/(X_2\ X_3)) + (\sigma_4/X_4)^2 = 1$$

$$(\sigma_3/X_3)^2 + (\sigma_1/X_1)^2 - ((\sigma_1\ \sigma_3)/(X_1\ X_3)) + (\sigma_5/X_5)^2 = 1$$

.....(2.2.6.3)

In this case the coefficients F_{ij} are as given below:

$$F_i = \begin{bmatrix} 0 \\ 0 \\ 0 \\ 0 \\ 0 \\ 0 \end{bmatrix} \quad ;$$

$$(F_{ij})_{12} = \begin{bmatrix} 1/X_1^2 & -1/(X_1\,X_2) & 0 & 0 & 0 & 0 \\ & 1/X_2^2 & 0 & 0 & 0 & 0 \\ & & 0 & 0 & 0 & 0 \\ & & & 0 & 0 & 0 \\ & & & & 0 & 0 \\ & & \text{Symm.} & & & 1/X_6^2 \end{bmatrix} \quad ;$$

$$(F_{ij})_{13} = \begin{bmatrix} 1/X^2 & 0 & -1/(X_1\,X_3) & 0 & 0 & 0 \\ & 0 & 0 & 0 & 0 & 0 \\ & & 1/X_3^2 & 0 & 0 & 0 \\ & & & 0 & 0 & 0 \\ & & & & 1/X_5^2 & 0 \\ & & & & & 0 \end{bmatrix} \quad ;$$

.....(2·2·6·4)

$$(F_{ij})_{23} = \begin{bmatrix} 0 & 0 & 0 & 0 & 0 & 0 \\ & 1/X_2^2 & -1/(X_2\ X_3) & 0 & 0 & 0 \\ & & 1/X_3^2 & 0 & 0 & 0 \\ & & & 1/X_4^2 & 0 & 0 \\ & & & & 0 & 0 \\ & & & & & 0 \end{bmatrix} ;$$

$$(F_{ij}\ \sigma_i\ \sigma_j)_{12} = 1 ;$$

$$(F_{ij}\ \sigma_i\ \sigma_j)_{13} = 1 ;$$

$$(F_{ij}\ \sigma_i\ \sigma_j)_{23} = 1 ;$$

.....(2.2.6.4)

Neither of the criteria put forward by Norris (1946 & 1950) include the linear terms F_i. Consequently, these criteria do not take into account the difference between the tensile and compressive uniaxial strengths of a given material. The second criterion represented by equation (2.2.6.3) is an improvement over that expressed in equation (2.2.6.1). It includes the coupling effect between the normal stresses, i.e. F_{12} , F_{13} and F_{23}. Nevertheless, the application of this criterion is restricted to the specially orthotropic case because it assumes that there is no coupling between

the normal and the shear stresses.

More recently, Azzi and Tsai (1965) modified Hill's (1948) criterion for unidirectional, fibre reinforced composite materials. The modified criterion has the following form

$$(\sigma_1/\sigma_{1\,(ult)})^2 + (\sigma_2/\sigma_{2\,(ult)})^2 + (1/\sigma^2_{3\,(ult)} - 1/\sigma^2_{x\,(ult)} - 1/\sigma^2_{y\,(ult)})\ \sigma_1\ \sigma_2 + (\sigma_6/\sigma_{6\,(ult)})^2 = 1 \qquad .....(2.2.6.5)$$

When applied to a plane stress situation, equation (2.2.6.5) can be expressed in the form of equation (2.2.5.3). The coefficients of F_i and F_{ij} will be as follow

$$F_i = \begin{bmatrix} 0 \\ 0 \\ 0 \\ 0 \\ 0 \\ 0 \end{bmatrix}; \quad F_{ij} = \begin{bmatrix} 1/\sigma^2_{1\,(ult)} & (1/\sigma^2_{3\,(ult)} - 1/\sigma^2_{1\,(ult)} - 1/\sigma^2_{2\,(ult)}) & 0 & 0 & 0 & 0 \\ & 1/\sigma^2_{2\,(ult)} & 0 & 0 & 0 & 0 \\ & & 0 & 0 & 0 & 0 \\ & \text{SYMM.} & & 0 & 0 & 0 \\ & & & & 0 & 0 \\ & & & & & 1/\sigma^2_{6\,(ult)} \end{bmatrix} \qquad .....(2.2.6.6)$$

This criterion has all the limitations similar to those mentioned when dealing with the Norris (1950) criterion.

Puppo and Evensen (1972) suggested a way of defining the principal strength axes in a composite structure. They introduced a parameter called the interaction factor, γ .

$$\gamma = 3\ T^2_{12}/(T_1\ T_2) \qquad .....(2.2.6.9)$$

where T_{12} is the shear strength of the structure.

T_1 is the uniaxial strength of the structure along the 1-direction.

T_2 is the uniaxial strength of the structure along the 2-direction.

The definition of the coordinate system is as shown below

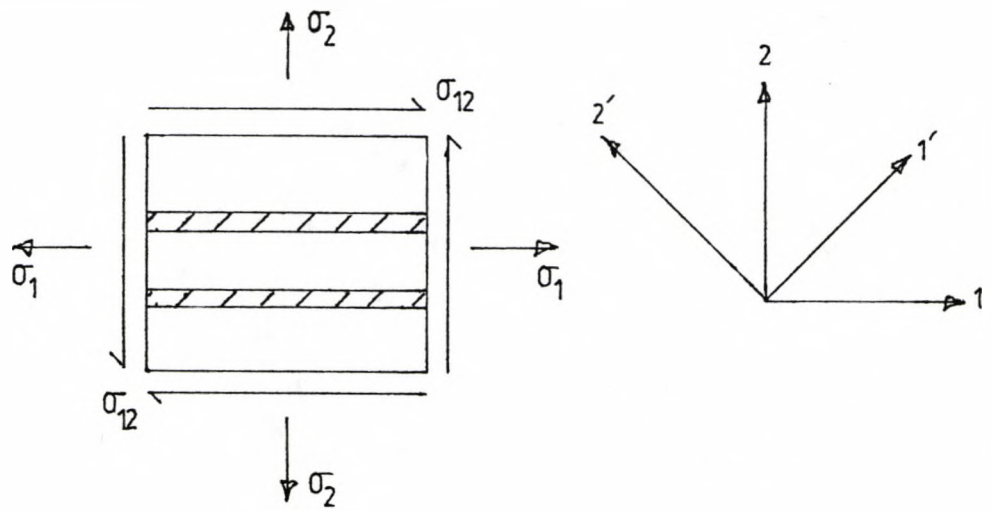

Fig 2.2.6.1. Lamina under Plane Stress.

When referring to the coordinate system 1'-2'

$$\gamma' = 3\ T_{12}^2 / (T_1, T_2)$$

.....(2.2.6.10)

The principal strength axes are defined as those for which the interaction parameter is a relative minimum with respect to transformation. Puppo and Evensen (1972) argued that in order to provide a facility for the transition from $\gamma=1$ to $\gamma=0$ a failure criterion must be composed of several equations which represent several intersecting surfaces in the (σ_1, σ_2, σ_3) stress space. They expanded their argument to the three dimensional case by defining two

extra interaction factors. Therefore, the interaction factors for a 3-Dimensional case are

$$Y_1 = 3\ T_{12}^2/(T_1\ T_2)$$

$$Y_2 = 3\ T_{23}^2/(T_2\ T_3)$$

$$Y_3 = 3\ T_{31}^2/(T_3\ T_1)$$

.....(2.2.6.11)

Subsequently, the failure criterion proposed by Puppo and Evensen (1972) has the following form

$$(F_{ij})_k\ \sigma_i\ \sigma_j = 1$$

.....(2.2.6.12)

i,j=1,2,3....6

and

k=1,2,3.

In other words, for a 3-Dimensional case the Puppo and Evensen (1972) failure criterion consists of three polynomial stress tensor equations. These equations contain only quadratic terms. The coefficients $(F_{ij})_k$ take the following forms

$$(F_{ij})_1 = \begin{bmatrix} 1/T_1^2 & -Y_1/(2T_2^2) & -Y_3/(2T_3^2) & & & \\ & Y_1/T_2^2 & -1/2T_1^2 & & & \\ & & Y_3/T_3^2 & & & \\ & \text{Symm} & & 1/T_{23}^2 & & \\ & & & & 1/T_{31}^2 & \\ & & & & & 1/T_{12}^2 \end{bmatrix}$$

.....(2.2.6.13)

$$(F_{ij})_2 = \begin{bmatrix} Y_1/T_1^2 & -Y_1/2T_1^2 & -1/2T_2^2 & 0 & 0 & 0 \\ & 1/T_2^2 & -Y_2/2T_3^2 & 0 & 0 & 0 \\ & & Y_2/T_3^2 & 0 & 0 & 0 \\ & \text{Symm.} & & 1/T_{23}^2 & 0 & 0 \\ & & & & 1/T_{31}^2 & 0 \\ & & & & & \frac{2}{T_{12}} \end{bmatrix}$$

$$(F_{ij})_3 = \begin{bmatrix} Y_3/T_1^2 & -1/2T_3^2 & -Y_3/2T_1^2 & 0 & 0 & 0 \\ & Y_2/T_2^2 & -Y_2/2T_2^2 & 0 & 0 & 0 \\ & & 1/T_3^2 & 0 & 0 & 0 \\ & & & 1/T_{23}^2 & 0 & 0 \\ & \text{Symm.} & & & 1/T_{21}^2 & 0 \\ & & & & & 1/T_{12}^2 \end{bmatrix}$$

.....(2.2.6.13)

For a plane stress situation equation (2.2.6.12) is reduced to

$$(F_{ij})_k \sigma_i \sigma_j = 1$$

.....(2.2.6.14)

where i,j=1,2 and 6

and

k=1,2.

The coefficients given in equation (2.2.6.13) are valid only for the specially orthotropic case. When considering the specially orthotropic materials under plane stress, equation (2.2.6.13) is then reduced to

$$(F_{ij})_1 = \begin{bmatrix} 1/T_1^2 & -\gamma_1/2T_2^2 & 0 \\ & \gamma_1/T_2^2 & 0 \\ & & 1/T_{12}^2 \end{bmatrix}$$

$$(F_{ij})_2 = \begin{bmatrix} \gamma_1/T_1^2 & -\gamma_1/2T_1^2 & 0 \\ & 1/T_2^2 & 0 \\ & & 1/T_{12}^2 \end{bmatrix}$$

.....(2.2.6.15)

For general orthotropic materials under plane stress, Puppo and Evensen (1972) demonstrated that

$$(F'_{ij})_1 = \begin{bmatrix} 1/T_1'^2 & -h(\gamma)/(T_1' T_2') & -g(\gamma)/(T_1' T_{12}') \\ & -1/T_2'^2 & -g(\gamma)/(T_2' T_{12}') \\ & & 1/T_{12}'^2 \end{bmatrix}$$

$$(F'_{ij})_2 = \begin{bmatrix} 1/T_1'^2 & -h(\gamma)/(T_1' T_2') & g(\gamma)/(T_1' T_{12}') \\ & -1/T_2'^2 & g(\gamma)/(T_2' T_{12}') \\ & & 1/T_{12}'^2 \end{bmatrix}$$

.....(2.2.6.16)

Where

$$g(\gamma) = (\gamma/12)^{1/2} \left(3f(\gamma) / (f(\gamma) - 4) + 1\right) f(\gamma)$$

$$h(\gamma) = 1 - (1/2)\, f(\gamma)$$

.....(2.2.6.17)

and

$$f(\gamma) = (1/10) \left(-(4 + 3/\gamma) + ((4 + 3/\gamma)^2 + 240/\gamma)^{1/2}\right)$$

$$\gamma = (3\, T'_{12}) / (T'_1\, T'_2)$$

.....(2.2.6.18)

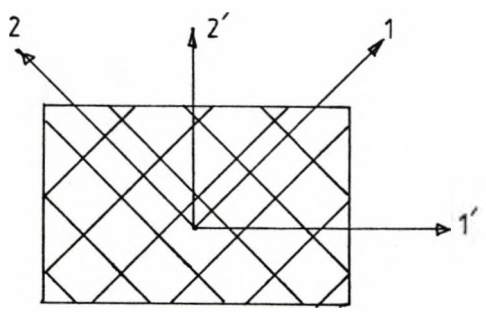

Fig 2.2.6.2. Transformation of Reference Coordinates.

Equation (2.2.6.16) is given with respect to the 1'-2' coordinate system as shown in fig 2.2.6.2. The distinction between specially and general orthotropic cases has been given by Ashton et al (1969).

Puppo and Evensen's (1972) criterion is similar to the Hill's (1948) criterion on one aspect. Both criteria use only the quadratic terms in their formulation. Though Puppo and Evensen (1972) pointed out the apparent paradox existing in the Hill-Type criterion. This contradiction arose because the original formula of Hill's (1948) criterion was not used in the coordinate transformation process as

explained by Wu (1974). In view of this similarity Puppo and Evensen's (1972) criterion shares many of the limitations experienced by Hill's (1948) criterion.

In order to take into account the difference in tensile and compressive stengths Puppo and Evensen (1972) imposed a condition such that the values of T_1 and T_2 must be chosen according to the signs of the normal stesses. No mention was made of the value of T_{12}. This ambiguity can lead to problems when one tries to apply the Puppo and Evensen (1972) criterion to composite structures with different values for positive and negative shear strengths.

The Puppo and Evensen (1972) criterion reviewed so far treats any laminated composite materials as homogeneous and anisotropic. The criterion is applied to the laminate as a whole.

Another approach currently available in predicting the failure of laminated composite structures is to carry out stress analysis on a given structure using the layer by layer basis. The stresses resulting from the applied external loads in each constituent lamina are calculated by assuming that the strains due to the external loads are the same for every constituent lamina. The law of elasticity is then used to evaluate the stresses corresponding to these strains. With these calculated stresses the chosen phenomenological failure criterion is utilised to predict the failure of the lamina. This process is repeated until all the laminae have failed, i.e. the failure of the laminate.

Tsai and Azzi (1966) have developed a method of strength analysis of laminated composites based on this approach which is also known as the classical Laminated Theory. The mathematical theory that they used is an extension of the Mathematical Theory of Elasticity, presented in detail by Sokolnikoff and Specht (1946). Tsai and Azzi (1966) included the thermo-effect in the analysis. However, in the present context only the mechanical excitation is of interest. Therefore, the thermo-excitation is purposely left out of this discussion. In deriving the theory for the stress analysis Tsai and Azzi (1966) made the following assumptions:-

(i) Each constituent layer of the laminated composite is quasi-homogeneous and orthotropic.

(ii) The layers are in a state of plane stress.

(iii) The layers or laminae behave elastically and hence obey Hooke's law of elasticity.

(iv) The normal to the geometrical mid-plane of the laminated plane or shell remains straight and perpendicular to this mid-plane while the laminated structure is in the deformed state.

(v) The interlaminar shear stresses are zero.

(vi) Every lamina has the same state of strains.

With these assumptions the following constitutive equations were derived.

$$\begin{bmatrix} N \\ M \end{bmatrix} = \begin{bmatrix} A_{ij} & B_{ij} \\ B_{ij} & D_{ij} \end{bmatrix} \begin{bmatrix} \epsilon^0 \\ \kappa \end{bmatrix}$$

$i,j = 1,2 \text{ and } 6.$

.....(2.2.6.19)

Where

$$\left[N \right] = \begin{bmatrix} N_1 \\ N_2 \\ N_6 \end{bmatrix}$$

.....(2.2.6.20)

$$\begin{bmatrix} N_1 \\ N_2 \\ N_6 \end{bmatrix} = \int_{-\frac{h}{2}}^{\frac{h}{2}} \begin{bmatrix} \sigma_1 \\ \sigma_2 \\ \sigma_6 \end{bmatrix} dz$$

.....(2.2.6.21)

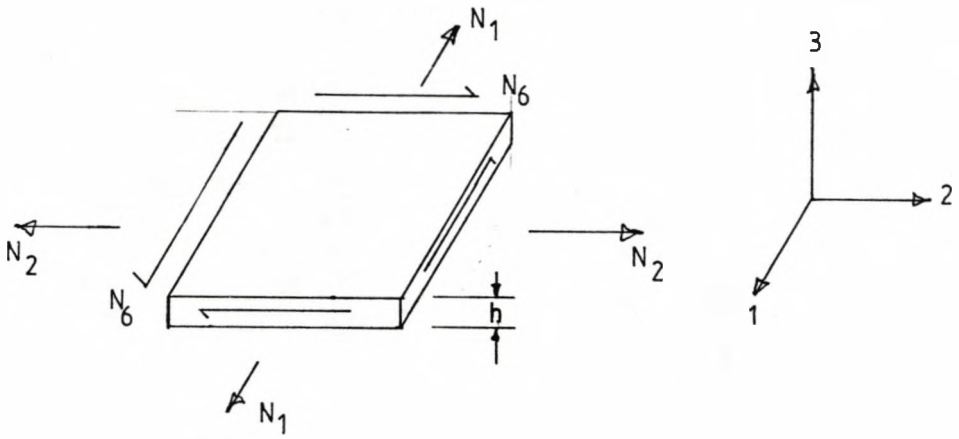

Fig 2.2.6.3. Notation for Laminate.

N_1 and N_2 and N_3 are each known as force per unit length. Since the functions

$$\sigma_1 = f_1(h)$$

$$\sigma_2 = f_2(h)$$

$$\sigma_6 = f_6(h)$$

.....(2.2.6.22)

are not continuous across the thickness of the laminate, piecewise integration has been resorted to. Consequently, the forces per unit length are expressed as

$$\begin{bmatrix} N_1 \\ N_2 \\ N_6 \end{bmatrix} = \sum_{m=1}^{n} \int_{h_{m-1}}^{h_m} \begin{bmatrix} \sigma_1 \\ \sigma_2 \\ \sigma_6 \end{bmatrix}_m dz \qquad .....(2.2.6.23)$$

Where m identifies the lamina and n is the total number of laminae. The in-plane stiffness matrix is

$$\left[A_{ij} \right] = \begin{bmatrix} a_{11} & a_{12} & a_{16} \\ a_{12} & a_{22} & a_{26} \\ a_{16} & a_{26} & a_{66} \end{bmatrix} \qquad .....(2.2.6.24)$$

and

$$a_{ij} = \sum_{m=1}^{n} (c_{ij})_m \, (h_m - h_{m-1}) \qquad i,j=1,2 \text{ and } 6.$$

Where C_{ij} are the components of the lamina stiffnesses. For an orthotropic lamina under plane stress

$$C_{ij} = \begin{bmatrix} c_{11} & c_{12} & 0 & 0 & 0 & 0 \\ c_{12} & c_{22} & 0 & 0 & 0 & 0 \\ 0 & 0 & 0 & 0 & 0 & 0 \\ 0 & 0 & 0 & 0 & 0 & 0 \\ 0 & 0 & 0 & 0 & 0 & 0 \\ 0 & 0 & 0 & 0 & 0 & c_{66} \end{bmatrix} \qquad .....(2.2.6.25)$$

B_{ij} is the stiffness coupling matrix and has the following form:

$$B_{ij} = \begin{bmatrix} b_{11} & b_{12} & b_{16} \\ b_{12} & b_{22} & b_{26} \\ b_{16} & b_{26} & b_{66} \end{bmatrix} ;$$

$$b_{ij} = \frac{1}{2}\sum_{m=1}^{n} (c_{ij})_m (h_n^2 - h_{n-1}^2) \qquad .....(2.2.6.25(i))$$

and D_{ij} is the flexural stiffness matrix with the following expression

$$\left[D_{ij} \right] = \begin{bmatrix} d_{11} & d_{12} & d_{16} \\ d_{12} & d_{22} & d_{26} \\ d_{16} & d_{26} & d_{66} \end{bmatrix} ;$$

$$d_{ij} = \frac{1}{3}\sum_{m=1}^{n} (c_{ij})_n (h_n^3 - h_{n-1}^3) \qquad .....(2.2.6.26)$$

The moments per unit length are

$$\left[M \right] = \begin{bmatrix} M_1 \\ M_2 \\ M_6 \end{bmatrix}$$

and

$$\begin{bmatrix} M_1 \\ M_2 \\ M_6 \end{bmatrix} = \sum_{m=1}^{n} \int_{h_{m-1}}^{h_m} \begin{bmatrix} \sigma_1 \\ \sigma_2 \\ \sigma_6 \end{bmatrix} z\,dz$$

.....(2.2.6.27)

$[\varepsilon^0]$ are the strains of the mid-plane and

$[k]$ are the curvatures of this mid-plane

while the laminate is subjected to a state of stress. The detail derivations of equations (2.2.6.19) to (2.2.6.27) have been given by Tsai and Azzi (1966) and Tsai (1964).

Given the applied loads, [N] and [M] are known. From equations (2.2.6.19) the quantities $[\varepsilon^0]$ and [k] of the laminate under the applied loads can be evaluated. Assumption (vi) implies that the deformations sustained by every lamina under the given applied loads are $[\varepsilon^0]$ and [k]. Using the following equations

$$(\sigma_i)_m = (c_{ij})_m \varepsilon_j^0 + z (c_{ij})_m k_j \qquad .....(2.2.6.28)$$

the stresses in the m^{th} lamina within the laminate can be computed. Tsai and Azzi (1966) applied Hill's failure criterion

$$F(\sigma_2 - \sigma_3)^2 + G(\sigma_3 - \sigma_1)^2 + H(\sigma_1 - \sigma_2)^2 + 2L\sigma_4^2 + 2M\sigma_5^2 + 2N\sigma_6^2 = 1 \qquad .....(2.2.6.29)$$

to the lamina to examine if it would fail under the system of stresses $(\sigma_i)_m$. When a lamina within the laminate has failed a redistribution of applied stresses amongst the remaining laminae still intact would take place. This process produces a new effective stiffness of the laminate and hence new values of [A], [B] and [D]. The procedure of predicting the failure of the lamina explained above is repeated until all the laminae have failed. Tsai and Azzi (1966) further assumed that the yielding and the ultimate strength were synonymous. They also assumed that the tensile and compressive strengths of a given structure were equal.

Tsai (1964) elucidated the method of evaluating the C_{ij} stiffness matrix from the material and geometric parameters.

Subsequently, The derivations of [A], [B] and [D] were given. He then went on to show how the value of [A], [B] and [D] for special cases like

(i) cross-ply and

(ii) angle-ply

could be obtained.

In using Hill's phenomenological failure criterion to predict the failure of a lamina, Tsai and Azzi's (1966) method of strength analysis of laminated composites shares those limitations of Hill's criterion mentioned by Wu (1974). Furthermore, the assumptions((i) - (vi)) made, imposed a severe limitation on their analysis. For non-metallic composite material like glass reinforced plastic, the stress corresponding to the elastic limit is small when compared to the ultimate strength. The material does not behave elastically beyond the elastic limit point. Also, the function

$$\sigma = f(\varepsilon)$$

.....(2.2.6.30)

is non-linear. Therefore, it is inaccurate to use equation (2.2.6.28) to evaluated the stresses present in the m^{th} lamina due to $[\varepsilon^0]$ and [k] when $[\varepsilon^0]$ are large compare to those at the point of elastic limit.

Tsai and Azzi (1966) used a laminated plate model for their analysis. Similar governing equations can be derived for laminate shell structures. Strictly speaking, Tsai and Azzi's (1966) method of strength analysis can only be applied to infinite laminate plates since interlaminar shear stress is present in finite laminate plates as has been shown by Puppo and Evensen (1970). In the Puppo and Evensen (1970) analysis they showed that the presence of the interlaminar shear stress was due to the existence of free edges. Pipes & Pagano (1970) and Pipes (1980) also treated the problem of interlaminar shear stress through the application of Theory of Elasticity. They employed the finite-difference solution technique. From their numerical analysis they confirmed the presence of interlaminar shear stress dealt with by Puppo and Evensen (1970). In addition, Pipes and Pagano (1970) found that the interlaminar shear stress was an edge effect which was restricted to an edge region approximately equal to the laminate thickness. These theoretical predictions were later substantiated experimentally by Pipes (1971). Pipes and Pagano (1970) also found that the interlaminar shear stress was high in the neighbourhood of the free edge with sign of a singularity at the intersection of the interface and free-edge. Puppo and Evensen (1970) and Pipes & Pagano (1970) suggested that delamination of the laminated plate at the free-edges was possible under uniaxial force. This phenomenon has been observed by Whitney and Browning (1972). Wang and Dickson (1978) also demonstrated the possibility of singularity at the intersection between free edge and the laminae interfaces. However, the existence of a stress singularity is, perhaps, a purely academic problem.

With all the shortcomings mentioned above, Tsai (1965) still found good agreement between the experimental and the theoretical results predicted by Tsai and Azzi's (1966) criterion. It must be pointed out that Tsai (1965) only considered lamina and laminated flat specimens under uniaxial force. It has been shown by Ashton et al., (1969) and Halpin et al., (1969) that the classical Laminated Theory can provide valuable information on the behaviour of laminated composites when subjected to stresses. It can be used as an aid in the analysis of composite materials.

Eckold et al., (1978) adopted the method used by Tsai and Azzi (1966) to calculate the stresses induced in a laminate when the given laminate structure was subjected to applied external forces. However, Eckold et al., (1978) employed the maximum stress failure criterion for the prediction of failure stresses. The accuracy of their theoretical prediction was improved by taking into account the following two factors:-

(i) The effect of different compressive and tensile strengths which was ignored by Tsai and Azzi (1966).

(ii) The non-linearity in the shear stress-strain response.

To accommodate for the second factor Eckold et al., (1978) fitted the expression

$$e_{12} = \sigma_{12}/G + B(\sigma_{12})^3 \qquad .....(2.2.6.31)$$

to the shear stress/strain curve. In equation (2.2.6.31) G and B are constants. Eckold et al., (1978) limited their failure criterion to filament wound materials.

Puck (1967) also developed a similar kind of analysis presented by Tsai and Azzi (1965). Puck (1967) concentrated on the plane stress case where the

$$[B_{ij}] = 0 \qquad .....(2.2.6.32)$$

Equation (2.2.6.32) is only true for symmetric laminate. Puck (1967) used the following equation as the failure criterion for the lamina.

$$(\sigma_{||}/\sigma_{||B})^2 + (\sigma_{\perp}/\sigma_{\perp B})^2 + (\tau_{\#}/\tau_{\#B})^2 = 1 \qquad .....(2.2.6.33)$$

where $\sigma_{||B}$, $\sigma_{\perp B}$ are the strengths paralled and perpendicular to the fibre under uniaxial load. $\tau_{\#B}$ is the shear strength under pure shear load. When expressed in tensor form as equation (2.2.5.3), equation (2.2.6.33) has the following appearance

$$F_{11}\,\sigma_1^2 + F_{22}\,\sigma_2^2 + F_{66}\,\sigma_6^2 = 1$$

$$\sigma_1 = \sigma_{||}\,, \quad \sigma_2 = \sigma_{\perp} \text{ and } \quad \sigma_6 = \tau_{\#} \qquad .....(2.2.6.34)$$

The coefficients of equation (2.2.6.34) are:

$$(F_i) = \begin{bmatrix} 0 \\ 0 \\ 0 \\ 0 \\ 0 \\ 0 \end{bmatrix}; \quad F_{ij} = \begin{bmatrix} 1/\sigma_{||B}^2 & 0 & 0 & 0 & 0 & 0 \\ & 1/\sigma_{\perp B}^2 & 0 & 0 & 0 & 0 \\ & & 0 & 0 & 0 & 0 \\ & & & 0 & 0 & 0 \\ & \text{Symm.} & & & 0 & 0 \\ & & & & & 1/\tau_{\#B}^2 \end{bmatrix} \qquad .....(2.2.6.35)$$

i,j = 1,2,3....6.

By excluding the linear terms, i.e. setting $F_i = 0$, Equation (2.2.6.33) cannot describe the difference between tensile and compressive stress induced failures. In addition, this equation is only applicable to the specially orthotropic case where

$$F_{16} = F_{26} = 0 \qquad .....(2.2.6.36)$$

Furthermore, it assumes that there is no interation between the stresses σ_1 and σ_2 which is grossly untrue. The condition for this assumption is

$$F_{12} = 0 \qquad .....(2.2.6.37)$$

The values of $\sigma_{\parallel B}$ and $\sigma_{\perp B}$ were not clearly defined as either tensile or compressive strengths. This ambiguity can present a problem since the tensile and compressive strengths are not usually equal.

As reviewed by Greenwood (1977), Schneider and Bardenheier (1975) used the following equation

$$-\sigma_\perp^2 / (\sigma_{\perp T}\, \sigma_C) + \sigma_\perp \left((\sigma_{\perp C} + \sigma_{\perp T}) / (\sigma_{\perp T}\, \sigma_{\perp C})\right) + (\tau_\# / \tau_{\#B})^2 = 1$$

.....(2.2.6.38)

to predict the fracture stress for the resin matrix. When equation (2.2.6.38) was incorporated into equation (2.2.6.33) Greenwood (1977) showed that the failure criterion for the resin matrix under plane stress became

$$(\sigma_{\parallel}/\sigma_{\parallel B})^2 - \sigma_\perp^2/(\sigma_{\perp T}\, \sigma_{\perp C}) + \sigma_\perp \left((\sigma_{\perp C} + \sigma_{\perp T}) / (\sigma_{\perp T}\sigma_{\perp C}\right) + (\tau_\# / \tau_{\#B})^2 = 1$$

.....(2.2.6.39)

By letting $\sigma_1 = \sigma_\parallel$, $\sigma_2 = \sigma_\perp$ and $\sigma_6 = \tau_\#$ equation (2.2.6.39) can be expressed as

$$\sigma_1^2 (1/\sigma^2_{\|\#B}) - \sigma_2^2 (1/(\sigma_{\perp T}\ \sigma_{\perp C})) + \sigma_2 ((\sigma_{\perp C} + \sigma_{\perp T})/(\sigma_{\perp T}\ \sigma_{\perp C})) + (1/\tau^2_{\#B})\,\sigma_6^2 = 1$$

.....(2.2.6.39(i))

which has a tensor form the same as that of equation (2.2.5.3). The strength coefficients of equation (2.2.6.39(i)) are:

$$(F_i) = \begin{bmatrix} 0 \\ (1/\sigma_{\perp T}) + (1/\sigma_{\perp C}) \\ 0 \\ 0 \\ 0 \\ 0 \end{bmatrix}; \quad F_{ij} = \begin{bmatrix} 1/\sigma^2_{\|\#B} & 0 & 0 & 0 & 0 & 0 \\ & 1/(\sigma_{\perp T}\ \sigma_{\perp C}) & 0 & 0 & 0 & 0 \\ & & 0 & 0 & 0 & 0 \\ & & & 0 & 0 & 0 \\ & & \text{Symm.} & & 0 & 0 \\ & & & & & 1/\tau^2_{\#} \end{bmatrix}$$

.....(2.2.6.40)

i,j = 1,2,....6.

According to Schneider and Bardenheier (1975) $\sigma_{\perp C}$ assumes negative numerical values. Equation (2.2.6.39) is an improvement over equation (2.2.6.33) because of the inclusion of the linear transverse term, i.e.

$$F_2 = 1/\sigma_{\perp T} + |1/\sigma_{\perp C}|$$

.....(2.2.6.41)

Nevertheless, it still suffers severe limitations similar to those experienced by equation (2.2.6.33).

In the analyses carried out by Tsai & Azzi (1966) and Puck (1967) the values of $[C_{ij}]$ were derived from $E_{\|}$, $E_{\perp}$, $\nu_{\|\perp}$, $\nu_{\perp\|}$, $G_{\#}$. These were in turn derived from the material properties of the constituents using the rule of mixtures (Ashton et al. (1969), Greenwood (1977) and Tsai (1964)).

All the phenomenological failure criteria that have been discussed so far require knowledge of the fracture strengths of the materials under the uniaxial stresses of compression, tension and pure shear. Furthermore, these strength values must be obtained experimentally. They vary with the constituent properties and the fabrication processes. Therefore, it is necessary that these strengths be determined for each given set of constituent properties and fabrication processes. Chamis (1969) introduced a two-level theory in trying to predict the strength behaviour of unidirectional filamentary composite materials with respect to their constituents.

Chamis (1969) also used the semi-empirical approach employed in the derivation of all other criteria reviewed so far. Chamis' (1969) theory is based on five strength criteria. Four criteria are used to characterize the strength behaviour of the materials under uniaxial stresses. The remaining criterion is required for describing the strength characteristic of the materials under the influence of combined plane stresses. In deriving the failure criteria, Chamis (1969) made a major assumption that the materials behave in a linear-elastic manner up to failure.

The fabrication process normally accounts for the following variables:

(i) void size,

(ii) void content,

(iii) void distribution,

(iv) filament spacing non-uniformity,

(v) residual stresses and

(vi) interfacial bond strength.

In order to take into consideration all such variables Chamis (1969) introduced the theory-experiment correlation factors into his criteria. These factors must be evaluated for each particular fabrication process. He then used the modified form of the rule of mixtures equations to relate the longitudinal tensile and compressive strengths to the material properties of the constituents. The resulting equations are as follow:

$$S_{11T} = S_{fT}(\beta_{fT}\,\bar{k}_f + \beta_{mT}\,\bar{k}_m(E_{m11}/E_{f11}))$$

.....(2.2.6.42)

and

$$S_{11C} = S_{mC}(\beta_{mC}\,\bar{k}_m + \beta_{fC}\,\bar{k}_f(E_{f11}/E_{m11}))$$

.....(2.2.6.43)

Where S_{11T} is the longitudinal tensile strength of the lamina.

S_{11C} is the longitudinal compressive strength of the lamina.

S_{fT} is the fibre bundle tensile strength.

S_{mT} is the matrix compressive strength.

$\bar{k}_m$ is the volume fraction of the matrix.

$\bar{k}_f$ is the volume fraction of the fibre.

β_{fT}, β_{mC}, β_{mT} and β_{fC} are the theory-experiment correlation factors.

E_{f11} and E_{m11} are the in-situ longitudinal moduli of fibre and matrix respectively.

Subscript:

f is fibre.

m is matrix.

T is tension.

C is compression.

l is lamina property.

The coordinate system used is as shown in fig 2.2.6.4.

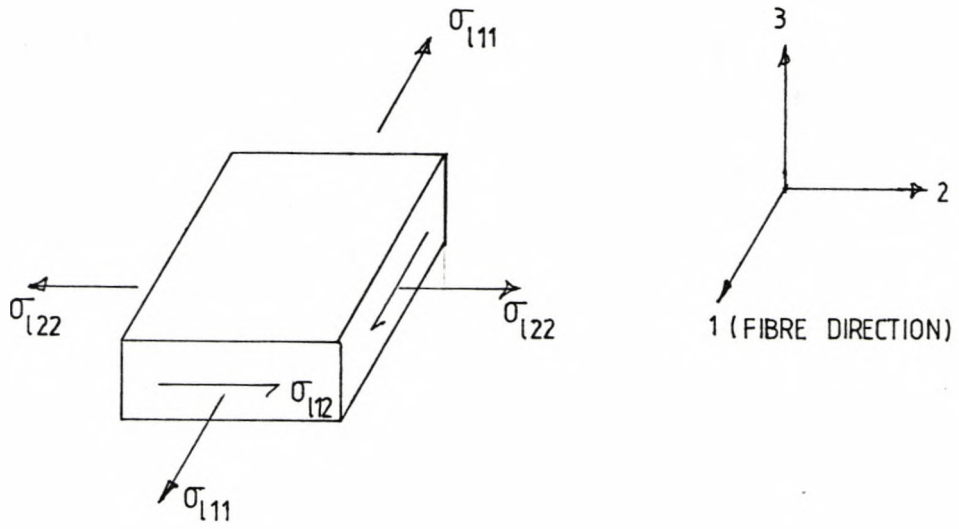

Fig 2.2.6.4. Coordinate System for a Lamina and Stress Notation.

Chamis (1969) argued that under longitudinal compressive loading it is possible for the lamina to fail by a combination of interface debonding and intralaminar shear. He approximated the condition by the expression

$$S_{l11C} = a_1 S_{l12S} + a_2$$

.....(2.2.6.44)

Here a_1 and a_2 are empirical curve-fit parameters. S_{l12S} is the intralaminar shear strength of the lamina. Chamis (1969) suggested that S_{l11C} be taken as the smaller of the two values computed from equations (2.2.6.43) and (2.2.6.44). The governing equations for transverse tensile, compressive and intralaminar shear failure stresses are respectively

$$S_{l22T} = \beta_{22T} \left(e_{mpT} / (\beta_v \Psi_{\mu 22})\right) E_{l22}$$

.....(2.2.6.45)

$$S_{l22C} = \beta_{22C} \left(\varepsilon_{mpC} / (\beta_v \Psi_{\mu 22})\right) E_{l22}$$

.....(2.2.6.46)

and

$$S_{l12S} = \beta_{12S} \left(\varepsilon_{mpS} / (\beta_v \Psi_{\mu 12})\right) G_{l12}$$

.....(2.2.6.47)

ε_{mpT} , ε_{mpC} and ε_{mpS} are the allowable matrix strains in tension, compression and shear. β_v is the void effect. E_{l22} and G_{l12} are the transverse and shear moduli of the lamina. $\Psi_{\mu 22}$ and $\Psi_{\mu 12}$ are the matrix-strain-magnification factors due to normal and shear stresses. The relations between $\Psi_{\mu 22}$, $\Psi_{\mu 12}$ and the material properties are given in Appendix 2. β_{22T} , β_{22C} and β_{12S} are the theory-experiment correlation factors. Equations (2.2.6.42) - (2.2.6.47) constitute the first level theory of Chamis (1969).

Chamis' (1969) second-level theory describes the strength behaviour of the lamina under a state of combined plane stresses. The governing equation for this strength criterion has the following form:

$$F(\sigma_l, S_l, K_{l12}) = 1 - \left((\sigma_{l11\alpha}/S_{l11\alpha})^2 + (\sigma_{l22\beta}/S_{l22\beta})^2 + (\sigma_{l12S}/S_{l12S})^2 - K'_{l12\alpha\beta} K_{l12} \left((\sigma_{l11\alpha}\, \sigma_{l22\beta}) / |(S_{l11\alpha}\, S_{l22\beta})|\right)\right)$$

.....(2.2.6.48)

$F(\sigma_l, S_l, K_{l12})$ is defined as follows:

$F(\sigma_l, S_l, K_{l12}) > 0$ - no failure

$F(\sigma_l, S_l, K_{l12}) = 0$ - onset of failure

$F(\sigma_l, S_l, K_{l12}) < 0$ - failure taken place.

S_l denotes the strength of the lamina under uniaxial stess. S_l can

be determined from the first level theory or measured experimentally. K_{l12} is a coefficient which has the following form:

$$K_{l12} = \{(1 + 4\upsilon_{l12} - \upsilon_{l13}) E_{l22} + (1 - \upsilon_{l23}) E_{l11}\} \Big/ (E_{l11} \; E_{l22} \; (2 + \upsilon_{l12} + \upsilon_{l13}) \; (2 + \upsilon_{l21} + \upsilon_{l23}))^{1/2}$$

.....(2.2.6.49)

Equation (2.2.6.48) is based on two postulates:

(i) The distortion energy under simple and combined loading remains invariant at the onset of failure,

(ii) the tensile and compressive properties of the lamina are the same up to the onset of failure.

But in general, the lamina does not possess the same material properties in tension and compression. Chamis (1969) compensated this observed phenomenon by introducing the theory-experiment correlation coefficient K'_{l12}. This was selected arbitrarily so as to give a good agreement between the theoretical and experimental results. Equation (2.2.6.48) is actually a modified form of the von Mises' failure criterion for isotropic materials, i.e.

$$(\sigma_{11} - \sigma_{22})^2 + (\sigma_{22} - \sigma_{33})^2 + (\sigma_{33} - \sigma_{11})^2 + 6(\sigma_{12}^2 + \sigma_{13}^2 + \sigma_{23}^2) = 8 K^2$$

.....(2.2.6.50)

Where K is the critical shear stress (Suh & Turner (1975)). It can be expressed in the tensor polynomial form similar to that of equation (2.2.5.3) and has the form

$$F_{11} \sigma_1^2 + F_{22} \sigma_2^2 + F_{12} \sigma_1 \sigma_2 + F_{66} \sigma_6^2 = 1$$

$$\sigma_6 = \sigma_{l12s} \qquad .....(2.2.6.51)$$

$$F_{ij} = \begin{bmatrix} 1/S^2_{l11\alpha} & ((-K'_{l12\alpha\beta}\ K_{l12})/|(S_{l11\alpha}\ S_{l22\beta})|) & 0 & 0 & 0 & 0 \\ & 1/S^2_{l22\beta} & 0 & 0 & 0 & 0 \\ & & 0 & 0 & 0 & 0 \\ & & & 0 & 0 & 0 \\ & \text{Symm.} & & & 0 & 0 \\ & & & & & 1/S^2_{l12} \end{bmatrix}$$

..... (2·2·6·52)

Though the strength coefficients F_{ij} are tensorial in nature, transformation of the F_{ij} matrix does not possess any physical meaning. This is because $K'_{|12\alpha\beta}$ and $K'_{|12}$ take up different values depending on the combination of applied stresses as illustrated by fig 2.2.6.5.

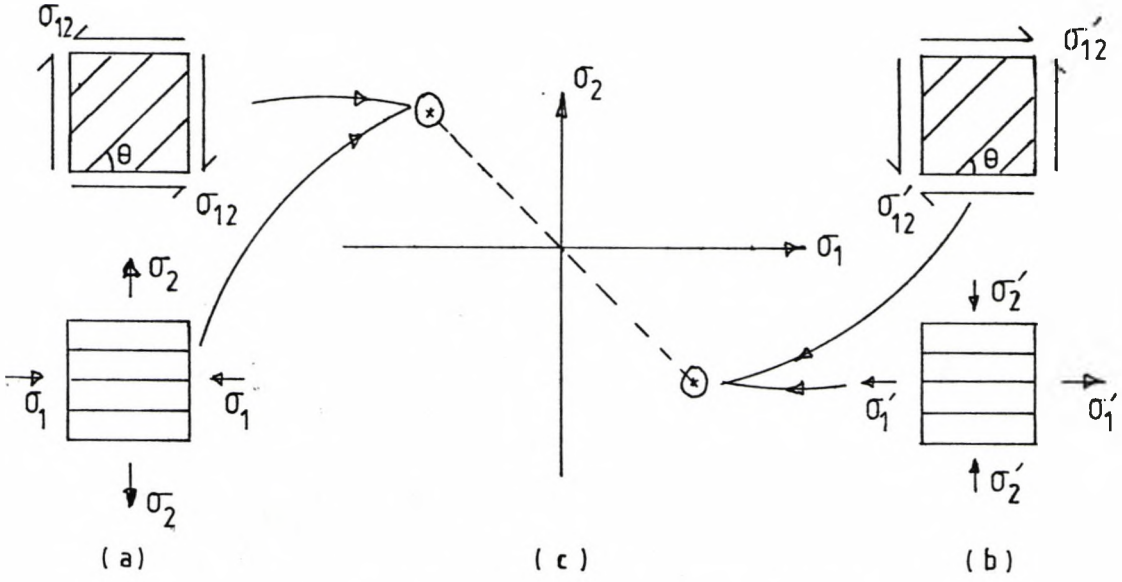

Fig 2.2.6.5. Two Systems of Pure Shear Stress.

Let the strength coefficients due to the state stress represented by fig 2.2.6.5 (a) be F_{ij} and that of fig 2.2.6.5 (b) be F'_{ij}. These systems of shear stress produce failure points on different quadrants of the σ_1—σ_2 stress space. Consequently,

$$F_{ij} \neq F_{ij}' \qquad .....(2.2.6.52a)$$

even when θ is the same in both cases. Therefore, to study the off-axis properties of an orthotropic material the external applied stresses must be transformed to the material axis.

As can be seen from equation (2.2.6.51) this criterion implies that there is no coupling between the shear and normal stresses, i.e.

$$F_{16} = 0 \quad ; \quad F_{26} = 0$$

.....(2.2.6.53)

It also assumes that

$$F_i = 0 \qquad .....(2.2.6.54)$$

With these assumptions, equations (2.2.6.53) and (2.2.6.54), it suffers the same limitations that have been mentioned earlier in this section.

In principle, Chamis' (1969) two-level theory is not valid beyond the elastic limit since he assumed that the material behaved in a linear-elastic manner. Nevertheless, the first-level theory offers a means of predicting the strength behaviour of the lamina with respect to the volume of fibre present.

As mentioned in the introductory section of this chapter, there is another approach to the study of failure behaviour of composite materials. This alternative is known as the micromechanics approach. The analysis is at a microscopic level. The stress distribution amongst the constituents of a given composite materials is examined. Detailed discussion of this topic is outside the scope of this chapter. Nevertheless, active work in this field is being pursued by others.

2.2.7. Experimental Stess Analysis - The Failure Characterization of Composite Materials:

The behaviours of the isotropic and the anisotropic materials under mechanical excitation differ considerably. It has been demonstrated by Halpin et al. (1969) that the method of mechanical

characterization for isotropic solids could not be applied directly to the anisotropic materials. Halpin et al (1969) also showed the effect of the coupling between the normal and shear stresses on the anisotropic material properties which if ignored could introduce serious error into the interpretation of experimental results.

In characterizing isotropic materials under uniaxial stress flat coupon specimens are frequently used for their simplicity. Unfortunately, it is not an easy task to generate a uniform state of stress in an angle-ply laminated flat coupon specimen. Pagano and Halpin (1968) discussed the influence of end constraint on the uniform stress field of coupon specimens under uniaxial tension. Using nylon-reinforced rubber Pagano and Halpin (1968) demonstrated the bending effect due to the end-clamping of the specimen which substantiated their analytical study on this subject.

Experimentalists have been forced to seek an alternative type of specimen because of the following two main problems :-

(i) the difficulty of generating a uniform state of stress in a flat laminated specimen.

(ii) edge effects (dicussed in Section 2.2.6) of flat laminated specimens.

The tubular specimen offers a means of overcoming the two problems mentioned above. Pagano et al (1968) carried out a study on the influence of end constraint in the mechanical testing of anisotropic cylinders. This study was based on the theory of elasticity. They considered a helically wound cylinder as shown below.

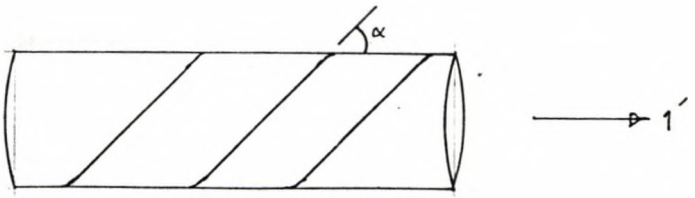

Fig 2.2.7.1(a). Helically wound tube - A Lamina

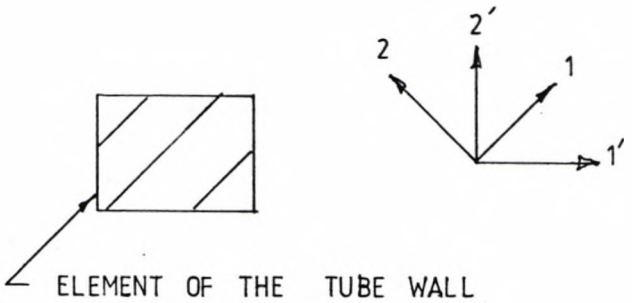

Fig 2.2.7.1(b). Coordinate system.

In plane stress case, the elastic constitutive equations in contracted notation form for an element of the tube wall are

$$e_i = S_{ij}\, \sigma_j \qquad .....(2.2.7.1)$$

Where S_{ij} are the compliances.

$i,j = 1',2',3'....6'.$

e_i are the strain responses.

σ_j are the applied stresses.

The strain-displacement relations are

$$e_{2'} = (1/r)(u + v_{,2'})$$

$$e_{1'} = w_{,1'}$$

$$e_{6'} = v_{,1'} + (1/r) w_{,2'} \qquad .....(2.2.7.2)$$

Note ',' denotes differentiation.

Using equations (2.2.7.1) and (2.2.7.2) and considering a cylinder under uniaxial tension along the 1' -direction Pagano et al., (1968) showed the existence of shear strain $\epsilon_{6'}$. This is because the compliance $S_{1'6'}$ is non-zero. Therefore, for a tubular specimen where $S_{1'6'}$ and $S_{2'6'}$ are non-zero free rotation about the tubular axis must be allowed before the following states of stress can be achieved:

(i)
$$\sigma_{1'} \neq 0, \quad \sigma_{3'} = \sigma_{2'} = \sigma_{4'} = \sigma_{5'} = \sigma_{6'} = 0$$

$$\sigma_{3'} = \sigma_r \qquad \text{.....(2.2.7.3)}$$

and

(ii)
$$\sigma_{2'} \neq 0, \quad \sigma_{1'} = \sigma_{3'} = \sigma_{4'} = \sigma_{5'} = \sigma_{6'} = 0 \qquad \text{.....(2.2.7.4)}$$

Pagano et al., (1968) also illustrated experimentally that if the condition

$$\epsilon_{6'} = 0 \qquad \text{.....(2.2.7.5)}$$

is imposed by clamping the ends of the tubular specimen instability would be introduced. Since in this case $\sigma_{6'}$ is now non-zero. Whitney and Halpin (1968) came to the conclusion that a tube clamped at one end and free to rotate at the opposite end could be used to characterize the mechanical properties of a fibre reinforce composite material.

Nevertheless, the phenomenon of instability which is commonly known as buckling must be considered seriously. An extensive amount of work has been done in this field. One of the objectives was to examine the stability of thin walled isotropic tubes under a complex state of stress. Treatment of this subject can be found in many text

books e.g. Flügge (1973), Johnson and Mellor (1973) etc. A theoretical analysis of buckling problems of heterogeneous anisotropic cylindrical shells under combined axial, radial and torsional loads was presented by Cheng & Ho (1963) and Ho & Cheng (1963). These analyses were based on thin shell theory of small deflections. Whitney and Sun (1975) concluded that buckling was a potential problem in the use of tubular specimens for composite material characterization. They found that in certain circumstances, the critical buckling load of the tube could be lower than the strength of the composite material estimated from the maximum strain criterion. Marlowe et al., (1974) determined experimentally the elastic torsional buckling strengths of a series of thin-walled angle-ply cylinders fabricated from the following type of materials:

(i) glass reinforced epoxy,

(ii) boron reinforced epoxy,

(iii) graphite reinforced epoxy composite materials,

(iv) non-metallic composite reinforced aluminum and

(v) non-metallic composite reinforced titanium.

A tremendous amount of work on the characterization of composite materials under simple uniaxial normal or pure shear stress has been carried out. However, discussion on these works has been left out deliberately due to the lack of space.

In the remainder of this chapter attention is focused on the characterization of composite materials under complex states of stress.

All the failure criteria that have been discussed in this chapter are purely mathematical models. They have been formulated for the purpose of predicting the failure conditions of a given composite material under a given state of stress. These models were not derived from the first principle of Physical Science. As such, there is no absolute verification for these models. Nonetheless, the accuracy of each model can be established experimentally. Many of these models required experiments that involved subjecting the specimens to a complex state of stress.

Hütter et al., (1974) have shown that it is difficult to generate a controlled biaxial state of stress in a flat plate specimen. To date, most work on the characterization of composite materials under a complex state of stress has been performed using tubular specimens for reasons that were mentioned earlier in this section. Care must be exercised in the experimental work since the experimental results reflect the method of testing, the specimen manufacturing process and the quality of the specimens.

Hütter et al., (1974) found that a unidirectional lamina under the two states of stress shown in fig 2.2.7.1 gave good agreement between their experimental data and the theoretical results calculated using the models of Norris (1950), Puck (1967) and Tsai (1965).

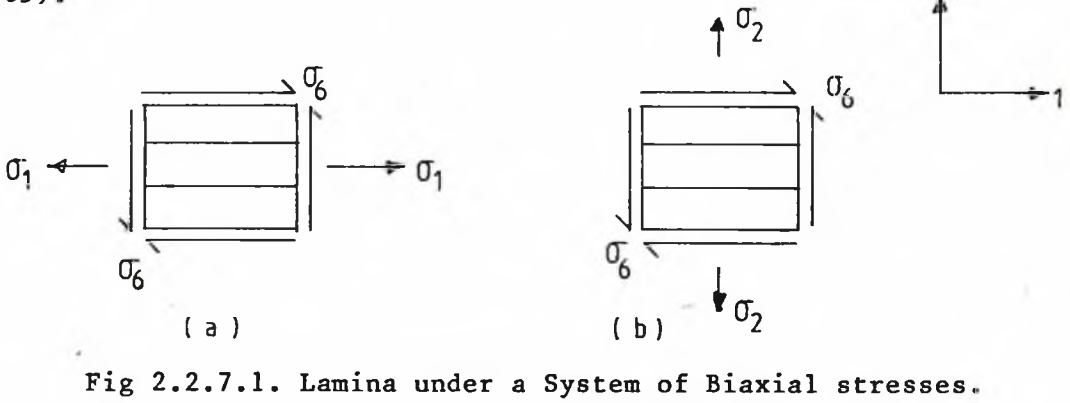

Fig 2.2.7.1. Lamina under a System of Biaxial stresses.

Tsai's model (1965) has the following form:

$$(\sigma_1/\sigma_{1y})^2 - (1/r)\,((\sigma_1\ \sigma_2)/(\sigma_{1y}\ \sigma_{2y})) + (\sigma_2/\sigma_{2y})^2 + (\sigma_6/\sigma_{6y})^2 = 1$$

.....(2.2.7.6)

where

$$1/r = \sigma_{1y}/\sigma_{2y}$$

But when they considered the following state of stress

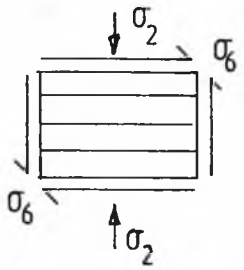

Fig 2.2.7.2. Lamina under Shear and Transverse Compressive Stresses.

the correlation between the experimental and theoretical results was poor.

The inadequacy of the existing ply-by-ply failure analysis, based on the Classical Lamination Theory, was voiced by Hütter et al. (1974). However, by modifying the ply-by-ply analysis to include

(i) the effect of differences in tensile and compressive strengths and

(ii) the non-linearity in shear stress-strain response

Eckold et al. (1978) reported good correlation between experimental and theoretical results. The theoretical model used by Eckold et al. (1978) was discussed in Section 2.2.6.

Soden et al., (1978) found good agreement between the experimental and theoretical data for $\pm$ 55 degrees tubular specimens but not for the $\pm$ 35 degrees specimens. Soden et al., (1978) used the Puppo and Evensen (1972) model to evaluate the theoretical data. The

experimental data was obtained from tests involving axial force and internal pressure as illustrated in fig 2.2.7.2.(i)

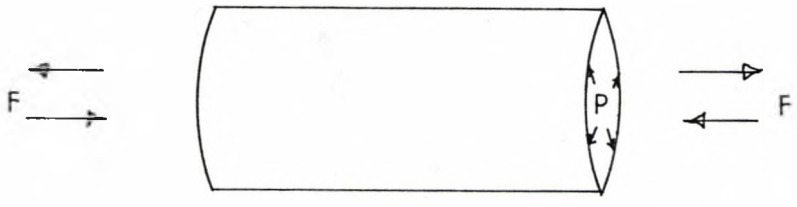

Fig 2.2.7.2(i) Tubular Specimen under Internal Pressure and Axial Force.

It must be pointed out that Soden et al.,(1978) simplified the analyses by ignoring the bending and twisting moments induced, since the specimens used were unbalanced with respect to the stacking sequence of the laminae.

Wu (1972) illustrated the accuracy obtained when applying the Tsai & Wu (1971) model (considering only the linear and quadratic terms) to predict the failure stresses of a lamina under the states of stress shown in fig 2.2.7.3.

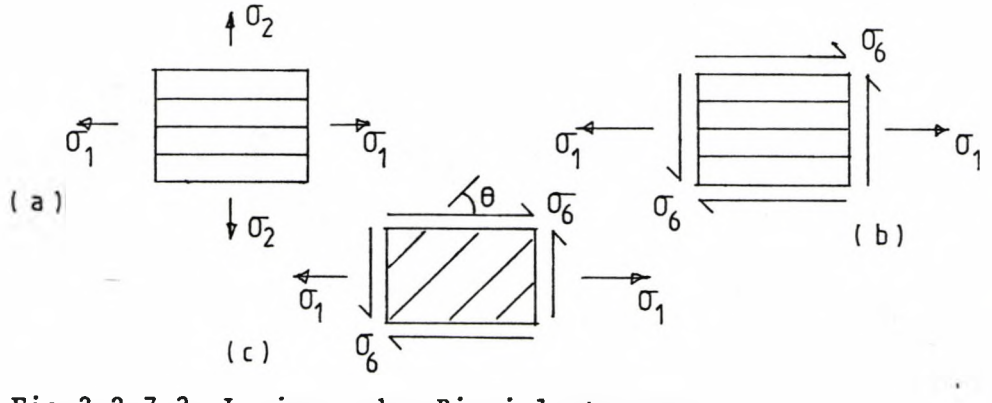

Fig 2.2.7.3. Lamina under Biaxial stresses.

(C) (i) $\theta = 15^{\circ}$, (C (ii)) $\theta = 30^{\circ}$, (C (iii)) $\theta = 45^{\circ}$, (C (iv)) $\theta = 60^{\circ}$

(C (v)) $\theta = 75^{\circ}$, (C (vii)) $\theta = 90^{\circ}$

However, Tennyson et al.,(1978) pointed out that it was too conservative to use only the linear and quadratic terms of the Tsai & Wu (1971) model in predicting the failure conditions of a lamina under a state of plane stress. Tennyson et al., (1978) showed tentatively that by including the cubic terms in the analysis a better performance in failure prediction by the Tsai & Wu (1971) model could be achieved. In order to reduce the effort in the evaluation of the interaction strength tensor components F_{ij} & F_{ijk} Tennyson et al., (1978) employed a hybrid method explained below.

By assuming material symmetry, identical strengths in both positive and negative shear and omitting the redundant terms the Tsai & Wu (1971) model is reduced to

$$F_1 \sigma_1 + F_2 \sigma_2 + F_{11} \sigma_1^2 + F_{22} \sigma_2^2 + F_{66} \sigma_6^2 + 2 F_{12} \sigma_1 \sigma_2 + 3F_{112} \sigma_1^2 \sigma_2 + 3F_{221} \sigma_2^2 \sigma_1 + 3F_{166} \sigma_1 \sigma_6^2 + 3F_{266} \sigma_2 \sigma_6^2 = 1 \qquad .....(2.2.7.7)$$

(Considering up to the cubic terms only.)

For a biaxial case where

$$\sigma_6 = 0$$

equation (2.2.7.7) can be rearranged to give

$$F_{12} = (1/2\, \sigma_1 \sigma_2)\,(1 - (F_1 \sigma_1 + F_2 \sigma_2 + F_{11} \sigma_1^2 + F_{22} \sigma_2^2 + 3F_{112} \sigma_1^2 \sigma_2 + 3F_{221} \sigma_2^2 \sigma_1)) \qquad .....(2.2.7.8)$$

Tennyson et al.,(1978) assumed that

$$\sigma_1 = k_1 \lambda \qquad \sigma_2 = k_2 \lambda \quad ; \quad \sigma_6 = k_6 \lambda \qquad .....(2.2.7.9)$$

where k_1 , k_2 and k_6 are constants for a given material and lamina orientation relative to an arbitrary set of structural axes. λ is a loading parameter. Substituting equation (2.2.7.9) into equation (2.2.7.7)

$$a\lambda^3 + b\lambda^2 + c\lambda + d = 0 \qquad .....(2.2.7.10)$$

is obtained where

$$a = 3(F_{112}\, k_1^2\, k_2 + F_{221}\, k_1\, k_2^2 + F_{166}\, k_1\, k_6^2 + F_{266}\, k_2\, k_6^2)$$

$$b = F_{11}\, k_1^2 + F_{22}\, k_2^2 + F_{66}\, k_6^2 + 2F_{12}\, k_1\, k_2$$

$$c = F_1\, k_1 + F_2\, k_2$$

$$d = -1$$

Tennyson et al.,(1978) considered the case where equation (2.2.7.10) has 3 real roots, 2 of which were equal. This case satisfied the physical interpretation of having only two distinct roots for two colinear loading paths as pointed out by Wu (1974). Subsequently, the constraint equation obtained is

$$27a^2 + a(4c^3 + 18bc) - 4b^3 - b^2 c^2 = 0 \qquad .....(2.2.7.11)$$

For a given material, Tennyson et al. (1978) used 4 angle-ply ($\pm\theta$) laminations to form 4 constraint equations similar to equation (2.2.7.11). The values of F_{12} , F_{112} , F_{221} , F_{166} and F_{266} were obtained by using the failure stresses of an optimal biaxial test (i.e. optimal σ_1/σ_2 ratio) and the 4 constraint equations obtained earlier. This approach reduces the amount of experimental work required to determine the interaction strength parameters F_{ijk} and F_{ij}.

Nevertheless, more work will be needed to validate this hybrid method.

It was rather unfortunate that Tennyson et al.,(1978) did not elaborate on the application of the lamina failure criterion to predict the failure of a laminate under a complex state of stress.

Owen and Griffiths (1978) found that, after highly subjective selection of their experimental data, there was a limited accuracy in the correlation between the predictions based on some of the theoretical models discussed earlier and that of the experimental observations. They reported that the best prediction of the observed fracture behaviour was provided by the following theoretical models:

(i) The Gol'denblat and Kopnov's criterion (1965) (explained in Section 2.2.3. with $\alpha = 1$ and $\beta = 1/2$)

(ii) The Tsai and Wu criterion (1971) (explained in Section 2.2.5; considering only the linear and quadratic terms)

(iii) The modified Marin's criterion reported by Franklin (1968) which has the form shown below.

$$F_1 \sigma_1 + F_2 \sigma_2 + F_{11} \sigma_1^2 + F_{22} \sigma_2^2 + F_{12} \sigma_1 \sigma_2 + F_{66} \sigma_6^2 = 1 \quad .....(2.2.7.12)$$

Where

$$F_1 = 1/X - 1/X' \quad ;$$

$$F_2 = 1/Y - 1/Y' \quad ;$$

$$F_{11} = 1/(X\,X') \quad ;$$

$$F_{22} = 1/(Y\,Y') \quad ;$$

$$F_{66} = 1/S^2 \quad ;$$

$$F_{12} = -K_2/(X'X)$$

K_2 is a constant evaluated from a test involving combined stresses.

X is the tensile strength parallel to the fibre.

X' is the compressive strength parallel to the fibre.

Y is the tensile strength perpendicular to the fibre.

Y' is the compressive strength perpendicular to the fibre.

S is the shear strength.

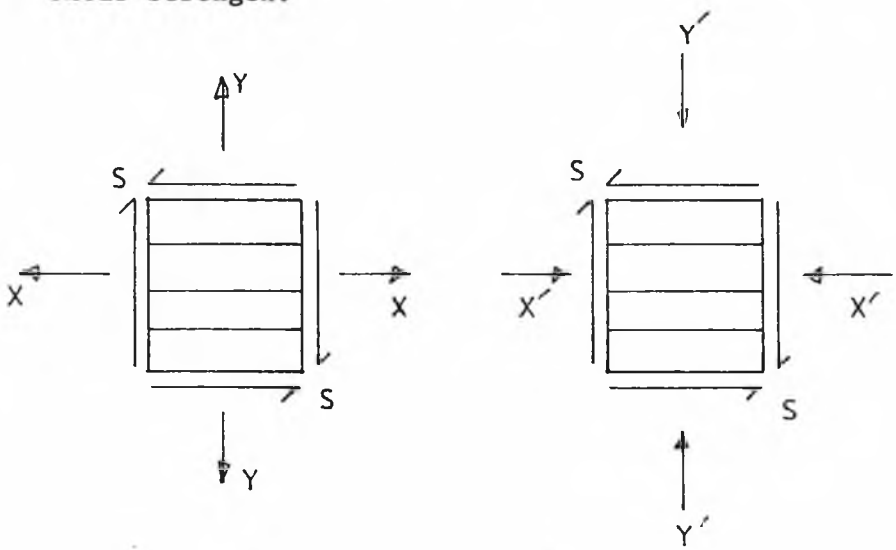

Fig 2.2.7.4 Notation for Equation (2.2.7.12)

Owen and Griffiths (1978) highlighted the problems due to the presence of joints and seams in tubular specimens. Owen and Rice (1981) reported the problem related to the fibre crimp. These artefacts are unavoidable when woven fabrics are used for the reinforcements and have a strong tendency to influence the experimental data. Owen and Griffiths (1978) pointed out the economic problem involved in the testing of anisotropic materials under complex states of stress. They suggested that simpler theoretical

models might be more useful to evaluate separately different regions of the failure surface.

Strength data are localised phenomena and they reflect local imperfections in the specimens. Consequently, these data tend to scatter. Statistical analysis has been used to analyse the failure behaviour of composite materials. However, the discussion of this topic is outside the scope of this chapter.

This chapter has reviewed some of the current works related to the characterization of failure behaviour of composite materials. An extensive review can also be found in Rowlands (1975).

Finally, it can be concluded that no one theoretical model can be used with absolute confidence. More effort will be needed in establishing some theoretical models which are more practical and acceptable.

Chapter 3: HARDWARE

3.1 Introduction

A multiaxial test rig as shown schematically in fig. 3.1 has been built. This test rig is able to exert three basic types of loads on a test specimen in any combination. The three basic loads are axial force, torque and internal pressure. The axial force is applied along the axis of the tubular specimen. It can be tensile or compressive force as required. The applied torque can be clockwise or anticlockwise.

Essentially the test rig consists of three load sources, viz:

(i) the actuator

(ii) the pressure intensifier and

(iii) the stepping motor.

Both the actuator and the pressure intensifier derive their power from a hydraulic pack. It is the actuator which provides the axial force to the test specimen. The pressure intensifier sends pressurised fluid into the test specimen so that it is pressurised internally. Modification can be made at the test section of the rig to provide means by which the pressurised fluid can be used to exert external pressure on the specimen. Clockwise or anticlockwise applied torque is exerted by the stepping motor via a reduction gear train. Servo-valves are used to control the flow of hydraulic power into the actuator and the pressure intensifier. They are of 2-stage type (Guillon (1961)).

The control unit is made up of the following components:

(i) the microcomputer,

(ii) the Analogue to Digital (A/D) converter,

(iii) the Digital to Analogue (D/A) converters,

(iv) the manual control device,

(v) the tape recorder,

(vi) the interface unit,

(vii) the translator module (The Superior Electrical Co.) and

(viii) the visual display unit (VDU).

The interface unit and A/D converter modify the electrical output of the load cells, pressure transducer, the linear variable displacement transducer(LVDT) and the strain gauges to a form suitable for processing by the microcomputer. Some of this data is used by the microcomputer to determine the current necessary action, while the rest of the data is stored on the cassette for further processing at a later stage. The LVDT measures the displacement of the cross-head (specimen end-grip). The main function of the A/D converter is to convert analogue signals into a digital form.

The torque motors in the servo-valves receive control signals from the microcomputer via the D/A converters and the interface unit. These D/A converters convert digital signals from the microcomputer into an analogue form. To drive the stepping motor the microcomputer sends a driving signal and the information on the direction of rotation to the translator module. This module then changes the driving signal into a switching sequence and drives the stepping motor accordingly.

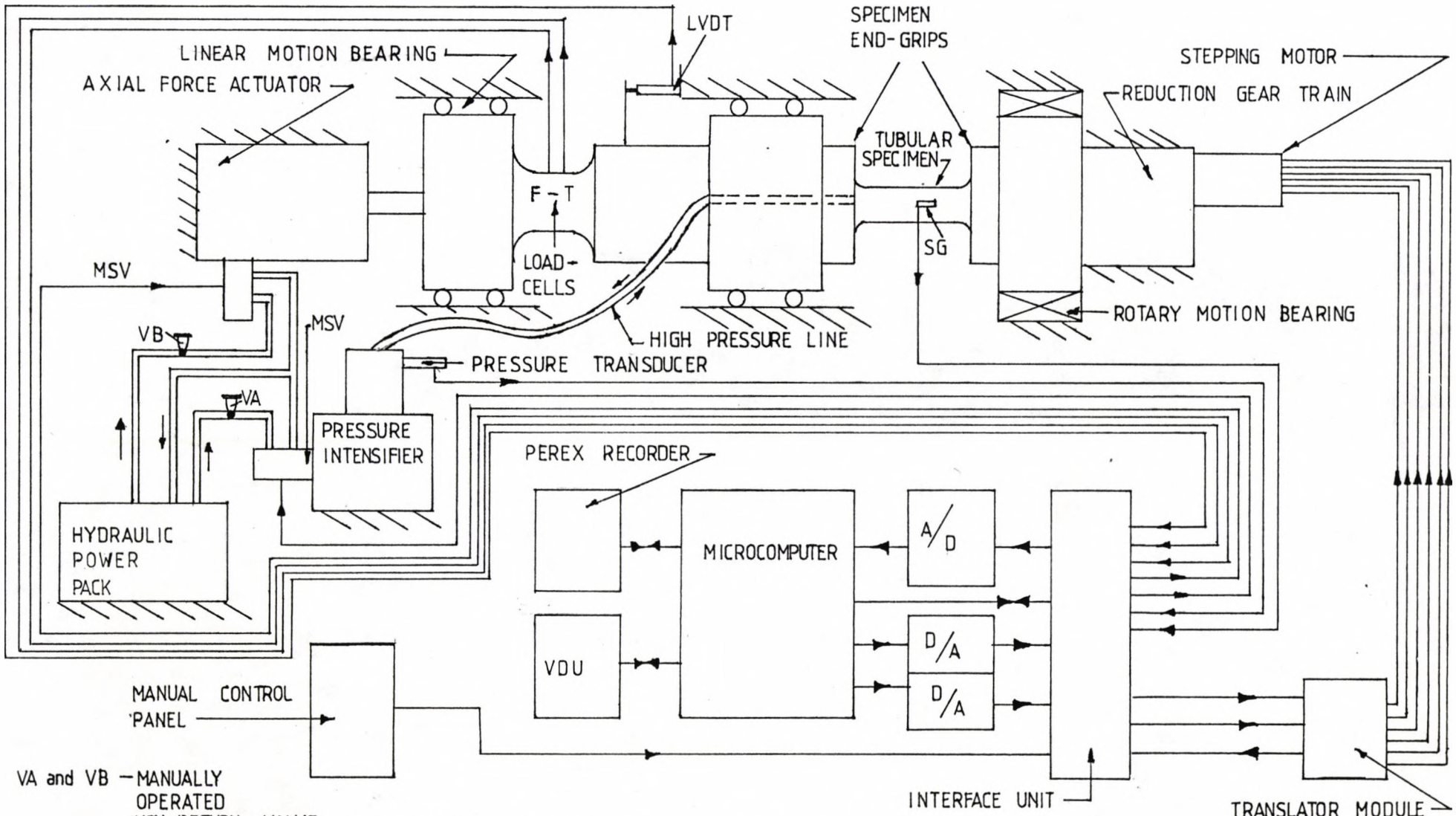

Fig 3.1 The Schematic Drawing of The Multiaxial Feedback Controlled Servo-hydraulic Test Rig.

The visual display unit provides a means of communication between the operator and the microcomputer.

During the mounting and dismounting of a test specimen, it is easier to control the test rig using the manual control device. However, it is the microcomputer that controls the test rig in the required manner throughout a test.

The control unit is flexible and the control sequences can be changed easily so that the control unit can be used to carry out different tests. To change the control sequences one only needs to alter the software used by the microcomputer. The library of software developed for this project will be described in Chapter 4.

The microcomputer will be described briefly in Section 3.2. The remainder of this chapter has been used to illustrate the functions of the interface unit in detail.

3.2 Microcomputer

An eight bit microcomputer has been chosen to form the main component of the control unit. It is relatively cheap. The central processor of the microcomputer is an eight-bit microprocessor. The detailed design and operation of the eight-bit microprocessor can be found in books such as McGlynn (1976),Altman (1975) etc. For ease of discussion it is necessary to explain a few terms used commonly in the microprocessor field.

The term eight-bit means that each instruction to the microprocessor contains information coded with eight bits. One can imagine eight electrical conductors as represented by eight boxes as shown in fig. 3.1(i), then each conductor constitute a bit. It can be high or low. A low state indicates that the D.C. voltage carried by the conductor is between 0 and 0.8 volts. A high state defines that the D.C. voltage of the conductor is between 3.2 to 5 volts. Very often low is represented by a '0' and high is equivalent to a '1'. Referring to fig 3.1(i), bit number 0 is known as the least significant bit (LSB). Whereas, bit number 7 is known the most significant bit (MSB). In this case those eight bits form a byte or a word.

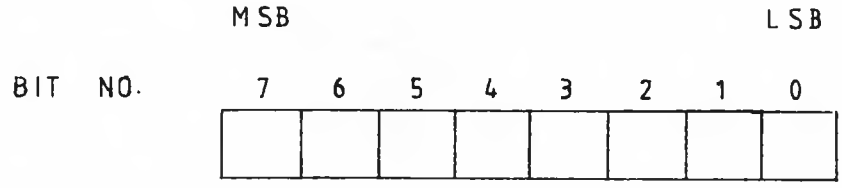

Fig 3.1(i) Configuration of a Byte

or a Word

The microcomputer has been structured such that it contains:

(i) two serial Input/Output ports,

(ii) 12 parallel Input/Output ports

(iii) 8 kilo bytes of Random Access Memory (8k of RAM)

(iv) 8k of Programmable Read Only Memory (PROM)

One serial Input/Output port links the microcomputer to a VDU. The communication between the microcomputer and the tape recorder is via the other serial Input/Output port. Two parallel Input/Output

ports have been used in conjunction with the interface unit.

Eight kilo bytes of RAM are used for storing temporary software and for the data acquisition process. RAM is a dynamic memory (Intel Corporation (1980)) which allows the microcomputer to write onto it or to read information already stored on it. Eight kilo bytes of PROM has been used to store all semi-permanent software. This type of memory only allows the microcomputer to read information stored previously by another process.

The total memory space can be expanded to 64k, if necessary. There are three built-in clocks within the microcomputer. One clock serves as a real time clock for the control process. A second clock has been programmed to generate a square wave which is then used to drive the stepping motor. The third clock also generates a square wave which is needed to operate the VDU.

The detailed design and operational theory of the microcomputer can be found in Intel Corporation (1978),(1976),(1977) and National Semiconductor Corporation (1978) given in the referrence listing. The series of detailed drawings showing the configuration of the microcomputer for the control unit and the memory map of the microcomputer are given in the software manual (Choo (1982)).

The tape recorder is used for experimental data acquisition and in addition, serves as an input terminal through which programs stored in a cassette can be loaded into the RAM. Further detail about the tape recorder can be found in Perex LTD (1978).

The A/D converter is a twelve-bit device. It has been multiplexed to read up to thirty-two channels of analogue input. Multiplex means the A/D converter can switch from one channel to the next. This converter is used in conjunction with the interface unit to read the signals coming from the transducers.

There are four D/A converters in the control unit. They convert the digital command signals from the microcomputer into analogue signals. After processing by the interface unit these analogue signals then drive the test rig.

The designs and operational theories of the A/D and the D/A converters are explained in the respective user manuals, National Semiconductor Corporation (1978) and Intel Corporation (1977).

3.3 Interface Unit

Before the microcomputer and the mechanical test rig can function coherently as a whole system an interface unit is required. The interface unit used in this case consists of three main parts viz:-

(i) the drivers,

(ii) the signal amplifiers and

(iii) the external interrupt system.

These three major and other minor parts of the interface unit will be described in detail in the following sections of this chapter.

3.3.1 Drivers:

The drivers amplify the power of the driving signal. There are three drivers, one for each load source. They function independently. Each has a direct link with the microcomputer as shown in fig 3.1. The drivers for the axial force and internal pressure sources are based on the same principle. They are known as the torque motor drivers. Therefore, only the function of the driver for the axial force source will be explained. A stepping motor has been used to provide torque to the test specimen as pointed out earlier. The operational principle of the stepping motor driver will be illustrated in Section 3.3.1.2.

3.3.1.1 Torque Motor Driver:

The servo-valve contains a torque motor. The operational theory of the servo-valve can be found in Guillon (1961).

The torque motor consists of two electro-magnetic coils. The motor is activated by passing direct current (D.C.) through these coils. Fig 3.2 shows the circuit of the torque motor driver. The components of the driver are an integrated circuit called 741 Operational Amplifier (Mullard LTD (1977)) and a resistor. Let I be the current that flows through the torque motor and ei be the driving signal from the microcomputer after D/A conversion, then

$$I=ei/R$$

where R is the resistance of the resistor

Therefore, $I=f(ei)$

Since the fluid power going into the actuator is a function of the I and the axial force is a function of the fluid power in turn.

Therefore, the axial force can be controlled by ei effectively.

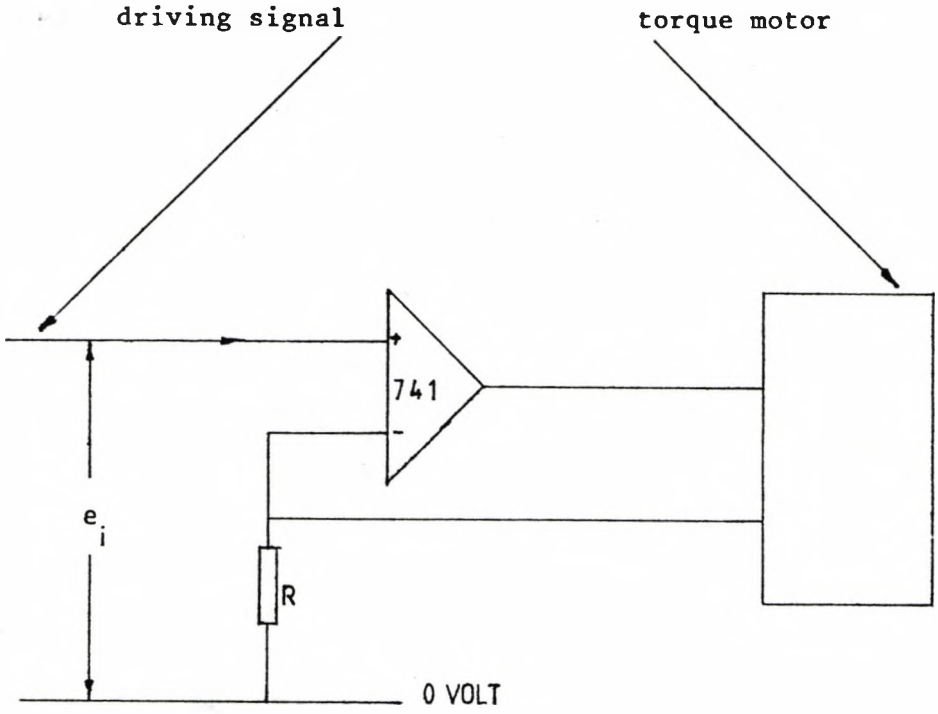

Fig 3.2 Torque Motor Driver.

Later, two analogue controllers were constructed to control the axial force actuator and the internal pressure intensifier. They improve the performance of the test rig and simplify the control software. These controllers receive command signals from the microcomputer and the response signals from the force and pressure transducers. Since, both controllers have an identical form, only the controller for the axial force actuator will be described.

The axial force actuator controller utilizes the principle of 'Proportional and Integral Control'. The theoretical analysis of this method can be found in most books on control theory, e.g. Schwarzenbach and Gill (1979). The block diagram of this controller is as shown in fig 3.2(i).

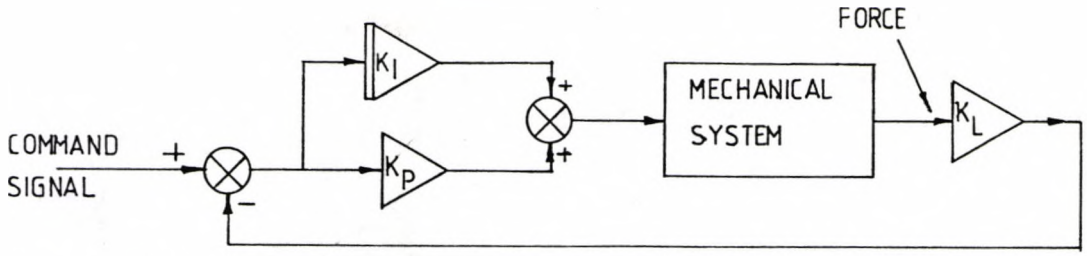

Fig. 3.2(i). Analogue Feedback System with Proportional and Integral Controller.

Similarly, strain signal can also be used as the feedback signal if strain is the required controlled signal. In this case, the force signal in fig 3.2(i) is replaced by the appropriate strain signal. The electronic circuit equivalent of fig 3.2(i) is illustrated in Appendix 3. The microcomputer uses bit numbers 3 and 4 of port **C4H** to switch the integrator on at the suitable time. Furthermore, these two bits have been used for control mode switching. At automatic mode the manual control signal is disconnected from the controller but the reverse is true at manual control mode.

3.3.1.2 Stepping Motor Driver:

The stepping motor, which provides torque to the test specimen, is driven by a digital signal. In this case a clock has been used to generate square wave pulses as shown in fig 3.3. It is called **Clock 0**, part of the microcomputer (Intel Corporation (1978)). The square wave is fed into two nand gates with open collectors to provide the required electrical power. The function of a nand gate is illustrated in fig 3.4. Let A be the input from Clock 0 and B be the input for controlling the condition of the output C. From the Truth Table shown in fig 3.4(iii) it can be seen that when the input B is '1' the output C will have an inverted form of input A. However, if input B is '0', then, the output C will be always high regardless of the input A. This is illustrated in fig 3.4(i) &(ii). Therefore, using

the arrangement shown in fig 3.3 it is possible to drive the stepping motor either in a clockwise or anticlockwise mode. The inputs B come from bit number 0 and 1 of port C4H of the microcomputer. The frequency of the square wave is a function of the clock count (Decimal). Hence the microcomputer can control the speed of the stepping motor by supplying different clock counts to Clock 0. The detailed operational theory can be found in Intel Corporation (1978). The speed of the stepping motor is related to the clock count N by

$$Fp=1/(Tc*N)$$

where Fp is the speed of the stepping motor and

Tc is the period of the clock.

This relation can be represented graphically by fig 3.4(iv). The microcomputer controls the stepping direction of the motor by supplying the appropriate signals to the inputs B. The Hex Inverters(H) (Texas Instruments (1981)) are required to invert the final outputs. In doing so the final output will have the same form as the input A for the active nand gate. The final output is sent to the translator module which converts it into the correct switching sequences to drive the stepping motor.

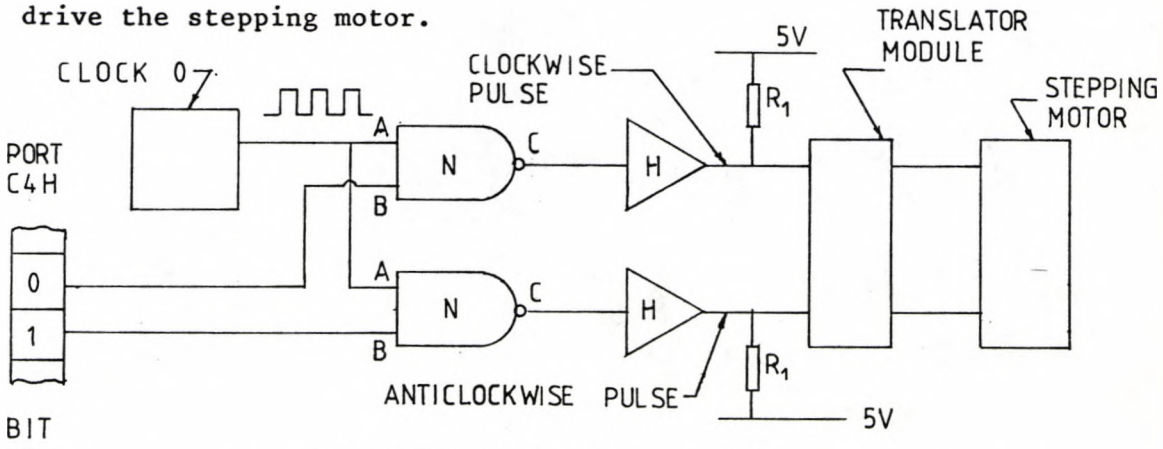

Fig 3.3 Stepping Motor Driver.

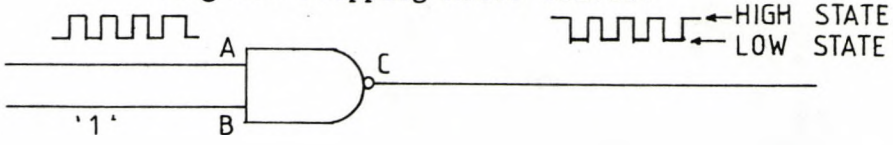

Fig 3.4(i) Nand gate in an 'activated state'

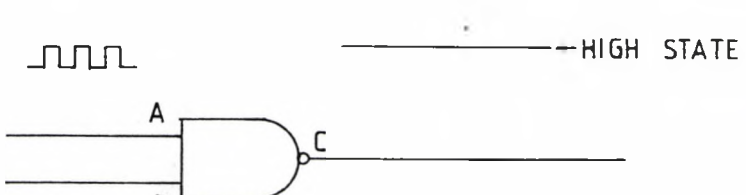

Fig 3.4(ii) Nand gate in a 'deactivated state'

The output will not drive the stepping motor.

A	B	C
1	1	0
0	1	1
0	0	1
1	0	1

Fig 3.4(iii) Truth Table of a nand gate

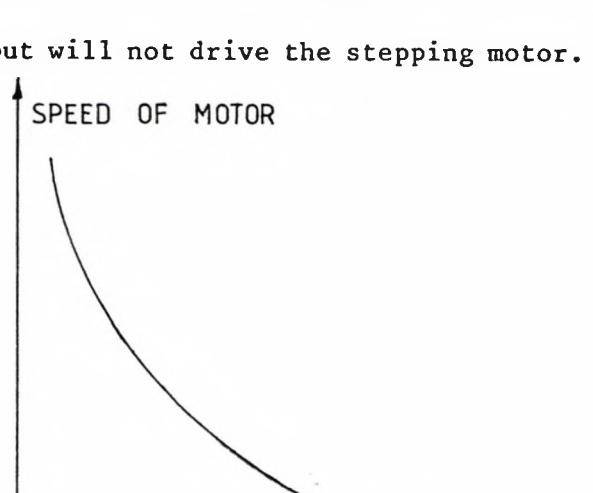

Fig 3.4(iv) The speed of the stepping motor vs clock count.

3.3.2 Signal Amplifiers:

The main tasks of the signal amplifiers are to amplify the low level (0 to 5 mv) signals from the transducers before sending them to the microcomputer. Amplification is necessary so that high resolution can be achieved. Two types of amplifiers have been used but certain

features of each are in common. For clarity they have been described in two separate sections.

3.3.2.1 Strain Gauge Amplifier:

Very often it is necessary to measure the strain on a test specimen which is in a stressed state. In this situation the strain gauge is connected to a three-quarter bridge to form a full Wheatstone bridge (Dove and Adams (1964)). The output from the Wheatstone bridge is then fed into an amplifier which provides the required amplification. The designs of all the Wheatstone bridges used in the experimental work were originally similar to that shown in fig 3.5. Rl and R2 are resistors of fixed values. Rs represents the strain gauge.

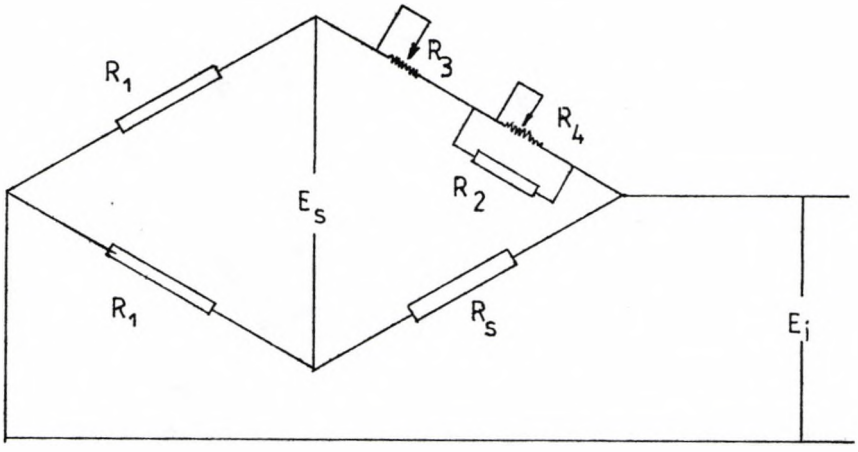

Note: Es is the excitation voltage.

Fig 3.5 Wheatstone bridge

R3 and R4 are variable resistors for the purpose of balancing the bridge. R3 is for coarse balance and R4 is for fine balance. The bridge was initially balanced while the strain gauge was in a strain free state. At balance, Ei was zero. The strain gauge was strained

simultaneously with the test specimen. This straining produced changes in resistance within the strain gauge. Consequently, an out of balance e.m.f. Ei was generated. Since the value of Ei is a function of the strain, the strain on the test specimen could be determined by measuring Ei. However, for ease in setting up the strain measuring device and the reduction of possible error due to variation of the resistance value of R3, the bridges have been altered slightly. R3 and R2 of each bridge have been removed. The bridges have been brought very near to the balance point using the resistor R4. The resistance value of R4 can be selected and fixed by a locking mechanism. Before every test, a set of reference data is recorded instead of balancing the bridges. This simplifies the setting up process.

The out of balance Ei was usually very small and amplification was necessary. A differential amplifier was used to minimize electrical noise which might otherwise mask the signal Ei. Figure 3.6 shows the lay-out of the differential amplifier.

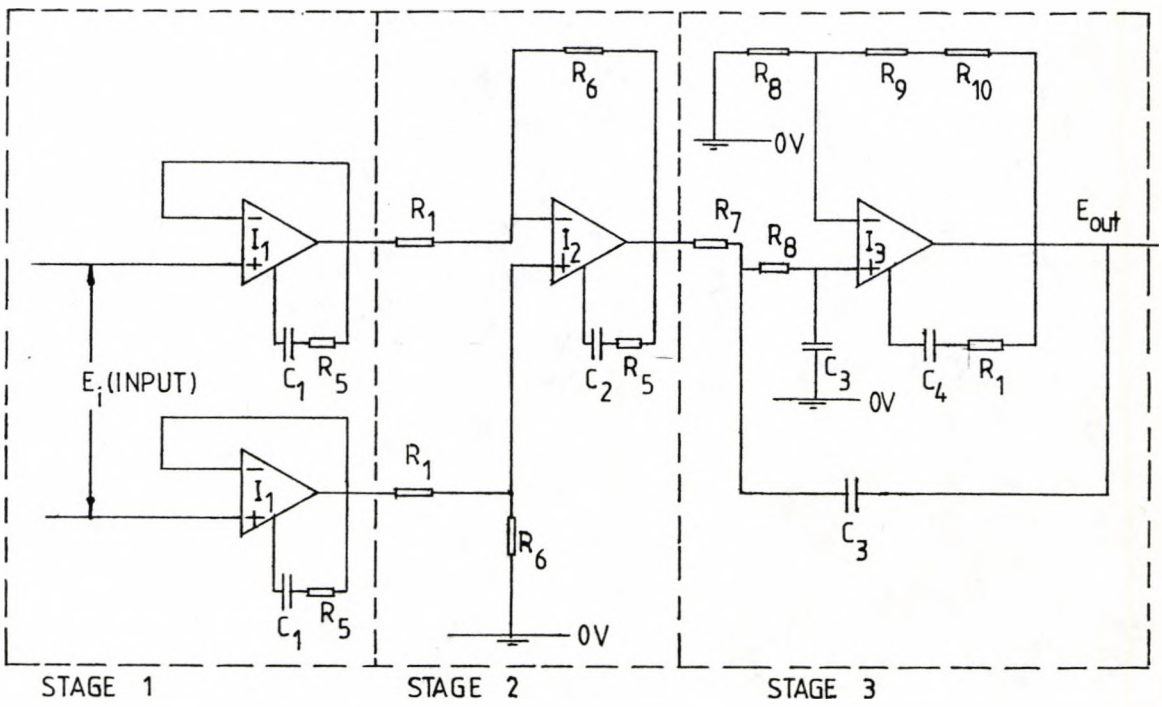

Fig 3.6 Differential Amplifier used in the Interface Unit.

There are three distinct stages in the differential amplifier. The first stage is called a buffer stage. Here, the two I1 offer an input impedance of about 2 Mega Ohms. The high input impedance has two advantages. Amplifier with high input impedance will draw only a very little amount of current from the input signal source. Hence the integrity of the signal is retained. In addition, the amplifier can be used to amplify signals from different transducers that have a large variation in the output impedance. This is because the output impedance is very small compared to the input impedance of the differential amplifier. Consequently, the performance of the amplifier is independent of the output impedance of the transducer.

The second stage provides an amplification gain of 16 dB. The output of stage-2 is then fed into the amplifier at stage-3. At the input of stage-3 the signal level is high enough to give a good signal to noise ratio. Hence the amplifier at stage-3 has a single-ended input. The amplification gain at this stage is only 3dB. Resistor R10 provides the amplification adjustment facility for stage-3. This resistor was removed later to allow for a fixed gain amplifier configuration.

Standard nulling method (Mullard LTD (1977)) has been adopted to null the amplifiers at stage-2 and stage-3. The input lines of the differential amplifier shown in fig 3.6 are short-circuit to the common (0 volt) and its output is connected to a digital voltmeter before carrying out the nulling operation. However, to carry out the

balance operation described earlier the input lines must be connected to the output of the Wheatstone bridge. When the differential amplifier is ready for use its output is then fed into the A/D converter which has formed an integral part of the microcomputer system. Relays have been used to do the switching of the input and output lines of the differential amplifier. The whole set-up of the differential amplifier, the Wheatstone bridge, the relays, the digital voltmeter and the A/D converter is shown schematically in fig 3.7. Relay A and B are controlled by the same switch. A separate switch operates relay C. This arrangement of the relays is necessary in order to ensure that the A/D converter always reads the amplified output of the Wheatstone bridge when the amplifier is being switched to the operation mode.

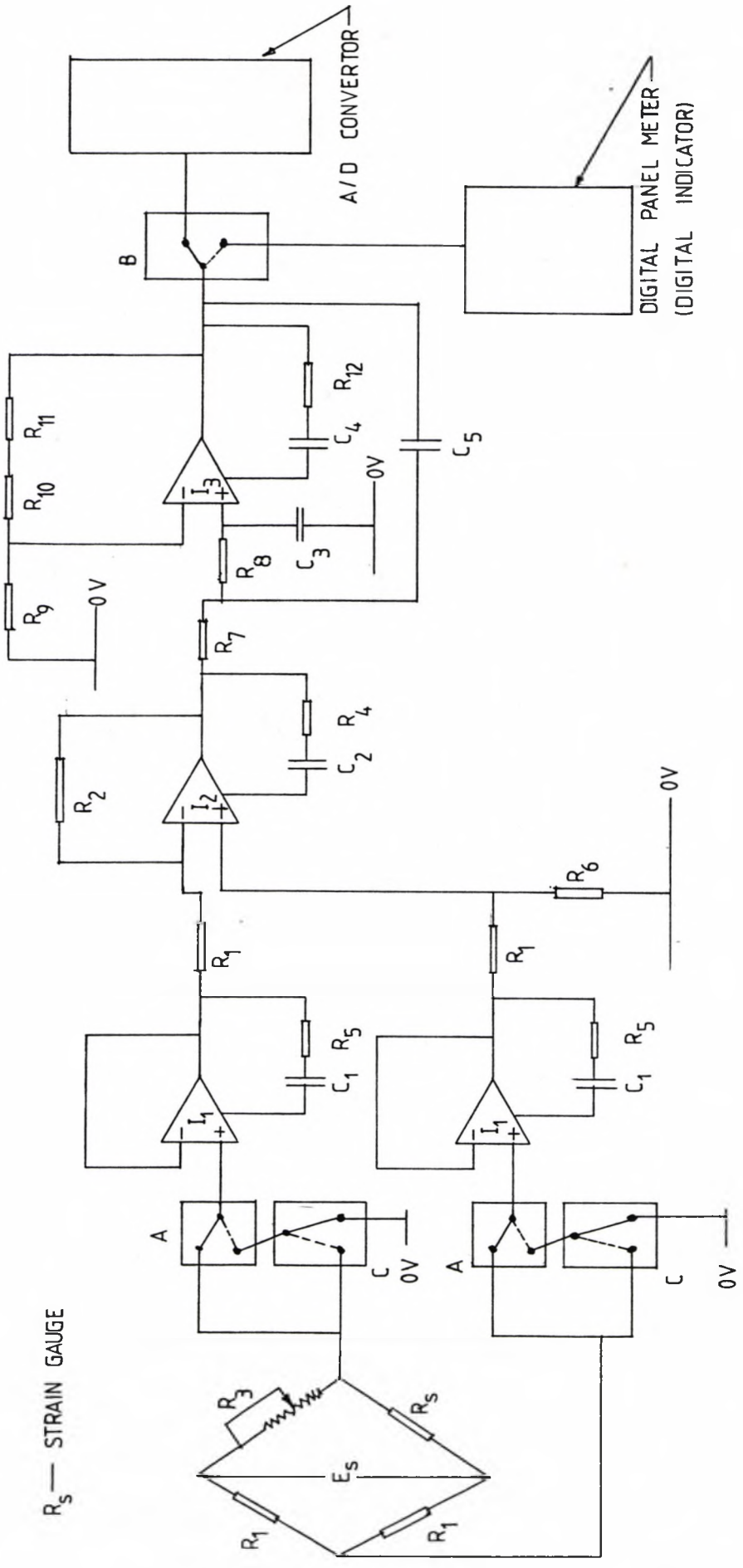

Fig 3.7 The Schematic Drawing Showing The Arrangement of The Wheatstone Bridge, The Differential Amplifier, The Digital Indicator and The A/D Converter.

3.3.2.2 Load Cell Amplifier:

The load cell referred to here consists of a balanced Wheatstone bridge at zero load. Therefore, no balancing operation is required. The differential amplifier needed, to amplify the output of the load cell, is the same as that shown in fig 3.6. The only exception is that the amplification at stage-3 is 10 dB instead of 3 dB. Hence, the lay-out of the amplifying system is similar to that shown in fig 3.7 with minor modification. In this case relay C is not needed. The input stage is simplified slightly as illustrated in fig 3.8.

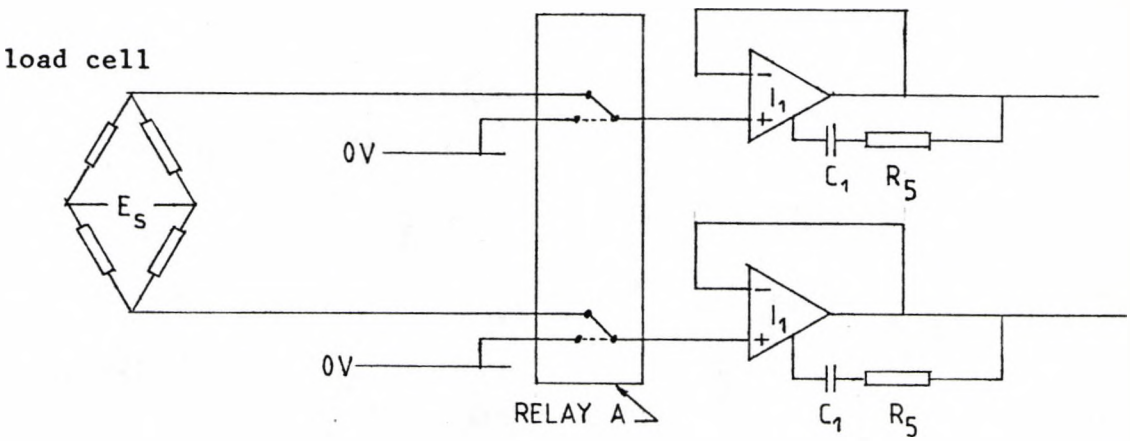

Fig 3.8 Input stage of the Load Cell Amplifiers.

Later, it was found that the axial force and the torsion load cells, produced by the Dr Lawrence's group, were not balanced at zero loads. Therefore, a slight modification was necessary to bring these two load cells to the balance point at zero loads as shown in fig 3.8(i).

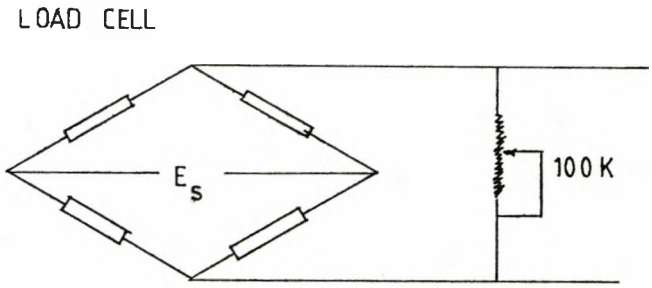

Fig 3.8(i) Load cell nulling method.

3.3.3 External Interrupt System:

The external interrupt system informs the microcomputer whenever pre-selected critical events occur. The vector interrupt method has been used (Intel corporation (1978)). With this information, the microcomputer can determine quickly the priority of events and carry out any necessary tasks efficiently. There are four units within the external interrupt system. They will be described in detail in Sections 3.3.3.1, 3.3.3.2, 3.3.3.3 and 3.3.3.4.

3.3.3.1 Weepage Interrupt Unit:

A tubular filament wound specimen might weep under internal pressure long before it bursts. The weepage produces minute liquid droplets on the outside surface of the specimen wall (Jones (1981)). These droplets increase gradually in size. A weepage interrupt unit has been used to determine accurately the applied loads and the resulting strains on the specimen at weepage. Figure 3.9 shows such an interrupt unit. It is used in conjunction with a pair of very thin copper wires. It is necessary to wind this pair of wires helically and loosely onto the test specimen. The helix angle subtained between the wires and the axis of the tubular specimen must be about 89 degrees and the distance between the pair of wire should be about 5mm. One wire is connected to a +5 volts D.C. power supply. While the other is connected to the input of the weepage interrupt unit. When a small of amount of conducting fluid touches both wires it will create a short circuit. Subsequently, a small D.C. signal will flow to the input of the unit.

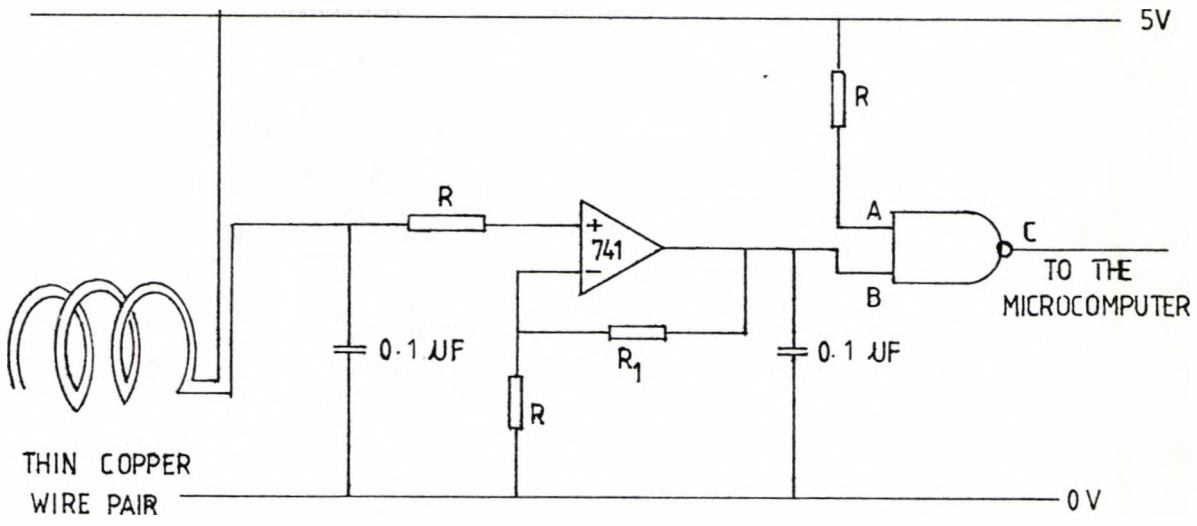

Fig 3.9 Weepage Interrupt Unit.

The first stage of the weepage interrupt unit consists of a single-ended input amplifier. This amplifies the signal to a D.C. voltage in the range of 3 to 5 volts. This amplified signal is then fed into a nand gate. The arrangement of the nand gate is such that its output is normally in a '1' state. In the presence of an amplified short-circuit signal due to weepage the nand gate output will change to a '0' state and consequently the microcomputer will be interrupted.

The two 0.1 microfarad capacitors are used to filter off any electrical noise that might otherwise trigger off the weepage interrupt unit.

3.3.3.2 Burst Interrupt Unit:

When a filament wound tubular specimen ruptures under the applied loads a strong vibration is produced. A burst interrupt unit has been built to detect this kind of vibration.

The burst interrupt unit consists of three main parts as listed below:

(i) a piezoelectric transducer,

(ii) an amplifier and

(iii)a nand gate.

The piezoelectric transducer is for transforming the mechanical vibration into an electrical signal. This signal is then amplified by a single-ended input amplifier. The nand gate changes the analogue output of the amplifier into a semi-digital form. Whenever the output of the amplifier is equal or greater than 3.2 volts the output C of the nand gate will be in a low state. In such circumstance the microcomputer will be interrupted.

The arrangement of the diodes and the capacitor at the output end of the amplifier is to limit the output voltage so that it ranges from 0 to 5 volts. As a result, the inputs A and B of the nand gate are protected against over-loading.

The amplifier as it is, provides a high input impedance which is required when amplifying signals from a piezoelectric transducer. The burst interrupt unit is illustrated in fig 3.10.

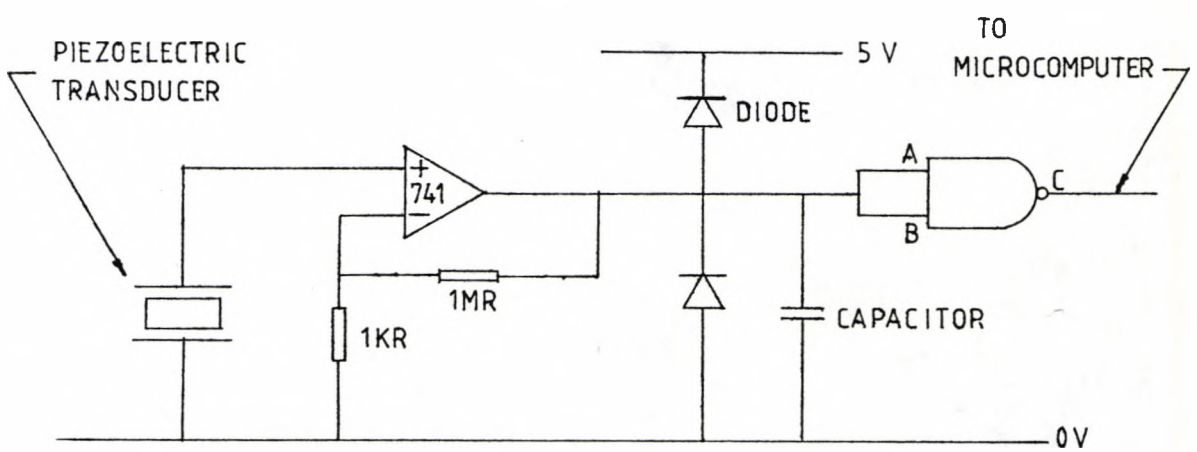

Fig 3.10 Burst Interrupt Unit.

3.3.3.3 Emergency Interrupt Unit:

There are two general purpose hand-held interrupt units and an emergency unit which have been based on the same principle. Therefore, only the emergency interrupt unit will be explained here.

Fig 3.11 shows the schematic drawing of the emergency unit. The switch is single-pole change-over type. Normally, contact B and C are closed. In this case, the output of the unit is in a high state. However, when the switch is being activated contacts A and C make. Consequently, the output of the unit becomes low and hence interrupts the microcomputer.

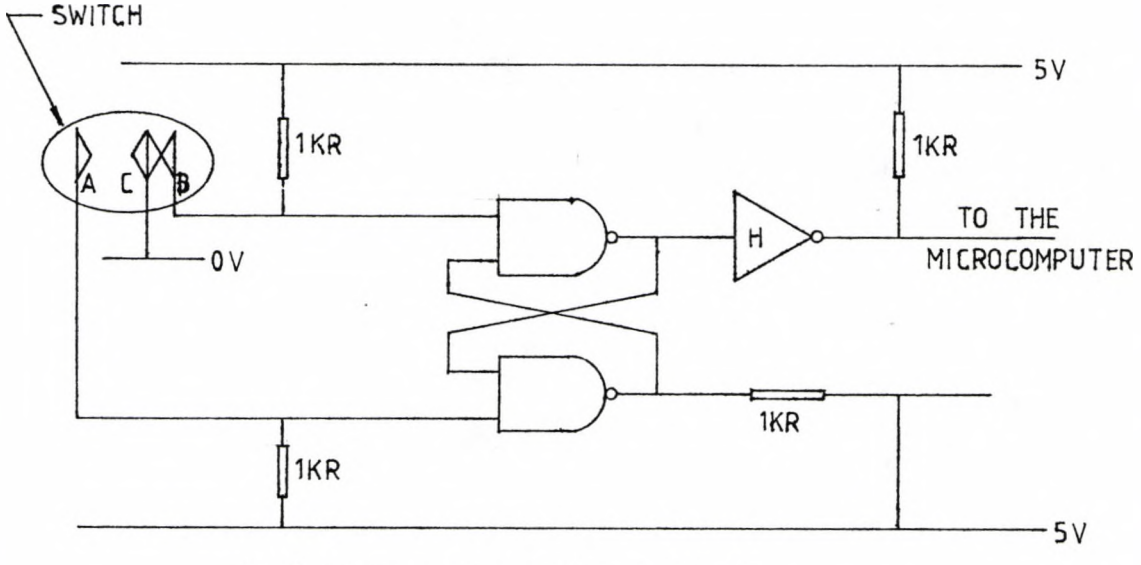

Fig 3.11 Emergency Interrupt Unit.

3.3.4 Hardware Self-check System:

The hardware self-check system performs two types of examination on the interface unit. First it examines the D.C power supplies, then, it checks the signal lines from the transducers.

There are three D.C. power supplies as listed below:

(i) +5 volts to all logic circuits.

(ii) +5 volts to all the load cells and the Wheatstone bridges which are for strain measurements.

(iii)+15, -15 and 0 volts to all operational amplifiers and manual control panel which will be described in Section 3.3.5. The power supply indicator illustrated in fig 3.12 has been used. Its output is fed into the microcomputer via port E8H (Intel Corporation (1978)). From this signal level the microcomputer will detect any power supply failure.

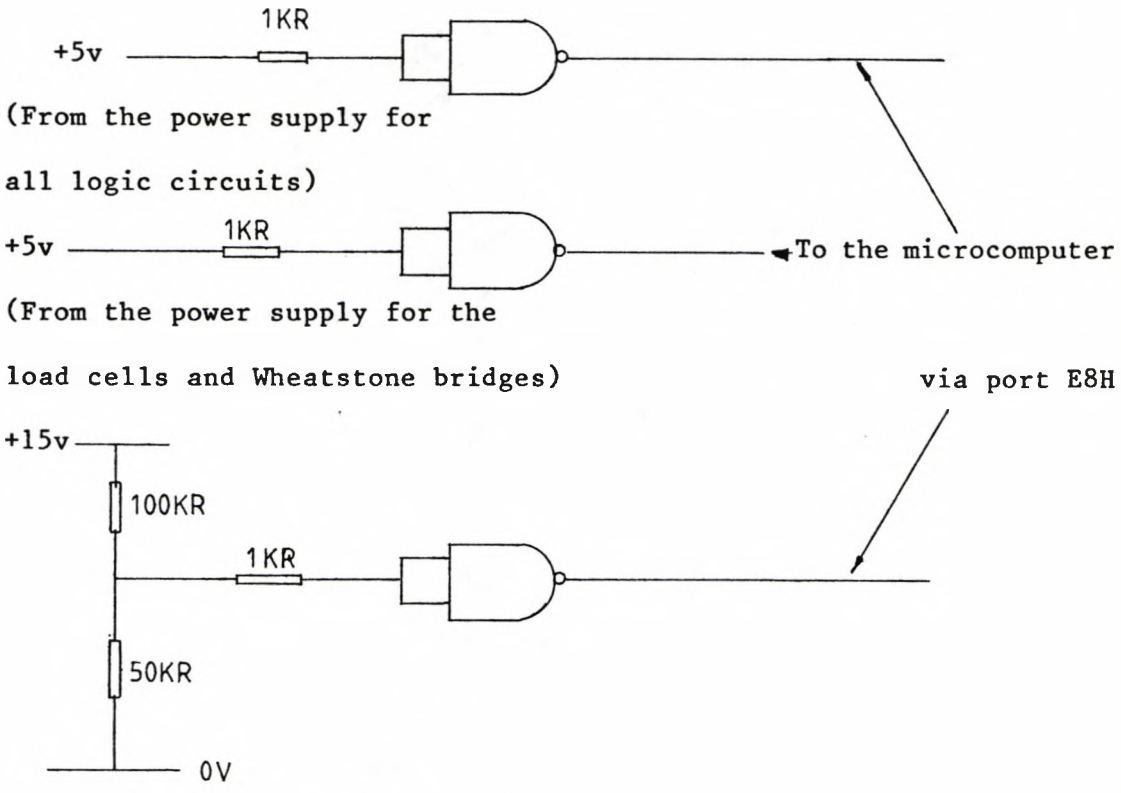

Fig 3.12 Power Supply Indicator.

To check a strain signal line connection, a dummy resistor RD has been used as shown in fig 3.13. Arm CD of the Wheatstone bridge has been arranged such that RD will be disconnected automatically in the presence of a strain gauge, Rs. However, as soon as the strain gauge Rs is removed from the bridge the contact between RD and the rest of the bridge will be completed. Since the value of RD is fixed, then by examining this output before an experiment begins the microcomputer will know if a strain gauge has been connected to the arm CD. This method has been adopted for checking all the strain signal lines.

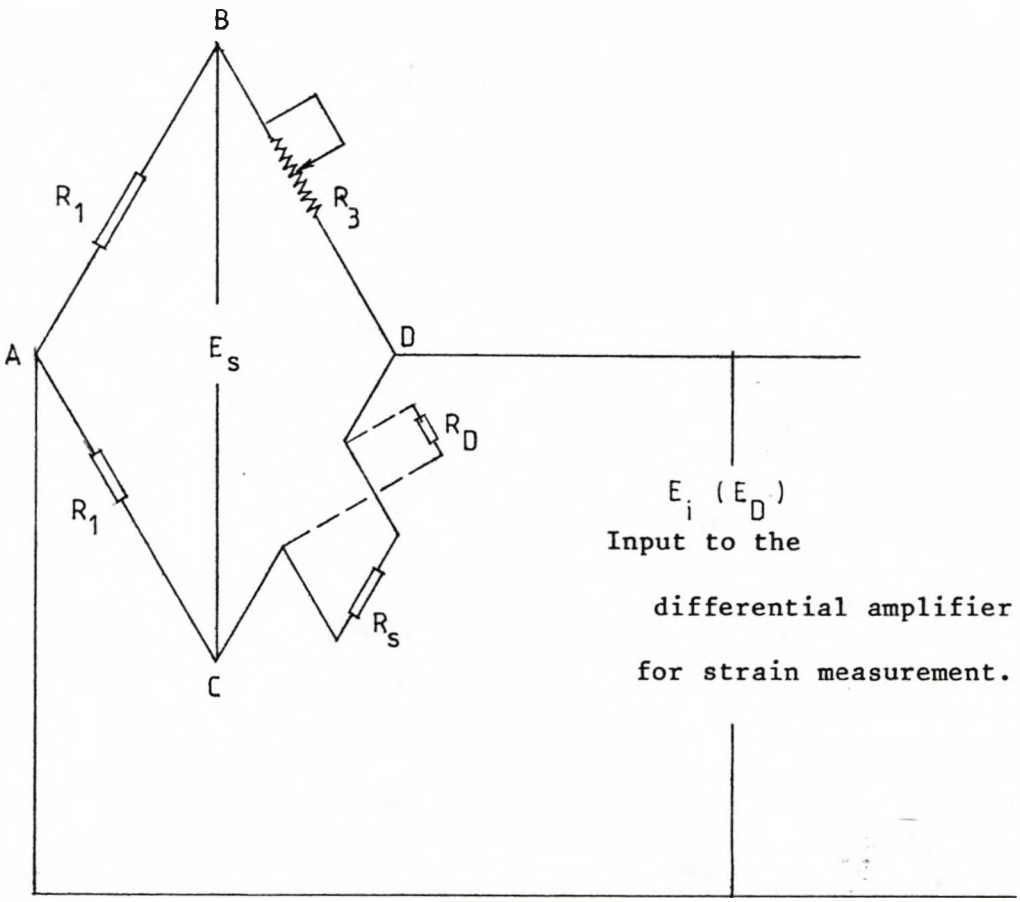

Fig 3.13 Strain Signal Line Connection Indicator.

Similarly a dummy Wheatstone bridge has been used for the purpose of checking the three load cell signal line connections.

This dummy bridge is connected automatically to any of the three load cell amplifiers whenever its contact with the load cell has been broken. Fig 3.14 shows the arrangement of the circuit.

load cell circuit.

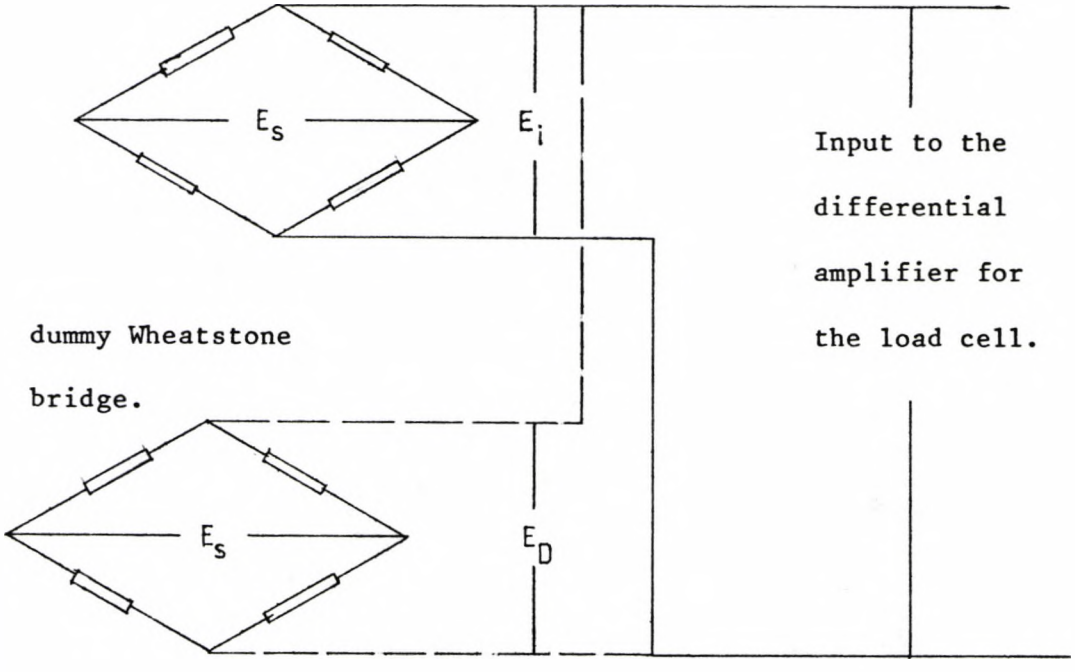

Fig 3.14 load cell signal line connection indicator .

In figures 3.13 and 3.14, E_i represents the actual transducer signal while E_D represents the dummy signal. E_D is fixed. At the beginning of an experiment E_i carried by any signal line must be less than E_D. If this condition is not satisfied, then, the microcomputer will assume that that particular signal line is not connected to the A/D converter.

3.3.5 Manual Control Device:

For mounting and dismounting of a test specimen it is easier to control the test rig manually.

The manual control method for the internal pressure and the axial force are based on the principle illustrated in fig 3.15. As can be seen, part of this figure is similar to fig 3.2. Therefore, the actual manual control consists of only two variable resistor A and B. A provides a coarse control while B affords a fine control on the axial force.

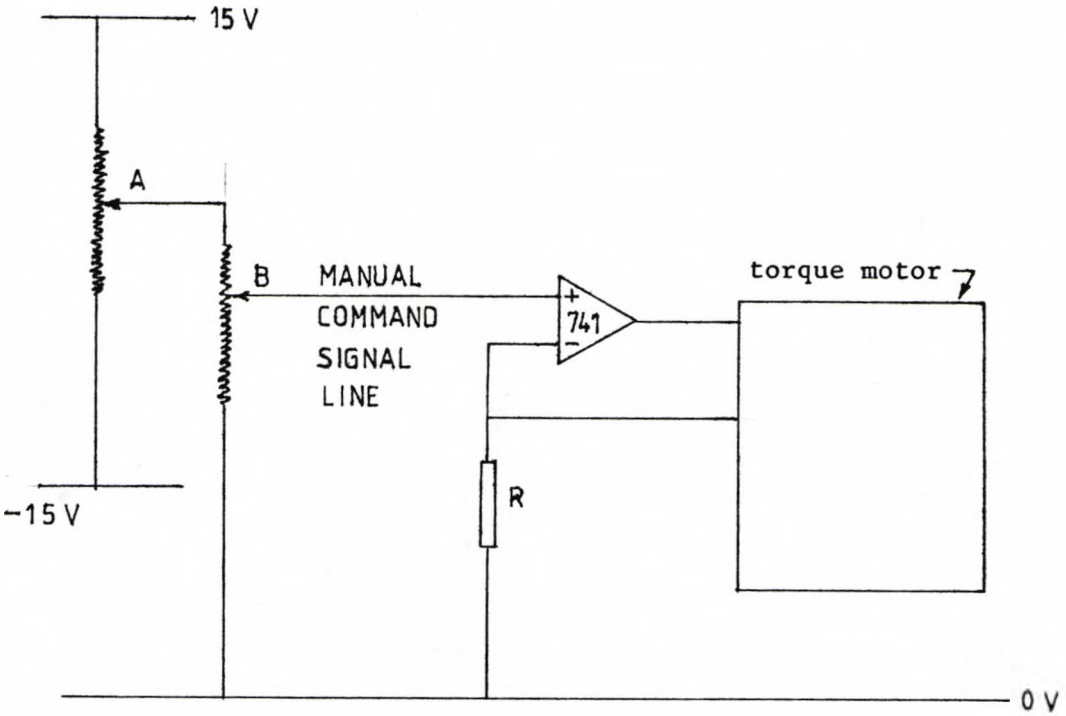

Fig 3.15 Manual Control for the Axial Force.

The manual command signal line has also been connected to the analogue controller for the axial force actuator as described in Section 3.3.1.1. Therefore, there are two sources of manual control each, for the axial force actuator and the pressure intensifier.

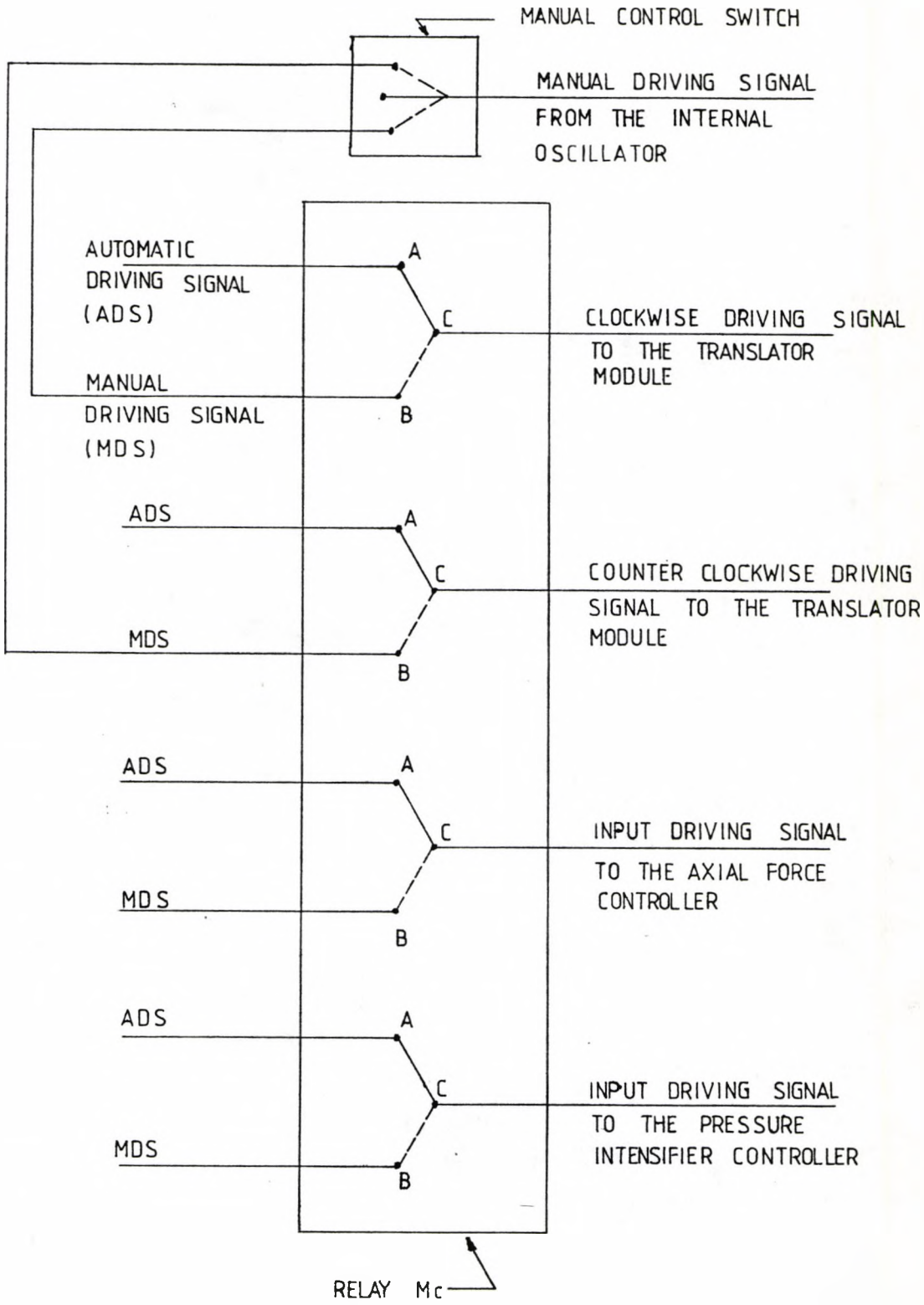

FIG 3.16 RELAYS FOR CHANGING THE MODE OF CONTROL

The stepping motor, which provides torque to the test specimen, can be controlled manually by means of a centre-biased switch. The manual driving signal for the stepping motor comes from the internal oscillator (The Superior Electric Co.). No manual driving signal is sent to the stepping motor/translator module when the centre-bias switch is not being operated. However, when activated it can be used to direct the manual driving signal in order to drive the stepping motor either clockwise or counter clockwise.

A relay package, which consists of four 2-pole relays, has been utilized to do the control mode switching as shown in fig 3.16. It has been given a name arbitrarily as 'Relay Mc'. When Relay Mc is activated all the relays will be switched to contact B. As such, the stepping motor and the torque motors will be ready to be driven by the manual control signals. On the other hand, as soon as Relay Mc is deactivated all the relays will switch to contact A. From now on the microcomputer will have complete control of the motors. Therefore, the test rig can be controlled either manually or automatically at any given instant; but not both at the same time.

The circuitry needed for operating Relay Mc is represented by fig 3.17. It consists of the input stage, a latch, a reset switch, an inverter and a Hex driver. When the input stage is used in conjunction with the extra circuitries as shown in fig 3.18 the output of bit number 2 and 3 can be manipulated to control the power supplies to the hydraulic pack and the stepping motor/translator module too. The latch retains the first set of information from bit number 2 and 3. Therefore, once the state of Relay Mc is set, it will

not be affected by any changes in information carried by these two bits. The Hex driver is required to provide enough power for activating Relay Mc. Owing to the inverting nature of the Hex driver, an inverter has been used so that the output of the Hex driver corresponds to the initial input at the input stage.

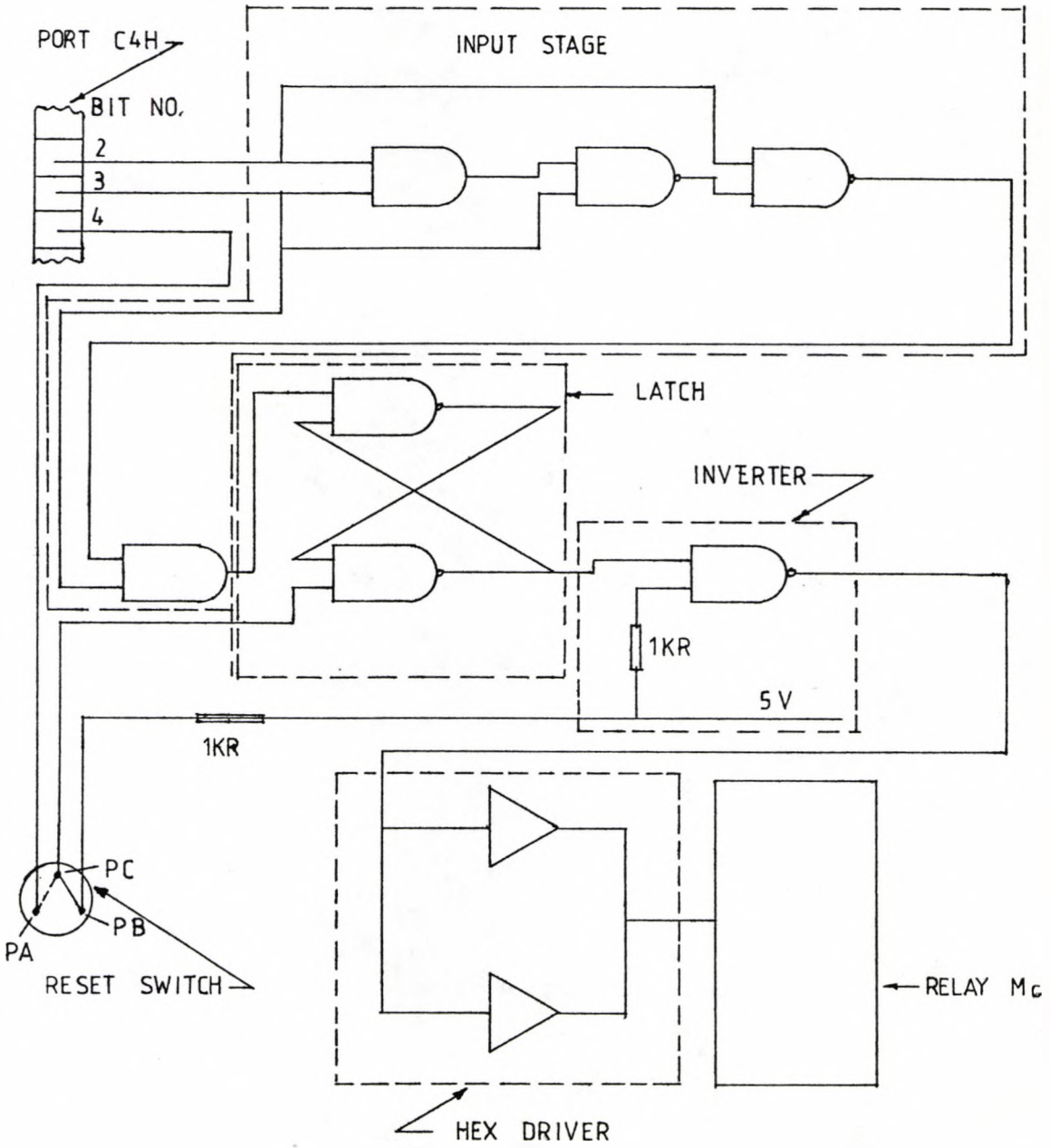

Fig 3.17 Relay Mc Switching Circuit

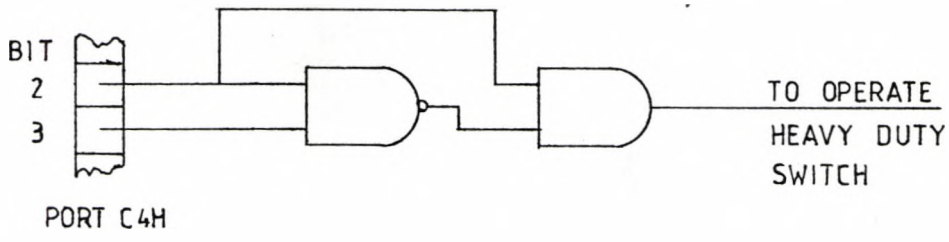

Fig 3.18 Extra circuitry for controlling the power supplies to the hydraulic pack and the stepping motor/translator module.

When in automatic control mode the initial output of bit number 2 and 3 must be ' 1 '. Furthermore, a ' 0 ' output at bit number 4 must be maintained. This is to ensure that the latch will not be affected when the Reset switch is operated accidentally. A ' 0 ' output at bit number 2 and 3 will switch the control mode from automatic to manual, provided the output of bit number 4 is ' 1 ' and the Reset switch has been switched so that contact PC is connected to contact PA. The Reset switch has contact PC always biased to contact PB. When it is being operated contact PC will be connected to PA temporarily. Therefore, the microcomputer can set the latch without human intervention since contact PB is always high.

The detailed circuit drawings of the interface unit has been given in Appendix 3.

Chapter 4: SOFTWARE

4.1 Introduction

With the advance in Computer technology Software has become an important field that deserves attention in its entirety. There are many books that deal with this topic specifically, such as Findlay and David (1978) , Texas Instrument Inc. (1975), Boulaye (1975) etc.

Software is a set of logical instructions which enables a computer to perform the required operations. It may be divided conveniently into two main categories, viz:-

(i) Programs written in high level languages and

(ii) Programs written in low level (or machine) languages.

High level languages are those which use words and symbols which programmers can understand without much difficulty. Programs written in a high level language have to be **compiled** by a computer. This is a process whereby the program is translated by the computer from the high level language to a low level one which it can understand. In the **compilation** process the **syntax** and the basic logic of the program are checked. If the **compilation** is successful, a **binary version** of the program will be produced by the computer.

Every instruction contains a constant number of **bits** (or binary digits (see Chapter 3, Section 3.2)). This number depends on the type of computer concerned. The computer would then use this **binary version** of the program to instruct itself to perform the necessary functions.

A program can be coded directly in binary. However, it is extremely difficult to write an operational program in this manner. To overcome this problem, computer manufacturers have encoded their individual instruction set into a **mnemonic form**. A program can then be written using these mnemonics which is less difficult to understand than is a combination of binary digits. The mnemonics are usually known as machine languages and are given the general name of **assembler languages**. **Cross-assemblers** are available for **cross-assembling** this type of program to produce a binary version of the mnemonic program. The cross-assembling process requires less computing time than the **compilation** process.

By simply changing the set of instructions (software) the same computer can be made to do different operations. It was because of this flexibility and the cost factor that the author chose a test rig with a feedback control system which is based on a microcomputer.

Having chosen the control system the selection of the language to be used for writing the control programs had to be made. Developing all control programs using any machine languages would be difficult, tedious and time consuming. This could offset the advantage offered by the software, i.e., flexibility. However, for certain purposes it is more convenient and enhances machine efficiency to write some routines in a machine language. These can be linked up to programs written in a high level language. A good example is the actual handling of hardware like the A/D converters.

High level language affords a means of developing control programs within a relatively short period. This would enhance the

flexibility of the control system. It was decided to develop the main control programs using a high level language. Those routines which handle hardware were to be written in a machine language called **assembler language.**

4.2 Assembler Language.

The maximum speed of operation of a microcomputer can be attained only if the programs are coded in binary form. Nevertheless, this is not being done here because of the difficulties pointed out in Section 4.1.

Assembler language provides a means of obtaining the highest efficiency of a microcomputer. A **cross-assembler** is used to convert an **assembler** program into binary form. The **cross-assembler** does not do any logic checking on the program while cross-assembling it. Even if a program has been cross-assembled successfully, it might still prove to be inoperative if the logic of the program is wrong. Therefore, the programmer must carry out thorough checking on the logic of his program. This involves tracing through the entire program to ensure that the microcomputer is performing a function in the required manner. These are the most time consuming and tedious operations within the programming process. A logic analyser is a very useful instrument for these tasks. Routines described in Sections 4.2.2 to 4.2.13 have been cross-assembled on the ICL 1906S computer in the Liverpool University Computer Laboratory. They have also been linked successfully to the control programs written in a high level language.

4.2.1 System Monitor:

This is a library of routines which initialises the microcomputer. It was supplied by the microcomputer manufacturer, National Semiconductor Corporation. Minor modification has been carried out by the author. A copy of the listing is available in the Composite Laboratory, Metallurgy and Materials Science Dept., University of Liverpool.

4.2.2 User Monitor:

The operator issues his commands to the microcomputer via the V.D.U., terminal. Messages from the microcomputer are printed on the V.D.U. To create a system whereby high level commands could be understood by the microcomputer and such that it prints high level messages, a User Monitor (Choo (1982)) has been developed . Access to this monitor is simply by pressing the CTRL and A keys simultaneously. An introductory message is printed to indicate that the User Monitor is ready.

Control parameters can be issued to the microcomputer using a set of commands. These commands and the messages from the microcomputer have been included in Appendix 4.1. On receiving a command the User Monitor will examine its validity. If valid, the microcomputer will perform the required operation. However, if the command is invalid appropriate error messages are given by the User Monitor. When it is ready to accept any input or command the sign '<-' is printed. It also checks the validity of the input control parameters to a certain extent. It is capable of prompting the

operator to type in the necessary control parameters, if so desired. This facility may be obtained by typing the word 'PROMPT'.

Protection of the mechanical components of the multiaxial test rig against over loading is provided by the control software developed. The User Monitor sets the default load limits for this purpose. However, these limits can be changed initially by giving the required values to the User Monitor. It will then overwrite the default values with those specified. This will enable the operator to limit the maximum load or loads on the specimen under test when necessity arises.

The Amplifiers mentioned in Chapter 3 possess fixed gains. In addition to those amplifiers, there is another differential amplifier on board the A/D converter. This amplifier has a programmable gain setting. The User Monitor gives a default gain of x1 automatically. This default value may be overwritten by the operator's new input. Hence the level of amplification of the input signals can be varied through software.

There are default values for the first and last channel numbers to be sampled by the microcomputer in any experiments. The control software was designed to sampled sequentially from the first to the last channel. Since by using the User Monitor it is possible to overwrite the default values, any required block of channels may be sampled. Full details concerning these defaults are given in Appendix 4.2

The User Monitor is also linked to the perex handling routines and magnetic tape readers which will be described in Sections 4.2.3 and 4.2.4 respectively. Therefore, the User Monitor is able to read programs or data which have been stored on any cassette tapes compatible to the perex 6041 cassette recorder mentioned in Chapter 3. As a result it is possible for the operator to select any control program and data, relevant to the required test, from a magnetic tape and load them onto the **core memory**, i.e. **RAM**, in preparation for the experiment.

Since the control system was designed to record automatically all experimental data in digital form, an empty **perex file** must be set up for this purpose before the experiment begins. **Perex files** are those created on the magnetic tape. The User Monitor can be instructed to open an empty perex file by giving the correct command followed by a file name consisting of three digits. The file name must be sequential i.e., in the ascending order. Details of the file name are given in Appendix 4.1 . Once a perex file has been opened no subsequent file can be set up and no perex file generated previously can be read until the open file has been closed. When one tries to set up an empty file in addition to the existing opened perex file, the User Monitor prohibits this operation and informs the operator that an empty perex file already exists. The User Monitor can be dictated to close any existing empty perex file by pressing the CTRL and C keys on the V.D.U. simultaneously.

Once the 'RUN' command has been issued, the User Monitor checks for the presence of a control program on the RAM. If the control program does not exist the operator will be given the appropriate

message. The User Monitor also checks whether an empty perex file has been set up for collecting experimental data. On detecting the absence of an empty perex file the User Monitor will then inform the operator. If the two examinations mentioned above were to be positive it will pass control to the selected control program. Further checks which have been mentioned in Sections 4.2.5 and 4.3 will be carried out. If any of these checks prove to be negative the control system will not initiate the experiment. These checks are necessary in order to ensure that all experiments are being carried out in the required modes and that sensible experimental data are being collected.

A simplified flow-chart explaining the operation of the User Monitor is given below.

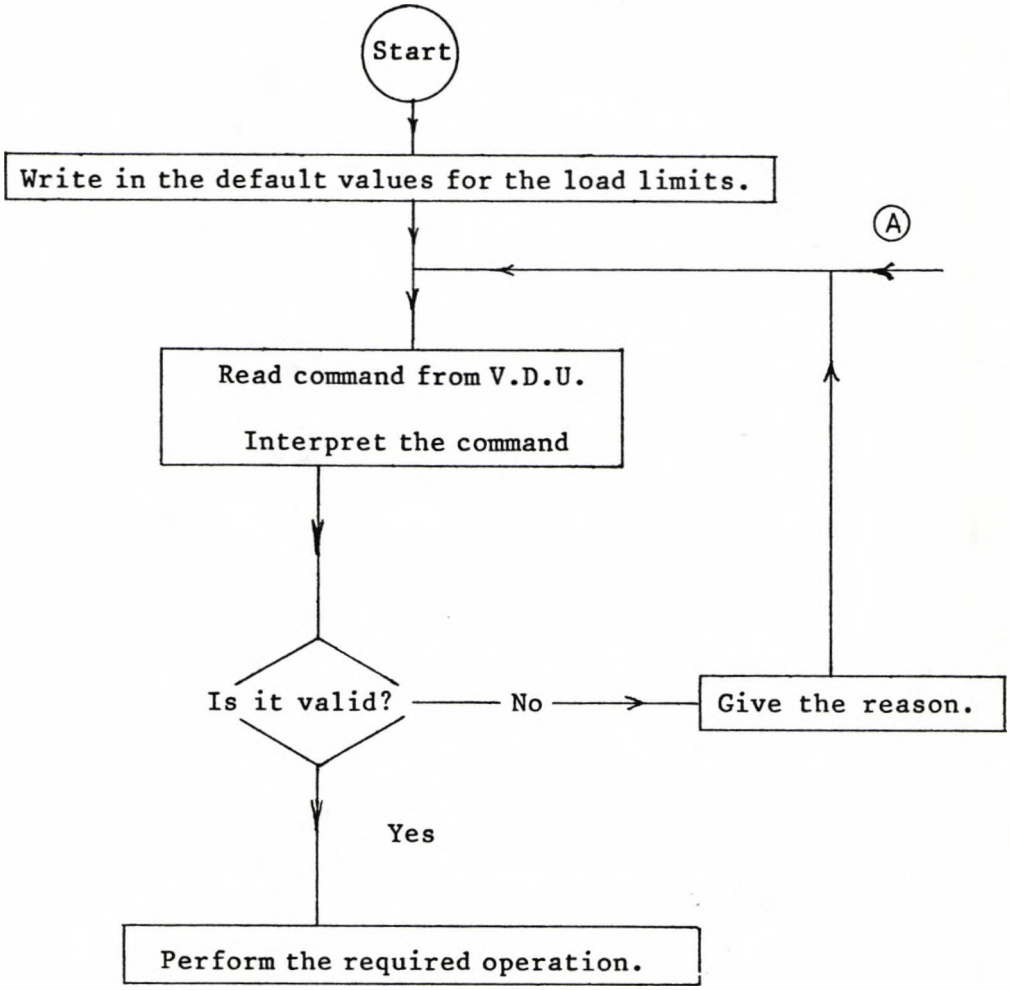

Fig 4.1 Flow-chart of the User Monitor.

The required operation can be any operations represented by the following flow-charts.

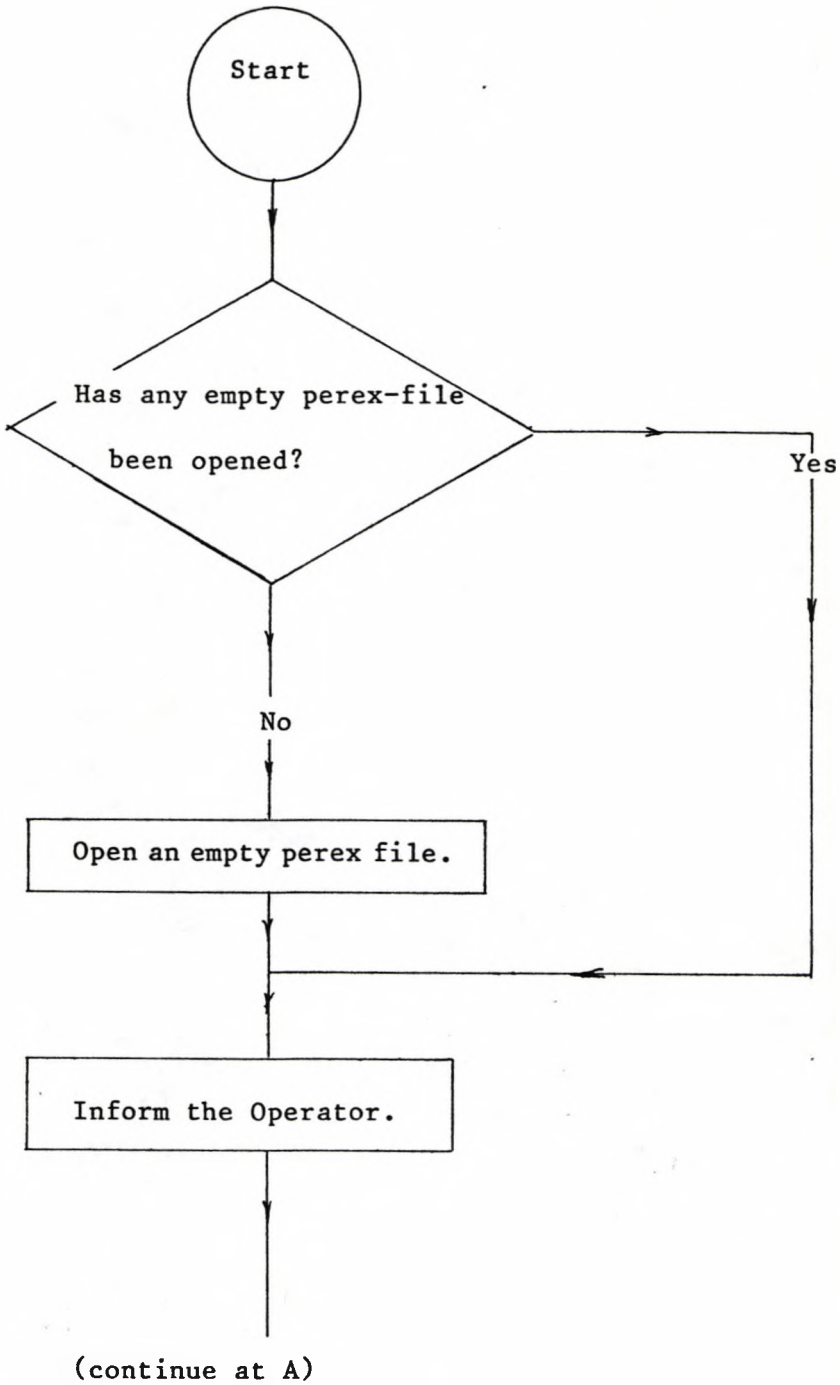

Fig 4.1(i) Preparation of a perex file for storing information.

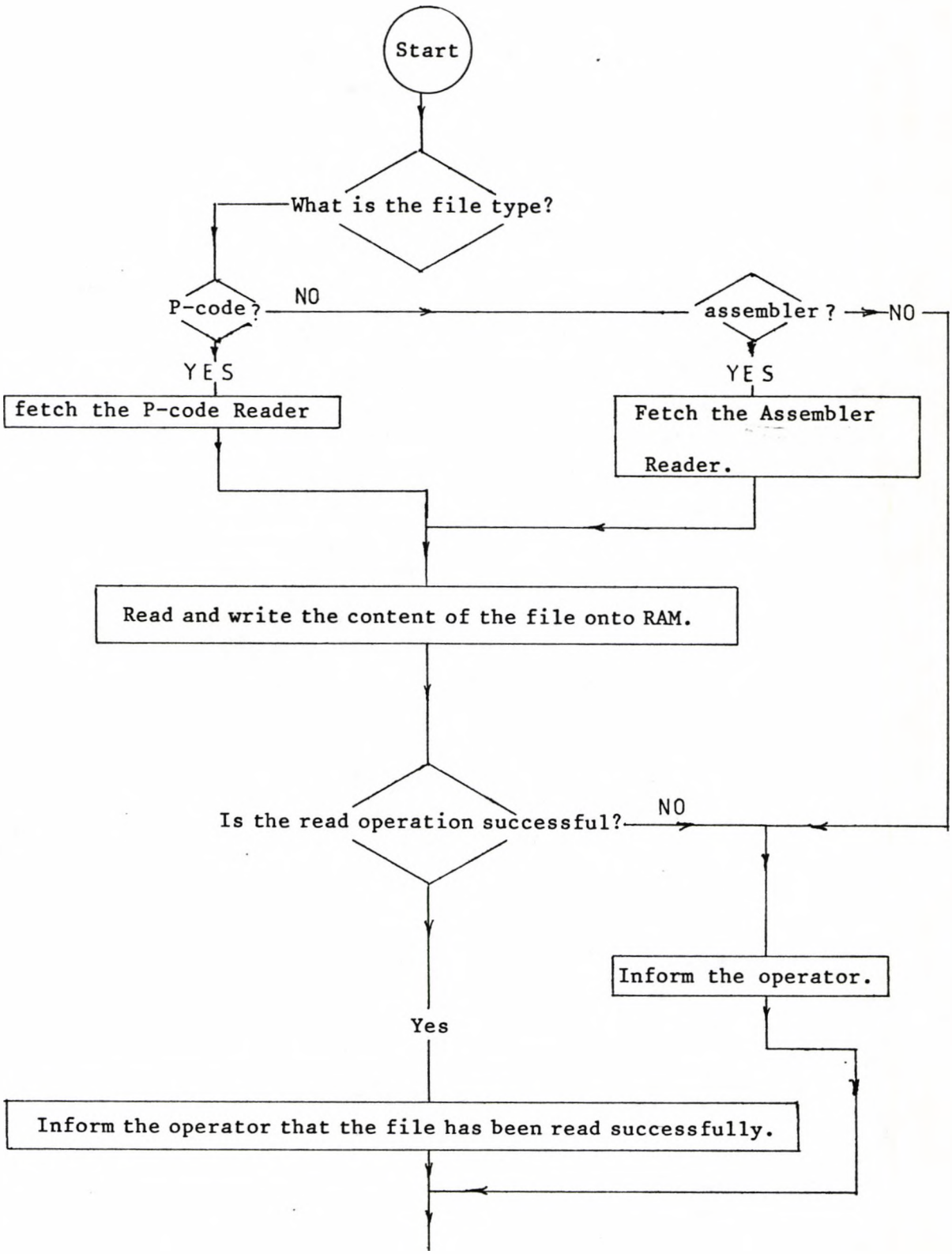

Fig 4.1(ii) The Read Operation.

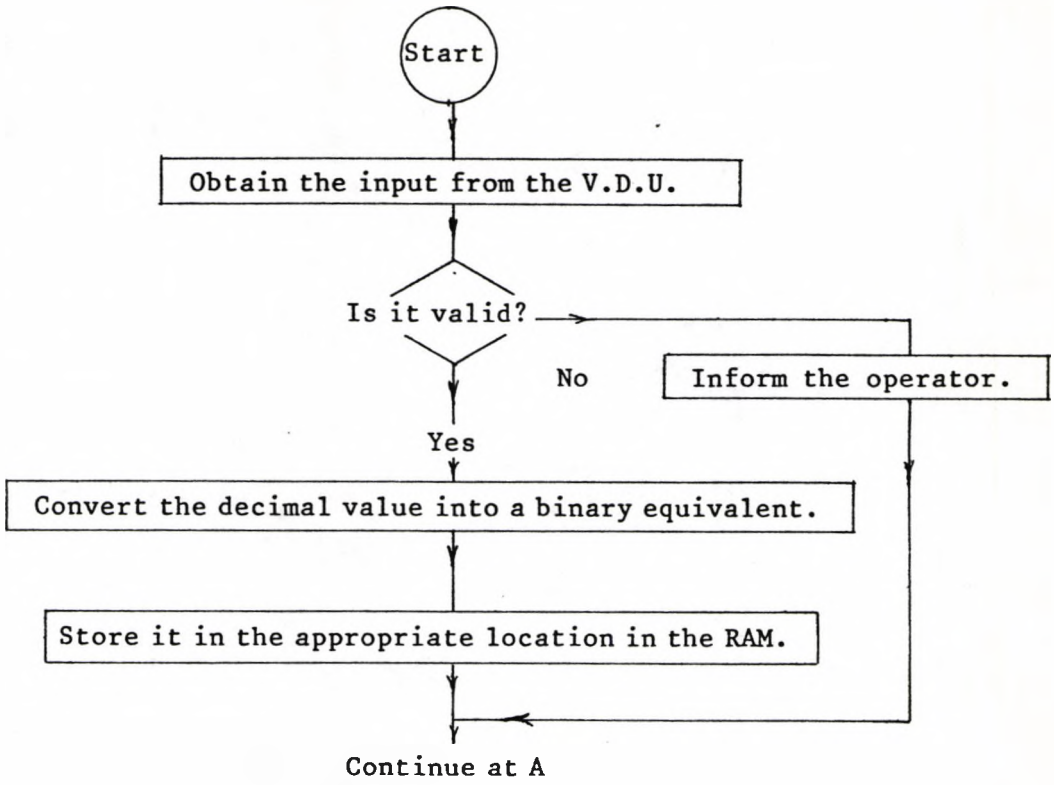

Fig 4.1(iii) The Control Data Input Operation.

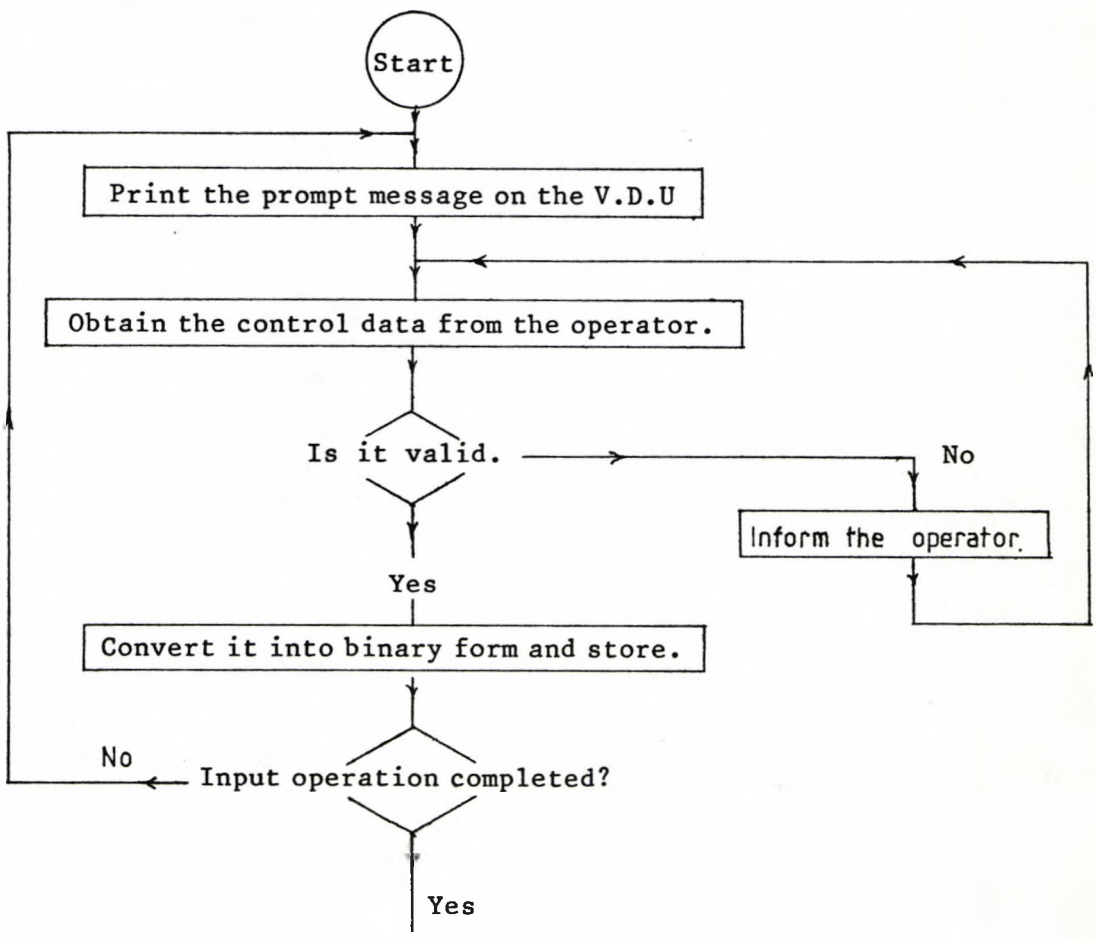

Fig 4.1(iv) The Prompt Operation.

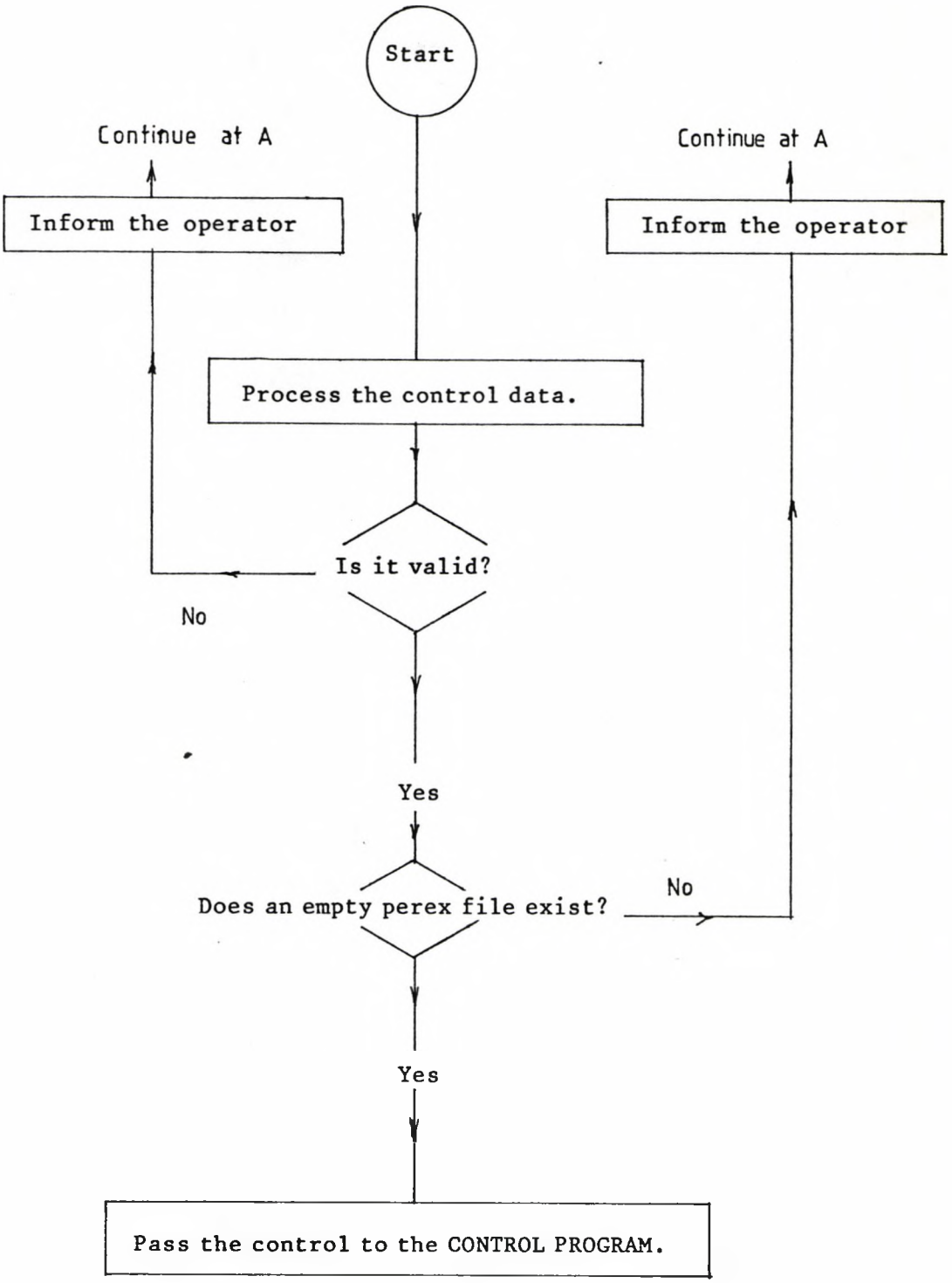

Fig 4.1(v) The Run Operation.

In any eight-bit processor the maximum **core memory** size is 64 kilo bytes. If the total space occupied by all the control programs were to be less than 64k and if these programs were fixed, then they could be stored conveniently and permanently in the **EPROM** (Erasable Programmable Read Only Memory). However, if the reverse were true, then, it would be highly undesirable to store these programs in the **EPROM**. In this case, some of the control programs would have to be stored in the same memory areas as others. This means that before those programs could be executed by the microcomputer the **EPROM** chips that contain these programs have to be put in the appropriate sockets and those that are already there would have to be removed. This physical movement of the **EPROM** chips in and out of their sockets repeatedly can introduce a possibility of damaging the electronic circuits. Therefore, an alternative method of storing the control programs was used. This method is more flexible. A minimum amount of programs, those that start up the system initially, are stored in the **EPROM** chips. The remaining control programs are stored in the cassette magnetic tapes. When the microcomputer is required to perform certain functions the corresponding control program is loaded onto the RAM from the magnetic tapes. In this way control programs can be changed as frequently as necessary. Furthermore, the magnetic tapes can be used to store a large number of programs and the microcomputer can be programmed to down load the required control programs onto the RAM at the appropriate time.

An exit point has been embedded in the User Monitor so that any utility programs (Choo (1982)), which have been loaded onto the specified locations in the RAM, can be accessed through the User Monitor. Two examples of these utility programs are

(i) the routine for listing the perex file on a V.D.U. or a printer,

(ii) the routine for copying another program from any specified RAM location into a perex file. The commands for executing these two routines are given in Appendix 4.1.

4.2.3 Cassette Recorder Handling Routines:-

The cassette recorder which has been described in Section 3.2 contains a microprocessor which does the perex file management. In this case it can be considered to be a slave microcomputer since it serves the master microprocessor only. Communication between the master and the slave is via an Intel 8251 Serial Interface Controller (Intel Corporation (1976))). When data are sent to the slave microprocessor, it stores the data in a buffer memory. As soon as this buffer is full the whole block of data collected is then transferred by the slave into the specified perex file. This file must be created before any transference of data takes place.

Choo (1982) has included some program segments under the title LPEREX (Weston (1979)) that handle the recorder. The present version of the LPEREX has been modified by the author in order to integrate it into SUZI, the User Monitor. More routines have been added to meet the requirements of the author. The facilities provided by these additional routines are described below.

At this stage the terms **static perex file** and **dynamic perex file** must be introduced. A **static perex file** is defined as one which contains permanently a fixed amount of information. In contrast, the amount of storage space in a **dynamic perex file** can be increased (but not decreased). A perex file is considered to be **dynamic** from the moment it is opened until just before the file closing procedure is carried out. Once a perex file has been closed, it is called a **static file.** The file closing procedure is as important as the opening procedure in an operation whereby information is being collected into a perex file. If, for some reasons, the power supply to the recorder were to be cut off accidentally in the presence of a **dynamic perex file,** then all the information in the whole track which contained that particular **dynamic perex file** would be lost. In order to safe guard all existing **static perex files** the last **dynamic file** must be converted into a **static** one while the power supply to the recorder is still on. It must be pointed out that there can be only one **dynamic file** at any time. When an experiment has been carried out successfully the master microprocessor will instruct the slave to carry out the above-mentioned operation automatically. However, as pointed out in Section 4.2.2, this operation can be carried out manually by typing 'CTRL/C' on the V.D.U. while the User Monitor is in command. Once the state of a perex file has been changed from **dynamic** to **static** any further similar instruction will be ignored by the slave microprocessor. The conversion process can proceed in one direction only, i.e. from **dynamic** to **static.** The flow chart of the routine that enables this conversion to take place is shown in fig 4.6. It must be added that information can be written onto a **dynamic perex file;** but the information already in it cannot be read. In contrast, the reverse is true for a **static perex file.**

The cassette that is suitable for the perex recorder is the 3M cassette which contains 4 tracks. A **dynamic file** can be created on anyone of these tracks. Once it has been generated on a track, information can be stored into the file continuously. On detecting the end of that particular track the slave microprocessor will change the **dynamic file** into a **static** ones automatically. Any further incoming information will be lost. Since this is highly undesirable if it were to occur before the completion of an experiment. In order to overcome this problem the physical link between the master and the slave microprocessor has the following safeguard characteristics.

As soon as the end of a track has been detected the slave microprocessor will close the final dynamic file on that track. It then interrupts and informs the master microprocessor. Once the master microprocessor has acknowledged the interruption, it goes to a special routine via a vector jump table. This special routine commands the slave to open another perex file on the next higher track. The master assumes the existence of a next track and that it has been initialised (Perex LTD. (1978)). If this is not the case, the operation fails and appropriate error messages are given at the V.D.U. However, when a new perex file has been opened successfully the master returns to continue the operation which it was performing just before the interruption from the slave. From then on any incoming information will be stored in the new **dynamic file**. This procedure may be repeated until there is no tracks left. In this way about 2 mega 8-bit bytes of information may be stored into a cassette continuously. The master microprocessor uses the cassette tracks sequentially.

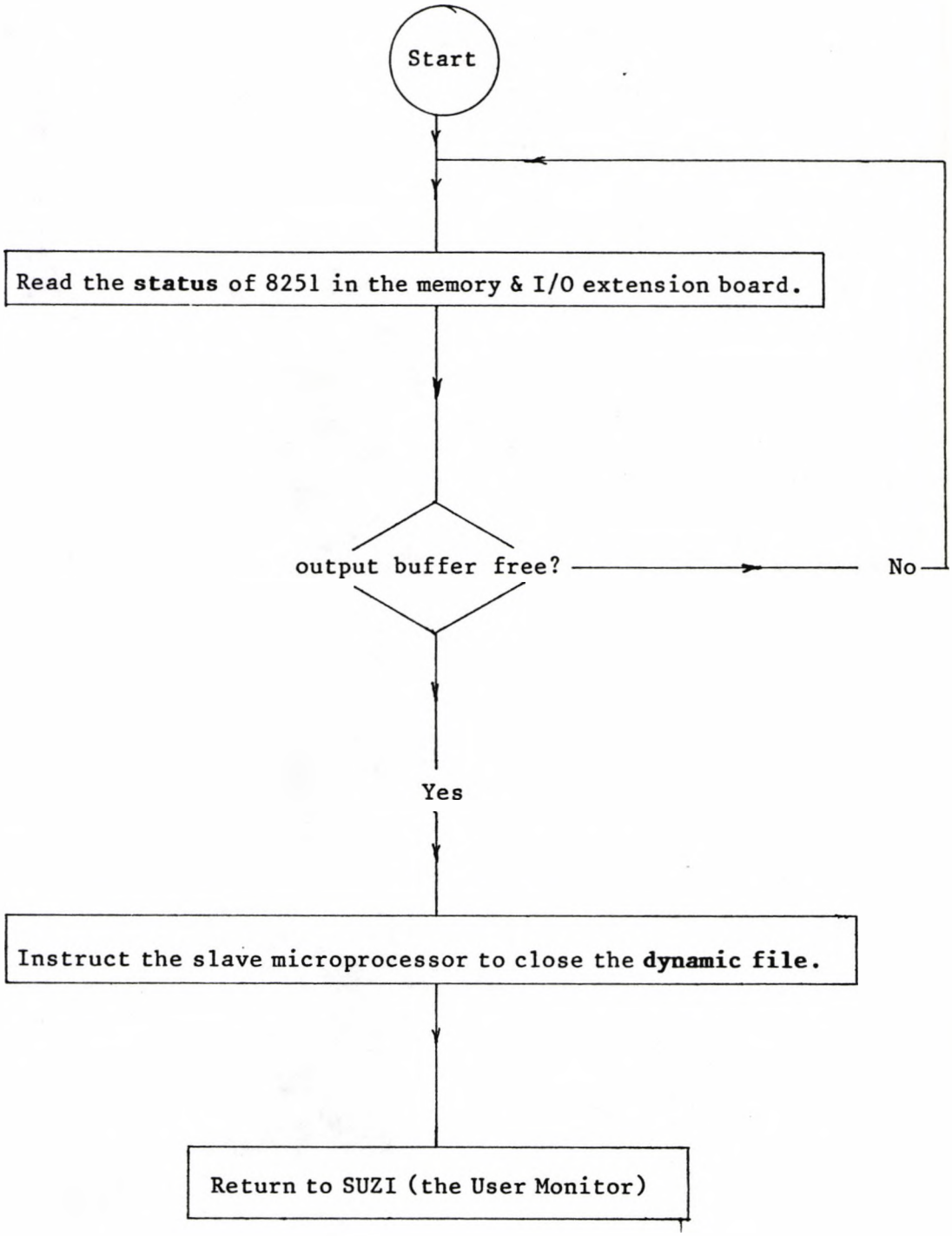

Fig 4.6 Flow-chart of the Routine for the status Conversion of File.

4.2.4 Readers:

Embedded in one of the **EPROMS** are two Readers (Weston (1979)) that read programs from a **static perex file** and store it in the **RAM** location specified in the file. Reader 1 reads the **cross-assembled** programs in **Intel format.** Reader 2 reads the **compiled Pascal** program codes called **P-codes.** These two Readers have been included here for the sake of completeness. They were modified to allow integration into the User Monitor. They operate at a **transmission speed** of 9600 **baud.** When the master microprocessor is under the control of the User Monitor, any of these Readers can be activated by giving the appropriate commands (see Appendix 4.1). The User Monitor records the read instruction before carrying out the operation. This is to enable it to take correct action should the read operation fails. A simplified flow-chart of these read procedures is given in fig 4.7. The listing of these Readers has been included by Choo (1982) under the library title INTEL.

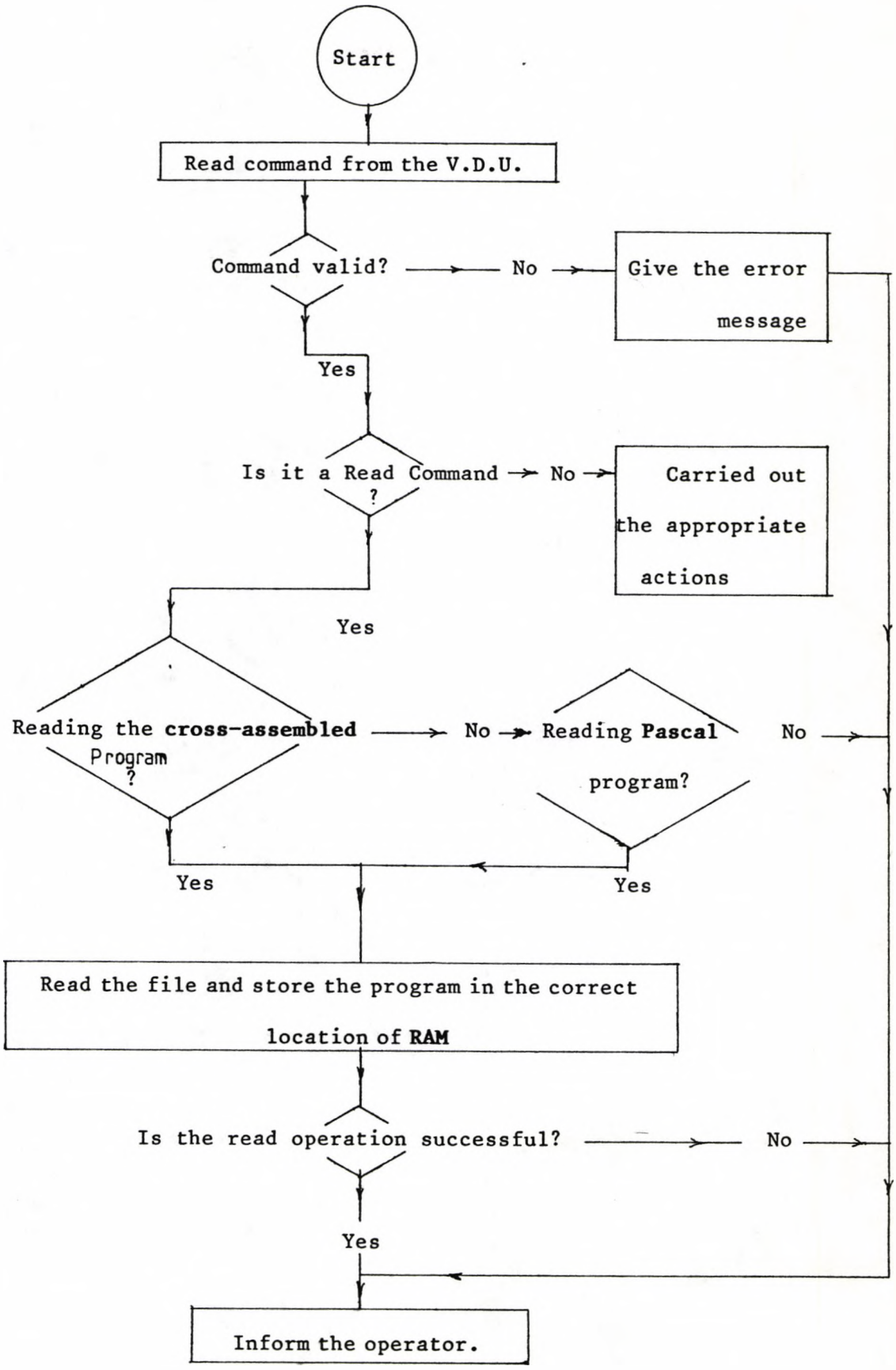

Fig 4.7 Flow-chart of the Read Operation.

4.2.5 System Initializing Routines:

Linking (Choo (1982) is the name of a library of **assembler** routines which are discussed in Sections 4.2.5 to 4.2.12. These routines have been linked to the control programs which have been written in the **Pascal language**. The **assembler** routines are mainly for handling the hardware, whereas the **Pascal** control programs do any necessary computations and work out what action needs to be carried out at any instant. Control is then passed to the corresponding **assembler** routine, which is in **Linking**, to carry out the action. On completing this task control is returned to the **Pascal** control programs.

This philosophy of software design has been adopted for speed both in the software development and the real time control processes. **Linking** begins with a Jump Table which is the means of connecting the **Pascal** control programs and the routines in **Linking**. The inclusion of this Jump Table enables one to make alterations to any routines within the **Linking** library without affecting the link as mentioned.

Before any experiment can be carried out using the multiaxial test rig the control system must be initialized. The system initialization operation is explained in this and the following paragraphs. As mentioned in Chapter 3, there exists a number of load combinations. Only one is required at a time. Therefore, to facilitate the load combination selection there must be an equal number of loading routines. As a result, the first step in this system initialization process is to obtain the correct entry address to the required loading routine. This address is then stored in a register

called SLRA, whose function will be explained in Section 4.2.11. At the time of the experimental work an alternative type of control software was developed. Consequently, the facility provided by register SLRA was not used.

The data sampling rate can be altered to suit one's needs. It is at this stage that a sampling indicator is set to the appropriate sampling rate. This indicator informs the master processor when to sample and record the experimental data (see Section 4.2.11.V).

The **Perex File Status Word** gives the master processor up-to-date information about the storage space available in the Perex File Store. It is reset during the system initialization process and will be set when the file store runs out. Once the master processor has detected that the **Perex File Status Word** is in a set condition it will stop sending experimental data to the slave microprocessor. Instead it stores any further incoming data in the **core memory**. It informs the operator about this action so that this block of data can be transferred later to new perex file.

Two other registers also need to be reset. They are the Table Pointer Register for the loading tables and the Interrupt Counter Register (see Section 4.2.11.V).

In a situation where a computer is being used to carry out experiments and to collect data automatically, some form of system self-checking is necessary to ensure that experiments can be carried out smoothly and that no data is accidentally lost. A limited amount of such self-checking operations have been included in the System

Initialzation process. Before carrying out the checking, two pair of **parallel I/O ports** i.e. **Port C4H** and **Port E8H** have to be initialized by the master processor. Once they are active external information, which flows through these ports, can be read by the master processor. It then interprets the external information to check that power supplies to the instrumentation and signal conditioners are on. It also makes sure that the data channels specified by the operators are connected properly. If any one of these checks fails the experiment will not be performed. Appropriate error messages will be printed on the V.D.U. screen. The functions of the individual bit of Ports **C4H** and **E8H** have been explained in fig 4.9.

When no hardware failure has been detected during the self-checking process the vector interrupt Jump Table is set up (see Section 4.2.11). Next the real time clock, which is used for timing the loading and data sampling processes (explained in Section 4.2.13(i)) is initialized and loaded with a clock counter value. The **interrupt mask register** (Intel Corporation (1976)) is activated so that external interrupt signals can flow freely into the microprocessor. Having completed the initialization process, the system initialization routine passes control back to the **Pascal** program but only after the loading process has been started.

The first and the last steps of system initialization change with the loading routine. Consequently, the number of initializing routines is the same as that of the loading routines. The general form of the initializing routines is shown in the following flow-chart.

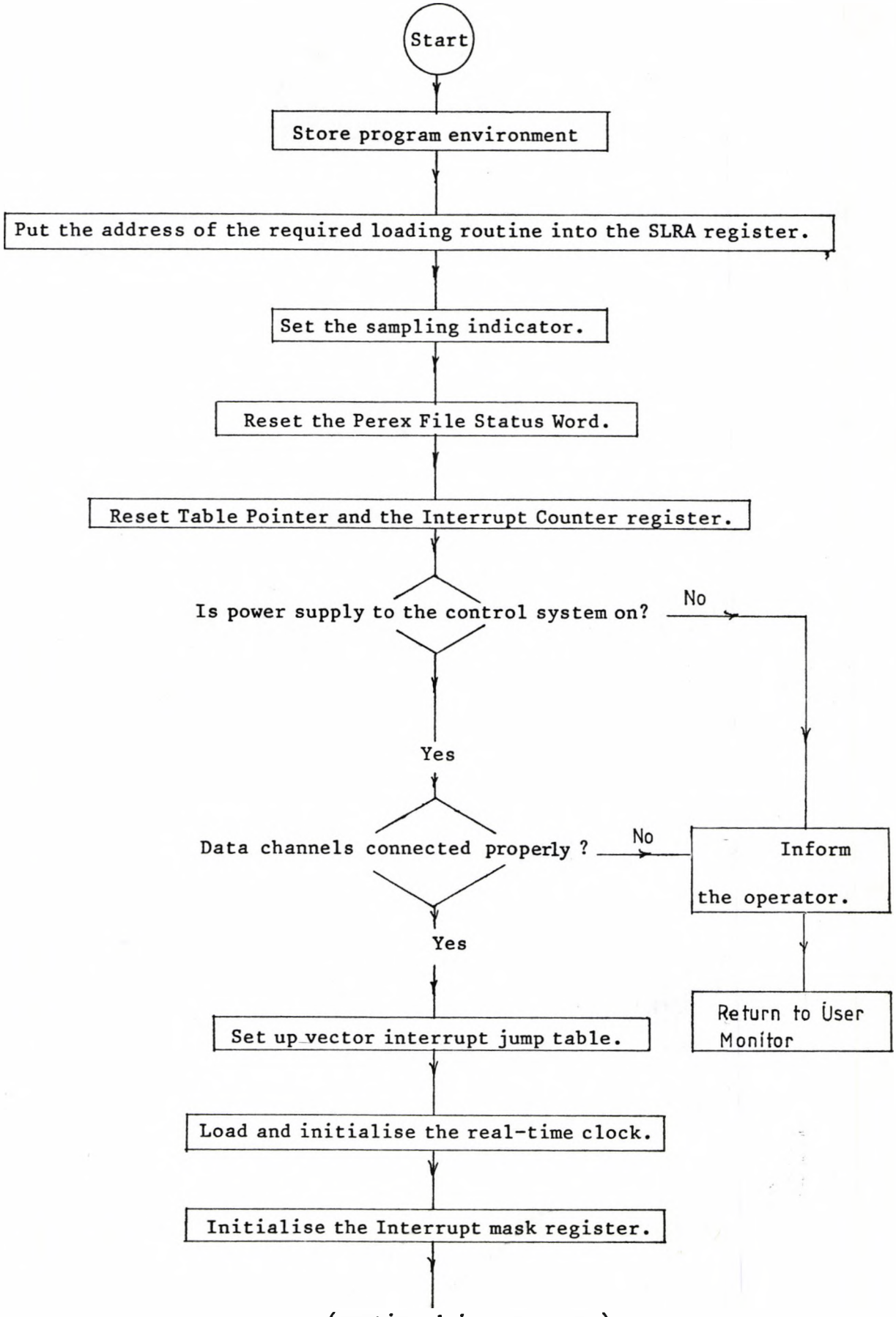

(continued in next page)

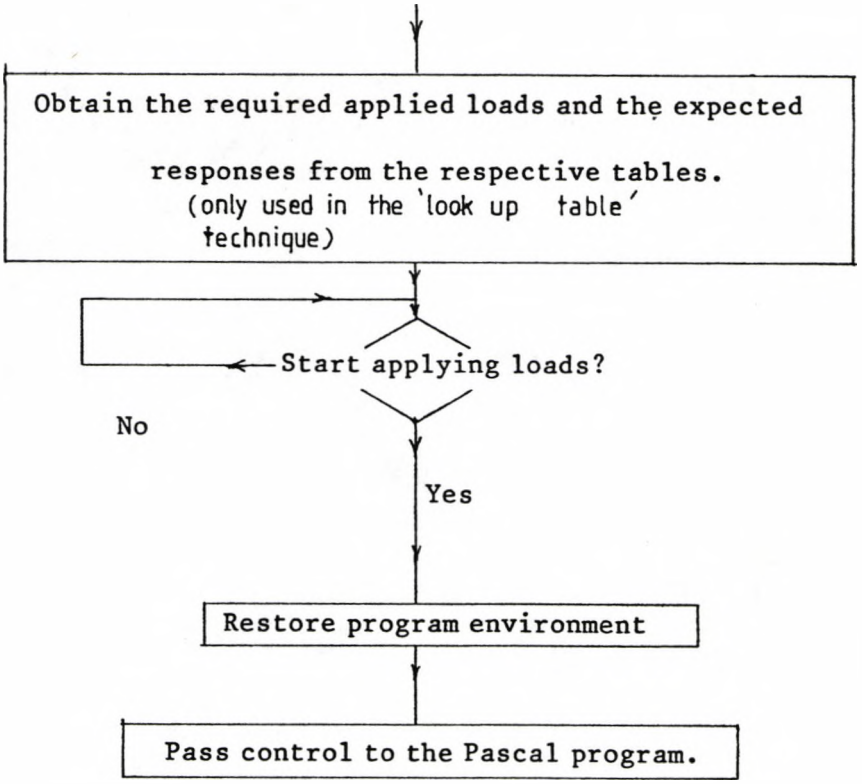

Fig 4.8 System Initializing Operation.

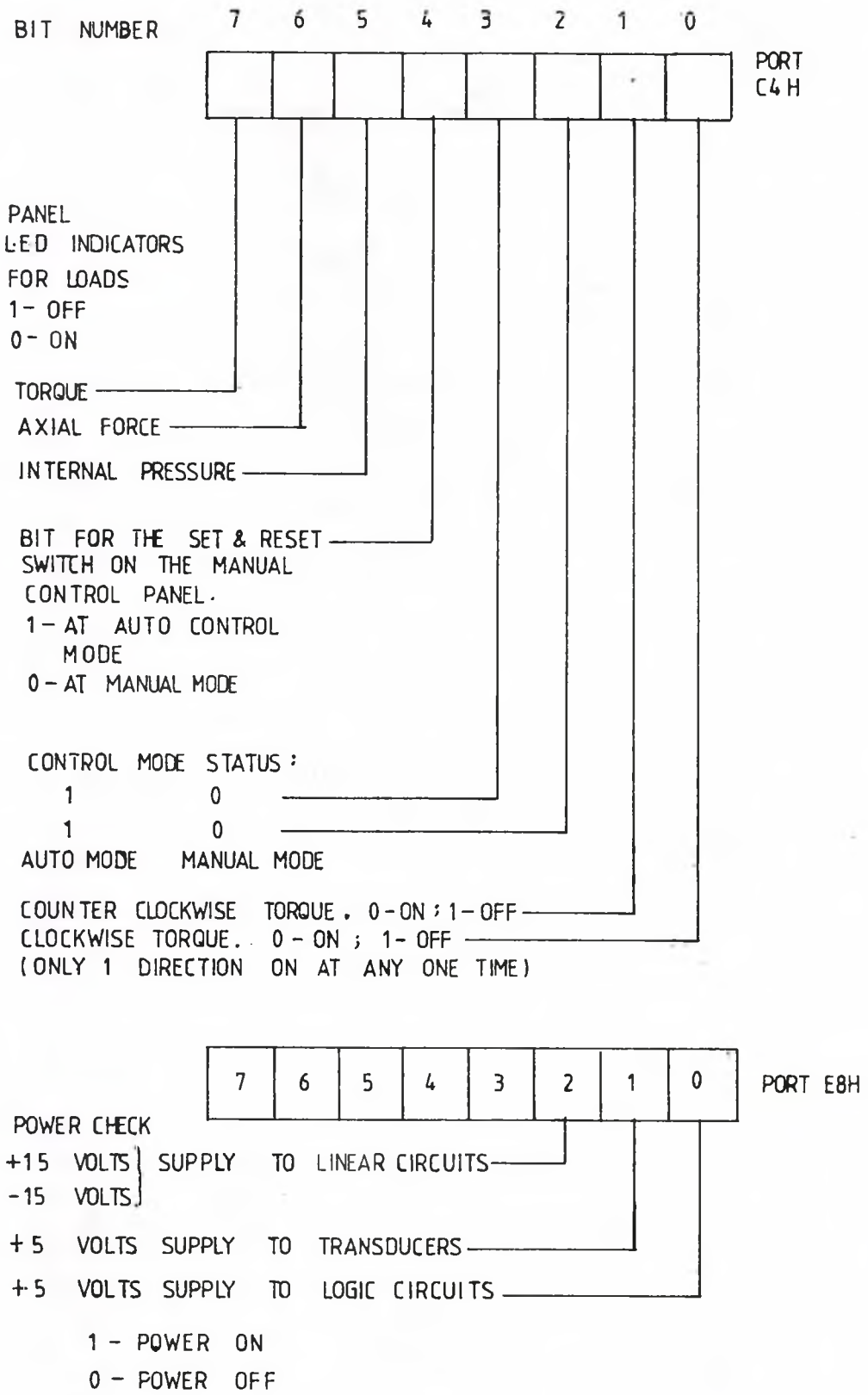

Fig 4.9 Functions of the Individual Bit of Ports C4H and E8H.

4.2.6 Loading Routines:

Loading routines (Choo (1982)) based on the 'look-up table' technique have been developed. They were used in conjunction with the SLRA register; but they were not used in the experimental work because a better alternative have been found. The improved method will be described in Section 4.3.1.

4.2.7 Digital to Analogue (D/A) Converter Handlers:

Four 12-bit D/A converters have been incorporated into the control system. For signals ranging from -10v to +10v, the attainable resolution is $20/2^{12}$ v i.e. 0.0049v. At present only two of these are being used. The other two can be used for further expansion.

Since they are based on the **memory mapping** principle (Intel Corporation (1977)), the software required to handle them is simple (Choo (1982) : D/A Handlers Section). On entering into any of these routines, the master processor fetches the driving signal, which is in digital form, and sends it to the appropriate D/A converter. One can then tap the equivalent analogue driving signal from the output port of the converter concerned.

4.2.8 Analogue to Digital (A/D) Converter Handlers:

The software which handles the A/D converter are more complicated than those which drive the D/A converter. Details of the basic operating principles for the A/D converter have been given in the manual (National Semiconductor Corporation (1978)). There are

two main routines under this section (Choo (1982)). They are SEQU and SEQ2. Both instruct the A/D converter to operate in a sequential mode i.e. to sample the data channels in ascending order with respect to the channel number.

The flow-chart for the routine called SEQU is shown in fig 4.10. On entering this routine the master processor sets up the specified number of channels to be read and their amplifier gains. A buffer is assigned by the master processor to store experimental data which is in binary form. This buffer has been called SAOB. In order to write onto the buffer a pointer is required. This is used to indicate the location which will be ready to accept information for storage and is set automatically by the master processor. Once the initial preparations have been carried out the sampling and conversion processes are initialised.

When an event of sampling and conversion has been completed, an experimental data block is formed. This data block begins with a letter H and terminates with a letter T. In order to achieve this data block format the master processor writes the letter H to the beginning of SAOB then advance the buffer pointer to the next empty location. The master repeatedly reads the **status** of the A/D converter. When the conversion process of a given channel has been completed, it will initialise the conversion process of the next channel. The digital signal of the current converted channel is read and stored in SAOB. This procedure is repeated until all the specified channels have been scanned. A letter T is then appended to the newly formed data block.

At this stage a second buffer called NBA is automatically assigned. A data dumping pointer is set up. It is called BUCK which tells the master the amount of information that is yet to be transferred onto the **perex file**. The initialisation of the 8251 **USART** (Intel Corporation (1976)), for the Perex, and the **enabling** of the Interrupt Process are performed next, in order to facilitate data transfer. From now onwards the Perex Recorder interrupts the master processor whenever it is ready to accept data. Meanwhile, the master carries out the task of converting the experimental data from binary to **ASCII-HEX** form and stores the new results into NBA. When the conversion operation has been completed, the master processor appends the new data block in NBA with a **Carriage Return, Line Feed, 00** and **Blank Space**. Having done this the master processor exits from the routine. The **ASCII-HEX** experimental data obtained can then be processed by the ICL1906S or IBM 4341 Computer.

The basic operations of SEQ2 are the same as those described in paragraph 2 and 3 of this section. In SEQ2, the master processor is instructed to read a specified number of channels and store the experimental data, in binary form, into a specified buffer.

4.2.9 Transient Experimental Data Sampling Routines:

When a test is in progress some of the feedback signals are used to compute the actions required at any given instant. Once used, these signals will be destroyed. Consequently they are called Transient Experimental Data. Since these signals are used internally by the master processor, the Transient Experimental Data is left in binary form after it has been converted from the analogue form by the A/D

converter. At present signals from three loads and the LVDT(which measures the relative displacement of the end clamps) are the only signals being used for this purpose.

These signals are obtained by a 2-step process. Assuming that the master processor is executing a **Pascal Control Program**, when a certain signal is required, the master will select the appropriate routine from a block of routines described in this section which consists of **assembler routines**, viz: TCSR,PCSR, FCSR,LVD1 and LVD2. Essentially, the master will be instructed by this particular routine to activate the A/D conversion process for the corresponding channel in a repetitive mode (National Semiconductor Corporation (1978)). As soon as this conversion process is completed the master will return to the **Pascal Control Program** and reads the required newly converted signal. In a similar way, signals from the strain gauges and other transducers can be used for the same purpose when necessity arises. However, it becomes obvious that more but similar types of routines will be required.

An additional routine called JOY has been included in this section. It initialises the A/D converter to operate in a sequential mode. The specified number of channels will be sampled and the digital signals are then stored in a buffer, which is set up by JOY automatically. JOY provides a means of sampling and storing extra temporary data. The buffer is used repeatedly for this operation. If necessary, these data can be converted into **ASCII-HEX** form and transferred onto a **perex file**.

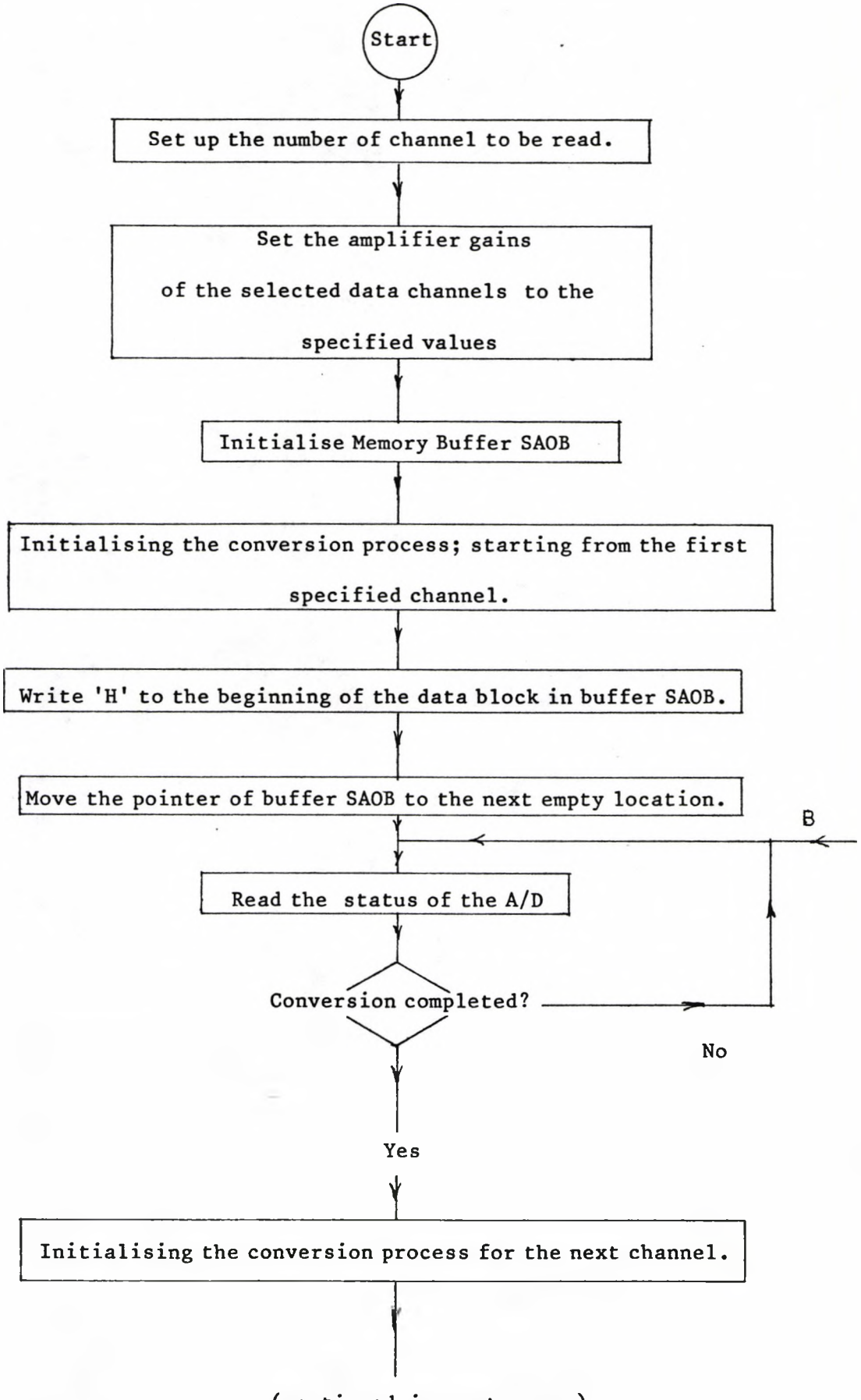

(continued in next page)

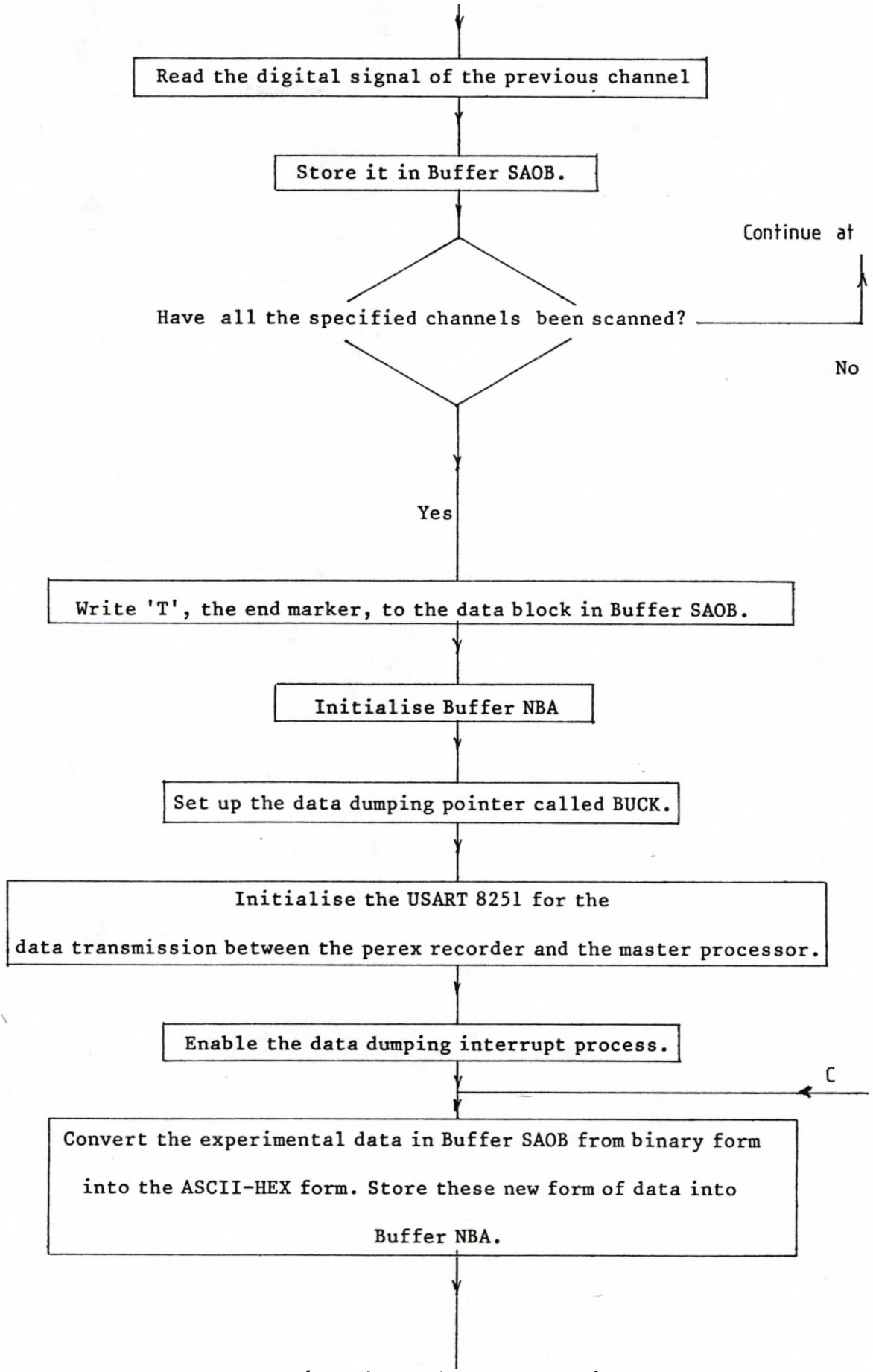

(continued in next page)

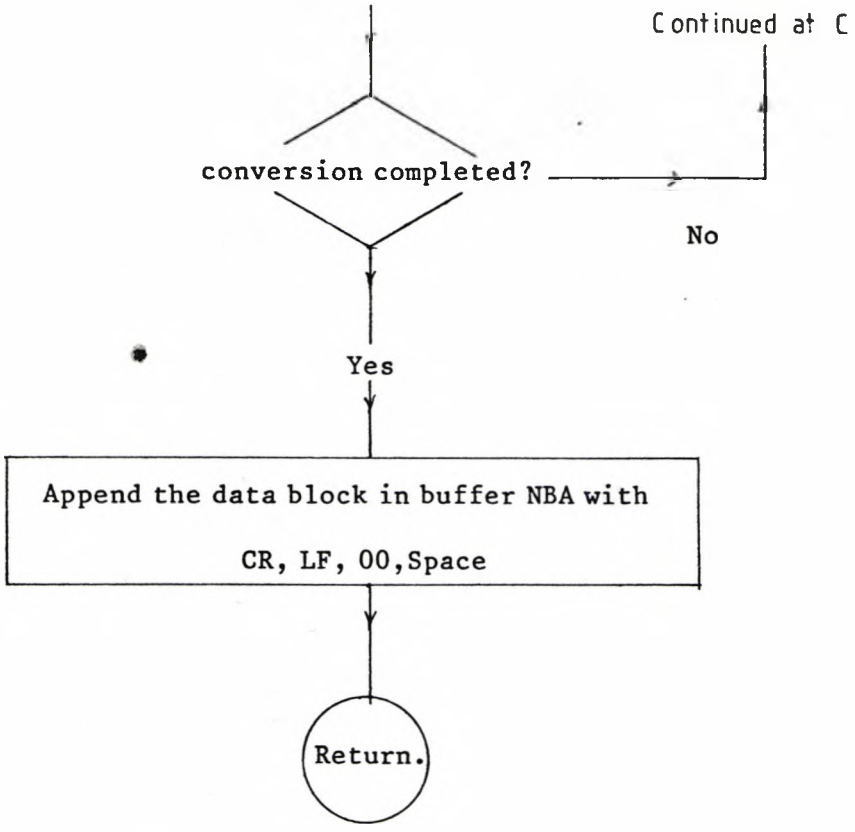

Fig 4.10 Flow-chart for the A/D converter handling routine 'SEQU'

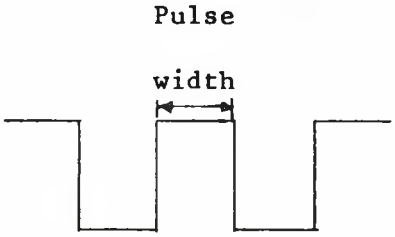

Fig 4.11(i) Square Wave.

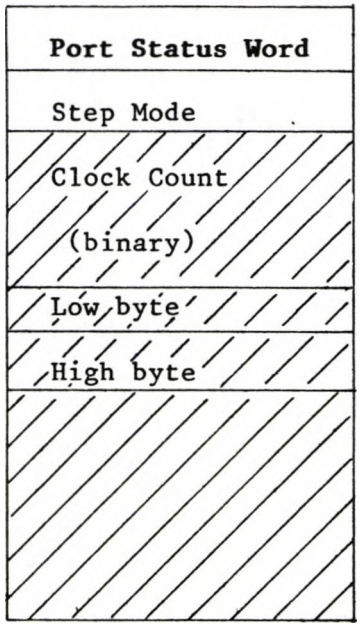

Fig 4.11 Torque Loading Table.

4.2.10 Pulse Train Generating Routines:

The applied torque on the specimen is provided by a stepping motor. A square wave signal is required to drive the stepping motor. For this purpose a built-in clock called **Clock 0**, which is within the microcomputer, has been used to generate the square wave pulse train. This clock can be activated by two routines which will be described in the following paragraphs in this section.

GCLR is called the General Clock Load Routine. The pulse frequency and pulse width (see fig 4.11(i)) can be varied by supplying **Clock 0** with different clock counts. GCLR always fetches the Port Status Word and the Step Mode from a torque loading table (if used) as shown in fig 4.11. These two pieces of information are **OR** and the result is sent to port **C4H**. Having completed the task it will then pick up the clock count indicated by a table pointer. Finally, GCLR supplies the **Clock 0** with the current clock count it has just obtained from the torque loading table.

Port Status Word contains information for switching those light indicators on the Driver Board Front Panel*. Furthermore, it also provides information on the control mode for the test rig, i.e. either automatic or manual. The **Port Status Word** is set by all the **Pascal Control Programs** automatically.

Step mode dictates whether the applied torque is clockwise or counter-clockwise. It has to be supplied by the operator before any experiment begins. However, this piece of information can be embedded

* Driver Board Front Panel is part of the Interface Unit.

in the torque loading table while the table is being prepared.

PULS provides the appropriate **Pascal Control Programs** with a means of altering the pulse frequency and hence the speed of the stepping motor. PULS fetches the clock count in the register called CLOCK. This clock count is provided by those **Pascal Control Programs** that need to have access to **Clock 0.**

4.2.11 Interrupt Service Routines:

In real-time control, one often encounters situations where certain operations need servicing continually but not continuously. Furthermore, it is possible that certain operations might only need to be serviced once throughout the entire real-time control period. Therefore, in order to improve the efficiency of a microcomputer, which performs the control, an interrupting technique has been introduced. External electronic circuits (See Section 3.3.3) have been used to generate interrupting signals whenever these operations need special attention. On acknowledging any interrupting signal the microcomputer will suspend temporarily its current task and carry out the required special service. Once completed it resumes the task it was performing before it was interrupted. A vector interrupting technique (Intel Corporation (1978)) was chosen. This offers further improvement on the microcomputer efficiency since the microcomputer knows exactly what needs to be done when it receives an interrupting signal without requiring additional information. There are eight Interrupt Service Routines in the **Linking Library** and each has its own characteristics. Consequently, it is easier to explain the functions of each individual routine separately. All necessary external circuits for generating the interrupt signal were described in Section 3.3.3.

4.2.11(i) Burst Interrupt Service Routine:

When a specimen bursts while it is being tested, the Burst Interrupt Service Routine will be executed. Essentially, it stops further interrupting before proceeding to record the experimental data corresponding to the rupture failure of the specimen. These data are stored temporarily in the buffer called MEMO. Next it examines the **status** of the **perex file** which is being used to collect experimental data. If there is no storage space left in the **perex file**, then the burst data will be left in MEMO and the operator will be notified after the test has been stopped. This is to ensure that critical experimental data will not be lost. On the other hand, if the **perex file** is still capable of accepting extra data the Burst Interrupt Service Routine will convert the burst and weepage data, if any, from binary to **ASCII-HEX** form and dump it onto the **perex file.**

4.2.11(ii) WISR (Weepage Interrupt Service Routine):

WISR captures the weepage data whenever a specimen weeps while a test is in progress. It stores these data in a buffer called WMEM in binary form. The Pascal Flag is set by WISR before the master processor exits from it. Throughout the period when WISR is command the interrupting process is activated. Therefore, any subsequent interrupting signal can still interrupt the microcomputer, provided it has a higher priority than the one which WISR is servicing (Intel Corporation (1978)).

4.2.11(iii) IRRP:

The maximum size of a **perex file** is limited by the physical length of the track on which the file is located. It has been pointed out in Section 4.2.3 that a special interrupt service routine is required to open a new **dynamic perex file** on the next higher track whenever the current one has run out. IRRP is that special interrupt service routine.

IRRP first stores the current content of the **Interrupt Mask Register**, port **ClH** (Intel Corporation (1976)). Then it masks out any interrupting signal with lower priority than its own. This means that the operation of transferring data onto a **perex file** is suspended temporarily. In order to maintain integrity in the last set of experimental data collected, just before the execution of IRRP, the NBA buffer pointer is pushed back one character space (Each location in the buffer called NBA represents one character space.). When a **dynamic perex file** has been opened successfully on the next higher track, IRRP will restore the **Interrupt Mask Register** with the previous content that it has stored. This is to ensure that the interrupting process is carried out in an orderly manner.

It must be clarified at this stage that the new **dynamic perex file** resulting from the above action always has a file name X00 where X is the corresponding track name. Therefore, if X00 already exists, failure of the above operation will occur even when there is room on track X. However, this failure can be avoided by leaving track X completely empty and fully initialised at the beginning of any experiment.

4.2.11(iv) IMR8:

Data is transferred from the **core memory** to the recorder one **ASCII-HEX** character at a time. The master processor send it to the **USART** (Intel Corporation (1976)). Transmission between the **USART** and the Perex Recorder is carried out by these two units without any supervision from the master processor. Since this transmission is not instantaneous the master processor will have to wait between the transferring of each **ASCII-HEX** character. Therefore, it becomes clear that experimental data can be moved more efficiently by interrupt technique. In this way the master processor can use the waiting time to do something useful. On acknowledging the interrupting signal from the **USART** the master processor will execute IMR8

IMR8 is responsible for transferring data from NBA into the specified **perex file** while an experiment is in progress. This level of interrupt (level 5) is **enabled** by SEQU described in Section 4.2.8. However, as soon as the master processor enters into IMR8, this same interrupt level is **masked out** and further interrupts from other levels are suppressed in order to create a unique state so that the integrity of the data under the process of transference is preserved. When all the data have been moved safely across to the **perex file**, IMR8 will **enable** all interrupt levels except level 5 and terminate its commanding role. On the other hand, if more data are to be transferred IMR8 will simply **enable** all interrupt levels. This will enable the remaining data in buffer NBA to be sent to the **perex file.**

4.2.11(v) INTR:

Regular load increments and data sampling are achieved with the aid of a real-time clock on board the microcomputer. This clock has been programmed to interrupt the master processor at an interval of 50 milliseconds. The clock used for this purpose is called **Clock 1**. The 50-millisecond interval can be altered by modifying the routine called MINI in the Utility Routines section (Choo (1982)). For each such interrupt the content of the interrupt count register is increased by one. The sampling rate factor is stored in register TSMP. The name implies that the content in TSMP will affect the rate of data sampling. Similarly, the loading rate factor is stored in LOIN. When the contents in the interrupt counter register and TSMP are equal INTR will command the master processor to do data sampling. On the other hand, if the interrupt count is equal to the value in LOIN, then, load or loads will be increased according to the specification given by the operator. However, if none of the above conditions are true no further action will be taken by INTR apart from incrementing the content of the interrupt count register.

Any experimental data sampled by INTR will be converted from binary to **ASCII-HEX** form. This type of data is transferred onto a **perex file** specified by the operator at the beginning of the experiment.

INTR can access the appropriate loading routine by a subroutine called LOAD (Choo (1982)). The content of SLRA register is used by the subroutine LOAD as an entry address for the suitable loading routine.

4.2.11(vi) EMSR:

In emergency circumstances the operator can override any normal program instruction by operating the emergency switch. This switch generates an interrupt signal which has the highest priority. When this level of interrupt is activated EMSR will command the master processor to shut down the whole test rig and inform the operator to carry out the required steps if he wishes to continue the test after the fault has been rectified.

EMSR does not close the current **dynamic perex file.** Therefore, the file can still be used to collect experimental data should the test be continued later.

4.2.11(vii) CREA and WHIT:

Interrupt service routines called CREA and WHIT are for general purpose .

4.2.12 COMP (experiment Terminating Routine):

When an experiment has been concluded, whether successful or not, the loads exerted on the test specimen will be reduced to zero. Control mode of the test rig will be switched from automatic to manual so that the specimen can be removed. Appropriate messages will be printed on the V.D.U. to inform the operator of the current state. The name of the **perex file** which was used to collect experimental data will also be listed.

If loading tables are used, the table **status words** can be embedded in the corresponding tables during the table preparation process. These **status words** are stored in special registers. They are used to determine if a required table is present in the **core memory**. If the check turns out to be negative, then the master processor will not start the experiment and the operator will be informed of the reasons. At the end of an experiment the registers which hold these **status words** will be reset by the COMP according the answers obtained from the operator.

Finally, the **dynamic perex file** which collects experimental data will be closed automatically by COMP. The operator then removes the cassette from the Perex Recorder and processes the experimental data as required.

4.2.13 Utility Routines:

These are the routines which carry out a major portion of the 'dirty jobs'. For example, before a message is printed a utility routine is required to fetch the message from a buffer. Another utility routine might be needed to send this message to the V.D.U. so that the message will be printed. There are many such routines in the **Linking Library**, but only one will be discussed here.

4.2.13(i) MINI:

MINI is the routine which initialises **Clock 1** (Intel Corporation (1978)) that regulates loading and data sampling (see Section 4.2.11(v)). The clock has a 2-byte register. A 2-byte value is loaded

into this register by MINI. Once initialised the clock will start counting down from the value which is in the register. When it reaches zero it will generate a signal to interrupt the master processor. This process is repeated until the clock is deactivated. The interrupt interval is dependent on the content of the clock register and can be changed by altering the content of this register.

4.2.14 Messages:

A library of vocabulary has been stored permanently in the **core memory** so that the control system becomes interactive. However, text needs a large storage space. Therefore, messages (Choo (1982)) have been compressed before they are retained in a limited **core** space.

4.3 Control Programs:

In general, before feedback or feedforward control is applied to a system its material behaviours are usually known. However, the material behaviours of the system under consideration are not understood fully. The systems mentioned here imply test specimens of different materials. The lack of knowledge of the material behaviours has ruled out the appliction of feedforward control in this situation. Furthermore, it also introduces difficulties into the feedback control utilized. Fortunately, the quasi-static nature of the experiments simplifies these problems to a certain extent. At present load control is used. This utilises the information on the loads exerted on the test specimen to derive the control actions required at any instant.

The main control programs can be written in **Pascal Language** which is high level language. It is relatively easy to write these programs since they follow closely the high level reasoning of the programmer. They can be understood easily, when compared to the machine language. Any programming error can be found and corrected quickly. Furthermore, the **syntax** of these programs is checked by the **Pascal Compiler**. Therefore, the programmer is relieved from the task of checking the basic logic of the programs. All the **Pascal Control Programs** described here were **compiled** using the ICL1906S Computer. A **P-code** version of each program has been produced. The **P-code** cannot be executed directly by the microcomputer. A **P-code** interpreter, which has been stored permanently in the **core memory**, is required to execute these control programs.

4.3.1 Functions of the Main Control Programs:

The library called **Linking** (Choo (1982)) begins with a jump table. This is the vital link between the **Pascal Control Programs** and some of the routines which are in **Linking**. The **Pascal Control Programs** gain access to these particular routines via the jump table.

If a "Run" instruction is issued while the User Monitor is in command, control will be passed directly onto the **Pascal Control Program** which is in the **RAM**. From now onward the microcomputer will not obey any instructions given by the operator via the V.D.U. The **Pascal Control Program** first prints out a list of loads to be exerted on the test specimen. In doing so the operator can double check that the required control program is in the **RAM**.

Overloading of the test specimen can be prevented by using the load limits. For each type of load there are two load limits -positive and negative load limits. Therefore, six variables are required to hold these load limits since there are three type of loads, viz., internal pressure, axial force and torque. The **Pascal Control Programs** assign these variables with the appropriate load limits before it takes an initial set of readings from the load cells while the loads exerted on the test specimen are still zero. This initial set of readings is used as a datum throughout the experiment. In addition, an initial set of data for the selected channels at zero loads is taken and dumped onto the specified **perex file** before an experiment commences. This set of readings will be used as datum for the data processing operation. These reference data are necessary since the absolute zero is difficult to obtain because most amplifiers tend to drift at zero input voltage.

Light indicators have been used to indicate which are the active load sources while an experiment is in progress. These indicators relied on the **Pascal Control Programs** or **Assembler Control Programs** to do the switching. During the process of switching on the appropriate indicators the test rig is also switched from manual to automatic control mode. At this stage the manual panel is deactivated.

In order to initialise the whole control system the control programs call the initialization routine concerned. All the activities described in Section 4.2.5 (Initialization Routines) will be carried out systematically.

The **Proportional and Integral** analogue controllers increase the capability of the microcomputer. Now the microcomputer is used to make decisions on the necessary action while an experiment is in progress. The above-mentioned analogue controllers act as slave drivers for the axial force actuator and the internal pressure intensifier. The required driving signals are generated by the microcomputer. They are sent to the slave drivers which ensure that the correct loading procedures for the specimen are achieved.

Some of the control software packages used in the experimental work have been written in **Assembler Language** and the flow-charts will be given in Chapter 5. The **assembled** control programs (Choo (1982)) for opened-loop control on the stepping motor, closed-loop control on the axial force actuator and the pressure intensifier are relatively simple. The closed-loop control software for the axial force actuator and the pressure intensifier have an extra task of switching the integrators in the analogue controllers. These integrators are switched off when the test rig is in a manual control mode; but they are switch into action when the test rig is in an automatic control mode. For closed-loop control on the stepping motor, the control software is more complicated. In general, complicated control software can be developed using high level language, in this case using **Pascal Language.**

The capabilities of the multiaxial test rig increase as more control software is developed.

4.4 Off-line Data Processing

Once the experimental data have been recorded on a magnetic tape it can be processed at a suitable time later. Routines described in this section have been used to carry out the processing operation. The processed data was listed on a high speed line printer. The necessary graphic outputs were obtained by using the GHOST Library (The GHOST GRAPHICAL OUTPUT SYSTEM NWD 26). All Off-line Data processing work was also carried out on the ICL1906S Computer in the Computer Laboratory, Liverpool University where the GHOST Library is available.

4.4.1 Editing of Input and Output Files:

The data processing sequence is illustrated in fig 4.18. It involves three stages of editing viz:-

(i) Raw data file editing,

(ii) Semi-processed data file editing and

(iii) Final output file editing.

4.4.1(i) Raw Data File Editing:

The raw experimental data gathered by the control system is divided into record form. Each record contains an experimental data block corresponding to a given instant. As pointed out in Sections 4.2.11(i), 4.2.11(ii) and 4.2.11(v) the control system employs two methods to acquire experimental data while an experiment is in progress.

Normally, the control system collects experimental data at regular intervals. However, the External Interrupt method is used to ensure that data corresponding to critical moments like weepage and burst are obtained. Unfortunately, the arrival of these interrupt signals is unpredictable. If one of these signals reaches the control system while it is collecting data using the former method, then that data record will be corrupted; but the critical data record resulted from the interrupt signal will be saved.

The main task of the raw data editing routine is to eliminate any corrupted data records which would otherwise cause failure in the data processing operation.

4.4.1(ii) Semi-processed Data File Editing:

In the **Pascal** data processing stage, which will be described later, a new data file is generated. It contains the table heading for the final output, control parameters for the **FORTRAN** processing stage and the semi-processed data.

It is necessary to edit the new data file so that the control data and the semi-processed data can be accessed readily. On completion of this editing stage the content of the new data file is divided and stored in different files. The heading for the final output is stored in a file called TITLE. The control data go into a file called CONDATA. Finally, the simi-processed data are retained in the User-specified data file.

4.4.1(iii) Final Output File Editing:

After the **FORTRAN** processing stage the processed data output file is merged with the TITLE to form the final output file. All the temporary work files are then erased.

4.4.2 **PASCAL** Data Processing Program:

When the data processing operation enters this phase, the edited raw data are converted from **ASCII-HEX** character code into decimal form. The **ASCII-HEX** character code is necessary to prevent data corruption. For numerical work it is easier to use a decimal form. The initial set of the raw data is used as a datum.

The heading of the final processed data file is generated by the **PASCAL** data processing program. The table heading of the final output file is needed to make the processed data meaningful.

A set of control parameters is calculated from the raw data input. These control parameters inform the **FORTRAN** data processing program the way in which the input data must be read. Furthermore, these control parameters also contain information which will be used in the applied loads, stresses and strains calculations.

The time corresponding to each set of experimental data is produced at this stage using the input information.

4.4.3 **FORTRAN** Data Processing Programs:

The input data for the **FORTRAN** data processing program comes from the semi-processed output file generated at the **PASCAL** data processing stage.

If there are more than three hundred sets of experimental data, then they will be averaged to produce three hundred sets at regular time interval. The time grid is set up for graph plotting purposes. For situations where there are three hundred sets of experimental data or less the averaging process will not be carried out.

In both cases, the applied loads, stresses and strains are calculated from the semi-processed input data. This procedure is repeated for weepage, burst and any other relevant data.

The following graphs:-

(i) Applied loads versus time,

(ii) Stresses versus time,

(iii) Strains versus time and

(iv) Strains versus applied stresses

are plotted. This part of the program can be expanded easily to plot any other graphs from the experimental data, if necessary.

The output data file produced at this stage is used in the final output file editing process explained in Section 4.4.1(iii).

The simplified flow-chart of the FORTRAN data processing program is shown in fig 4.19

The complete listing of the Off-line data processing programs can be found in Choo (1982). The principles used in calculating the loads and strains from the corresponding electrical signals recorded are given in the software manual (Choo (1982)).

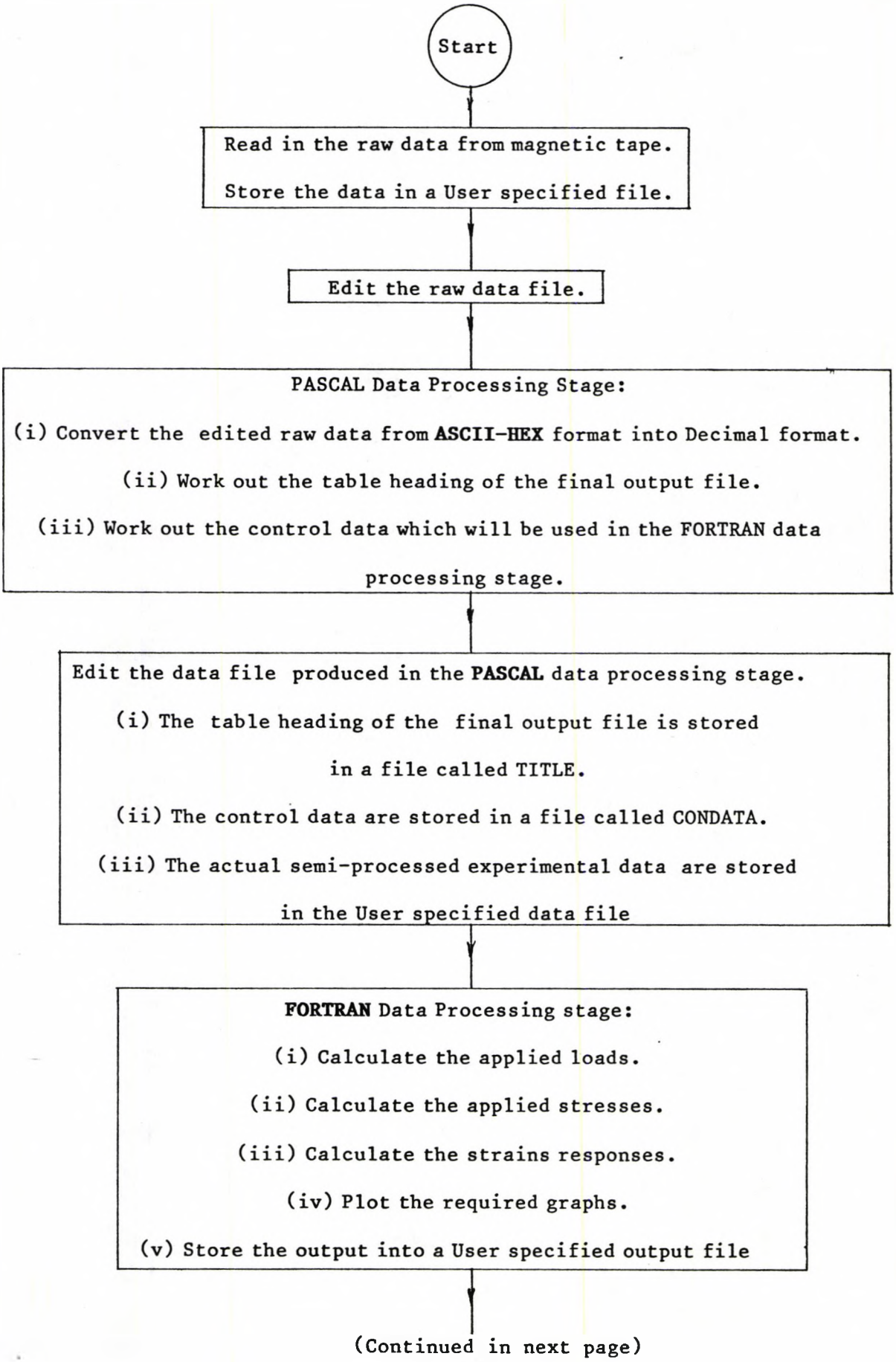

(Continued in next page)

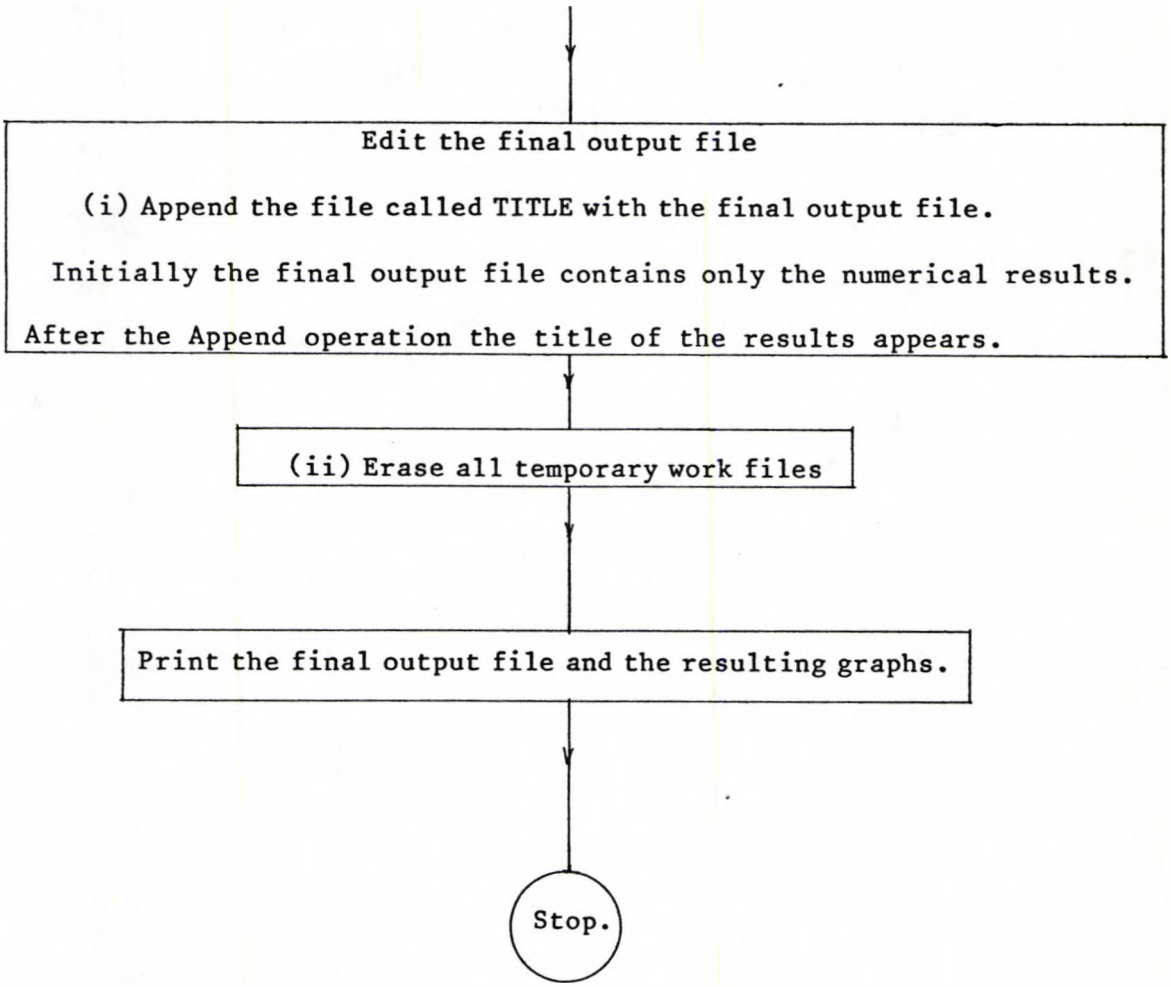

Fig 4.18 Flow-chart of the Data Processing Operation.

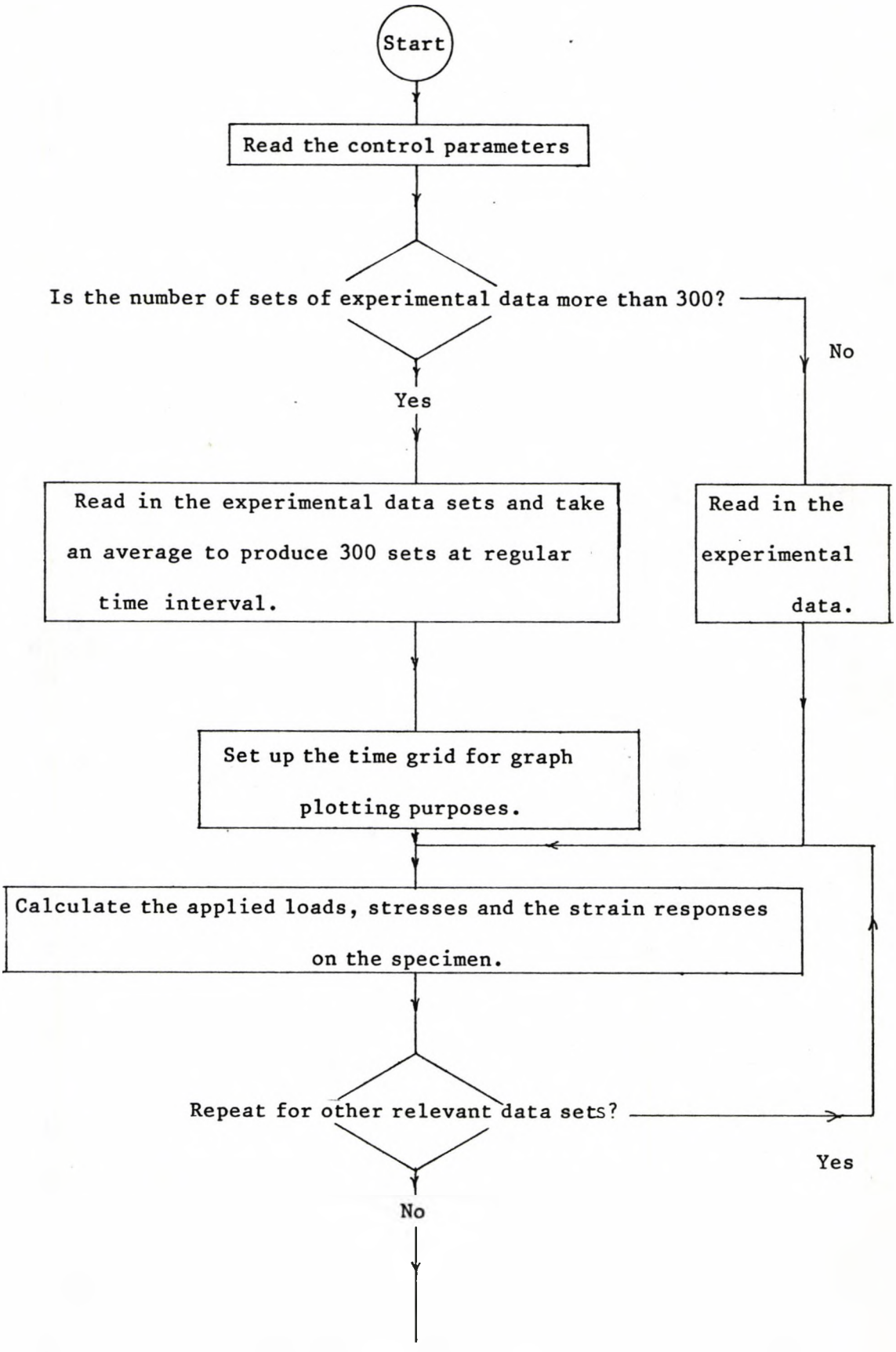

(Continued in next page.)

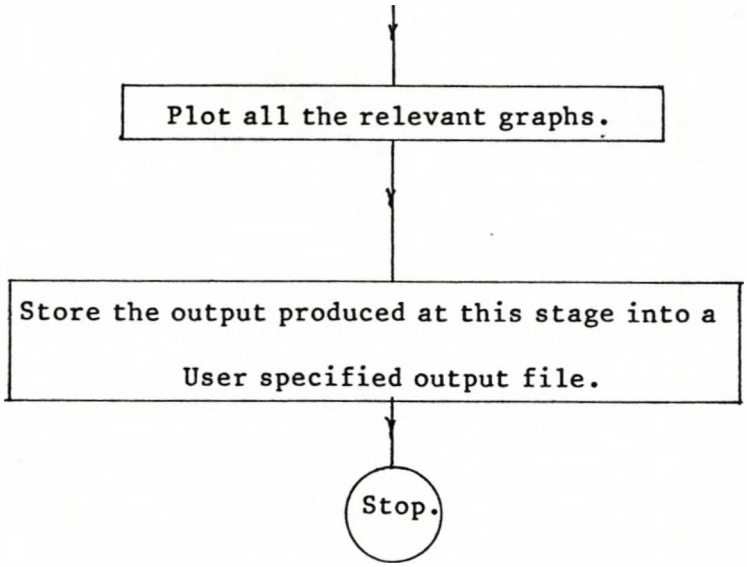

Fig 4.19 **FORTRAN** Data Processing Operation.

Chapter 5: EXPERIMENTATION

5.1 Introduction

This chapter is divided into 3 main sections to explain the experimental work carried out. Section 5.2 describes the specimen preparation process. It gives a detailed account of the constituents used, the technique of making specimens and their dimensions.

The procedure for setting up a test and the capabilities of each test program are illustrated in Section 5.3. The available test programs are represented here by flow-charts.

Finally, the work on the microscopic study is elaborated in Section 5.4. The term fracture surface has been used in the text of this chapter. It means the physical fracture surface of the specimen and not the mathematical failure surface predicted using a theoretical model.

5.2 Specimen Preparation

In this section, the details of specimen preparation are described. This account is subdivided into the following sections for ease of presentation.

5.2(a) Material Components:

The constituents of the non-metallic composite materials used in this project were:

(i) polyester resin, which formed the matrix, and

(ii) E-glass fibre, which served as the reinforcement.

Initially, the polyester was in a liquid form. Part of the specimen making process involved adding a catalyst and an accelerator, which were also in liquid form, to the polyester. It was then mixed thoroughly to produce a homogeneous mixture. The proportion of each component used is given in Table 5.2.1.

Table 5.2.1. Chemical Composition of the Polyester Mixture

Constituent	Percentage by Volume.
Crystic 272 - Isophthalic acid based unsaturated polyester resin.	100
Initiator - Methyl Ethyl Ketone Peroxide (supplied by Scott Bader as 'M')	1.0
Accelerator - Cobalt Naphthanate (Supplied by Scotter Bader as 'E')	0.5

The E-glass was obtained from Pilkington with the trade name 'Equirove'. Two types of glass fibre were used. One consisted of 2400 tex and the other was a 1200 tex glass. The diameters of both types of glass were almost identical. The word 'tex' means individual glass fibre. Therefore, a 2400 tex glass bundle consists of 2400 individual fibres. The individual glass fibre was coated with a thin layer of silane to promote good bonding between the glass fibre and the polyester matrix. Interface bonding between the reinforcement and the matrix is an important topic in composites and

has been studied, for instance, by Gatwood (1982).

5.2(b) Specimen Making Technique:

Tubular specimens were used in all the experiments carried out. These specimens were produced using the Filament Winding Technique. This technique has been described in detail by Legg (1980), Jones (1981) and Hogg (1981). The Filament Winding Machine consists of four major components; viz,:-

(i) a digital controller,

(ii) a mandrel

(iii) a bath

(iv) a carrier.

and is illustrated in fig 5.2.1.

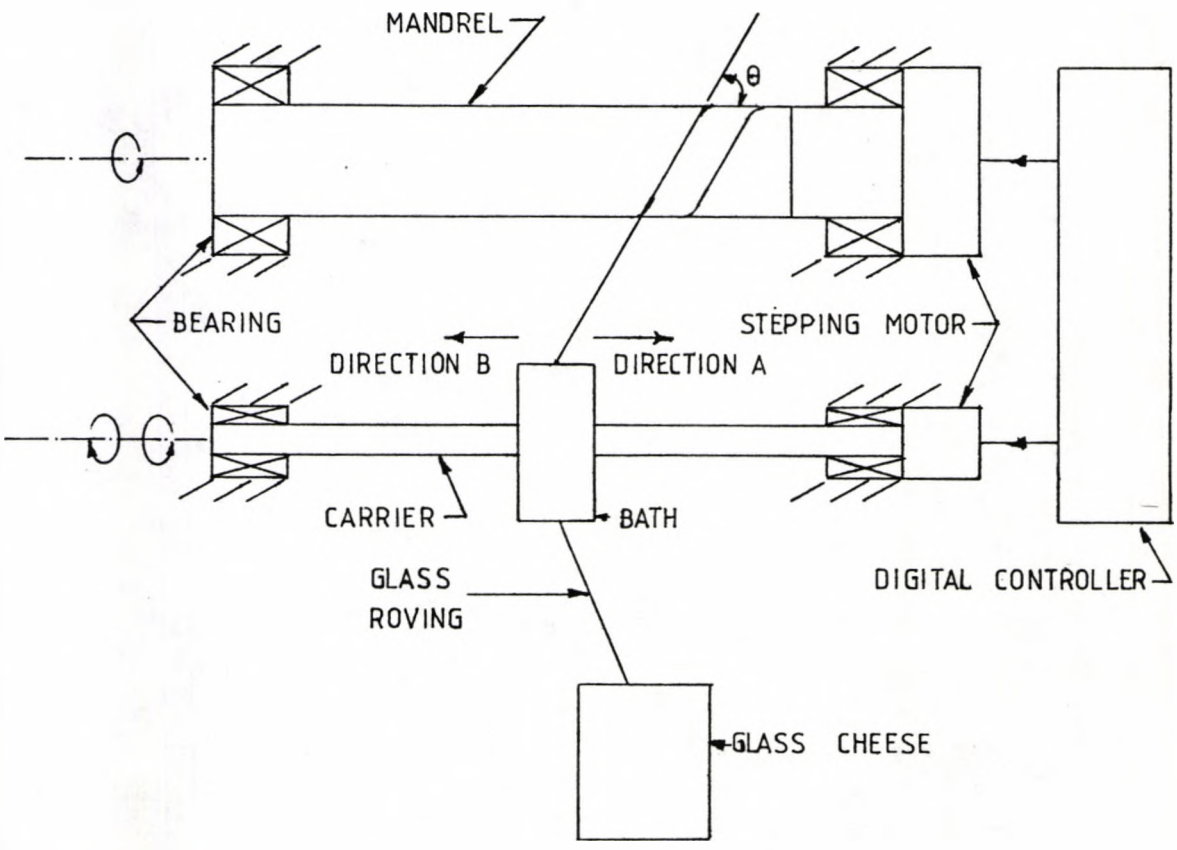

Fig 5.2.1. Filament Winding Process.

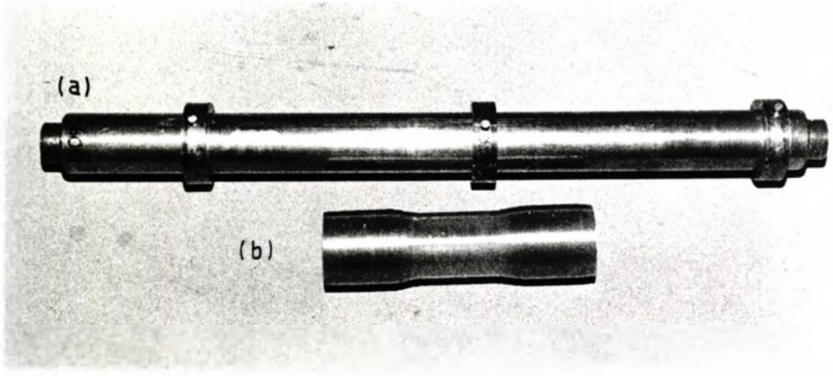

Plate 5.2.1(a) Metallic Stops and Mandrel Assembly.

(b) Hoop Wound Specimen.

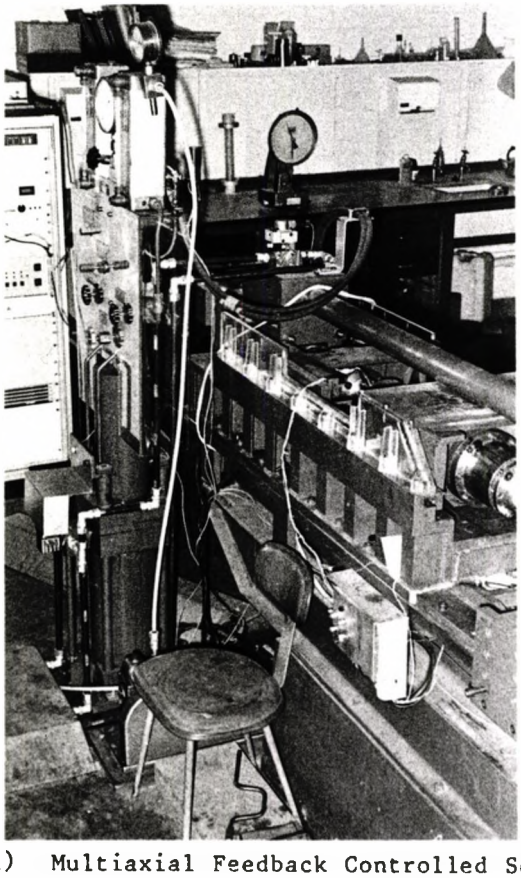

Plate 5.3.1(a) Multiaxial Feedback Controlled Servo-hydraulic Test Rig --- Test-bed.

The polyester mixture mentioned in Secton 5.2.(a) was placed in the bath. Glass roving from a cheese was drawn through the bath and wound onto a mandrel. In the process, the glass fibre was wetted with polyester mixture. The carrier, which could be made to rotate in either direction, subsequently induced the bath to move either in direction A or B. The relative motion between the mandrel and the bath could be varied to produce different winding angles θ shown in fig 5.2.1. The movements of the mandrel and the bath were controlled by the digital controller.

In the present work, the winding angle $\theta = 89.5^{\circ}$ was chosen. The tube produced at this angle is known as a hoop wound tubular specimen. Metallic stops, shown in fig. 5.2.2, were placed on the mandrel to obtain specimens of the required length. More important, these stops enabled the end-faces of a specimen to be perpendicular to its axis (see fig 5.2.3). Prior to the winding process, the stops and the mandrel were covered with a layer of releasing agent to prevent the polyester mixture from sticking onto them permanently.

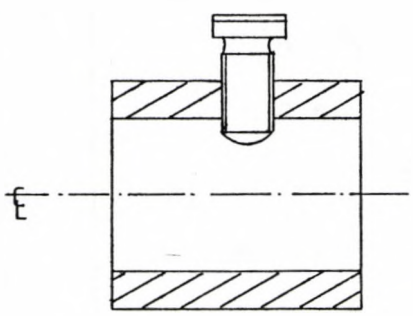

Fig 5.2.2 Metallic Stops

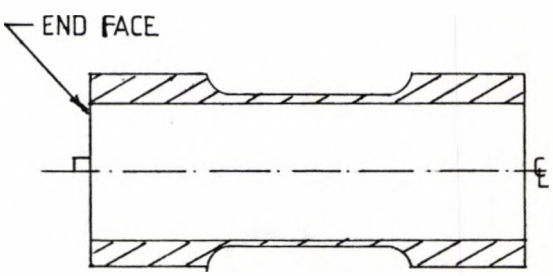

Fig 5.2.3. Hoop Wound tube.

The assembly of metallic stops and the mandrel is shown in Plate 5.2.1(a). In a hoop wound tube, the mandrel was covered completely by every layer of winding. When the winding process was completed the mandrel was kept rotating by a spinner until the polyester resin

mixture had gelled. The gelling stage took about 5 hours to complete. Gelling means that the polyester resin turned from a liquid into solid state. The gelled tube, while still on the mandrel, was post cured at 80° C for 4 hours. It was then let to cool down. The heating and cooling cycle was carried out gradually to reduce the thermo-residual stress build-up in the specimen. At room temperature the hoop wound tube was removed from the mandrel with the aid of a pneumatic press as illustrated schematically in fig 5.2.4. The hoop wound tubes in the present work were each a true lamina.

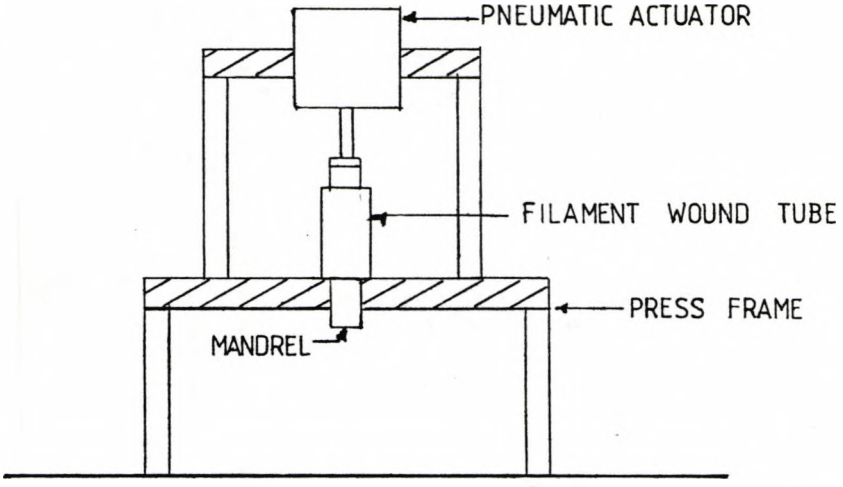

Fig 5.2.4. Pneumatic Press.

5.2(c) Reinforcement of the Ends of the Specimen:

A tubular structure is, in general, a strong structure. To test it upto failure requires a pair of end-grips which can effectively transmit the loads from the test rig onto the test section of the tubular specimen. Due to the buckling problem the gauge length of the tubular specimen is usually kept to the minimum. This was to ensure that no buckling occurred prior to material failure. In order to induce fracture at the gauge length, end reinforcements must be provided at both ends of the specimen. Daniel et al. (1980), Duggan &

Bailie (1980) and Guess & Haizlip (1980) have carried out finite element analyses on the stress distribution in composite specimens with various forms of end reinforcements. They reported stress discontinuities in the transition between the reinforced end and the test section of the specimen. Daniel et al. (1980) and Duggan & Bailie (1980) suggested means of minimizing the stress discontinuities.

All the hoop wound specimens used were reinforced at their ends by further hoop winding while the specimens were in the pre-gelled stage. The glass used for this purpose was 2400 tex E-glass; the resin mixture was the same as that used in making the specimen. It was found that this type of reinforcement worked satisfactorily. Most specimens failed at the test section. Plate 5.2.1(b) shows the appearance of a typical hoop wound specimen.

5.2(d) Dimensions and Configuration of the Specimens:

According to Pagano & Whitney (1970) the stress field across a highly anisotropic cylinder is far from uniform. Using an approach which consists of combining a modified plane strain elasticity solution and shell theory, Pagano & Whitney (1970) carried out a parametric study on different composite materials. This study was used as a guideline for deciding on the dimensions of the hoop wound specimens.

The dimensions and configurations of the hoop wound specimens were as shown in Table 5.2.2 and fig 5.2.5 respectively.

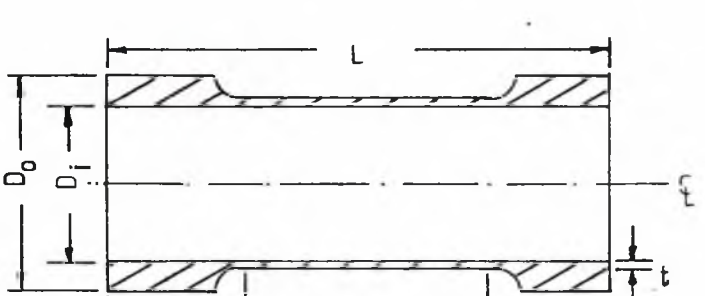

Fig 5.2.5 Configuration of The Hoop Wound Specimen.

Table 5.2.2. Dimensions of Hoop Wound Specimens:

Specimen Group	L mm	D_o mm	D_i mm	l_e mm	l_g mm	t mm
A	320	88.9	76.0	76.5	167	1.5 to 1.9
B	320	88.9	76.0	90.0	140	1.7
C	320	88.9	76.0	90.0	140	1.3
D	320	88.9	76.0	90.0	140	1.4
E	320	88.9	76.0	90.0	140	1.7
F	320	88.9	76.0	105.0	110	1.7
G	320	88.9	76.0	105.0	110	1.9
H	320	88.9	76.0	105.0	110	1.9

Specimens in groups A to C were made from 2400 tex 'Equirove' glass and those in groups D to H were made with 1200 tex 'Equirove' glass. It was found that buckling occurred in specimens from groups C and D. The buckling took place while the specimens were being tested in the torsion & compression mode. All specimens subsequently made were to have an average wall thickness of 1.7 to 1.9 mm and a gauge length of 110 to 140 mm.

The internal and external diameters of the ends of the specimens were measured using a pair of calibre. The wall thickness of the specimens was measured using a device described by Legg (1980), which is illustrated in fig 5.2.6.

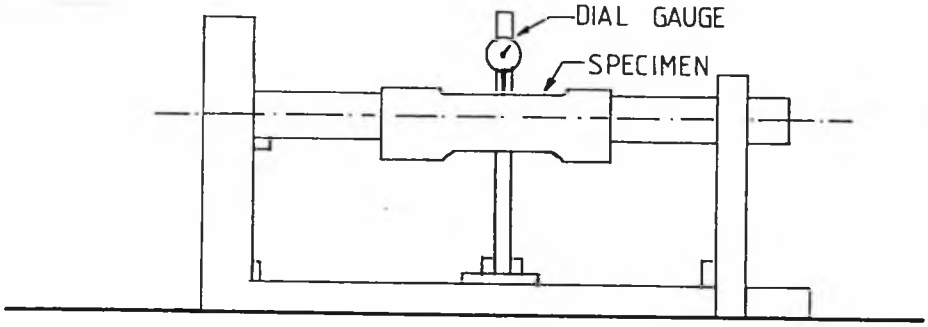

Fig 5.2.6. Wall Thickness Measuring Device.

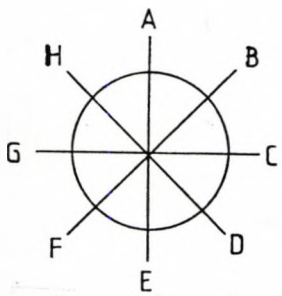

Fig 5.2.7(a) End-view of a Specimen.

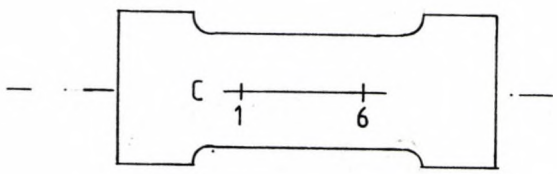

Fig 5.2.7(b) Side-view of a Specimen.

Each specimen was marked with 8 points at equal intervals. A line parallel to the specimen axis was drawn through each point shown in fig 5.2.7(a). At the gauge length the line was marked with 6 points at equal intervals as illustrated in fig 5.2.7(b). The wall thickness of the specimen was measured at these points. Therefore, 48 wall thickness readings were obtained for each specimen. Four internal diameter readings were taken at each end of a specimen. They were taken across points A & E, B & F, C & G etc, as can be seen from figure 5.2.7(a).

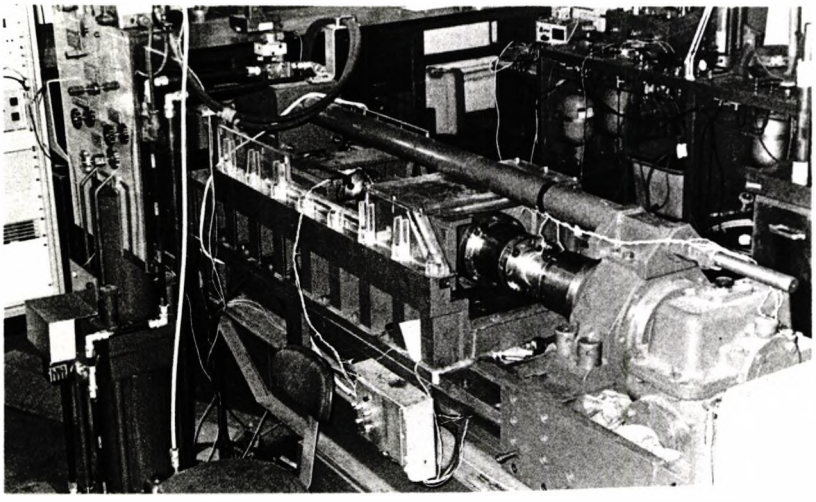

Plate 5.3.1(a) Multiaxial Feedback Controlled Servo-hydraulic Test Rig --- Test-bed.

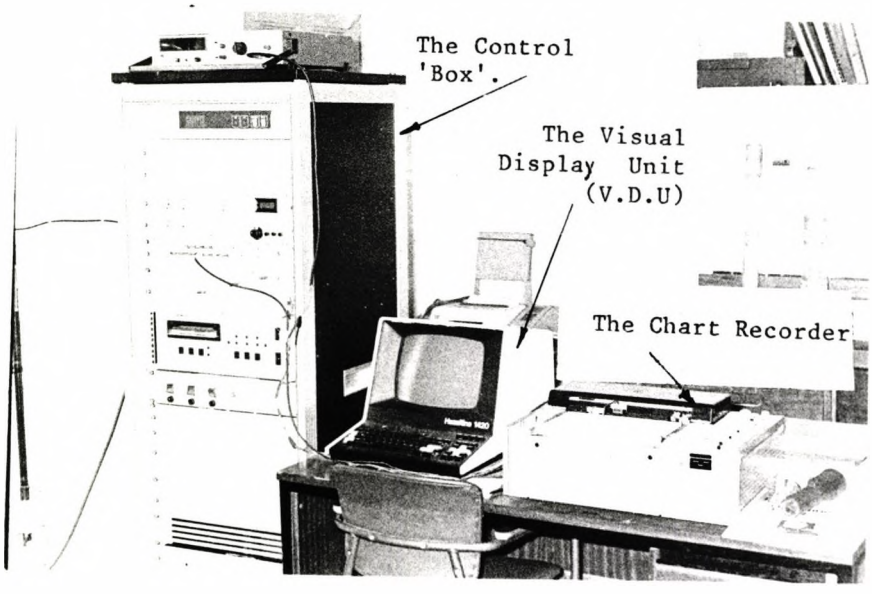

Plate 5.3.1(b) Multiaxial Test Rig ---- Control System.

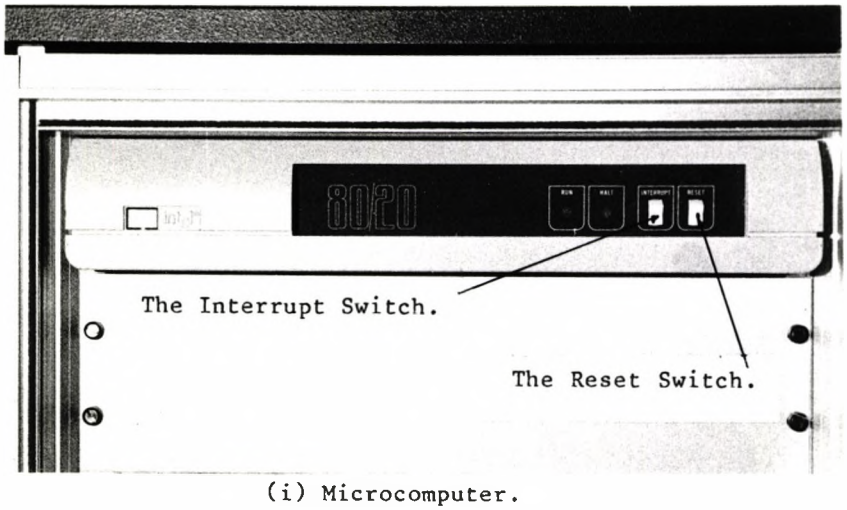

(i) Microcomputer.

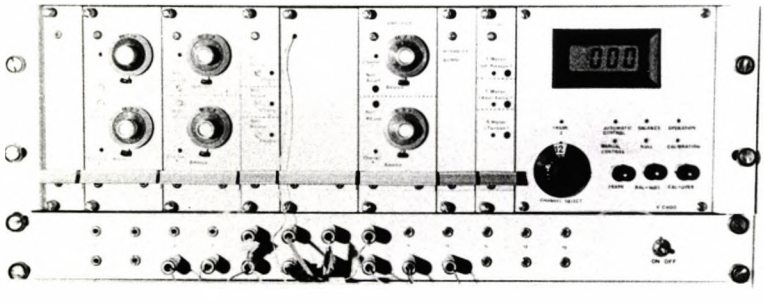

(ii) Interface Unit.

(iii) Perex Recorder.

Plate 5.3.1(b)

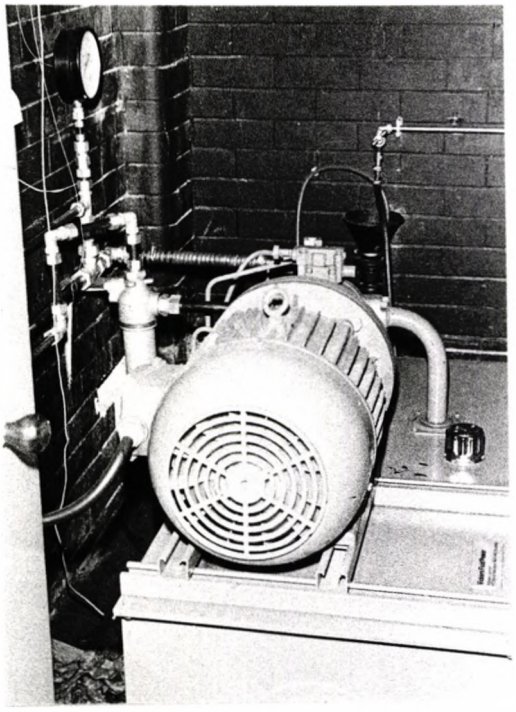

(i) The Hydraulic Pump

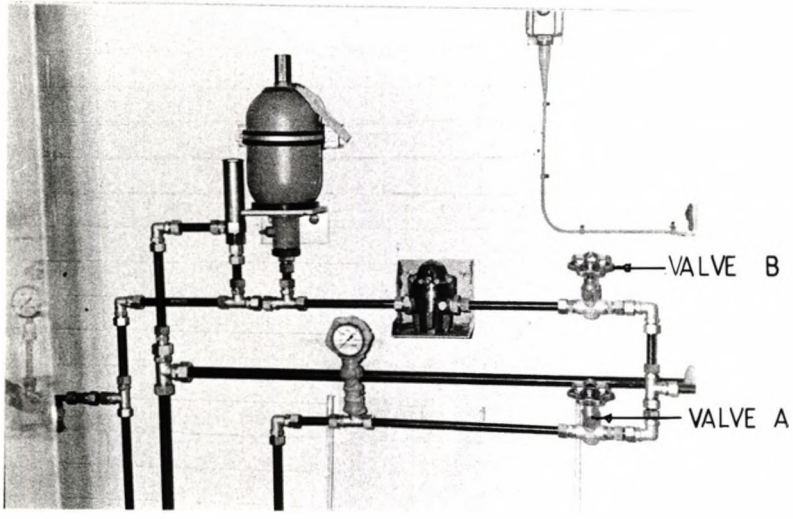

(ii) The Hydraulic Power Lines.

Plate 5.3.1(c) Multiaxial Test Rig ---- Hydraulic Power Pack.

5.3 Testing Procedures

When the test rig was first switched on it was allowed to warm up. The control system usually took 15 to 30 minutes to reach the steady temperature state, whereas, the hydraulic system required longer than 30 minutes. For ease of description a schematic drawing of the test rig in block diagram form is shown in fig 5.3.1. For more detail on the test rig, reference can be made to fig 3.1 or Plate 5.3.1.

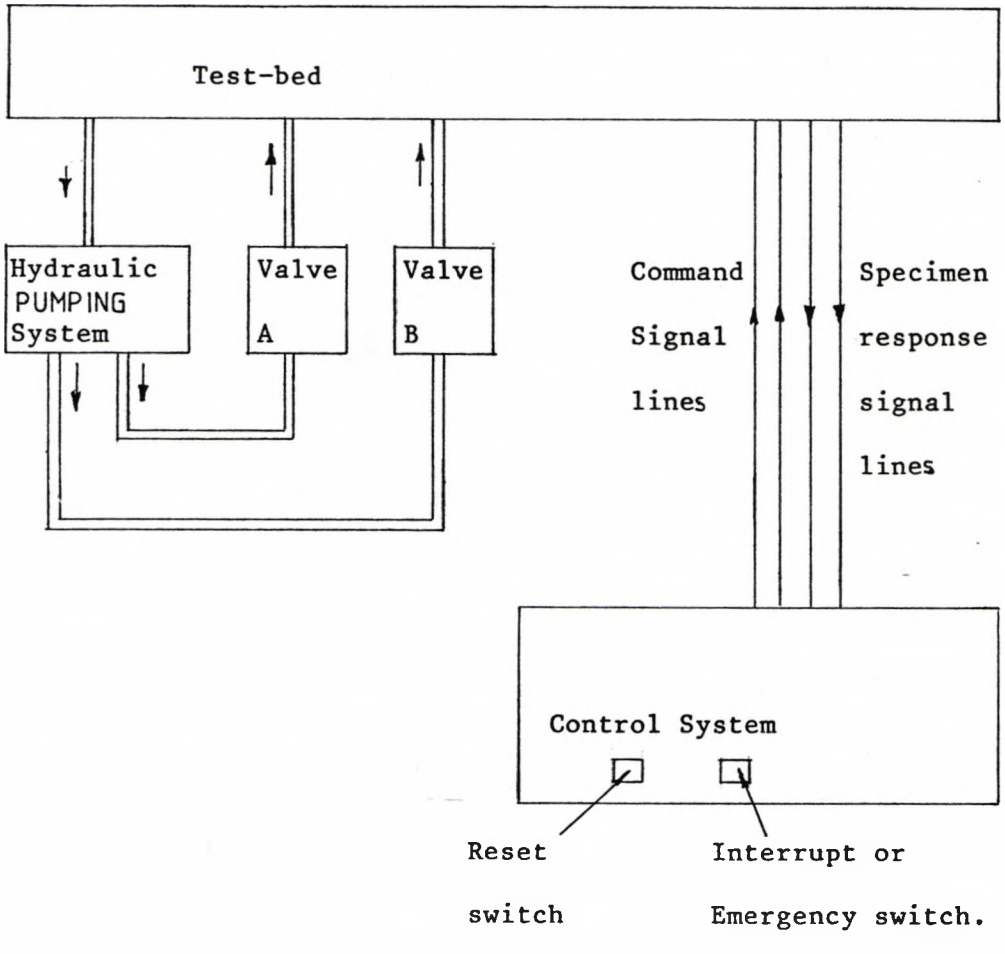

Fig 5.3.1. Block Diagram Representation of the Multiaxial Test Rig.

For tests involving internal pressure the cross-bar, shown in fig 5.3.4, was placed into position to take the axial force generated by the internal pressure. Consequently, the internal pressure exerted only hoop stress on the specimen. A vacuum was created in the specimen with a vacuum pump prior to filling the specimen with fluid for pressurization. A protective screen made of steel and polycarbonate plates was used to contain the expected explosion of the specimen. The transparency of the polycarbonate allowed the progress of the specimen under stress to be observed right up to failure. The assembly of the end thrust elimination device is shown schematically in fig 5.3.4.

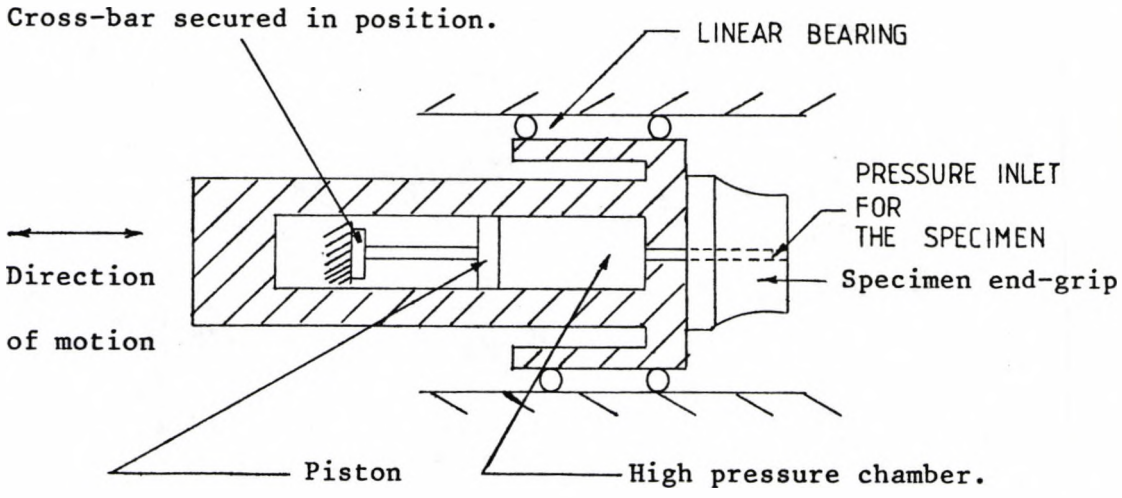

Fig 5.3.4. End Thrust Elimination Device.

Before the hydraulic system was switched on, it was important for valves A & B to be in the 'off' position; they were then opened when the hydraulic system was running smoothly.

While the systems were warming up, the required test program was loaded into the microcomputer. The following control parameters were given to the microcomputer via the V.D.U. as follow:

(i) The data sampling rate

(ii) The first data channel to be sampled.

(iii) The last data channel to be sampled.

(iv) The name of the magnetic tape file on which experimental data were to be stored.

(v) The amplifier gain for each of the data channels to be sampled.

(vi) The loading rate. This consisted of three sub-parameters for axial force and internal pressure, viz.,

(a) the axial force incremental step

(b) the internal pressure incremental step

(c) the time interval for each increment.

With these sub-parameters the microcomputer would generate the ramp loading as shown in fig 5.3.2 with loading rate determined by the load incremental step and the time interval for each increment.

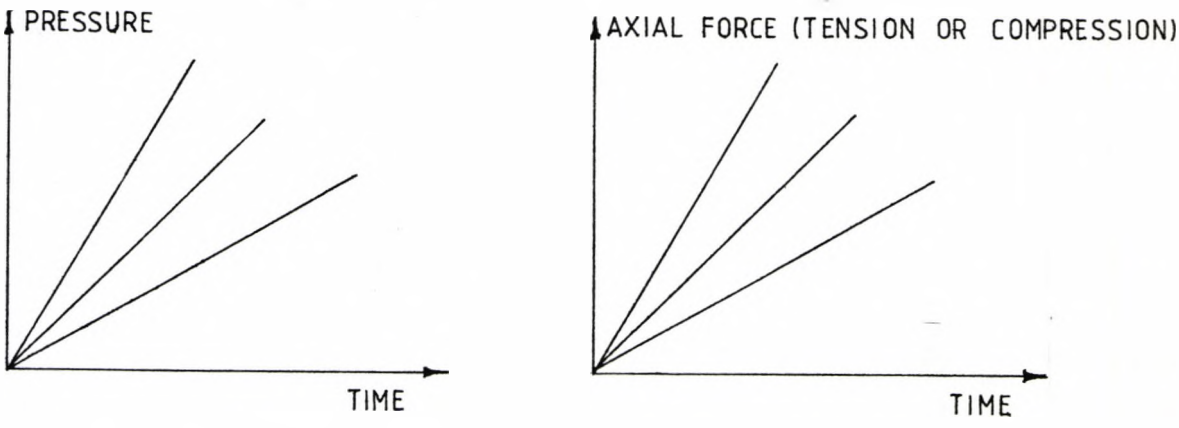

Fig 5.3.2. Ramp Loading Mode.

At the time of experimental work, no torque feedback control program was available. Therefore, for shear test the constant end-grip

angular displacement rate was used. To achieve this two sub-parameters were typed into the microcomputer.

(d) the step mode; this determined whether to twist the specimen in clockwise or anticlockwise direction.

(e) the end-grip angular displacement rate.

(vii) Hold factor. This parameter was necessary only in tests that involved holding the internal pressure or the axial force constant at certain stages of the test. This facility was available for pressure and axial force loading only.

(viii) Lag factor. In tests where one load started later than the other, this parameter was required. It was irrelevant to other test modes. Apart from the test program two more programs were also needed to be loaded into the microcomputer. They were:

(a) the system initialising program,

(b) the data sampling program.

During the specimen mounting stage the multiaxial test rig was in manual control mode. By bringing the end-grips to the correct position the specimen was then secured on this pair of end-grips. The complete assembly of specimen and end-grips is as shown in fig 5.3.3 and Plate 5.3.1.

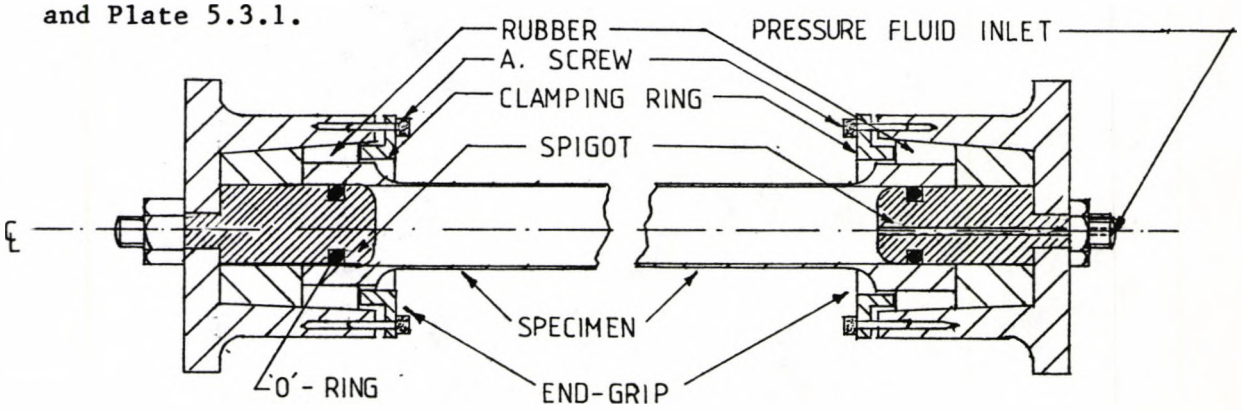

Fig 5.3.3. Assembly of Specimen With End-grips.

In tests where strain gauges were required, they were connected to the control system at this stage. The test began when a run command was issued to the microcomputer.

Test programs (Choo (1982)) shown by figures 5.3.5 to 5.3.10 were used in the experimental work. All these programs were run in conjunction with all the subroutines explained in Chapter 4. The data sampling procedure and test stoppage on specimen failure were carried out through interrupt operations explained in Chapter 4. The functions of initialisation of the control system have also been described in Chapter 4. The loading mode of each program has been illustrated next to each flow chart. The detailed program represented by each flow-chart can be found in Choo (1982). The notation used in the loading mode diagrams assumed the following convention shown in fig 5.3.11.

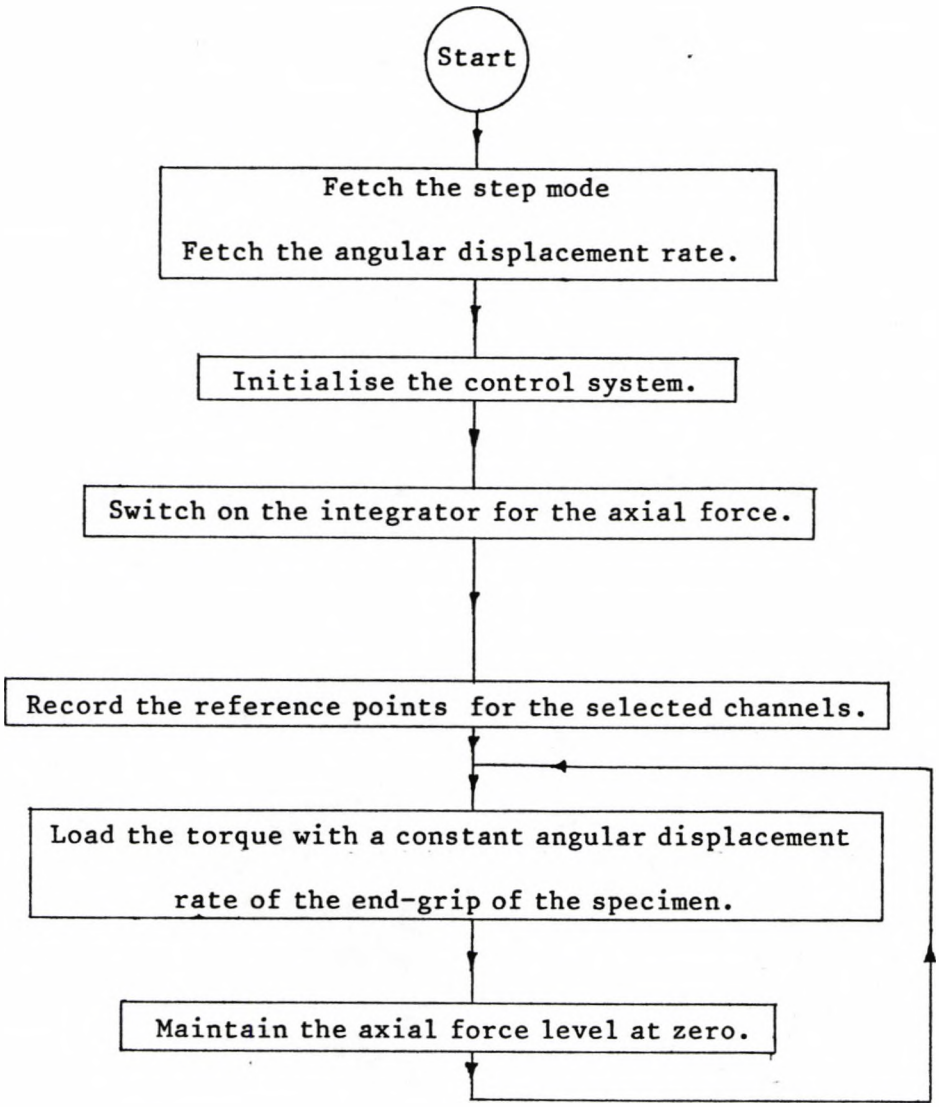

Fig 5.3.5 Pure Shear Test Program Flow-chart.

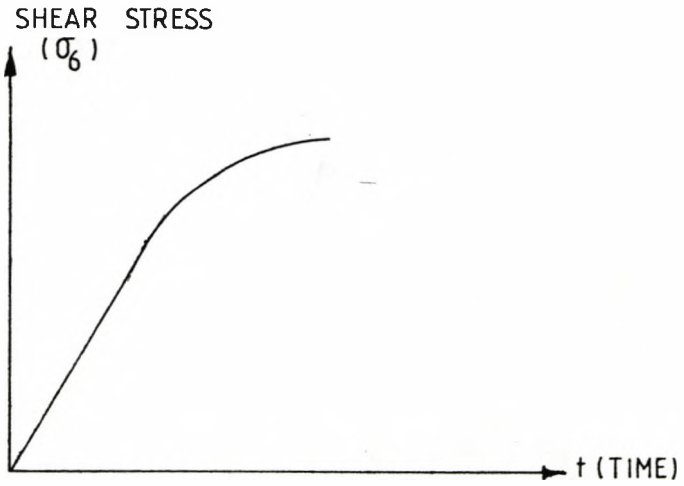

Fig 5.3 5(i) Loading mode.

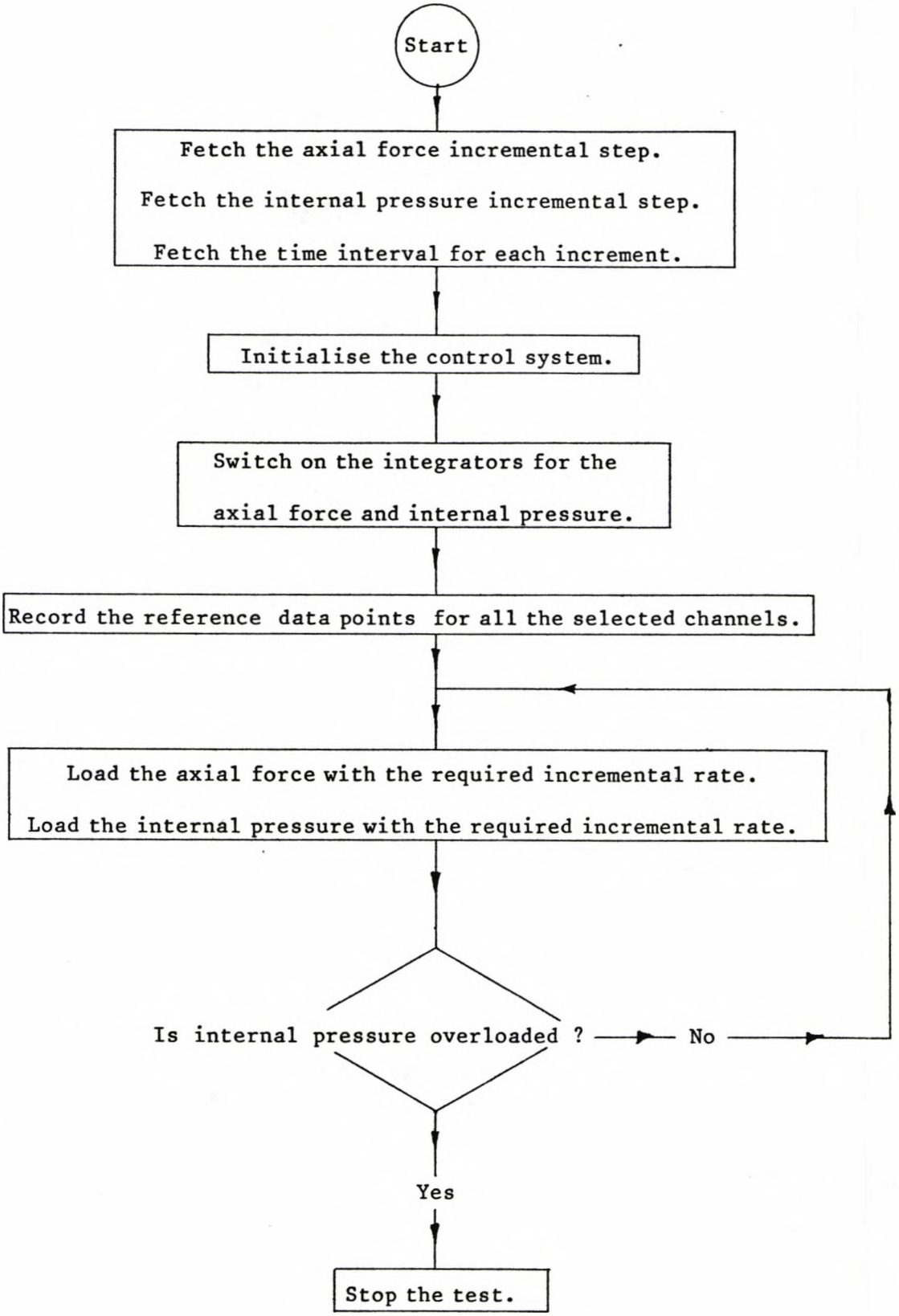

Fig 5.3.6 Axial Force & Internal Pressure Test Program Flow-chart.

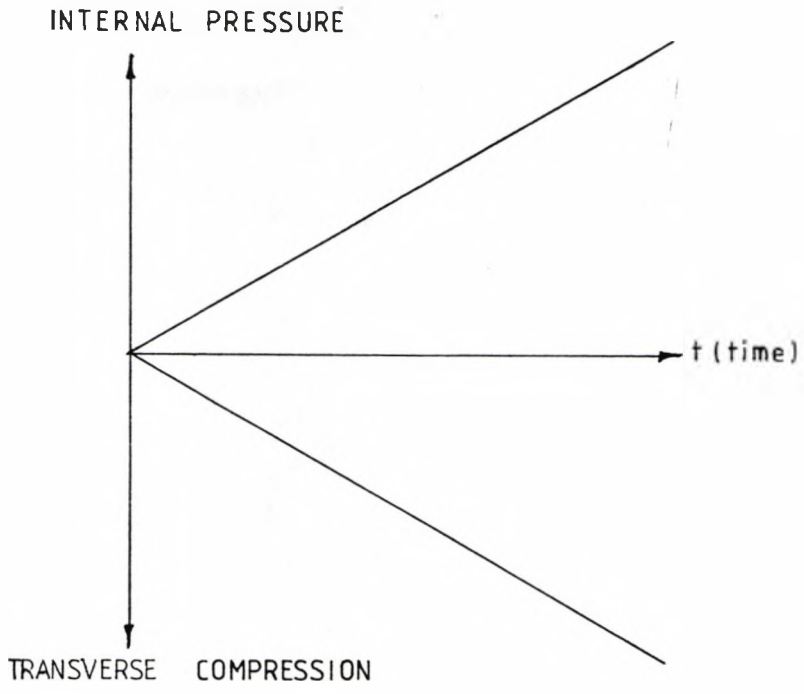

Fig 5.3.6(i) Internal Pressure & Compression Loading Mode.

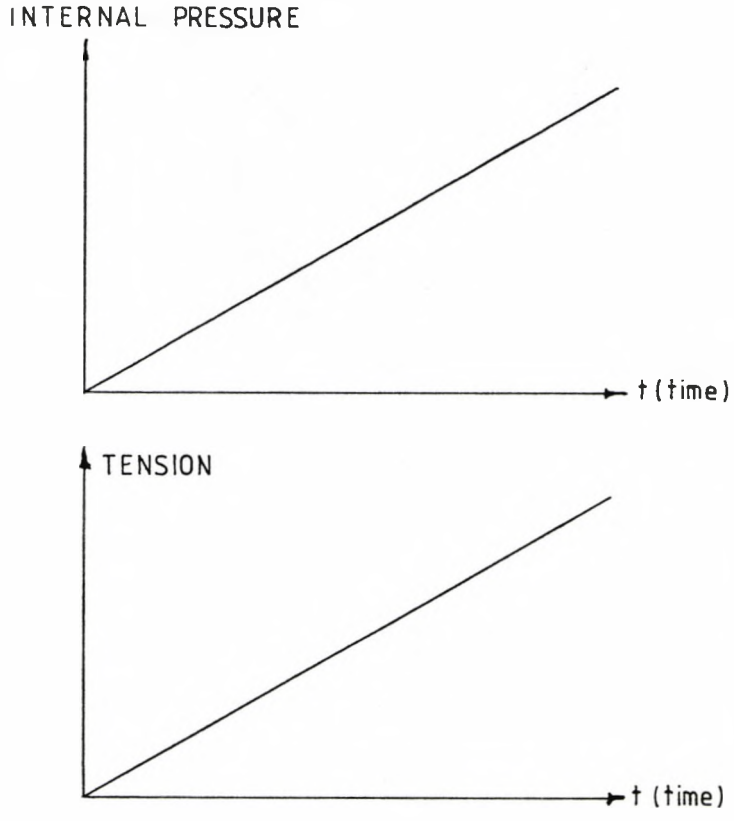

Fig 5.3.6.(ii) Internal Pressure & Tension Loading Mode.

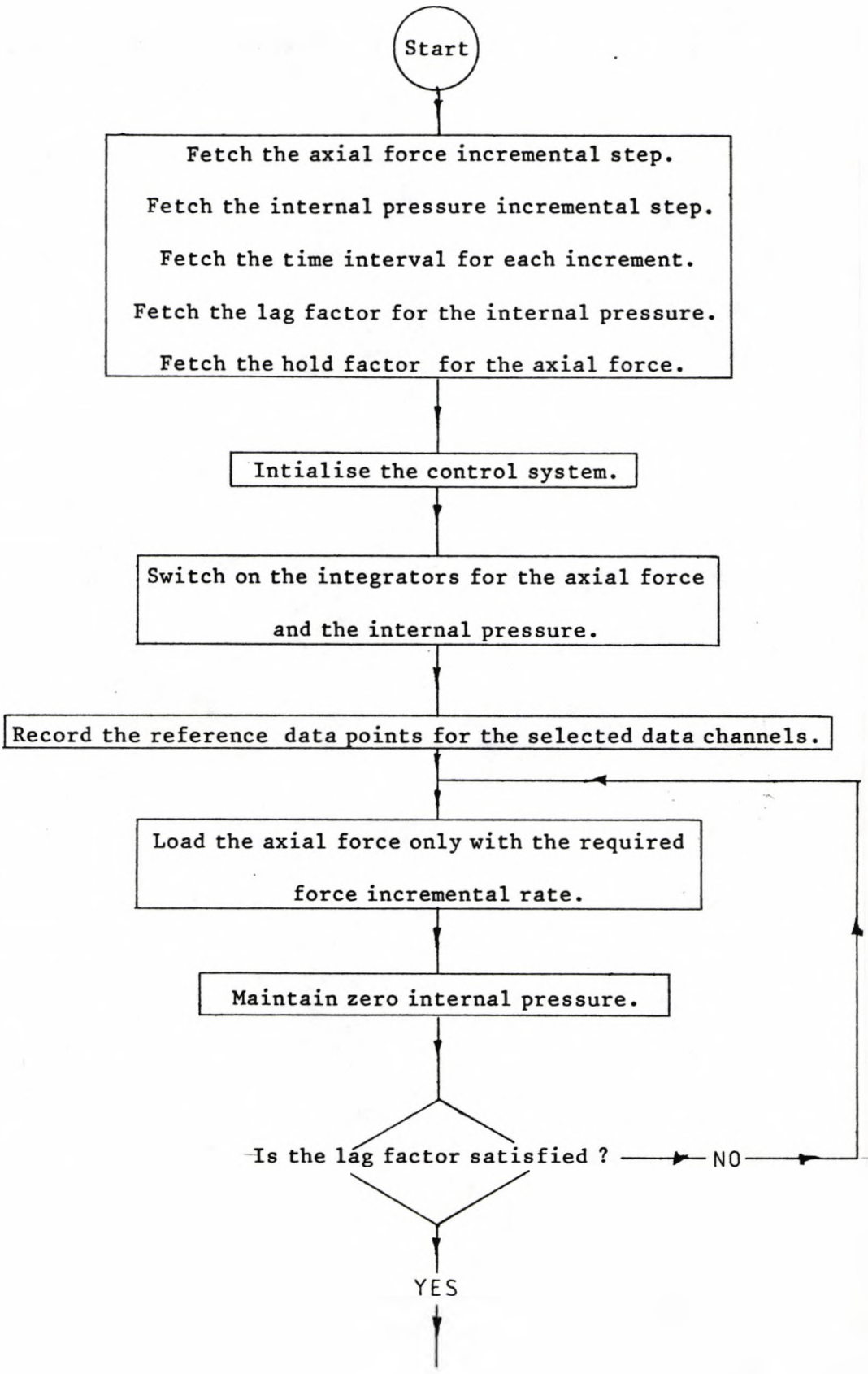

(Continued in next page)

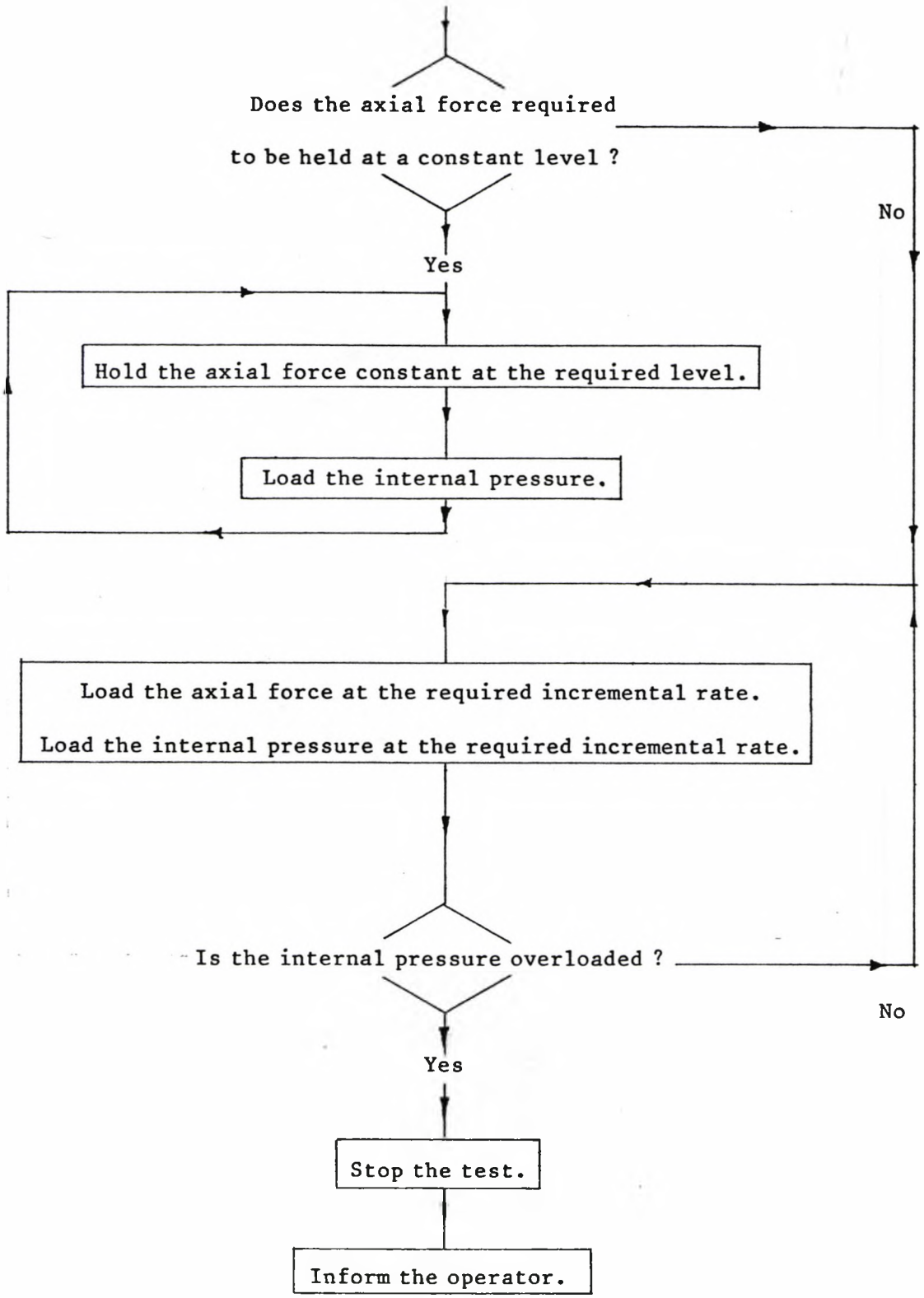

Fig 5.3.7 Axial force & Internal Pressure Test Program Flow-chart With Lag and Hold Facilities for the Internal Pressure and Axial Force Respectively.

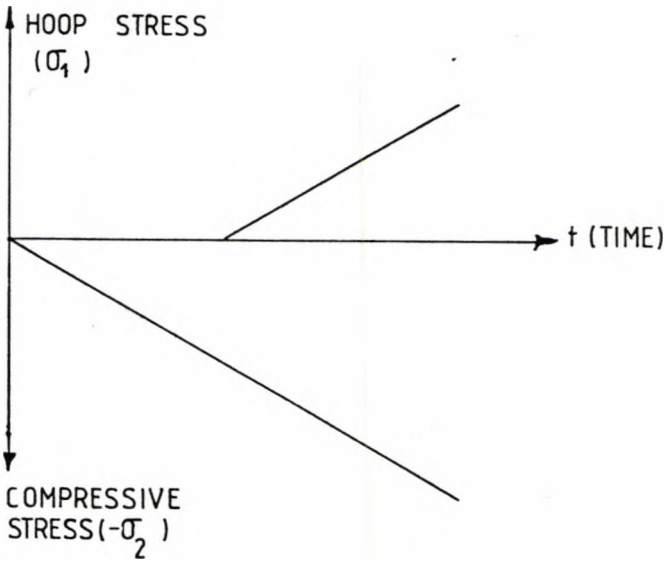

Fig 5.3.7(i) Loading Mode With Lag On σ_1.

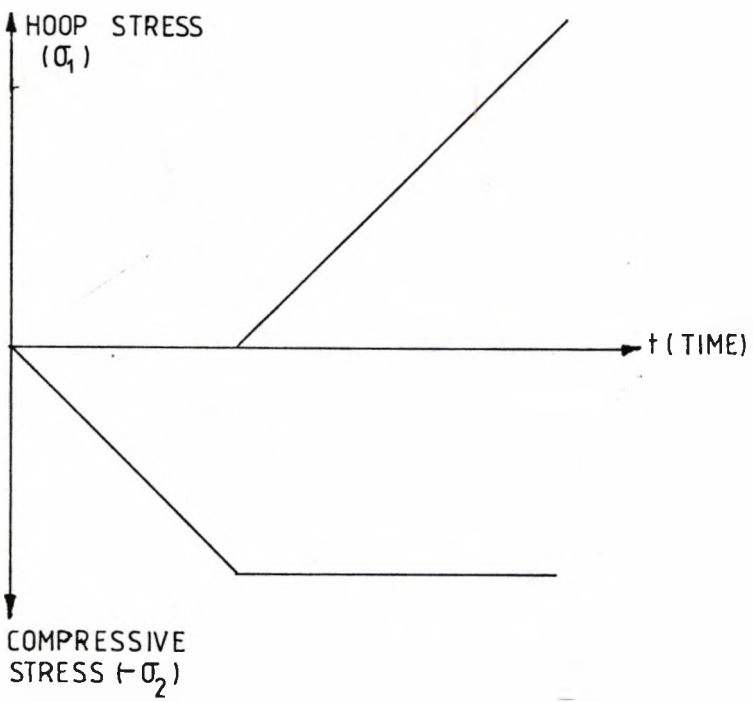

Fig 5.3.7(ii) Loading Mode With Lag On σ_1 and Hold On $-\sigma_2$.

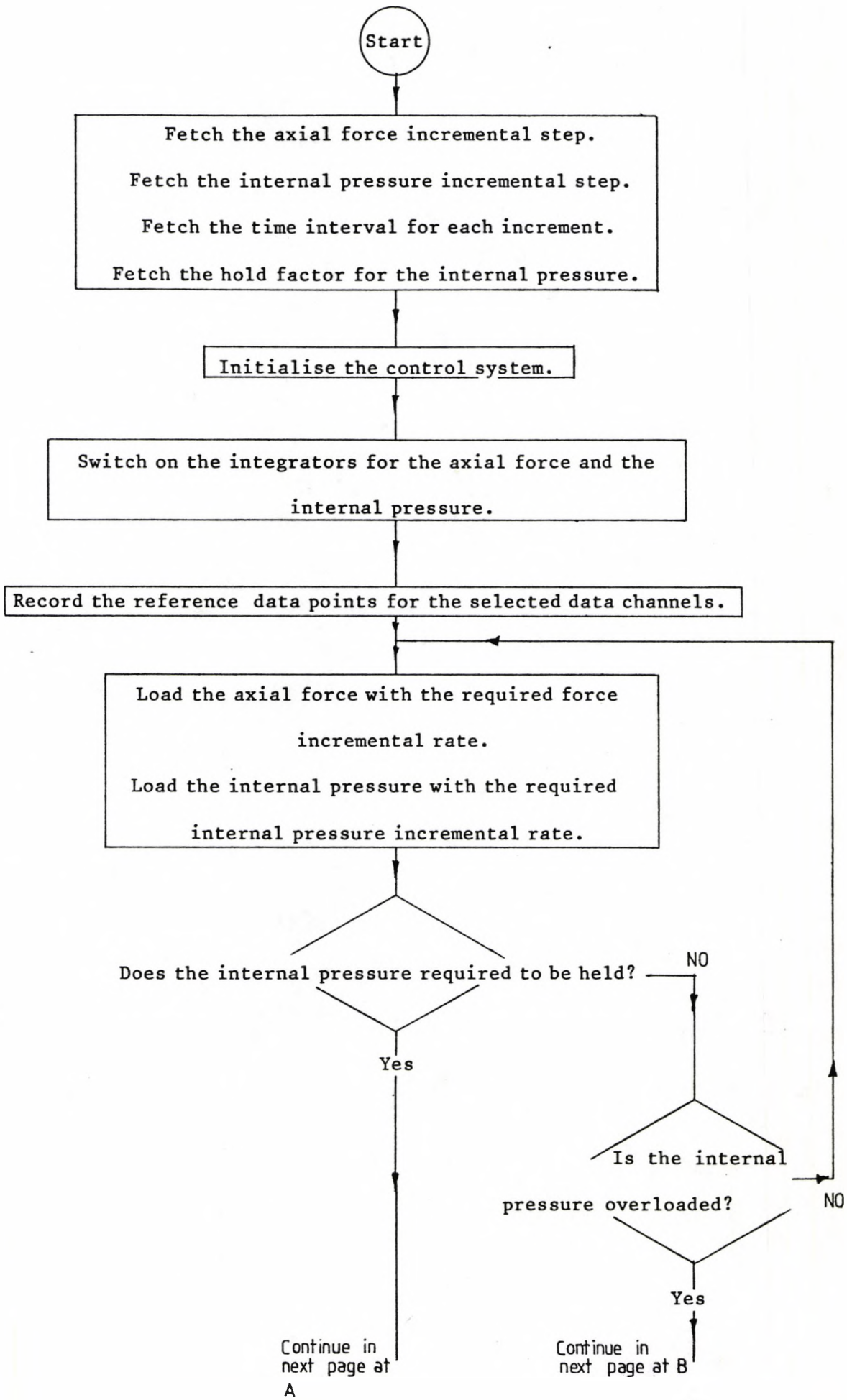
Start
Fetch the axial force incremental step.
Fetch the internal pressure incremental step.
Fetch the time interval for each increment.
Fetch the hold factor for the internal pressure.
Initialise the control system.
Switch on the integrators for the axial force and the internal pressure.
Record the reference data points for the selected data channels.
Load the axial force with the required force incremental rate.
Load the internal pressure with the required internal pressure incremental rate.
Does the internal pressure required to be held?
NO
Yes
Is the internal pressure overloaded?
NO
Yes
Continue in next page at A
Continue in next page at B

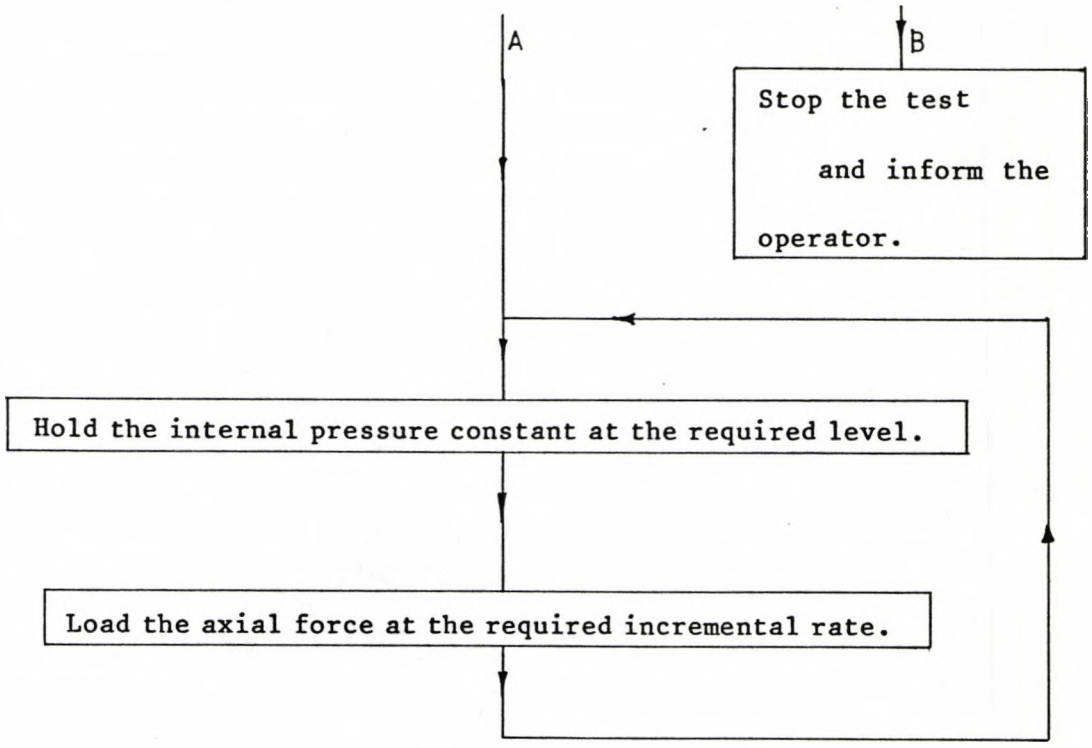

Fig 5.3.8 Axial Force & Internal Pressure Test Program Flow-chart With Hold Facility for the Internal Pressure.

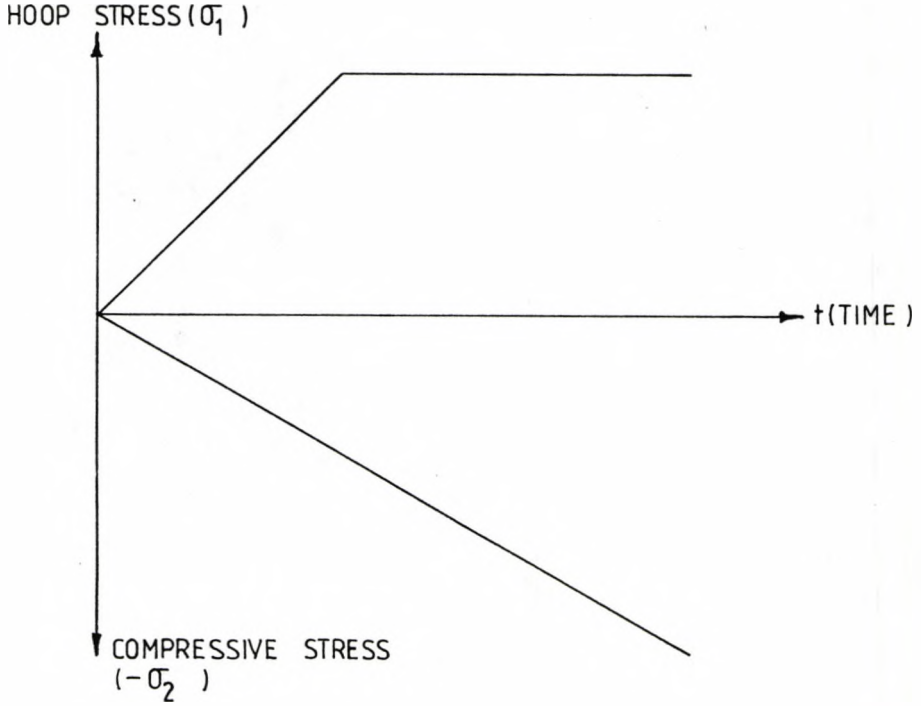

Fig 5.3.8.(i) Loading Mode with Hold On σ_1 .

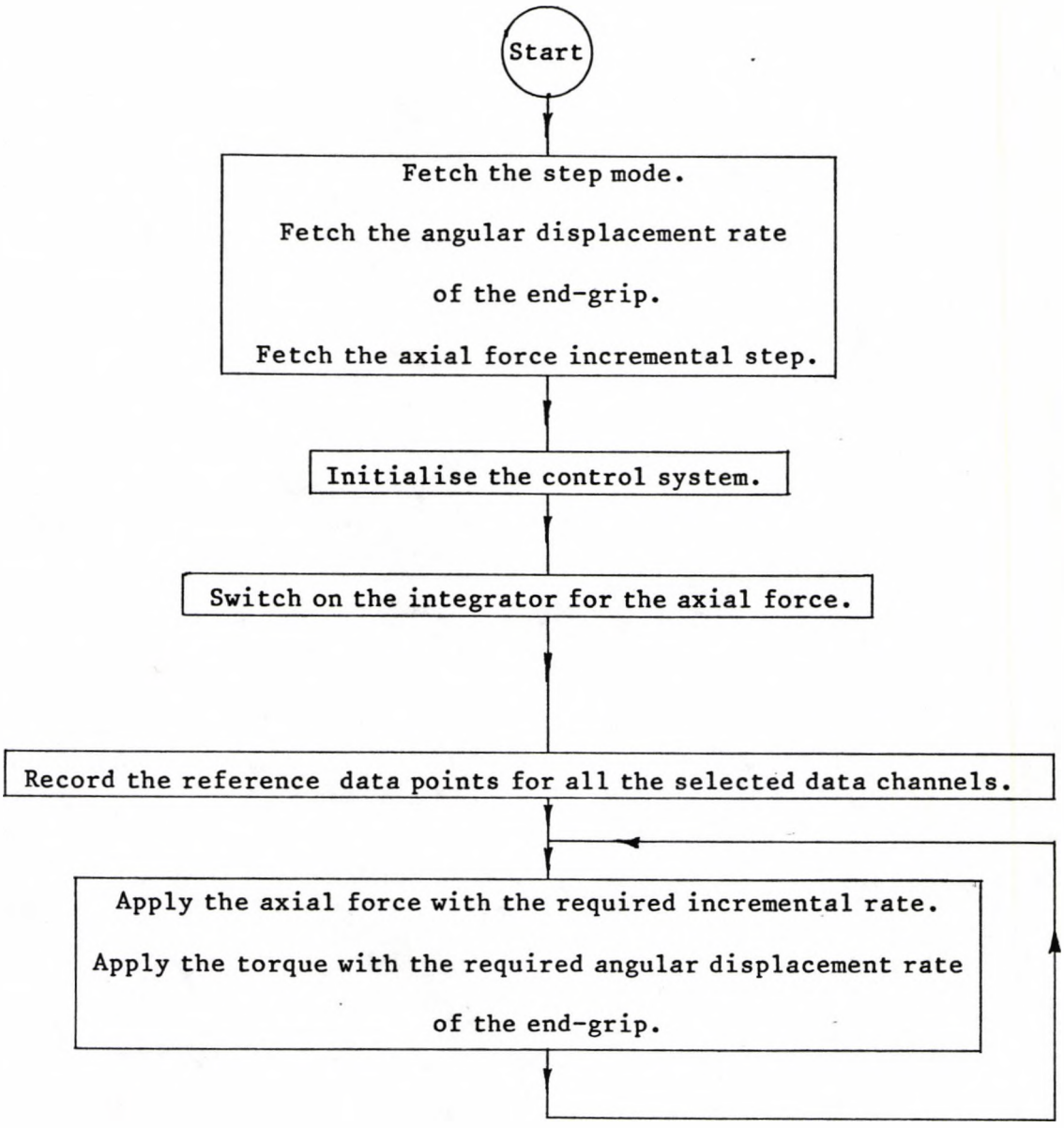

Fig 5.3.9 Axial Force & Torsion Test Program Flow-chart.

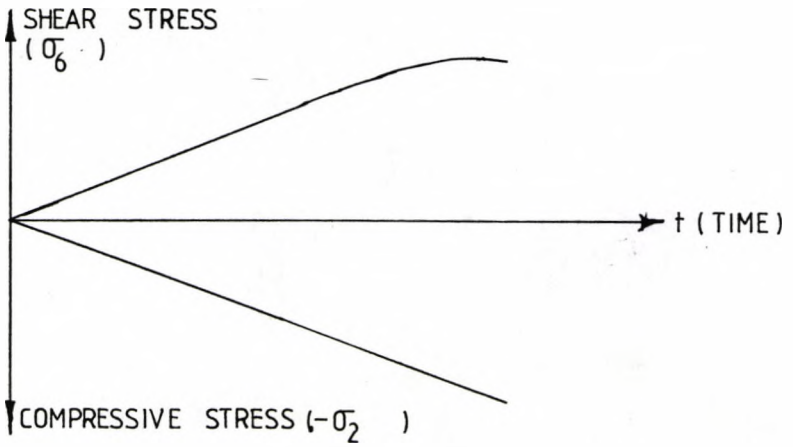

Fig 5.3.9(i) Axial Force & Torsion Loading Mode.

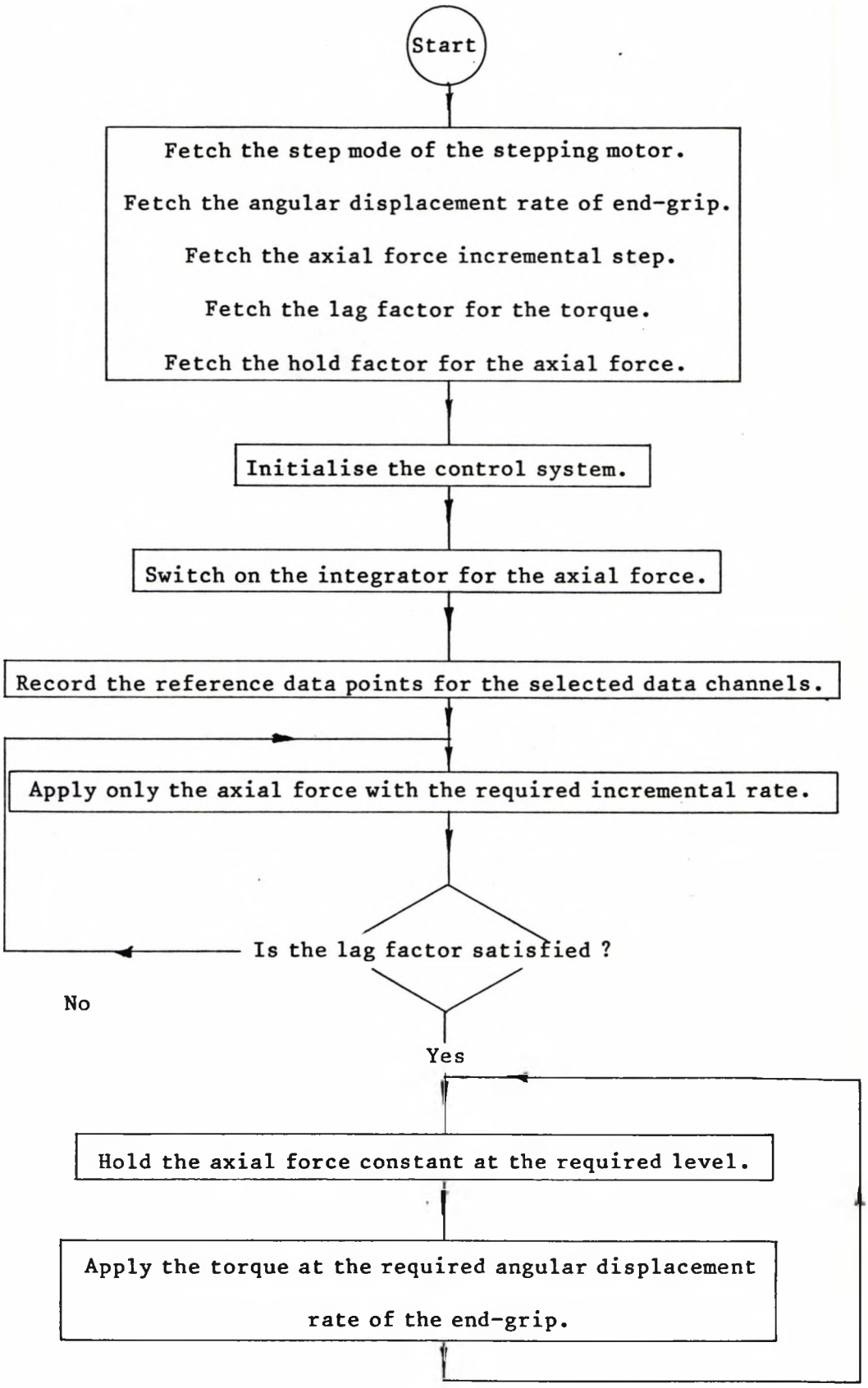

Fig 5.3.10 Axial Force & Torsion Test Program Flow-chart with Hold Facility for the Axial Force.

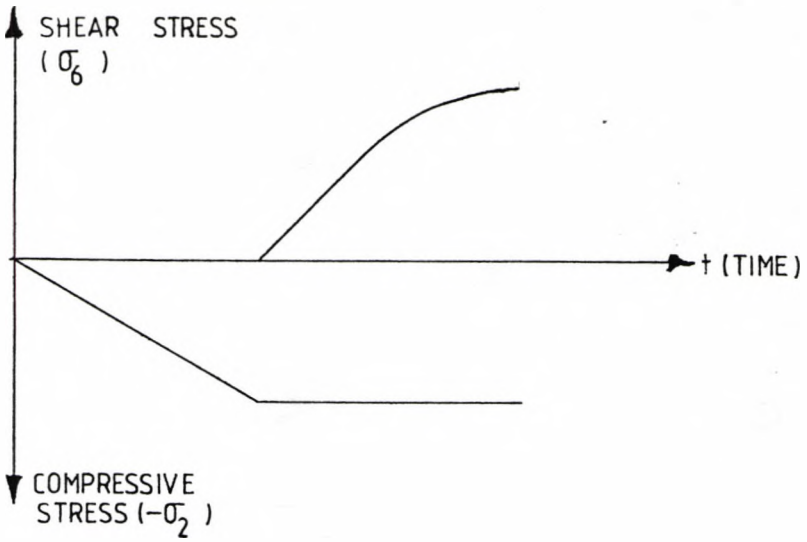

Fig 5.3.10(i) Axial Force & Torsion Loading Mode.

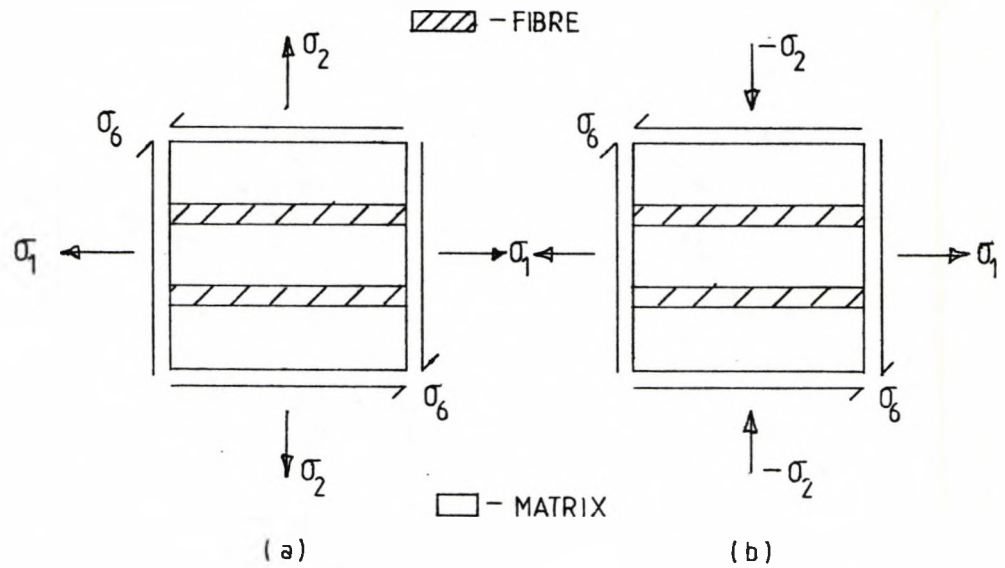

Fig 5.3.11 Notation Convention of Stresses Acting on An Element of The Unidirectional Lamina.

Loading modes shown in figures 5.3.6.(i), 5.3.7(i)&(ii), 5.3.8(i), 5.3.9(i) and 5.3.10(i) were utilised to study the loading path dependency of the failure conditions of the composite unidirectional laminae.

The detailed set of operational instructions is given in the software manual (Choo (1982)).

5.4. Microscopic Examination of the Physical Fracture Surface

Scanning microscopy was carried out on the physical fracture surfaces of some specimens tested. The fracture surfaces of one half of each specimen from the selected group were marked as shown in fig 5.4.1.

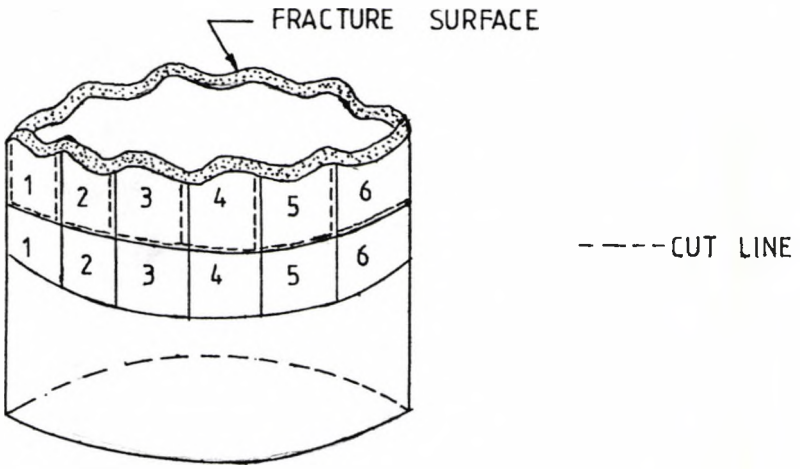

Fig 5.4.1 Marking of Fracture Surface.

Each was cut along the dotted lines. Sections of the fracture surface were removed from the rest of the specimen. All the cutting was done with a jeweller's saw. The marking was for the purpose of recognition later.

Each section of the fracture surface was washed in an ultra-sonic oscillator for about 15 minutes. Deionized water was used in the washing process. To fracture surfaces obtained from tests in which internal pressure was involved, detergent was added in the washing process to remove the layer of vegetable oil left on the surface of the specimens. In this case, each section of the fracture surface was washed in an ultra-sonic oscillator with detergent and deionized water for 20 to 30 minutes. It was rinsed with warm water and then washed in fresh detergent and deionized water for another 20 minutes.

The rinsing operation was repeated. Finally the section of the fracture surface was washed with fresh deionized water for a further 20 minutes.

Each section of a fracture surface was dried in a desiccator. It was then put into the sputter machine for a fine layer of gold to be deposited on the fracture surface. Later it was examined carefully in a scanning electron microscope.

Whenever necessary, the above process was repeated on the other half of each specimen. The location of cuts was changed so that the picture of an 'uninterfered' fracture surface could be built up.

For optical microscopy work, the region of interest was cut off from a specimen which had been tested as shown in the diagram below.

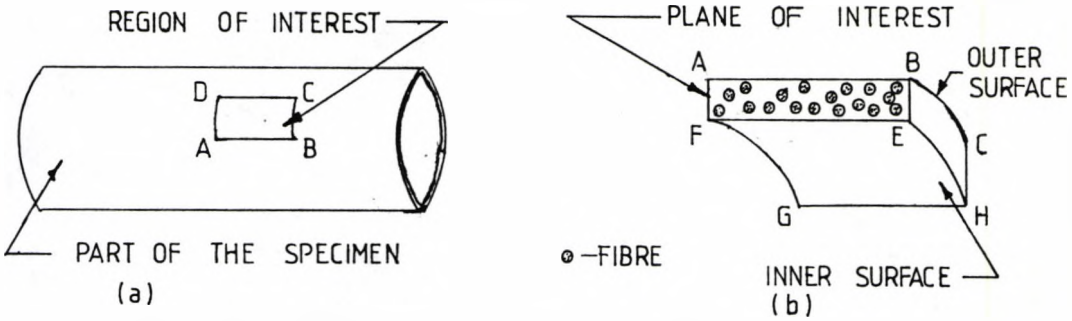

Fig 5.4.2 Section From the Region of Interest.

Figure 5.4.2(a) illustrates the region of interest. When cut, a section (fig 5.4.2(b)) was obtained. It was mounted in 'scandiplast', which cured at room temperature, so that the plane of interest (ABEF) could be polished. Plane ABEF was ground using grids of 180, 400 and 1200 sequentially. Next it was washed with alcohol using an ultrasonic vibrator for 2 minutes. This was followed by polishing from 6 down to $\frac{1}{4}$ micron using diamond paste. The washing procedure was repeated for 2 minutes at the end of each polishing stage.

However, the final wash was for about 25 minutes. The section was then dried again in a desiccator. Now Plane ABEF was ready for examination under the Reichert optical microscope.

Chapter 6:

EXPERIMENTAL RESULTS & ANALYSIS

6.1 Introduction

Hoop wound tubular specimens were used in all the experimental work throughout this project. It was relatively easy to generate a required system of biaxial stress using such specimen configuration. Under a given state of stress, a hoop wound tube was assumed to behave like a flat unidirectional lamina. The terms 'unidirectional lamina' and 'hoop wound tube' are used synonymously in the following discussion, unless otherwise stated.

The failure behaviour of laminae under the following conditions was examined:

(i) combined transverse tension and shear stress parallel to the fibre axis (σ_2— σ_6)

(ii) transverse compression ($-\sigma_2$)

(iii) pure internal pressure which produces hoop stress on the specimen (equivalent to tensile stress parallel to the fibre axis)

(iv) combined hoop stress and transverse compression (σ_1—($-\sigma_2$))

(v) combined transverse compression and shear stress parallel to the fibre axis.(($-\sigma_2$)— σ_6)

The effects of loading paths on the failure conditions of the laminae in the combined σ_1—($-\sigma_2$) and ($-\sigma_2$)— σ_6 stress spaces were studied and are discussed in Sections 6.3.1.4 and 6.4.

6.2 The $\sigma_2 - \sigma_6$ Stress Space

The failure behaviour of the unidirectional laminae in the above mentioned stress space was studied. In order to induce this combination of stresses on a lamina, a hoop wound thin wall tubular specimen was used. Transverse tension and torsion were applied to the specimen as shown in figure 6.2.1.

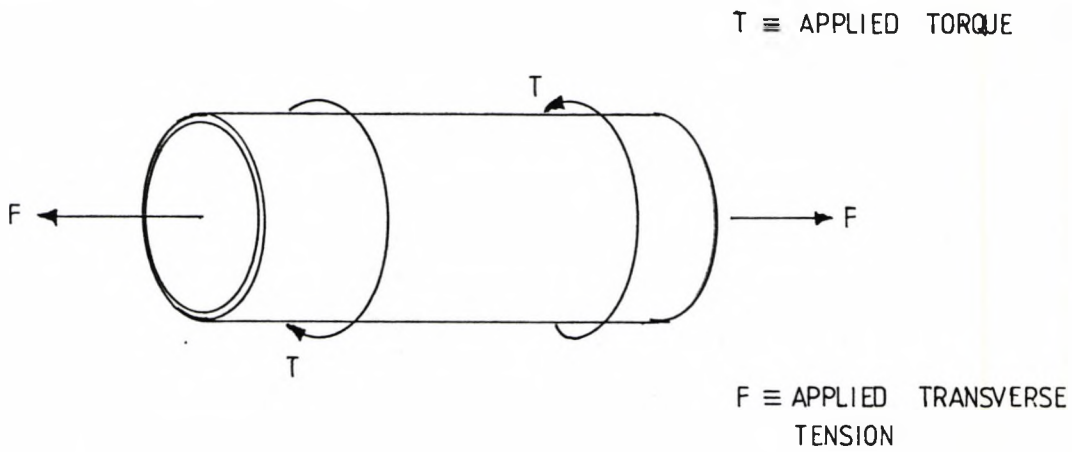

Fig 6.2.1 Hoop Wound & Thin Wall Specimen Subjected to Torsion and Transverse Tension.

From fig 6.2.1 the applied stresses existing in an element of the specimen wall are illustrated in fig 6.2.2.

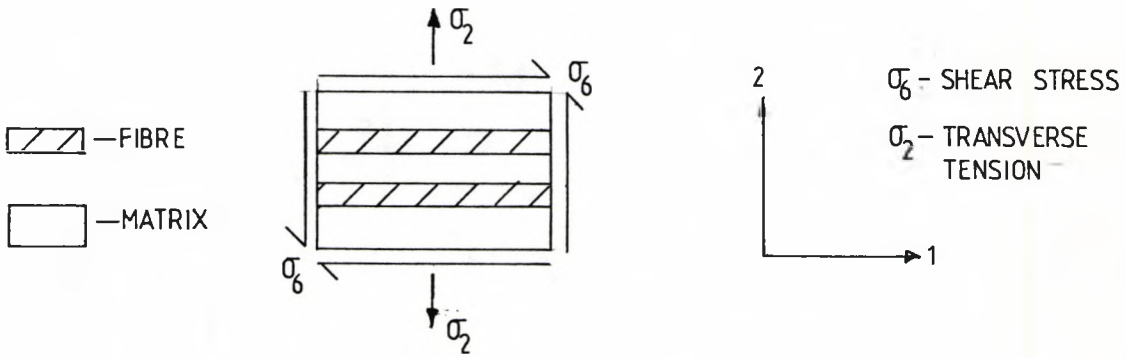

Fig 6.2.2 A Lamina Under a System of Biaxial Stress Resulting from the Applied Loads of Axial Tension & Torsion.

At the time of the experimental work no torque feedback program was available. The torsional loads were applied to the specimens by driving the stepping motor with fixed rotational speed. However, the rate of change of applied transverse tensile stress($\frac{d\sigma_2}{dt}$) was varied to produce the loading paths on the $\sigma_2 - \sigma_6$ stress space as shown in figure 6.2.3.

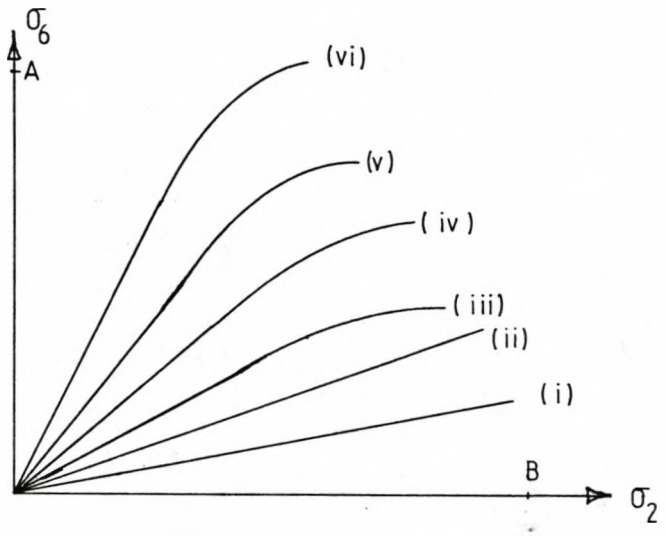

Fig 6.2.3 Paths Along which Experiments were Performed.

Experimental data points A and B were obtained by testing hoop wound tubular specimens under pure shear and pure transverse tension respectively.

An initial objective was to examine the effect of loading paths on the failure surface of a unidirectional lamina. It was decided that in order to carry out a study four sets of experiments were needed, as shown in fig 6.2.4. The failure points along paths (i), (iii), (iv) and (vi) were determined from experiments described earlier. Subsequently, experiments would be carried out along paths OFF' and OGG' etc.

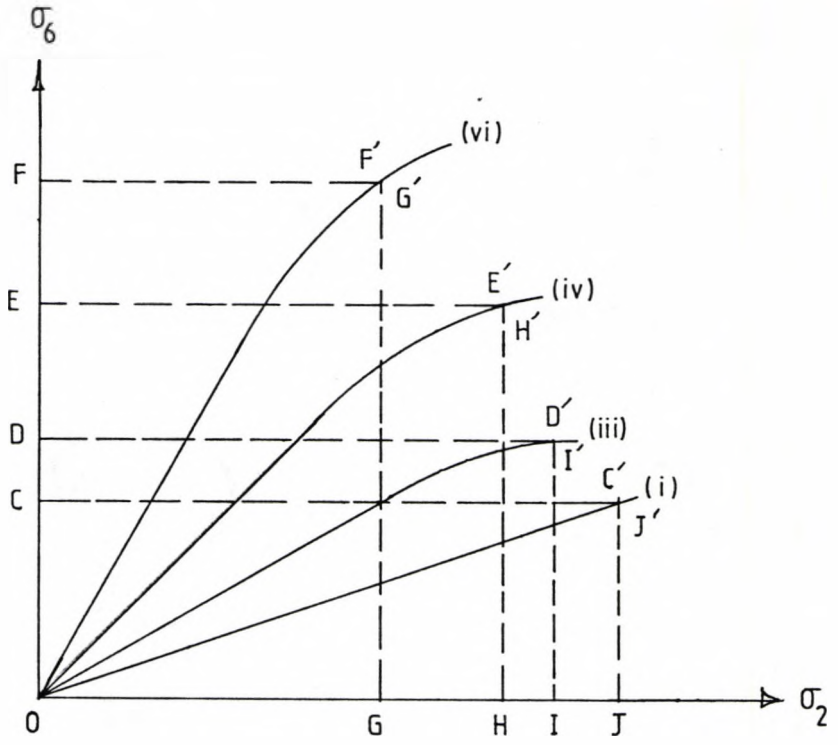

Fig 6.2.4 Loading Paths Chosen to Examine Their Effects on The Failure Surface in The $\sigma_2 - \sigma_6$ Stress Space.

The resin matrix used was 'crystic 272' and the reinforcement was 'Equirove' 2400 tex fibre.

Due to the irregularity of the outside wall, 64 specimen wall thickness readings for each specimen used in this work were recorded. The average values of internal diameter and wall thickness were used in the stress calculations. The transverse tensile stress, σ_2, was calculated using equation (6.2.1).

$$\sigma_2 = F/A \qquad .....(6.2.1)$$

where F is the applied transverse tension

and A is the cross-sectional area of the specimen.

The shear stress, σ_6 , was evaluated from equation (6.2.2)

$$\sigma_6 = 3T/(2\pi a^3(1 - (b/a)^3)) \qquad .....(6.2.2)$$

Where T is the applied torque

$\bar{d}_i$ is the average internal diameter of the specimen.

$\bar{t}$ is the mean wall thickness of the specimen.

$$a = (\bar{d}_i/2) + \bar{t} \qquad .....(6.2.3)$$

$$b = (\bar{d}_i)/2 \qquad .....(6.2.4)$$

The derivations of equations (6.2.1) and (6.2.2) were based on the equilibrium of the system (specimen). Therefore, they are valid both in the elastic and plastic domains, provided that the change in the value of A (eq (6.2.1)) is not significant. The derivation of equation (6.2.2) is given in Appendix 6.

No audible emission could be detected throughout any of the tests performed in the $\sigma_2 - \sigma_6$ stress space. Nevertheless, it was possible that the audible 'noise' was emitted but masked by the noise generated by the test rig. All the observed specimen failures were catastrophic. There were two types of fracture:

(i) For the tests where the shear stress component was greater than 62 MN/m^2, the specimen tended to fracture in three sections as shown in the diagram below.

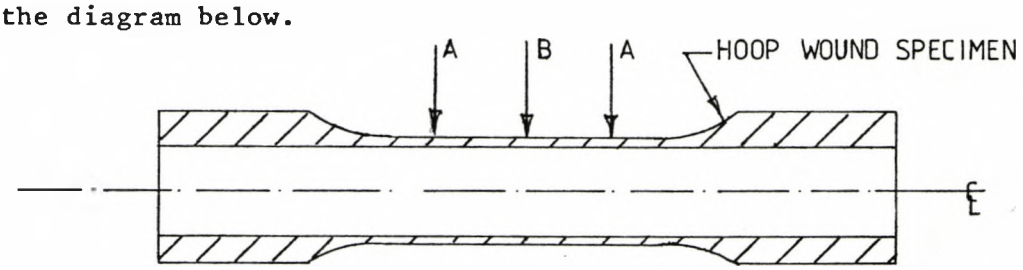

Fig 6.2.5 Mode of Fracture.

A - Primary Fracture Zone (near complete separation)

B - Secondary Fracture Zone (small crack)

This mode of fracture also occurred in pure shear tests.

(ii) When the shear stress component at failure was less or equal to 62 MN/m^2, the specimen fractured at only one zone. The fracture in this case was a complete separation.

The experimental results along the paths shown in fig 6.2.3 are plotted in the σ_2 — σ_6 stress space (fig 6.2.6). In general, one would expect a large degree of data scatter in this stress space due to the presence of σ_2.

Careful examination of the specimens prior to the tests revealed yellow streaks. Along these streaks voids were visible. The locations of these streaks were marked clearly on each specimen before it was tested. For those tests with failure shear stress component less than 62 MN/m^2, fracture always occurred in one of the marked regions. As pointed out by Puck & Schneider (1969) and other workers, material failure is a localised phenomenon; the failure strength of a material tends to be influenced by local defects. Transverse tensile strength is very sensitive to these material defects. The yellow streaks mentioned so far were probably due to excessive size. From this observation it may be concluded that the experimental data scatter seen in fig 6.2.6 was probably due to the void and localised poor interface bonding between fibre and resin matrix. In addition, the experimental data scatter could also be due in part to the following factors:-

(i) the small but unavoidable variation in volume fraction shown in Table 6.1.

(ii) the variation of specimen wall thickness throughout the gauge length of the specimen.

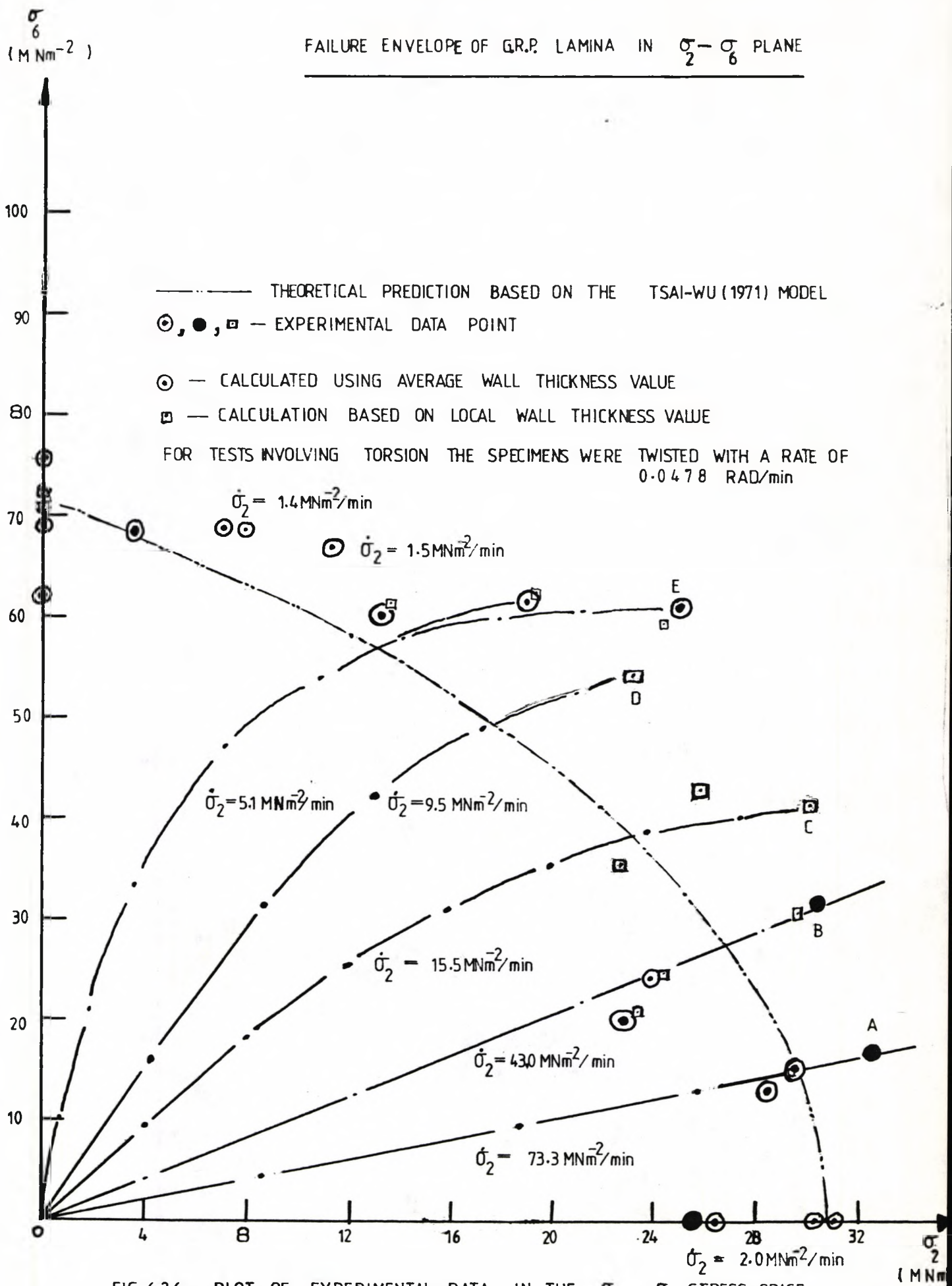

FIG 6·2·6 PLOT OF EXPERIMENTAL DATA IN THE σ_2 — σ_6 STRESS SPACE

Table 6.1 Volume Fraction of the Specimens tested in the $\sigma_2 - \sigma_6$ Stress Space.

Specimen	Volume Fraction
1058	0.388
1057	0.432
1067	0.444
1055	0.413
1060	0.439
1052	0.377
1051	0.393
1063	0.407
1062	0.418
1061	0.436
1065	0.441
1109VC	0.495
1107VC	0.477
1111VC	0.467
1112VC	0.497
1114VC	0.529
1098	0.388
1105	0.522
1117VC	0.464
1118VC	0.467
1121VC	0.454

In the $\sigma_2 - \sigma_6$ stress space, the Tsai & Wu (1971) criterion reduces to

$$F_2\,\sigma_2 + F_{22}\,\sigma_2^2 + F_6\sigma_6 + F_{66}\,\sigma_6^2 + 2F_{26}\,\sigma_2\,\sigma_6 = 1 \qquad .....(6.2.7)$$

Since the case considered here is a specially orthotropic one,

$$\therefore \quad F_{26} = 0 \qquad .....(6.2.8)$$

Furthermore, if it is assumed that the negative and positive shear strengths are identical, then

$$F_6 = 0 \qquad .....(6.2.9)$$

The final form of equation (6.2.7) becomes

$$F_2\,\sigma_2 + F_{22}\,\sigma_2^2 + F_{66}\,\sigma_6^2 = 1 \qquad .....(6.2.10)$$

The theoretical prediction based on equation (6.2.10) can be seen in fig 6.2.6. The uniaxial strength parameters used for the evaluation of F_2 , F_{22} and F_{66} are as given Table 6.2.

Table 6.2. Strength Parameters.

Uniaxial Strength	MN/m^2
Transverse Compression ($-\sigma_2$)	-122.16
Transverse Tension (σ_2)	30.68
Pure Shear (σ_6)	71.10
Strength Tensor	
F_2	$0.0244085 \times 10^{6}/Nm^{-2}$
F_{22}	$0.0002668 \times 10^{12}/(Nm^{-2})^2$
F_{66}	$0.000198 \times 10^{12}/(Nm^{-2})^2$

It was not meaningful to make a comparison between the experimental data and the theoretical prediction based on the Tsai & Wu (1971) criterion because of the poor experimental results.

In an attempt to reduce flaw and irregularity of wall thickness 'Equirove' 1200 tex glass was chosen for subsequent experimental work. There was a great improvement in the quality of the specimens produced with this type of glass.

Due to the sensitivity of the transverse tensile strength of a lamina to local flaws, a large number of tests would be necessary before a conclusion could be drawn with confidence from the experimental data obtained. However, time was very limited at this phase of the research project. It was decided to concentrate the effort on the stress space that involved transverse compressive stress rather than transverse tensile stress. Since the transverse compressive strength was relatively less susceptible to flaws in a lamina, the effect of loading paths in the $(-\sigma_2)-\sigma_6$ stress space were examined and the results are discussed in Section 6.4. Those experiments chosen as shown in fig 6.2.4 were abandoned.

6.3 The σ_1—$(-\sigma_2)$ Stress Space

Using the **Proportional and Integral** controllers (explained in Chapter 3) it was relatively easy to program the multiaxial test rig to execute a test involving axial force and internal pressure.

Hoop wound specimens with 1200 tex glass fibre were used to examine the failure behaviour of laminae under the biaxial stresses, involving hoop (tensile) and transverse compressive stresses. Only the best specimens, containing no observable yellow streaks or voids, were selected for the experimental work. The nominal dimensions of these specimens are given in Table 5.2.2 under specimen groups E, F and G. Initially, the nominal wall thickness $\bar{t}$ and the gauge length of the specimens were 1.7 mm and 140 mm respectively. In order to ensure that buckling did not occur, these dimensions were changed to 1.9mm and 110mm. No obvious signs of buckling were observed in specimens from group E to G during testing.

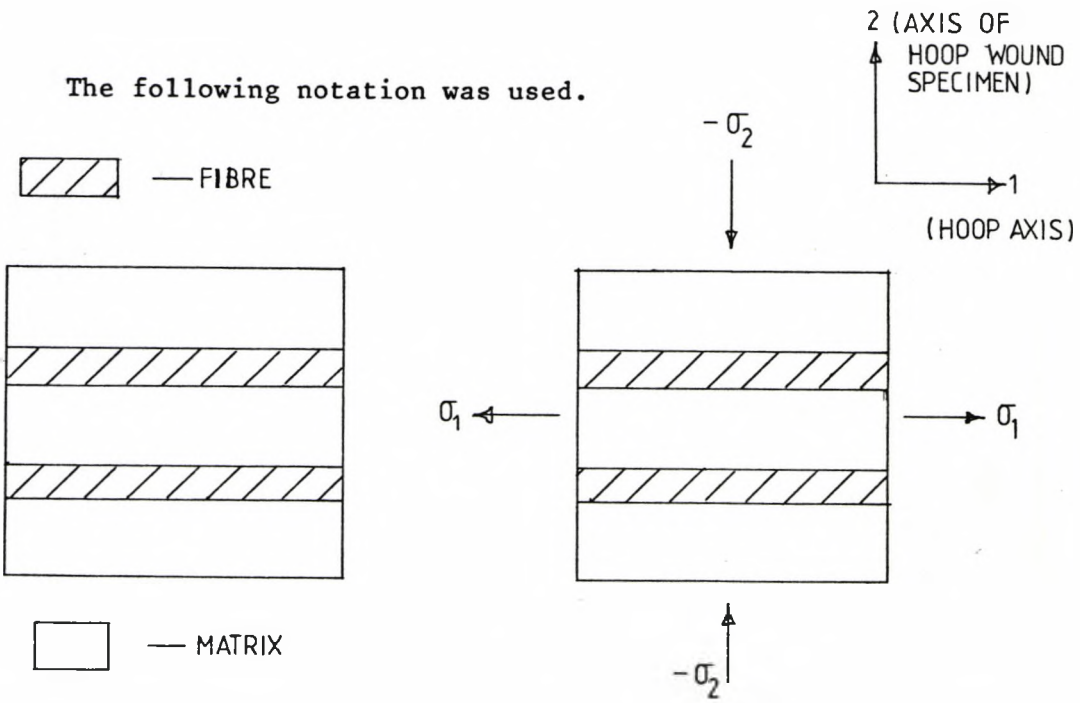

Fig 6.3.1 Lamina Representation

Fig 6.3.2 Coordinate System and Notation.

The failure loci (2-Dimensional Representation) in the $\sigma_1 - (-\sigma_2)$ stress space were established using the loading paths illustrated in fig 6.3.3.

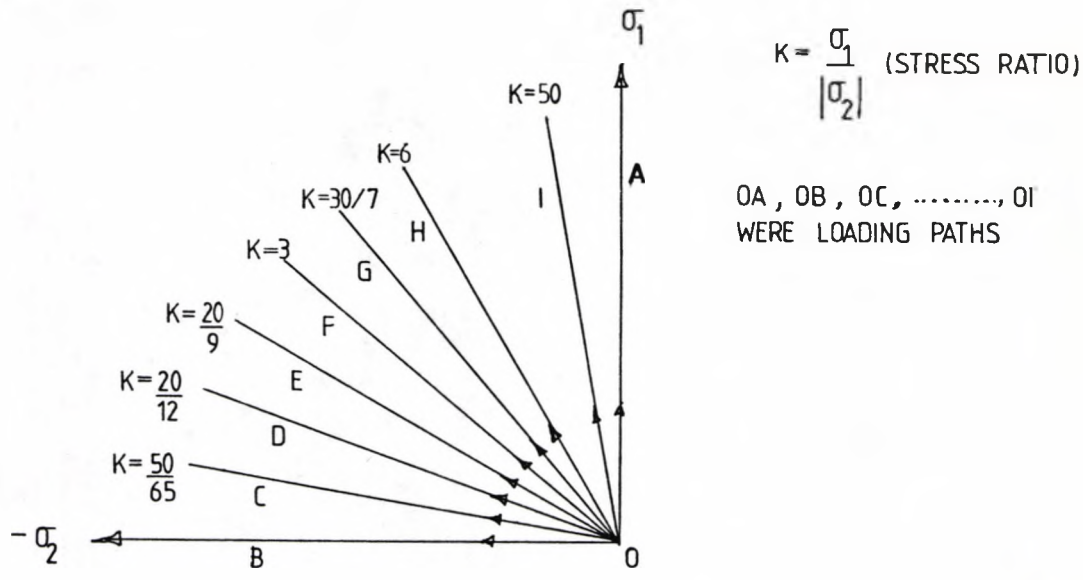

Fig 6.3.3 Experimental Determination of the Failure Surface in $\sigma_1 - (-\sigma_2)$ Stress Space.

The effect of loading path was examined in the regions of the $\sigma_1 - (-\sigma_2)$ stress space shown in fig 6.3.4.

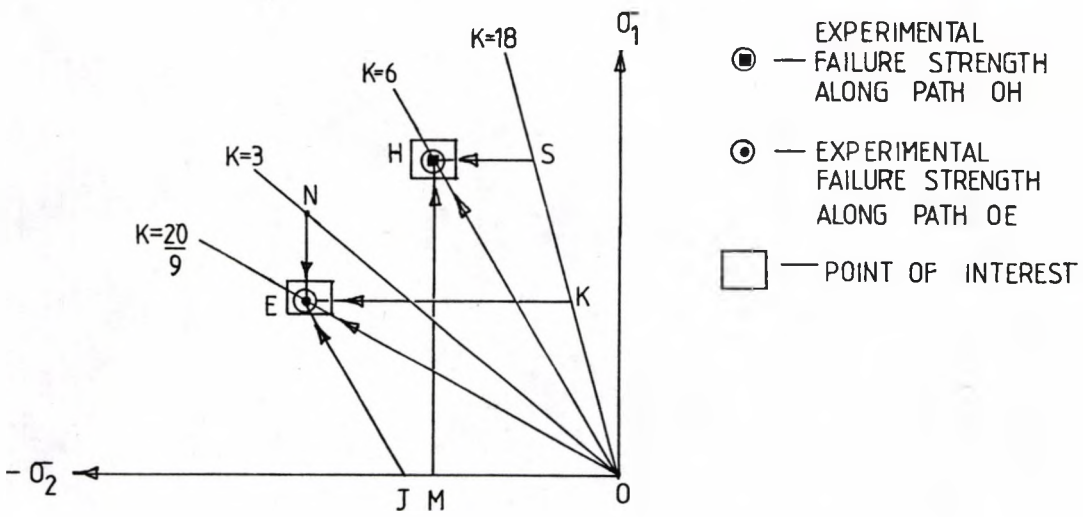

Fig 6.3.4 Experiments Devised for the Examination of the Effect of the Loading Path.

The failure strengths of the laminae along path OE and OH obtained earlier were used to plan the loading paths OJE, OKE, OMH and OSH. Hoop wound specimens were loaded along these new paths. This exercise was designed to study the dependency of the strength of a lamina upon the loading paths for a given stress ratio. Detailed discussion on this topic will be presented in in Section 6.3.1.4.

6.3.1 Modes of Failure of a Unidirectional Lamina in the σ_1 — ($-\sigma_2$) Stress Space:

In this stress space there are two distinct modes of failure for a lamina:

(i) Resin (matrix) failure.

(ii) Fibre (reinforcement) failure.

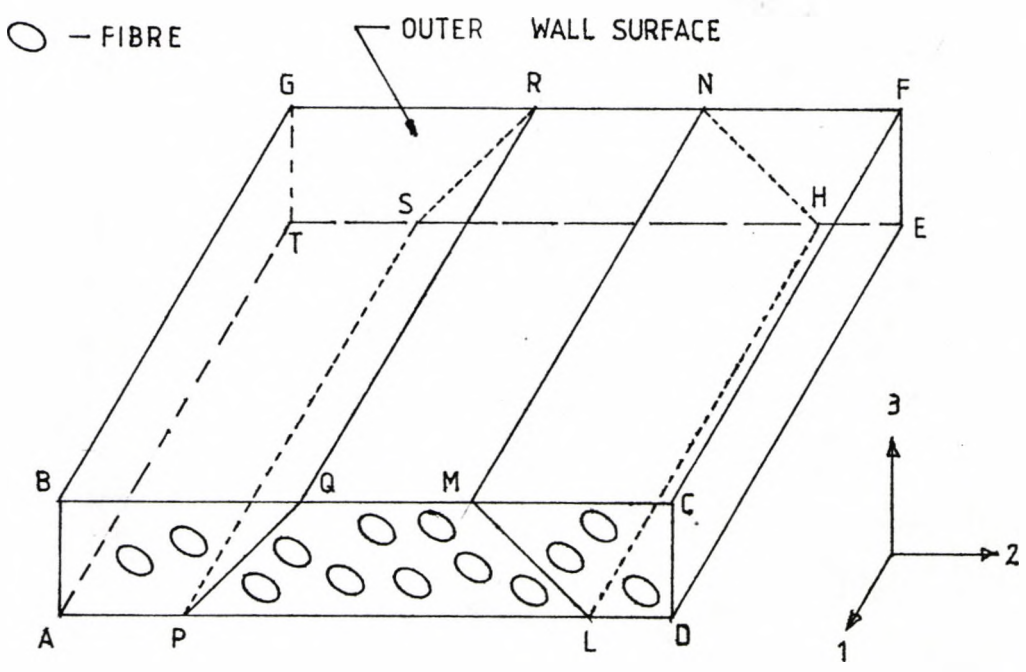

Fig 6.3.5 A Small Element of A Hoop Wound Specimen Wall.

Figure 6.3.5 shows an element of the cylindrical wall of a hoop wound specimen. In the stress space concerned the element can be subjected to transverse compression($-\sigma_2$), tension parallel to the fibre(σ_1) or a combination of both. In circumstances where matrix failure is dominant, the weak planes in the element are those parallel to plane HLMN or PQRS.

6.3.1.1 Failure Behaviour of a Unidirectional Lamina Under Pure Transverse Compression ($-\sigma_2$):

With reference to fig 6.3.5 the transverse compressive stress on the element can be represented in a 2-Dimensional space (fig 6.3.6)

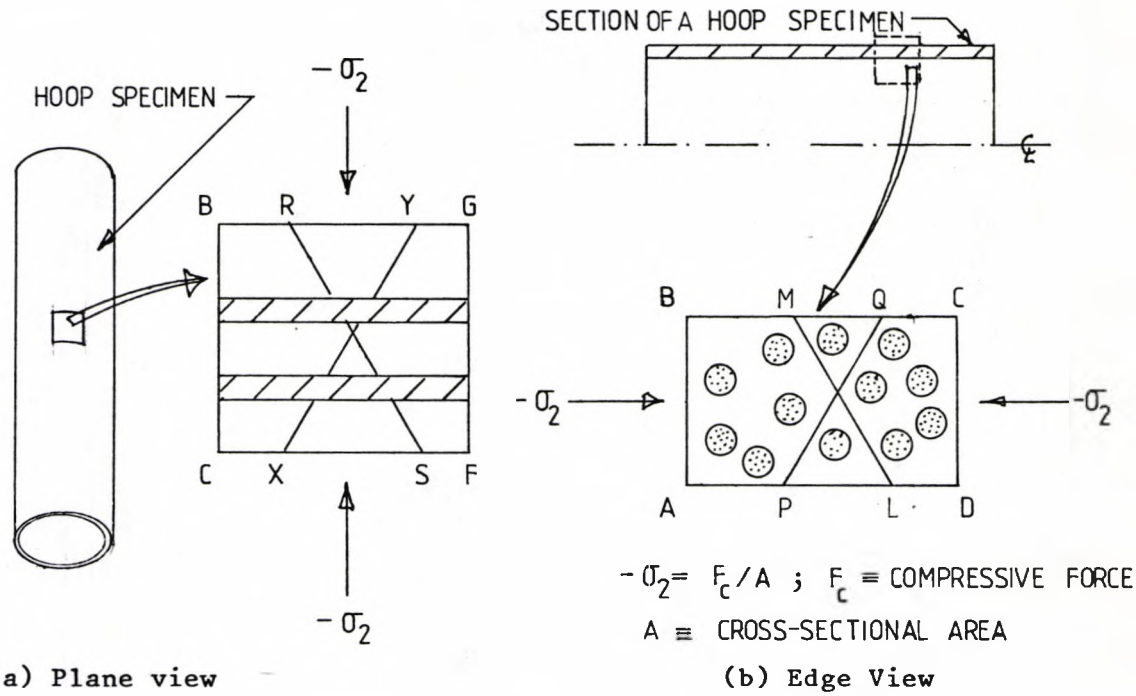

(a) Plane view (b) Edge View

Fig 6.3.6 A Lamina Under Transverse Compression ($-\sigma_2$)

Comparing figures 6.3.6(a) & (b) it can be argued that fracture would be more likely to occur along plane PQ or LM rather than along plane XY or RS. Here, fracture was assumed to be caused by shear stress existing on a plane which was at an oblique angle to the direction of

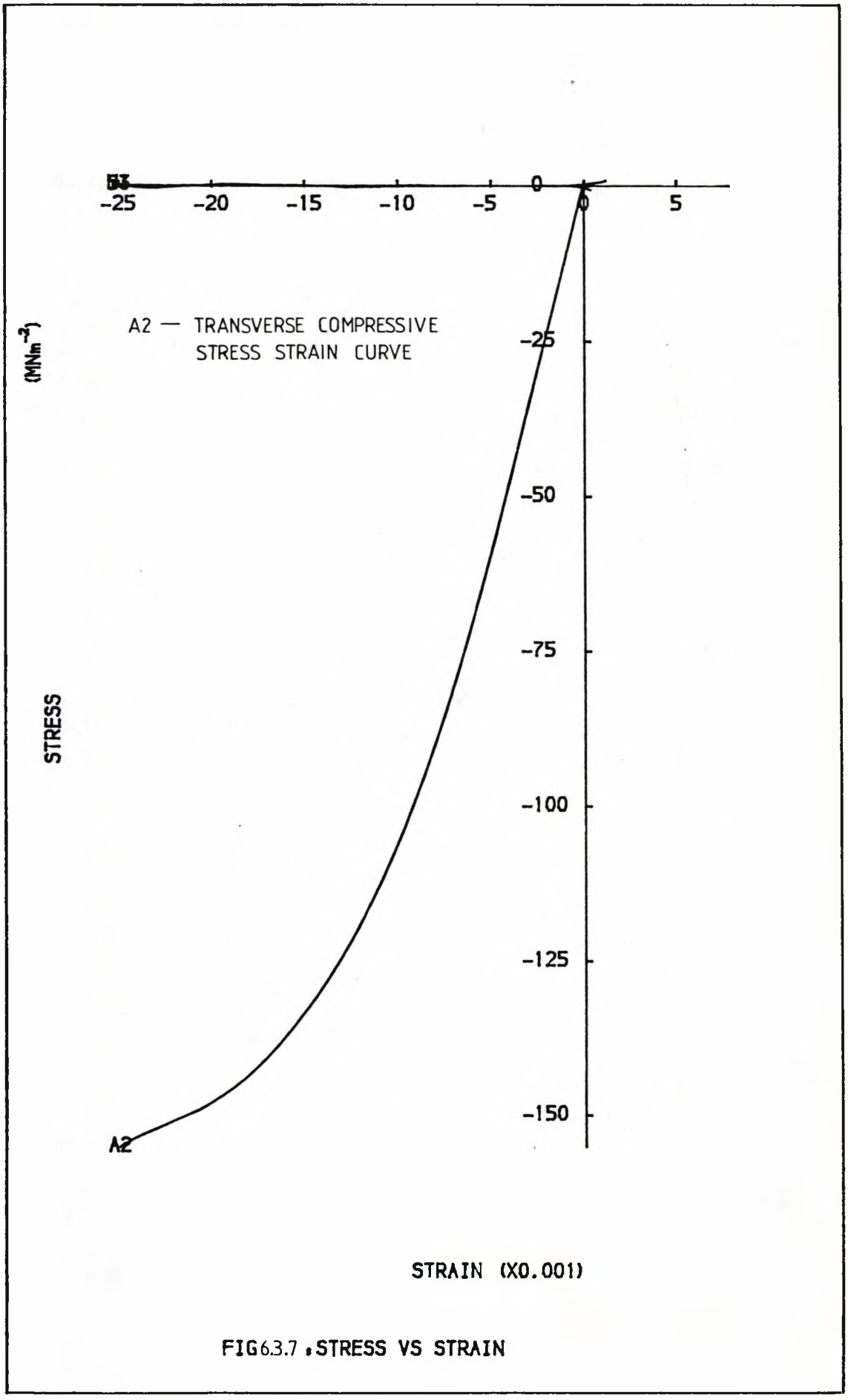

FIG6.3.7 .STRESS VS STRAIN

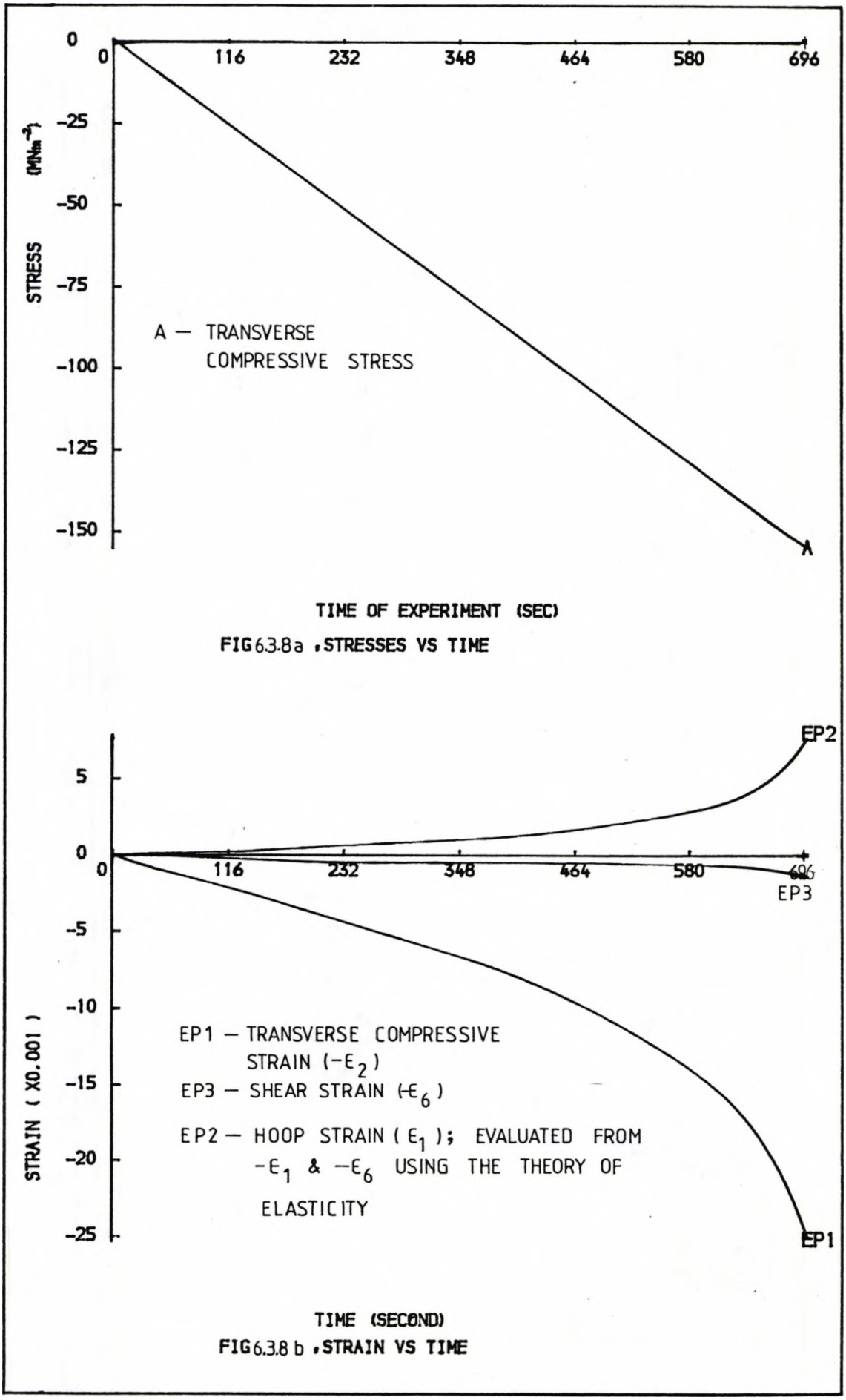

FIG 6.3.8 a , STRESSES VS TIME

FIG 6.3.8 b , STRAIN VS TIME

the applied transverse compressive stress. Figure 6.3.7 is a typical pure transverse compressive stress-strain curve. Figure 6.3.8 shows the loading history of the specimen. As shown in fig 6.3.7 there was a considerable amount of plastic deformation. In fact, the elastic limit was just over -60 MN/m^2. It must be the matrix that was plastically deformed, since the glass reinforcement behaved elastically in a quasi-static testing condition. It is conceivable that plastic flow can occur in the matrix on planes RS, XY, LM and PQ. But it is planes LM and PQ that provide an ideal condition for a fracture surface to be initiated.

Microscopic examination of the fractured specimens tested in pure transverse compression revealed an interesting result that gave support to the concept discussed in the prece ding paragraph. After a test, shiny white streaks were visible. These streaks existed randomly along the gauge length. An example of these white streaks is shown in Plate 6.3.1. A small section of the tubular specimen containing the white streaks was removed. This was prepared as explained in Chapter 5 for examination using a Reichert optical microscope. The plane of interest was perpendicular to the axis of the fibre, as illustrated in fig 6.3.9.

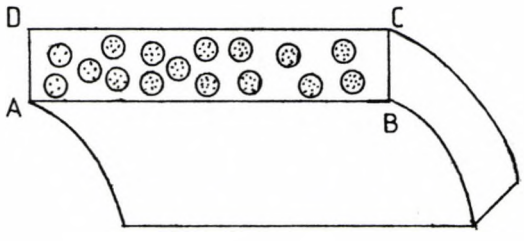

Fig 6.3.9 Section of a Hoop Wound Tubular Specimen with White Streaks

Optical micrographs 6.3.1(a) & (b), 6.3.2(a), (b) & (c) show the shear deformation in the matrix as envisaged. Since there was no visible crack, the white streaks could only have been caused by the

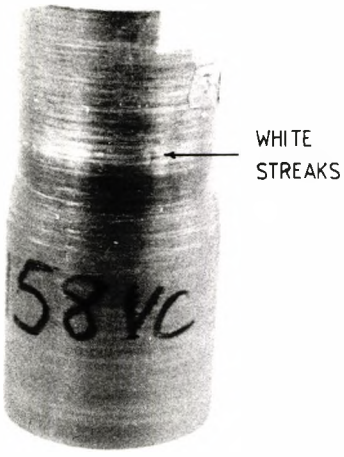

Plate 6.3.1 Part of a Hoop Wound Specimen Tested - Showing the Shiny White Streaks.

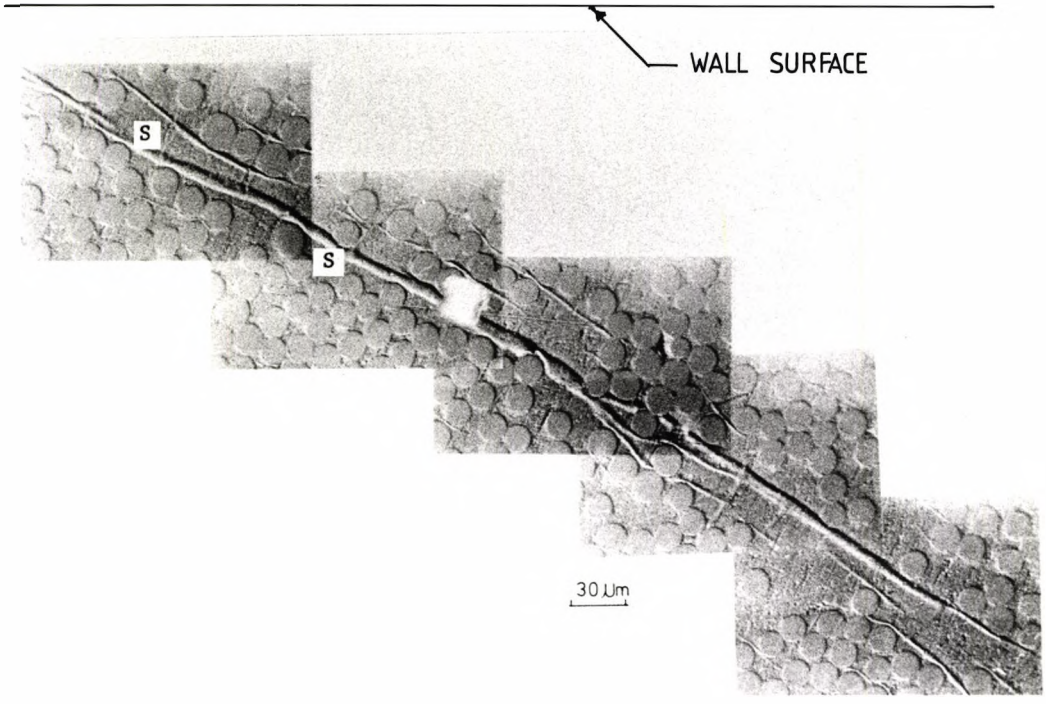

Optical Micrograph 6.3.1a Shear Deformation in the Matrix of the Specimen Tested in Pure Transverse Compression(S)

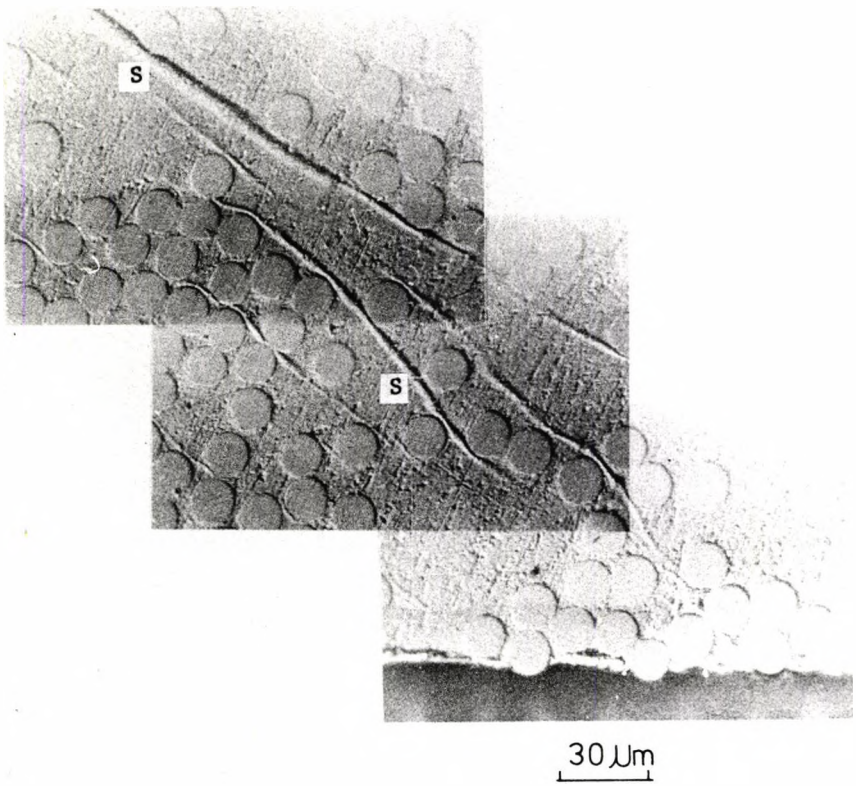

Optical Micrograph 6.3.1 b Shear Deformation in the Matrix of the Specimen Tested in Pure Transverse Compression.

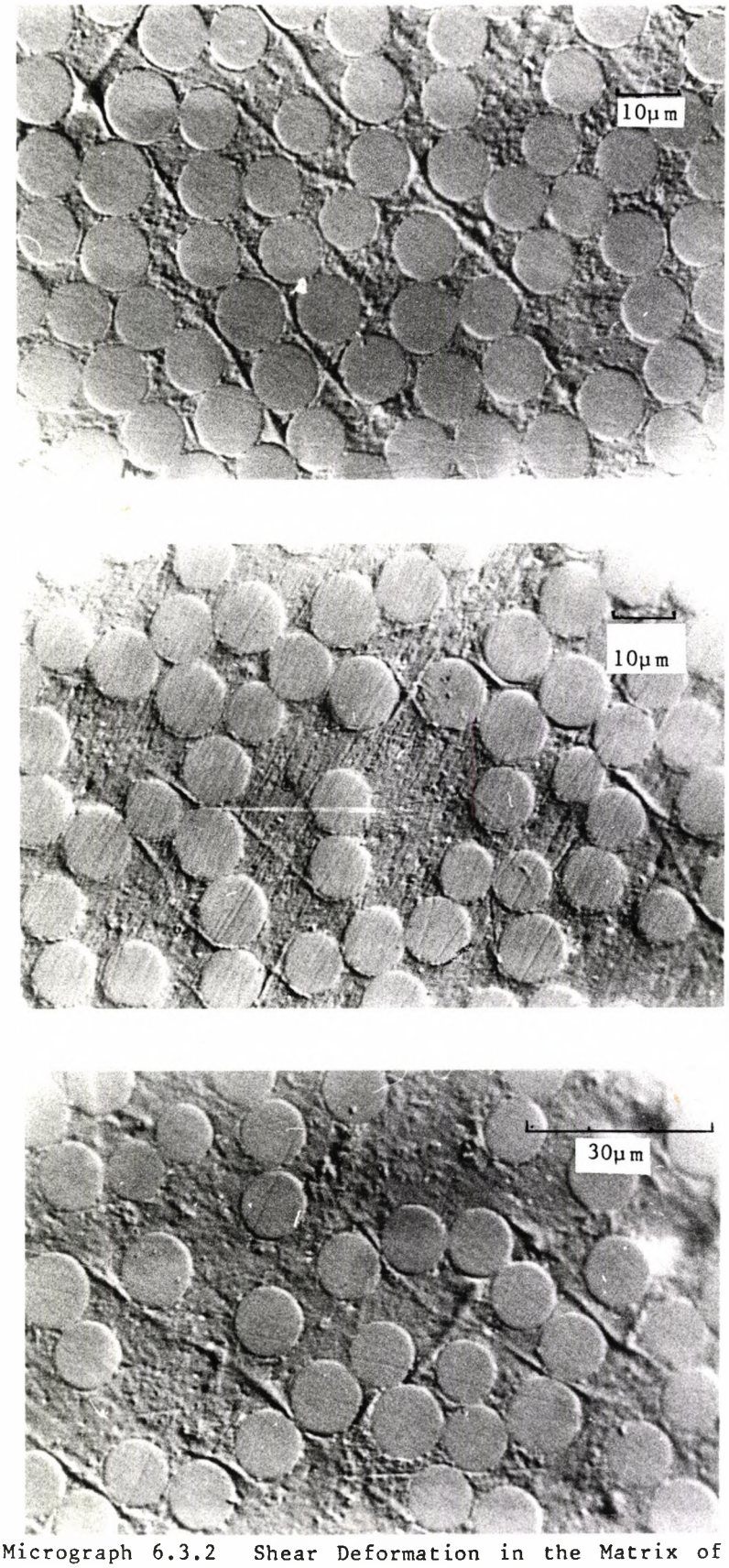

Optical Micrograph 6.3.2 Shear Deformation in the Matrix of the Specimen Tested in Pure Transverse Compression.

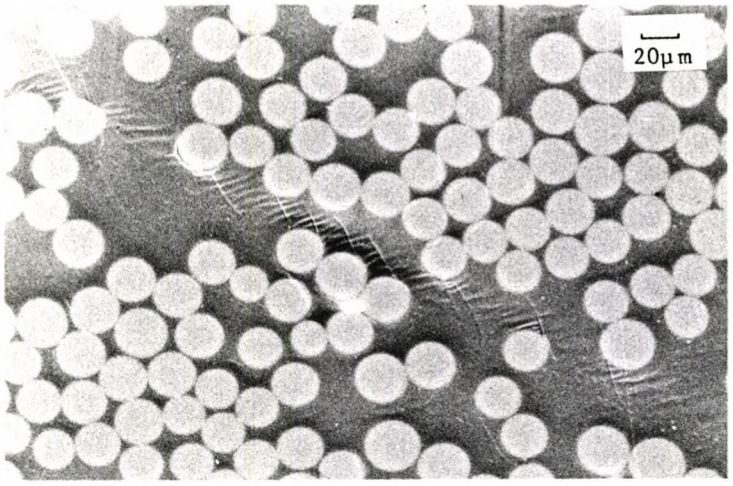

a

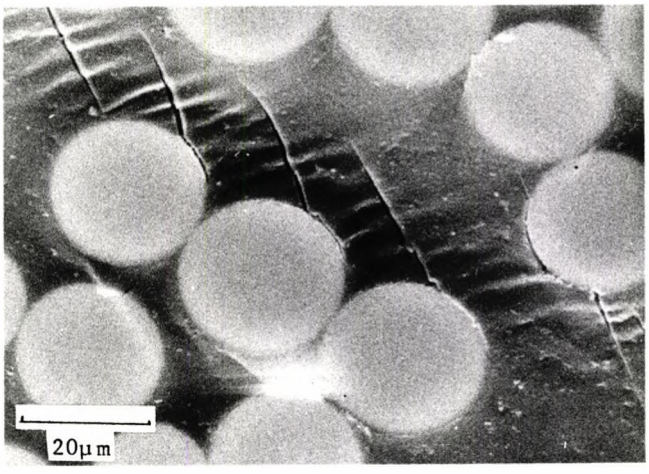

b

Scanning Micrograph 6.3.1 Part of the Modified Appearance of the Shear Deformed Matrix Shown in Optical Micrograph 6.3.1(a).

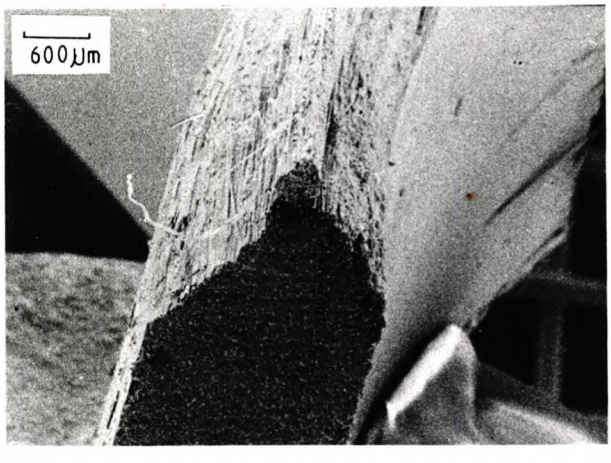

Scanning Micrograph 6.3.2 Profile of the Fracture Surface Due to Pure Transverse Compression.

change in the refractive index of the deformed region of the matrix due to an alteration of its density. The ridges existing on the highly polished plane might be attributed to the permeability of the deformed area to alcohol. Alcohol absorbed during the long wash at the last stage of the washing procedure probably produced the ridge-like appearance. When the polished specimen corresponding to the optical micrograph 6.3.1 was examined under the electron scanning microscope, small hairline cracks were found along the region occupied previously by the ridge as shown in scanning micrograph 6.3.1 (a) & (b). The heat generated by the sputtering process (see Chapter 5, Section 5.4) and the scanning microscope together with the vaccum environment could have probably caused the alcohol to evaporate and hence the disappearance of the ridges. The process of polishing and microscopic examination was repeated on the plane of interest of the specimen section. It was found that occasionally no ridge-like phenomenon could be observed. This suggested that the shear deformed zones were initiated randomly along the gauge length of the tubular specimen as well as along the fibre direction. These zones then increased in size with increasing applied transverse compressive stress. Sometimes, these damage zones merged to form a larger one. Fracture of the lamina finally took place when a damaged region was formed continuously along the fibre direction and across the thickness of the lamina. Scanning micrograph 6.3.2 shows the profile of the fracture surface so formed.

The Mohr's circle of stress (Timoshenko & Young (1968)) is a very useful graphical representation of the stresses present in an element, especially when it is under a state of applied biaxial stress. As a simple example the stresses on different planes of two

individual elements subjected to applied transverse compressive stresses are represented by the corresponding Mohr's circles shown in the two sketches presented in fig 6.3.10. The following assumptions are made when applying the principle of Mohr's circle of stress:

(i) the element considered is remote from the point of load application so that the non-uniformity of stress distribution due to the point of introduction of load is small and can be ignored,

(ii) the fibre /matrix interface bonding is perfect,

(iii) the effect due to the difference in the moduli between the fibre and the matrix is negligible,

(iv) the effects of shrinkage stress, the local non-uniformity of stress and the stress concentration due to the presence of fibre are small and can be neglected.

(v) the transverse stress (due to the longitudinally applied stress) arising from the difference in the Poisson's ratios of the fibre and matrix is insignificant and can be neglected.

The term 'General Assumptions' is given arbitrarily to these assumptions for ease of reference later. They have been applied to all the ensuing oversimplified analyses, unless otherwise stated. The average values of the stresses are used for the construction of the appropriate Mohr's circles.

On the macroscopic scale it is assumed that the transverse compressive stress is uniformly distributed throughout the lamina. As such the plane of maximum shear stress is at 45 degrees to the applied transverse compressive stress. The plastic shear deformation zone which appears subsequently is expected to lie on the same plane. However, on the microscopic scale the stress distribution is far from

uniform throughout the lamina. The direction of growth of the plastically deformed zones can be affected by the localised non-uniformity of the stress field due to the presence of glass fibre reinforcement. The deflection of the path of growth of the damage zone is shown in optical micrograph 6.3.1. There is a strong indication that the local non-uniform stress field is one of the factors which prevented the formation of the deformed zones on the 45-degree plane as mentioned above.

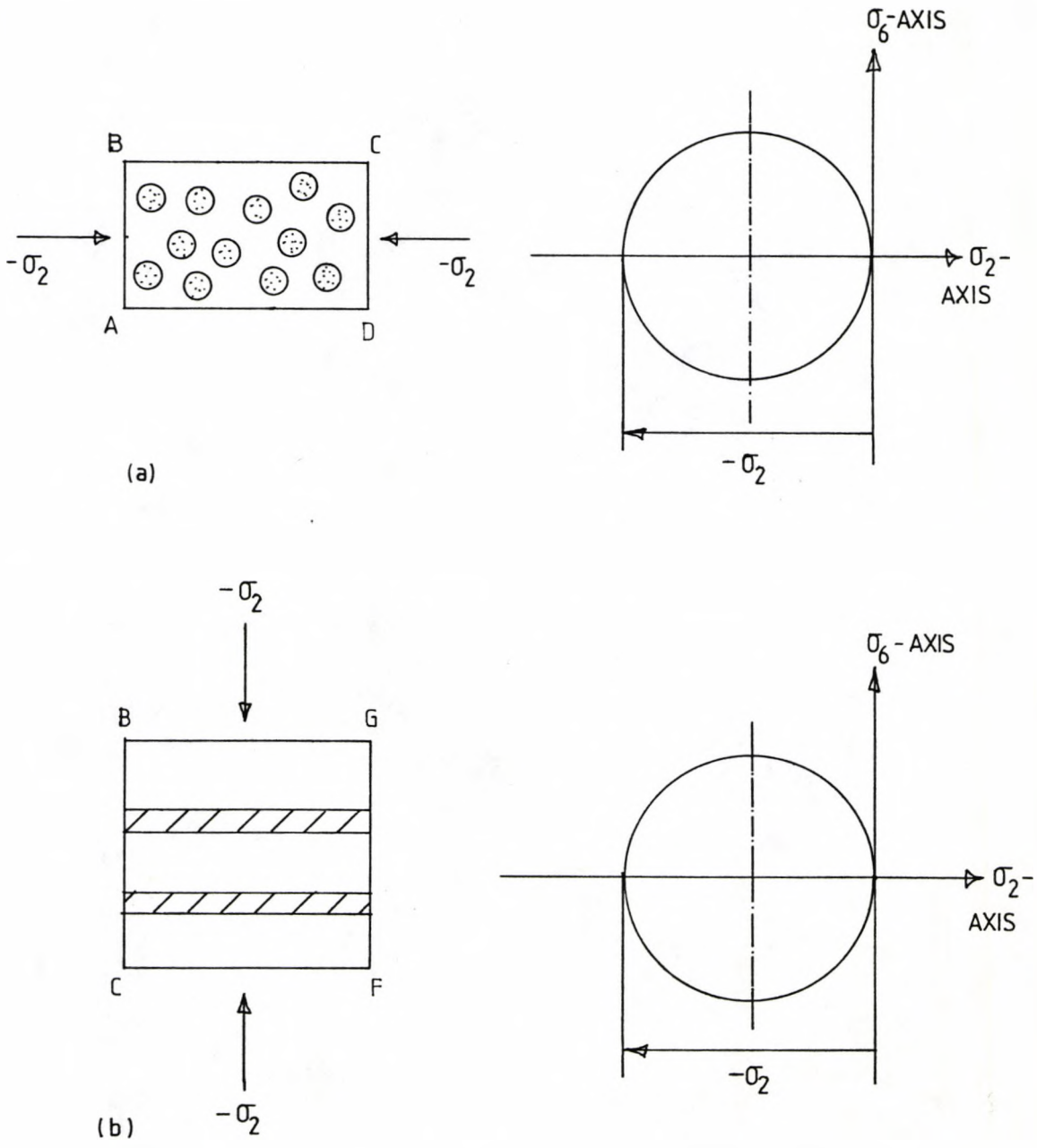

Fig 6.3.10 Graphical Representation of Stresses on an Element of a Unidirectional Lamina.

6.3.1.2 Failure Behaviour of a Unidirectional Lamina Under Pure Internal Pressure (σ_1):

In this loading condition, the plane perpendicular to the direction of the fibre (Plane ABCD in fig 6.3.5) is not important. Attention should now be focused on the other two planes illustrated below.

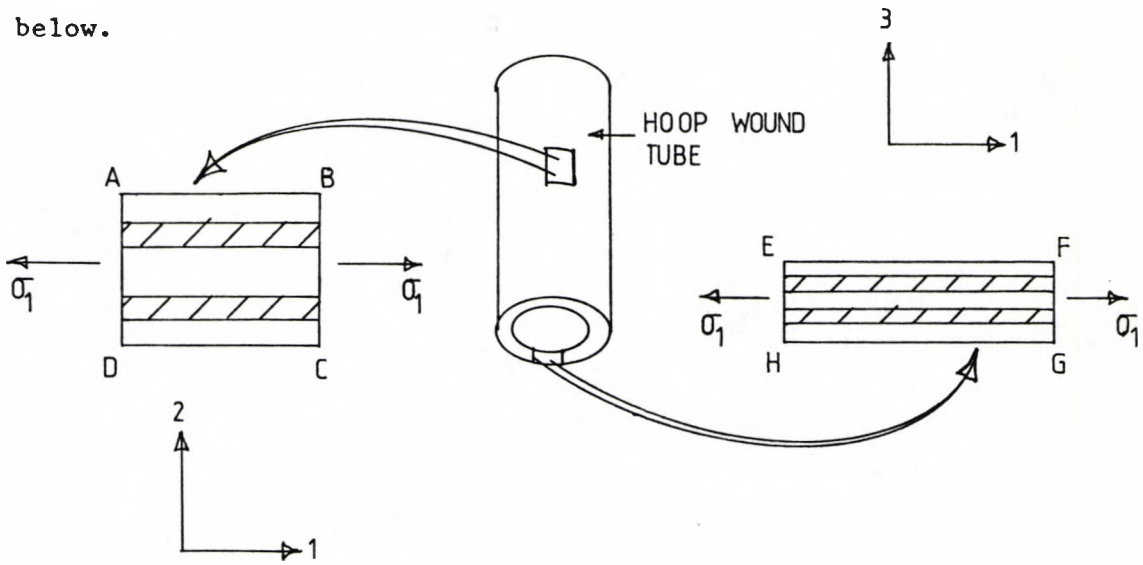

Fig 6.3.11 Unidirectional Lamina Under Pure Tensile Stress Parallel to the Fibre.

The hoop stress due to the internal pressure was calculated using the formula

$$\sigma_1 = P_i \ (\bar{d}_i + \bar{t}) / (2\bar{t})$$

.....(6.3.1.2.1)

Where P_i is the internal pressure

$\bar{d}_i$ is the mean internal diameter of the tubular specimen

$\bar{t}$ is the mean wall thickness of the tubular specimen.

Under the pure internal pressure loading, the unidirectional lamina exhibits its highest strength. This is because the applied stress is parallel to the fibre reinforcement. The constitutive equations that

govern the elastic behaviour of the lamina are

$$e_i = S_{ij}\ \sigma_j \qquad .....(6.3.1.2.2)$$

$i,j = 1,2....6$

Where e_i are the strain components of the lamina

S_{ij} are the compliance components

σ_j are the stress components

For pure internal pressure loading

$$\sigma_1 \neq 0;\ \ \sigma_2 = 0;\ \sigma_6 = 0;\ \sigma_3 \neq 0 \qquad .....(6.3.1.2.3)$$

However, the effect of radial stress $(-\sigma_3)$ has been ignored since its magnitude is small and has no significance in the present situation. By substituting equation (6.3.1.2.3) into (6.3.1.2.2) and considering only the 1-direction the following equation is obtained.

$$e_1 = S_{11}\ \sigma_1 \qquad .....(6.3.1.2.4)$$

Figure 6.3.12 is a plot of hoop stress (σ_1) versus hoop strain (ϵ_1) obtained from a test involving pure hoop stress. It indicates that S_{11} in equation (6.3.1.2.4) is a constant, i.e., ϵ_1 is a linear function of the applied stress σ_1 for the unidirectional lamina tested. The fibre reinforcement and the resin matrix were assumed to have the same strain in 1-direction. Such a strain was induced solely by the applied internal pressure. The stress distribution on the fibre and the resin of a unidirectional lamina can be evaluated in the following way.

$$e_{1f} = (S_{ij})_f\ \sigma_{1f} \qquad .....(6.3.1.2.5)$$

$i,j = 1,2,.....6$

Where ϵ_{if} are the strain responses of the fibre in the 1-direction.

$(S_{ij})_f$ are the compliance components of the fibre.

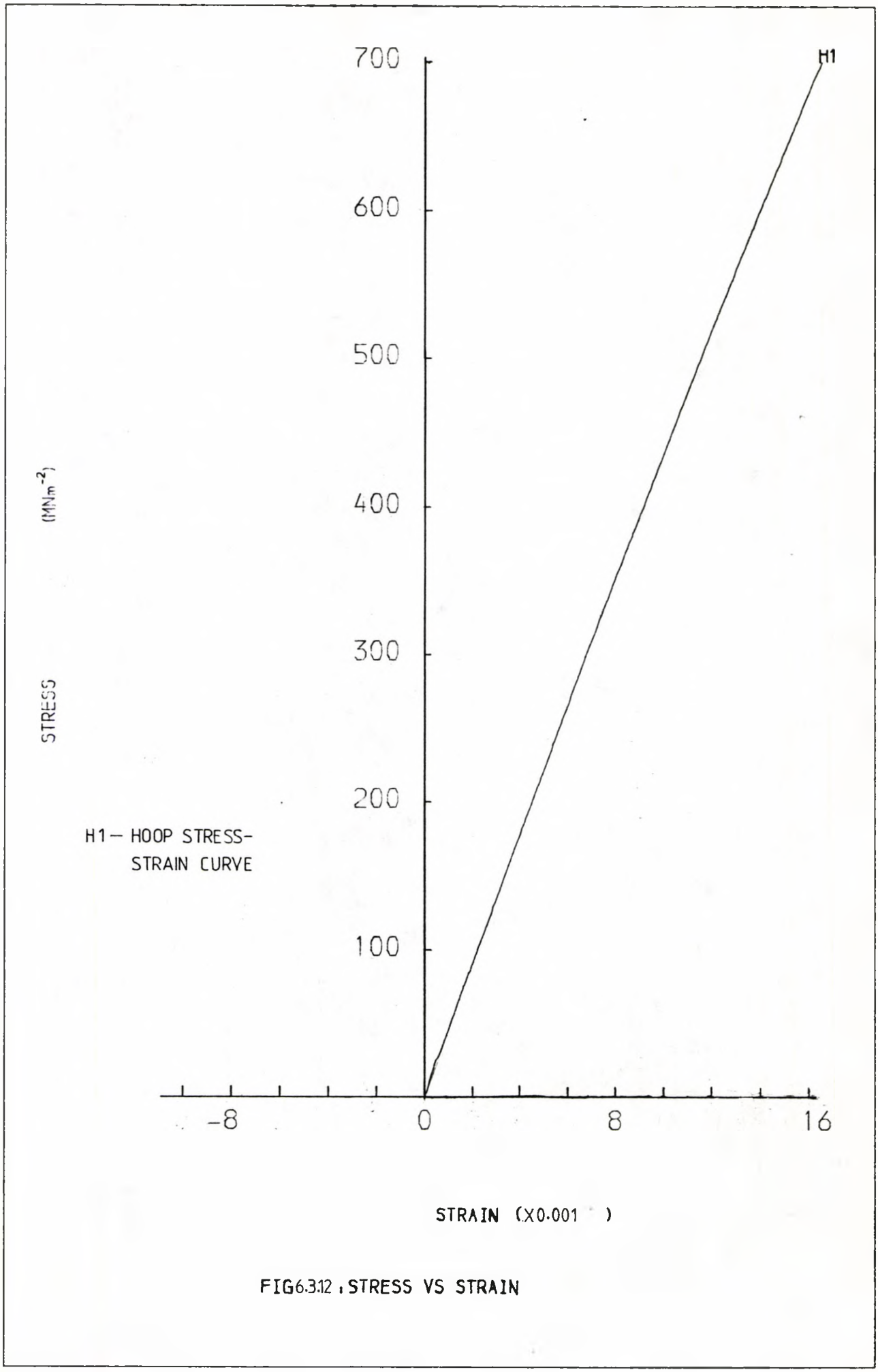

FIG6.3.12 : STRESS VS STRAIN

In pure internal pressure loading condition

$$\sigma_{2f} = \sigma_{6f} = 0$$

Therefore,

$$e_{1f} = (S_{11})_f \, \sigma_{1f} \qquad .....(6.3.1.2.6)$$

But from the assumption made on the strain response

$$e_1 = e_{1f} = e_{1m} \qquad .....(6.3.1.2.7)$$

Where ϵ_1 is the strain of the unidirectonal lamina in the 1-direction.

ϵ_{1f} is the strain of the fibre in the lamina along the 1-direction.

ϵ_{1m} is the strain of the resin in the 1-direction.

By substituting equations (6.3.1.2.4) & (6.3.1.2.7) into equation (6.3.1.2.6) the following equation emerges.

$$S_{11}\sigma_1 = (S_{11})_f \, \sigma_{1f} \qquad .....(6.3.1.2.8a)$$

Rearranging equation (6.3.1.2.8a) produces

$$\sigma_{1f} = (S_{11}/(S_{11})_f)\,\sigma_1 \qquad .....(6.3.1.2.8b)*$$

But the 'rule of mixture' states that

$$\sigma_1 = \sigma_{1f} v_f + \sigma_{1m} (1 - v_f) \qquad .....(6.3.1.2.16)$$

From equations (6.3.1.2.8b) and (6.3.1.2.16) σ_{1f} and σ_{1m} can be computed once the values of σ_1 , v_f, S_{11} and $(S_{11})_f$ are known.

Another method of computing the values of σ_{1f} and σ_{1m} from the applied stress σ_1 is elaborated as follow.

Assuming a linear stress-strain relation of resin,

$$\sigma_{1m} = E_{1m} \, e_{1m} \qquad .....(6.3.1.2.20)$$

* Note: the following equations do not exist.
Equations (6.3.1.2.9) to (6.3.1.2.19) except (6.3.1.2.16)

and

$$\sigma_1 = E_1 \varepsilon_1 \qquad \text{.....(6.3.1.2.21)}$$

but

$$\varepsilon_1 = \varepsilon_{1m} \qquad \text{.....(6.3.1.2.22)}$$

Combining equations (6.3.1.2.20), (6.3.1.2.21) and (6.3.1.2.22) it is possible to show that

$$\sigma_{1m} = \frac{E_{1m}}{E_1} \sigma_1 \qquad \text{.....(6.3.1.2.23)}$$

Once the values of v_f and σ_1 are determined equations (6.3.1.2.23) and (6.3.1.2.16) can be used to calculate the values of σ_{1f} and σ_{1m}.

At the point of failure of the lamina, the stress parallel to the fibre carried by the resin is less than its own failure strength. It was found that the failure strain of the lamina in the 1-direction is about 1.60%. Whereas, the failure strain of pure resin is 2.05 %. Therefore, in the case of pure tensile loading parallel to the axis of the fibre, it is very unlikely for a crack to form on the resin and precipitate the catastrophic failure of the lamina.

In general, it is accepted that the fibre reinforcement carries most of the load applied along its axis. As such,the fracturing of the fibre has a pronounced effect on the integrity of the unidirectional lamina (since the matrix cannot sustain the level of applied load that causes fibre fracture). Therefore, the stress on the fibre becomes the critical factor.

In addition to the General Assumptions given in Section 6.3.1.1 it is also assumed that all of the fibres are parallel and experience the same level of stress up to the point just prior to failure of the

lamina. Based on these assumptions the failure stress of fibres within the lamina can be computed by considering a single fibre. This is an oversimplified view. In reality fibres with poor surface finish will fail first and incurring a redistribution of stresses amongst other intact fibres. As a result, all the fibres do not fail simultaneously. Nevertheless, refined failure analysis was prevented due the lack of time. Figure 6.3.14 is a graphical representation of the stresses present in different planes of a fibre that intercept its own axis.

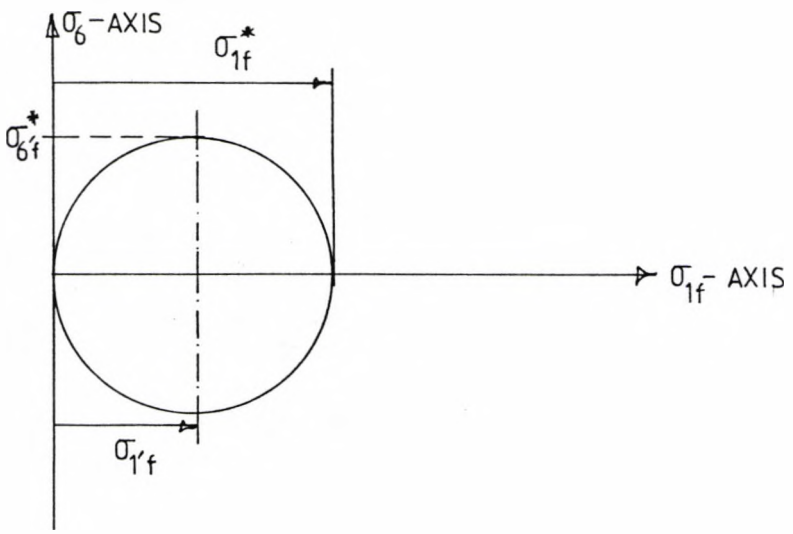

Fig 6.3.14 Mohr's Circle Representation of Stresses Present in the Fibre.

σ_{1f}^* is the fracture tensile strength of the fibre acting along the axis of the fibre. $\sigma_{6'f}^*$ is the shear stress acting on the two complementary planes which are at 45 degrees to the axis of the fibre. $\sigma_{1'f}$ is the tensile stress acting normal to these planes.

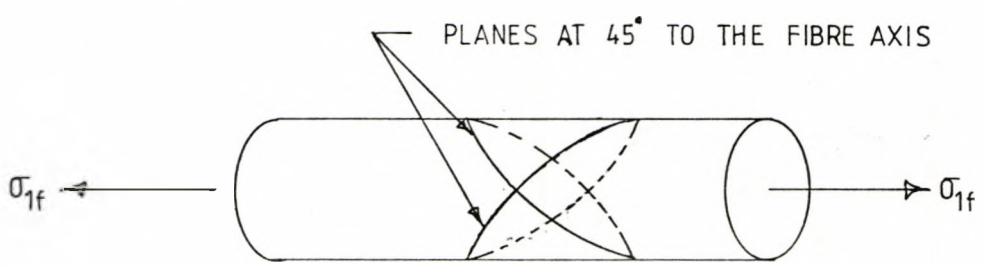

Fig 6.3.15 A Fibre under Tensile Stress.

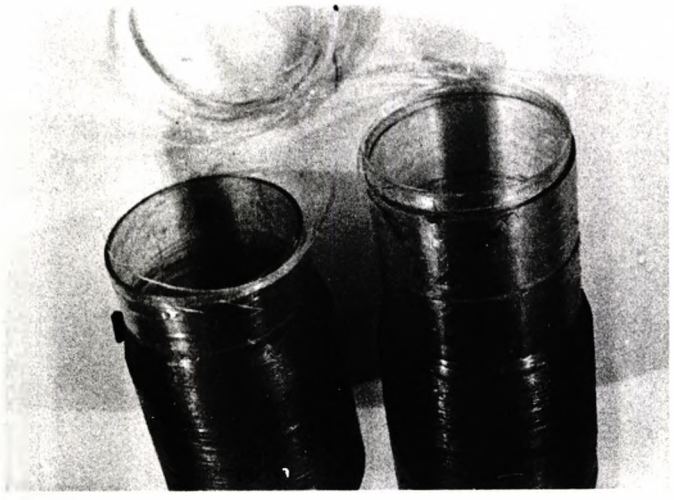

Plate 6.3.2 Typical Fracture Mode Due to Pure Internal Pressure.

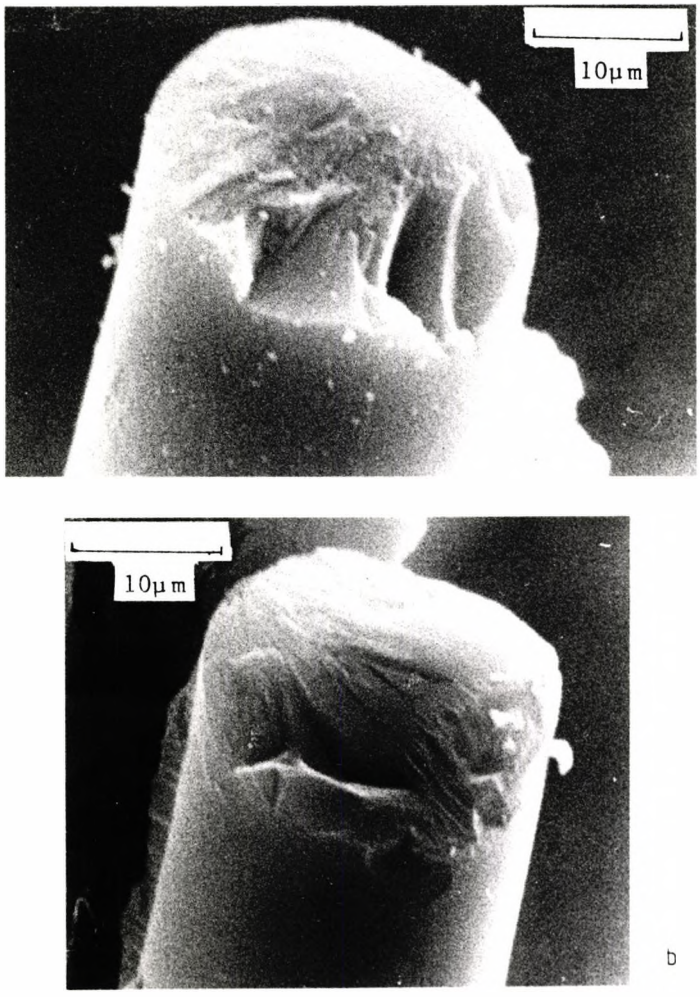

Scanning Micrograph 6.3.3 Fibres Fractured in Tensile Mode.

a

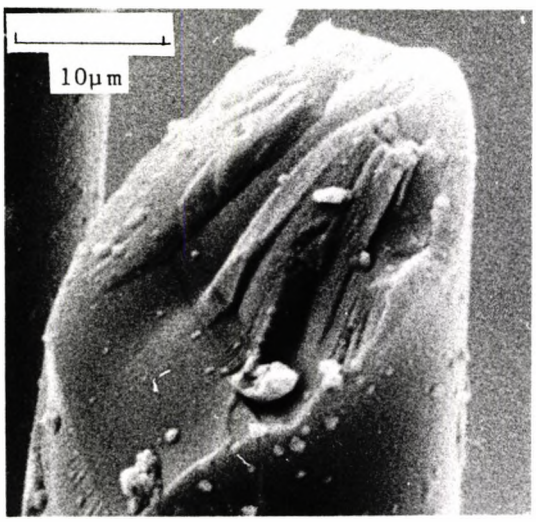

b

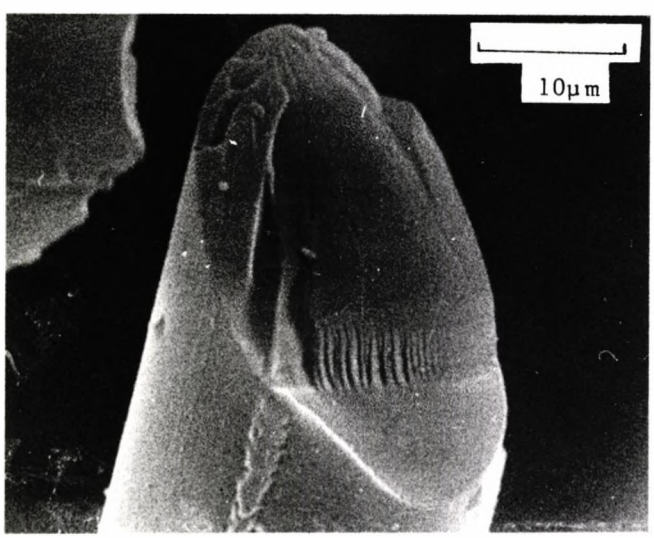

c

Scanning Micrograph 6.3.4 Fracture Surface of Fibre.

In fig 6.3.15 it can be seen that there are an infinite number of planes that can intercept the fibre at 45 degrees to its axis. Tensile fracture of a fibre can be viewed as proceeding in the manner represented by fig 6.3.16. An example of tensile fracture surface of a fibre can be seen in scanning micrograph 6.3.3.

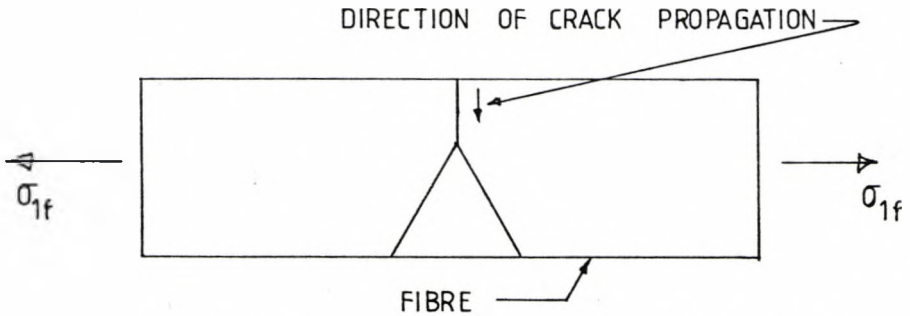

Fig 6.3.16 Tensile Fracture Mode in A Fibre

A shear mode of fracture would probably occur on an oblique plane which intercepts the axis of the fibre at a certain angle. From figures 6.3.14 and 6.3.15 it can be seen that for a shear fracture mode to materialise $\sigma^{*}_{6'f}$ must be the failure initiating stress. The presence of σ_{1f} would assist the crack opening process. However, no concrete evidence of fibre fracture initiated by shear stress was found. Another commonly observed type of fibre fracture surface which resulted from pure internal pressure tests on hoop wound tubes is shown in scanning micrograph 6.3.4. There are numerous other ways in which a fibre can fracture, due to the powerful influence of the surface finish of the fibre.

It appears that either σ^{*}_{1f} or $\sigma^{*}_{6'f}$ shown in fig 6.3.14 can be viewed as the fracture strengths of the fibre. Either of them can be used in conjunction with equation (6.3.1.2.8b) to compute the fracture stress

of a unidirectional lamina parallel to the fibre in a biaxial stress case ($\sigma_1 / -\sigma_2$), provided that fibre fracture is a critical factor and that S_{11} and $(S_{11})_f$ are given. Nevertheless, as will be shown later in Section 6.3.1.3 the limited experimental data seem to agree better with the theoretical prediction based on σ_{6f}^* . The application of σ_{1f}^* and σ_{6f}^* will be illustrated in Section 6.3.1.3. From fig 6.3.14 it is clear that

$$\sigma_{1f}^* = 2\sigma_{6f}^*$$

.....(6.3.1.2.24)

For all the hoop wound specimens tested under pure internal pressure a typical fracture mode (Plate 6.3.2) was observed. In general, the fracture surfaces from such tests are complicated. It is impossible to present a complete explanation for the whole fracturing process since further detailed experimentation could not be pursued due to the time constraints. In attempting to gain some insight into the failure behaviour of a unidirectional lamina under σ_1 an over-simplified model is put forward as follows.

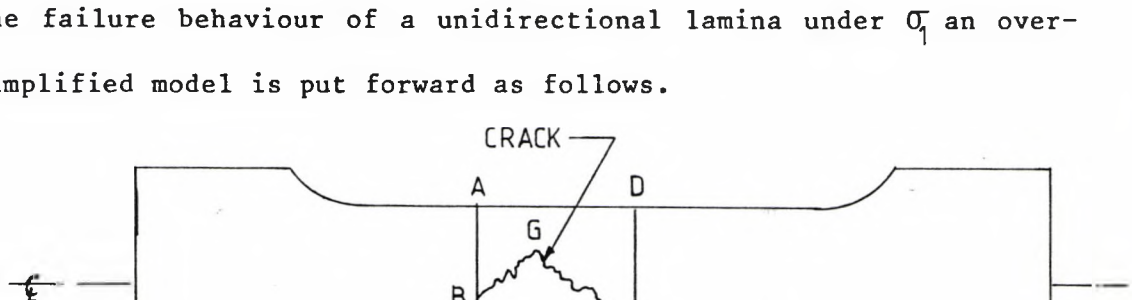

Fig 6.3.17 Failure of Hoop Wound Specimen Under Internal Pressure.

As a whole, the crack on the fibre was assumed to be initiated by shear stress, σ_6' , at 45 degrees to the axis of the fibre. When the fibre has fractured completely the crack propagates through the matrix and meets the next fibre. Assume that fig 6.3.17 shows a hoop wound specimen in an advanced stage of the failure process. The crack

has travelled through the wall thickness of the specimen. Furthermore, the crack BGE is assumed to be continuous. The region of the specimen bound by the circumferential lines ABC and DEF enters into a new phase of the fracturing process. The damaged area can be assumed to behave as two cantilevers as shown in fig 6.3.18. Now, the internal pressure has an additional effect of inducing a uniformly distributed force acting perpendicular to the cantilevers. This tends to push the damaged area outward relative to the rest of the specimen as seen in fig 6.3.19. Shear deformation on the matrix in planes XX and YY, shown in fig 6.3.19, was assumed.

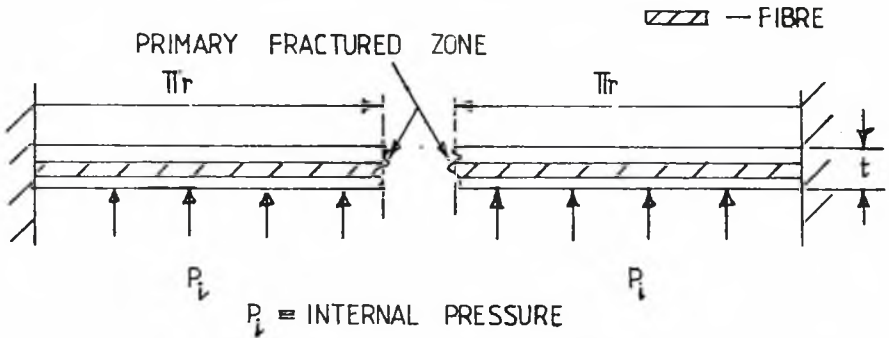

Fig 6.3.18 Cantilever Loading on the Damaged Area.

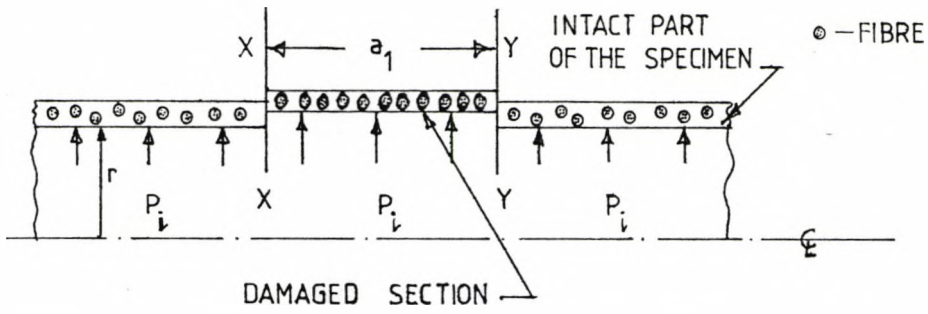

Fig 6.3.19 Cantilever Bending Effect on the Damaged Area in a More Advanced Stage of Fracturing Process.

The fracture shear stress, σ_6^* , determined from pure shear test on hoop wound specimens was used for the derivation of equation (6.3.1.2.26) .

Let A_t be the cross-sectional area of the specimen at plane XX or YY.

A_d be the area of the damaged area.

Therefore,

$$A_t = 2\pi rt$$

$$A_d = 2\pi r a_1 \qquad \text{.....(6.3.1.2.24i)}$$

By considering the equilibrium state of the damaged section illustrated in fig 6.3.19 it can be demonstrated that

$$P_i A_d = 2\sigma_6 A_t + f(\text{flexural stiffness})$$

$$\text{.....(6.3.1.2.25)}$$

$$P_i 2\pi r a_1 = 2\sigma_6 2\pi rt + f(\text{flexural stiffness})$$

Therefore,

$$a_1 = 2(\sigma_6/P_i)\ t + f(\text{flexural stiffness})$$

$$\text{.....(6.3.1.2.26)}$$

Equation (6.3.1.2.26) can be used to estimate the value of a_1 for a given biaxial stress state.

The 'shear fracture' surface seen in fig 6.3.20 was thought to have formed in a progressive manner. In the nature of this mode of fracture, the damage is mainly incurred in the matrix. Therefore, attention was focused on the damage to the matrix. To this end, the outer surface of a hoop wound specimen was coated with a thin layer of resin while it was still in the pre-gelled state. The specimen was subsequently tested under pure internal pressure. It was hoped that more information could be extracted from the resulting fracture surface so that a better understanding about the fracturing process might be attained.

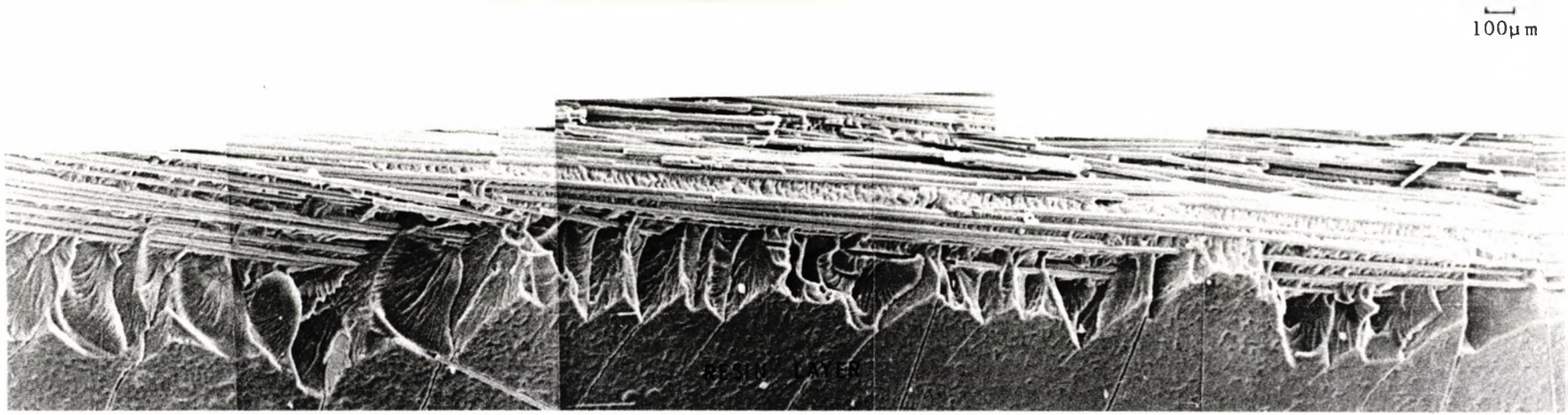

Scanning Micrograph 6.3.5 Secondary Fracture Surface Produced When a Hoop Wound Specimen was Subjected to Pure Internal Pressure. Attention was Focused on the Outer Resin Layer.

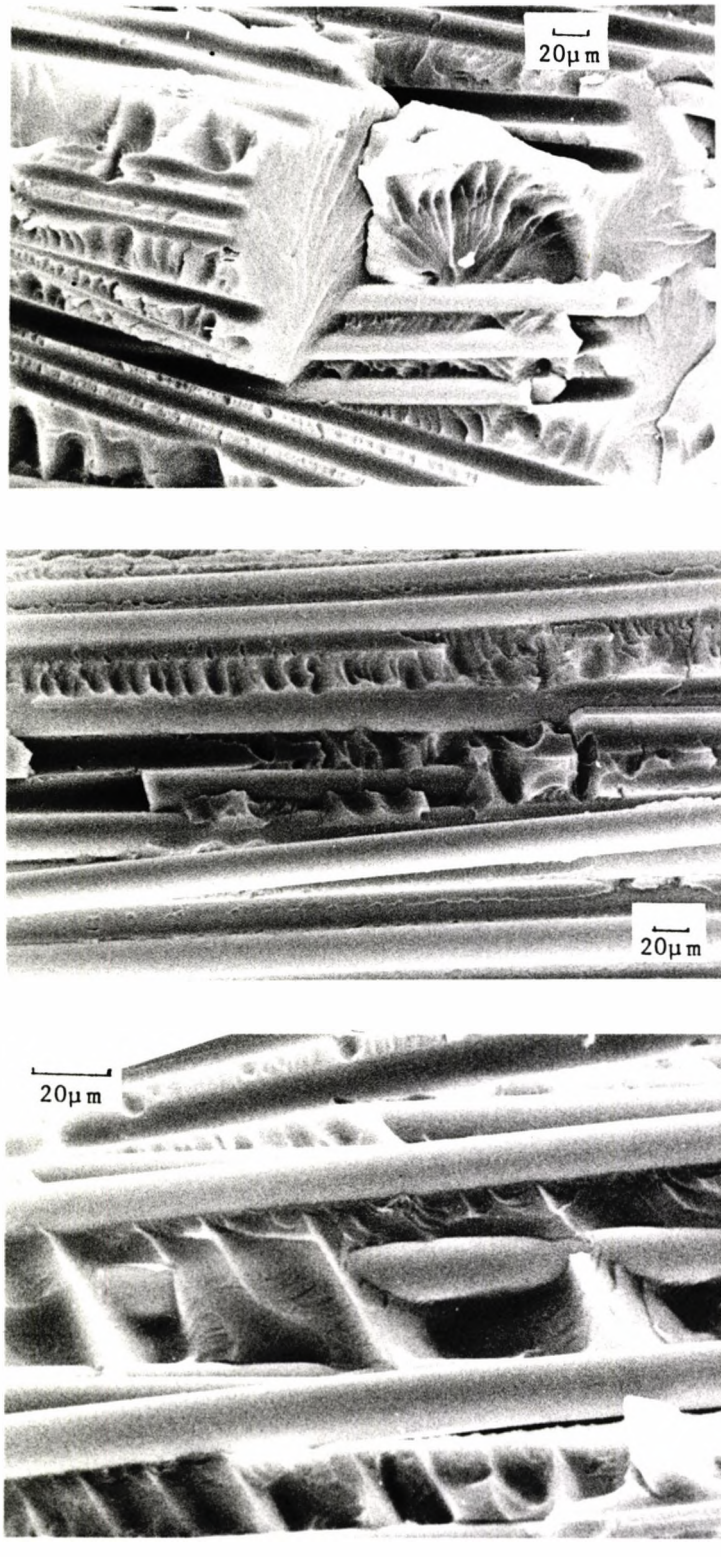

Scanning Micrograph 6.3.6 Secondary Fracture Surface of a Hoop Wound Specimen Produced by Internal Pressure Loading.

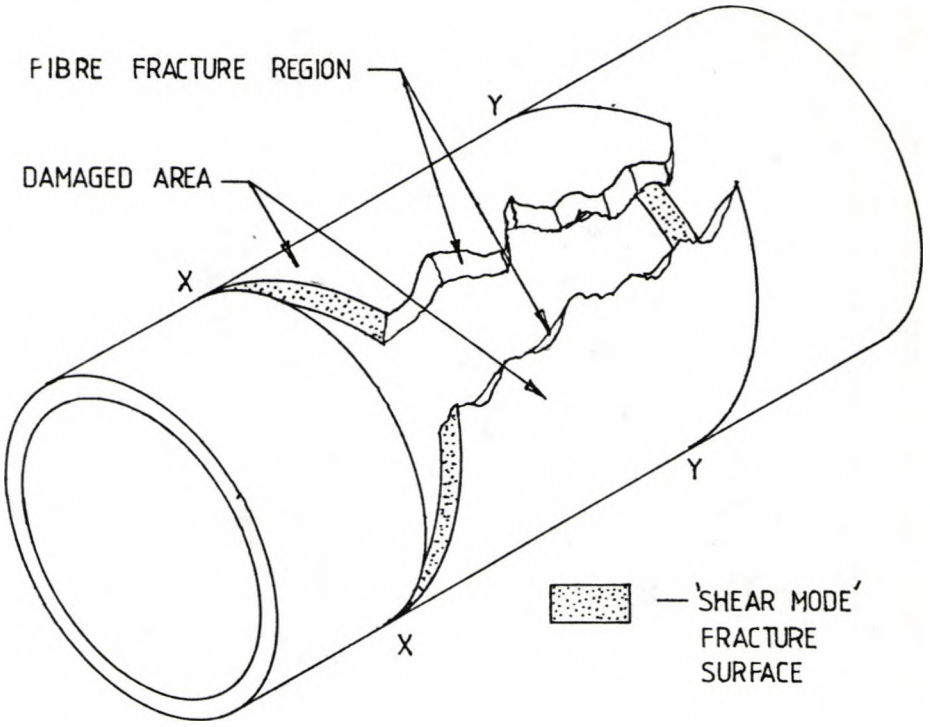

Fig 6.3.20 Oblique View of the Fracture Zone in Hoop Wound Specimen Due to Pure Internal Pressure Loading.

Scanning micrographs 6.3.5 and 6.3.6 (a),(b) & (c) represent the results obtained from this experiment. A section of the 'shear fracture' surface is shown in scanning micrograph 6.3.5. It can be seen that the fracture surface of the outer resin layer is serrated. The crack nucleating centres exist throughout the entire fracture surface of the resin layer. There are two possibilities as to how the resin layer fractured:

(i) Cracks nucleating in different locations of the resin matrix. Each of these minute cracks grow in size and probably merge with others until a continuous fracture surface is formed eventaully.

(ii) The cracks nucleating centres are formed along the crack path one at a time.

Resin fracture surface marking shows that most cracks in the resin matrix were nucleated in the vicinity of the fibres. It must be pointed out that the local fracture surface was at an oblique angle to the fibre axis as can be observed in the scanning micrgraph 6.3.5. It is quite conceivable that the local fracture was following the shear planes of the resin due the applied hoop stress. Scanning micrograph 6.3.6 (a), (b) & (c) give evidence that this fracture process extended across the thickness of the specimen wall. The appearance of the fibre A shown in scanning micrograph 6.3.6 (c) can be explained by the process illustrated in fig 6.3.23 (a) & (b).

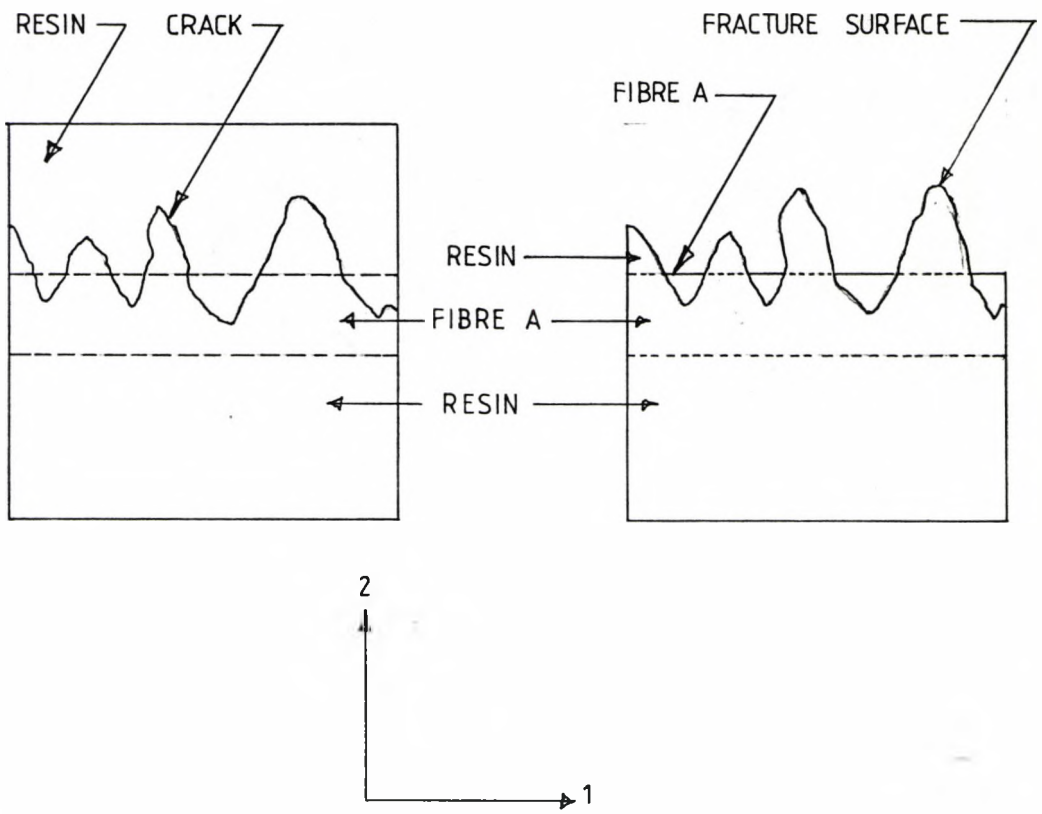

Fig 6.3.23 Formation of A Fracture Surface in An Element of A Specimen Wall.

6.3.1.3 Failure Behaviour of A Unidirectional Lamina Under Different Stress Ratios ($\sigma_1 / |-\sigma_2|$):

Having investigated the failure behaviour of unidirectional laminae under pure transverse compression and pure tensile stress parallel to the fibre axis, attention is now directed towards the combined-stress ($\sigma_1 / -\sigma_2$) situation. The General Assumptions were applied in deriving the criterion for matrix failure presented in this section. It will be demonstrated later that this theoretical model is valid only in the region where

$$\sigma_1/|-\sigma_2| \leqslant 3 \qquad .....(6.3.1.3.5)*$$

As explained in Section 6.3.1 for a unidirectional lamina, where the matrix failure controls its integrity, the weak planes are those parallel to plane HLMN or PQRS shown in fig 6.3.5.

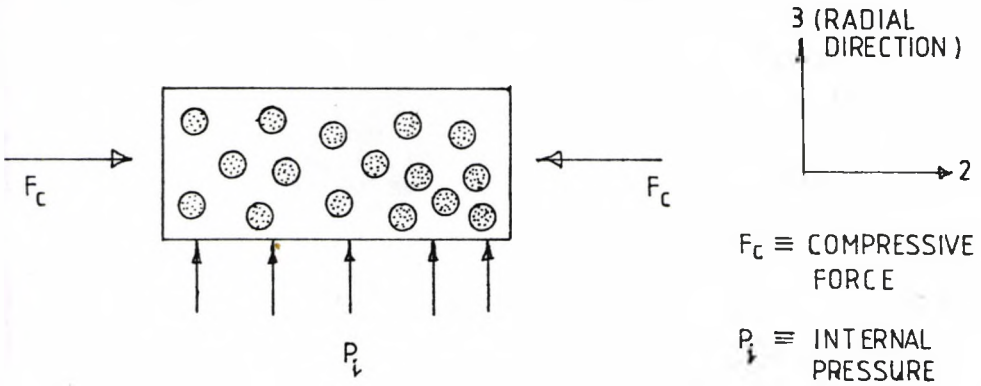

Fig 6.3.27 The Applied Loads Exerted On The Plane of Interest In A Unidirectional Lamina.

The applied internal pressure in a tubular specimen has the effect of inducing a compressive stress along the 3-axis (radial axis) as illustrated in fig 6.3.27. The magnitude of this compressive stress is small compared to other applied stresses. In most circumstances, it is ignored in the stress analysis. However, it will be shown later that the effect of this radial compressive stress, $-\sigma_3$, on the above-mentioned weak planes is profound. Utilizing the elastic

* - Note: the following equations and figures do not exist:
equations (6.3.1.3.1) to (6.3.1.3.4), (6.3.1.3.6) to (6.3.1.3.15) and (6.3.1.3.18)
figures 6.3.24, 6.3.25 and 6.3.26

analysis it can be demonstrated that the distribution of the radial stress across the wall thickness of the specimen is governed by the following equation:

$$\sigma_3 = ((P_i\, a^2) / (b^2 - a^2))\,(1 - (b^2/r^2)) \qquad .....(6.3.1.3.19)$$

with the definitions of the parameters illustrated in fig 6.3.28.

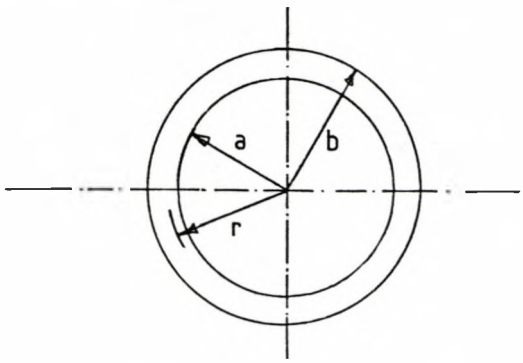

Fig 6.3.28 End-view of a Tubular Specimen.

For a given P_i the relation between $-\sigma_3$ and r is sketched in fig 6.3.29.

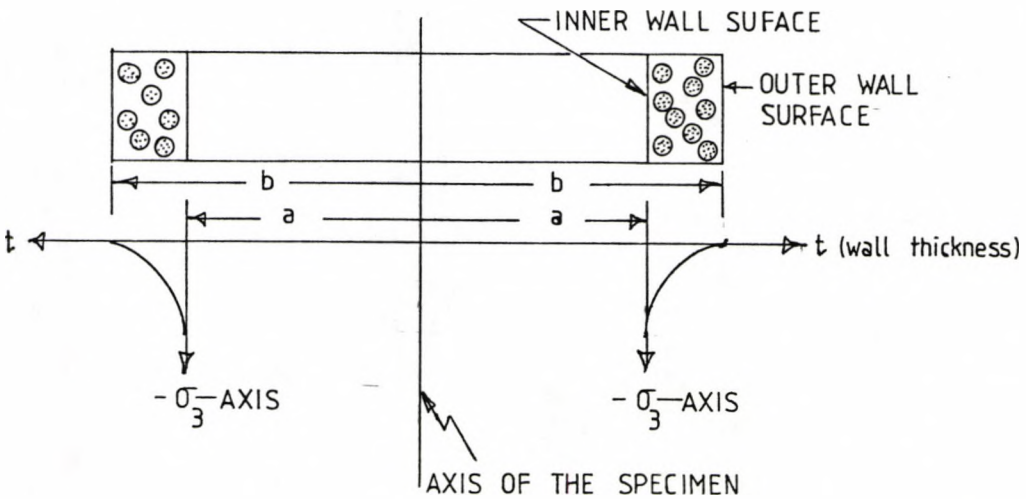

Fig 6.3.29 Distribution of the Radial Stress Across the Wall Thickness of a Hoop Wound Specimen.

In the ensuing analytical work the radial compressive stress is assumed to be given by the following equation.

$$-\sigma_3 = -P_i \qquad \text{.....(6.3.1.3.20)}$$

Now consider an element of the plane of interest under a system of biaxial stress generated by the applied loads which satisfied the condition

$$\sigma_1 / |-\sigma_2| \leqslant 3 \qquad \text{.....(6.3.1.3.5)}$$

The system of biaxial stress given in fig 6.3.30 can be represented by a Mohr's circle (MC2) plot as can be seen in fig 6.3.31.

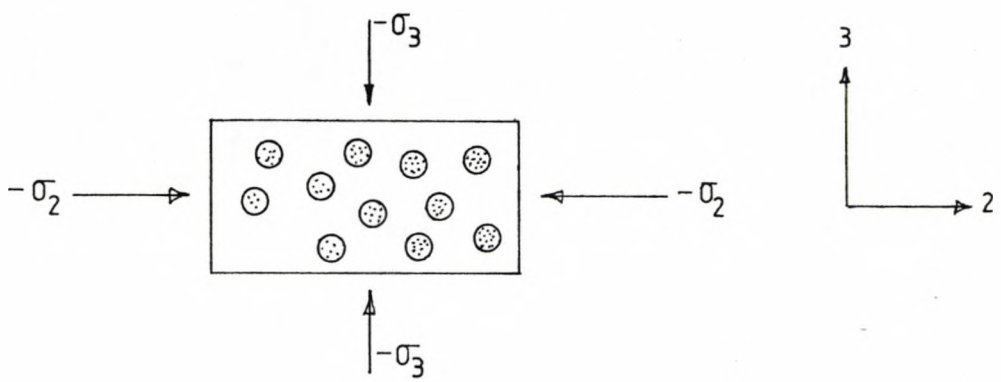

Fig 6.3.30 The Plane of Interest Under a System of Biaxial Stress.

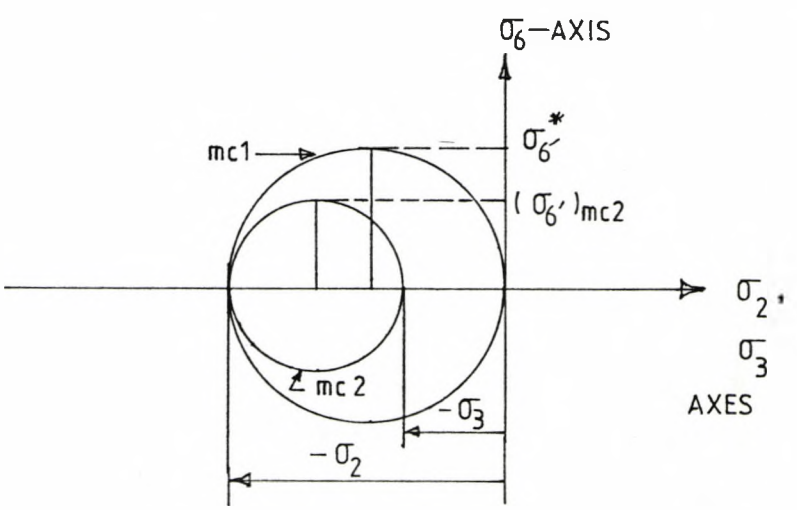

Fig 6.3.31 Mohr's Circle Plot of the System of Stress given in fig 6.3.30

At this stage, it is assumed that the matrix and the fibre each experience the same magnitude of transverse compressive stress. Since the matrix failure is important in the present discussion, the Mohr's circles sketched in fig 6.3.31 are assumed to represent the stresses in the matrix. The Mohr's circle (MC1) due to pure transverse compression, $-\sigma_2$, is for comparison purposes. In this loading condition equation (6.3.1.3.21) is true.

$$-\sigma_3 = 0 \qquad .....(6.3.1.3.21)$$

From fig 6.3.31 it can be deduced that the application of $-\sigma_3$ effectively reduces the size of the stress Mohr's circle and hence the shear stress present in the matrix on the plane of interest. Consequently, the onset of plastic deformation is delayed. This phenomenon was observed experimentally. Figure 6.3.32 is a transverse compressive stress-strain plot for four loading paths which have been mapped out in fig 6.3.33. The rate of transverse compressive stress increment for all four cases was the same.

From fig 6.3.32 it can be seen clearly that the transverse compressive stress at the onset of plastic deformation of the matrix was increasing with the internal pressure.

At the elastic domain, there was an apparent reduction in the transverse Young's Modulus of a lamina when subject to biaxial stresses (σ_1 vs $-\sigma_2$). This was due to the Poisson's effect of the hoop stress (σ_1) on the axial compressive strain.

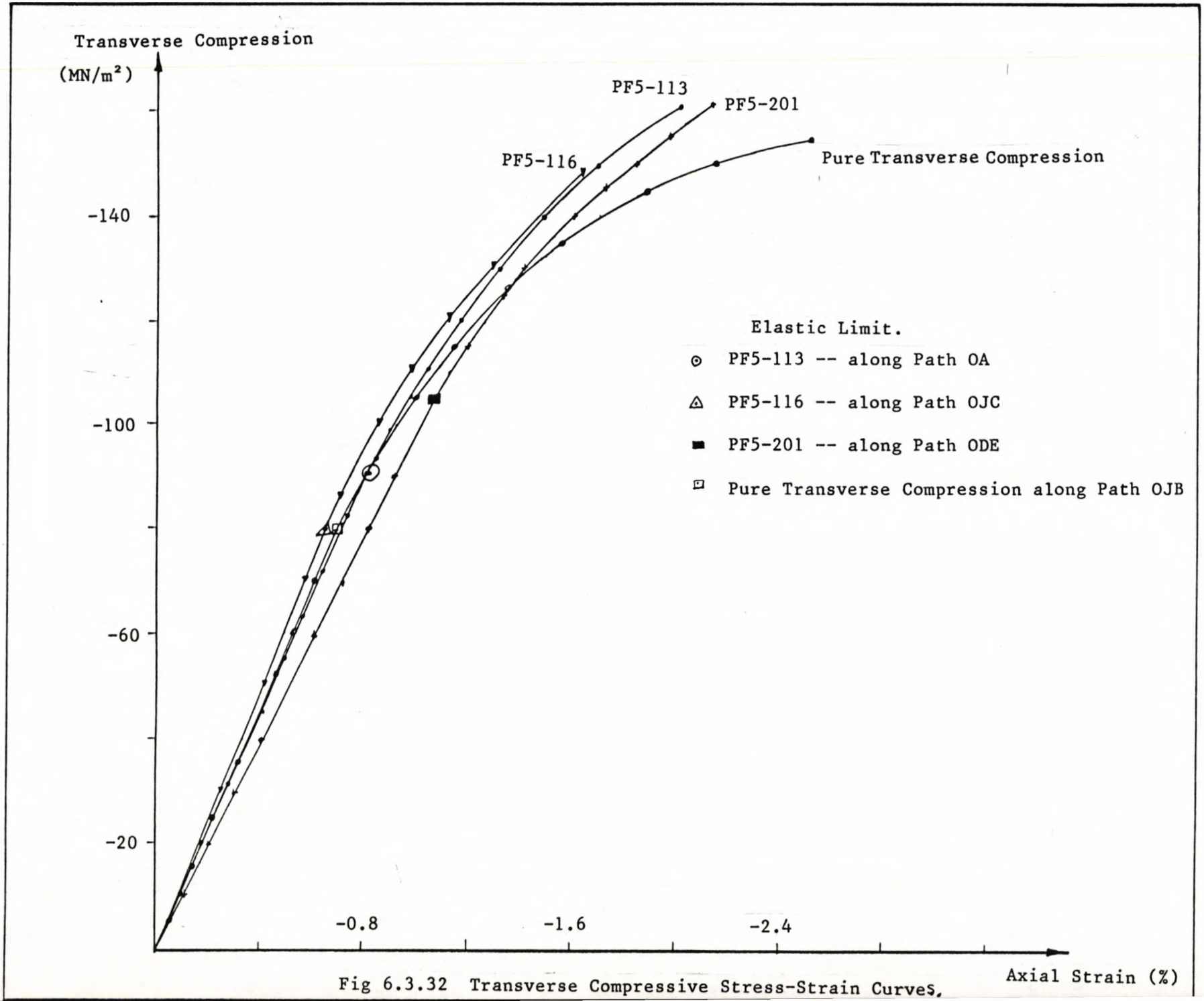

Fig 6.3.32 Transverse Compressive Stress-Strain Curves.

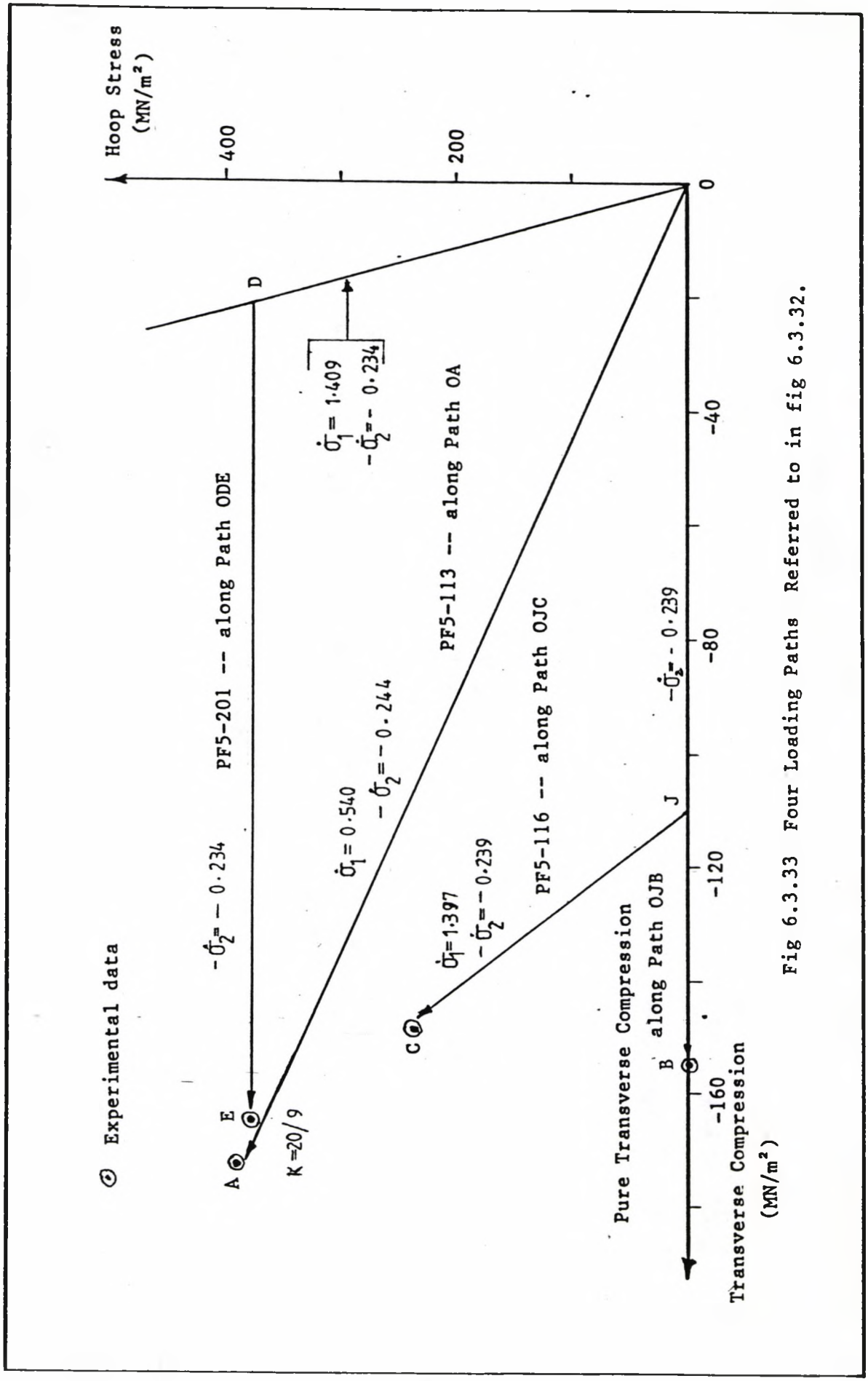

Fig 6.3.33 Four Loading Paths Referred to in fig 6.3.32.

It was demonstrated in Section 6.3.11 that in pure transverse compression ($-\sigma_2$) the plastic shear deformation of the matrix occurred in the following manner shown in fig 6.3.34 and led to the final catastrophic matrix failure.

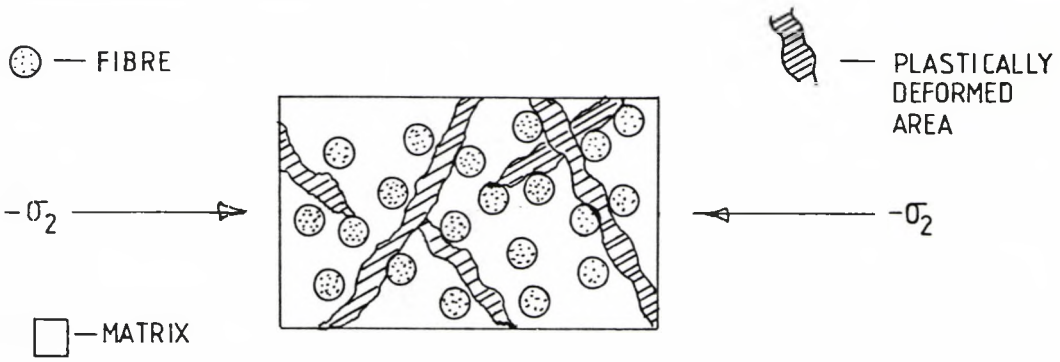

Fig 6.3.34 Plastic Deformation of the Matrix Due to Transverse Compression ($-\sigma_2$).

It is assumed that such matrix failures take place only when the maximum shear stress ($\sigma_{6'}$)$_m$ in the shear plane has fulfilled the requirement

$$(\sigma_{6'})_m \geq \sigma_{6'}^* \qquad .....(6.3.1.3.22)$$

$\sigma_{6'}^*$ is the maximum shear at the point of matrix failure due to pure transverse compressive stress, i.e.,

$$\sigma_{6'}^* = \left|-\sigma_2^*\right|/2 \qquad .....(6.3.1.3.23)$$

Where $-\sigma_2^*$ is the transverse compressive stress measured at the point of fracture of the unidirectional lamina.

Polakowski & Ripling (1966) and Ward (1971) have discussed the increment of shear strengths of a large number of materials with hydrostatic pressure.

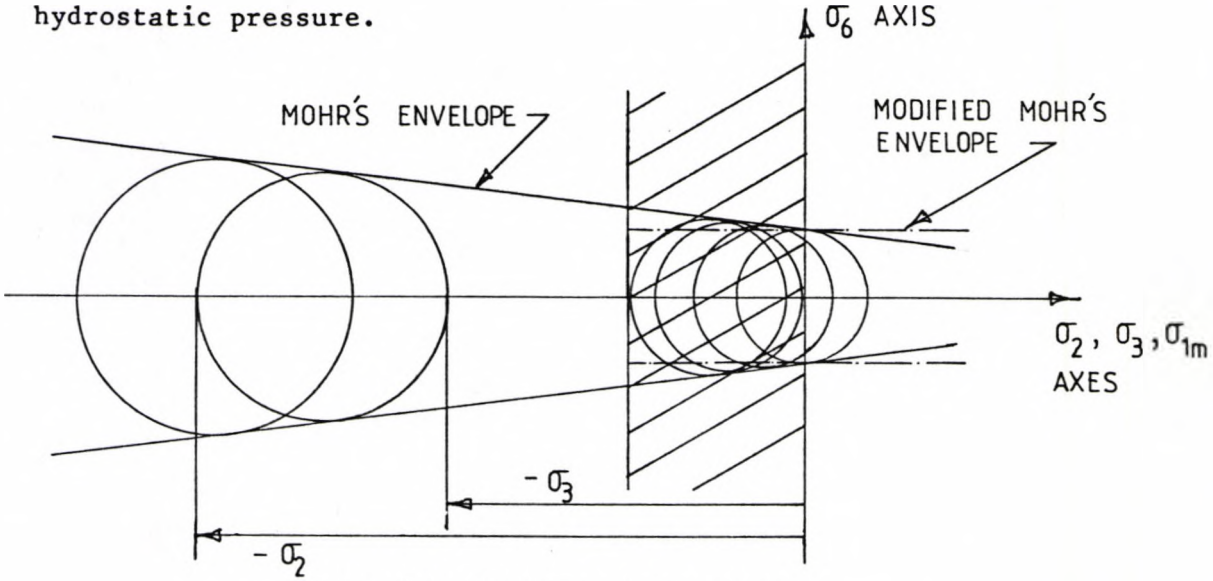

Fig 6.3.34(i) Mohr's Envelope.

A simple form of such variation is shown in fig 6.3.34(i). In the present context only the shaded region is of relevance. The failure behaviour of the matrix is assumed to be governed by the modified Mohr's envelope given in fig 6.3.34(i). It is clear that such a modified envelope will introduce a small error into the stress analysis currently being pursued. Nevertheless, the error is small enough for the assumption implied by equation (6.3.1.3.22) to be justified.

If a similar mode of matrix failure is assumed for the case presented in fig 6.3.30, then equation (6.3.1.3.22) can be used as a criterion for the matrix failure. By re-examining fig 6.3.31 it becomes clear that for

$$(\sigma_6')_{mc2} = (\sigma_6^*)' \qquad \text{.....(6.3.1.3.24)}$$

to be true, either ($-\sigma_3$) has to be reduced to zero or ($-\sigma_2$) is increased further. Therefore, the introduction of the internal pressure apparently increases the transverse compressive strength of a unidirectional lamina. The limited experimental data also indicate the existence of such a feature as is illustrated in fig 6.3.35.

From MC2 in fig 6.3.31 it can be shown geometrically that

$$(\sigma_{6'})_{mc2} = (|-\sigma_2| - |-\sigma_3|)/2 \qquad .....(6.3.1.3.25)$$

When the criterion

$$(\sigma_{6'})_m \geq \sigma_{6'}^* \qquad .....(6.3.1.3.22)$$

is used, then replacing ($\sigma_{6'}$)$_m$ by ($\sigma_{6'}$)$_{mc2}$ and combining equations (6.3.1.3.22) and (6.3.1.3.25) the following expression can be obtained.

$$|(-\sigma_2 - (-\sigma_3))/2| \geq \sigma_{6'}^* \qquad .....(6.3.1.3.26)$$

Now it may be recalled from Section 6.3.1.2 that

$$P_i = (2\sigma_1 \bar{t}) / (\bar{d}_i + \bar{t}) \qquad .....(6.3.1.3.27)$$

But from equation (6.3.1.3.20) the relation between $-\sigma_3$ and the P_i is

$$-\sigma_3 = -P_i \qquad .....(6.3.1.3.20)$$

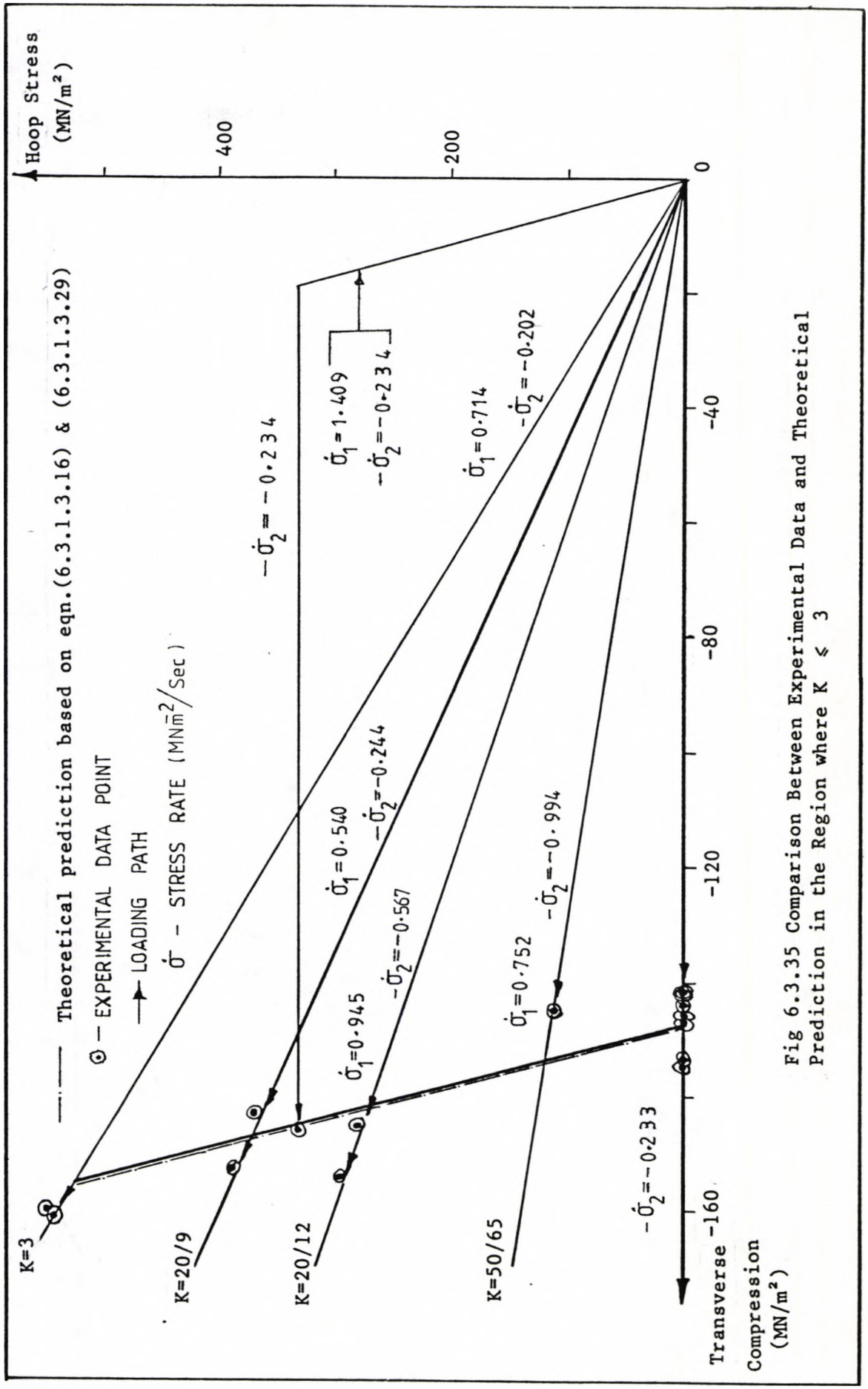

Fig 6.3.35 Comparison Between Experimental Data and Theoretical Prediction in the Region where K ≤ 3

Substituting equation (6.3.1.3.27) into (6.3.1.3.20) the following equation is produced.

$$-\sigma_3 = -(2\sigma_1 \bar{t}) / (\bar{d}_i + \bar{t})$$

.....(6.3.1.3.28)

let

$$K = |\sigma_1 / -\sigma_2| \qquad .....(6.3.1.3.16)$$

By combining equations (6.3.1.3.26), (6.3.1.3.28) and (6.3.1.3.16) the following criterion is obtained

$$\left|(-\sigma_2 - (-\sigma_2 K)(2\bar{t} / (\bar{d}_i + \bar{t})))/2\right| \geq \sigma_6^*$$

i.e.

$$|-\sigma_2| \geq 2\sigma_6^* / ((1 - 2K\bar{t} / (\bar{d}_i + \bar{t}))$$

.....(6.3.1.3.29)

Equations (6.3.1.3.29) and (6.3.1.3.16) were used to compute the transverse compressive and hoop stresses of a lamina at failure for various stress ratios K that satisfy the condition

$$|\sigma_1 / - \sigma_2| \leq 3 \qquad .....(6.3.1.3.5)$$

The value of $\bar{t}$ and $\bar{d}_i$ chosen for the computation were:

$$\bar{t} = 2 \text{ mm}$$

$$\bar{d}_i = 76 \text{ mm} \qquad \text{.....(6.3.1.3.30)}$$

The estimation of the failure stresses based on this model was compared with the experimental data. The agreement between the two sets of data is shown in fig 6.3.35. One possible reason for the experimental data scatter may be the unavoidable variations in $\bar{d}_i$ and $\bar{t}$ of the tubular specimen. As can be seen from equation (6.3.1.3.29) the failure stresses σ_1 and $-\sigma_2$ are influenced directly by the values of $\bar{d}_i$ and $\bar{t}$.

It was found that for all the tests performed with a stress ratio K which satisfied the condition

$$\sigma_1 / |-\sigma_2| \leq 3 \qquad \text{.....(6.3.1.3.5)}$$

the hoop wound tubular specimens failed in a definite way. The fracture process resembled that characteristic fracture mode of a hoop wound tubular specimen subjected to pure transverse compression. The white streaks shown in Plate 6.3.1 appeared in all the specimens tested. When sectioned along the plane perpendicular to the fibre axis and examined under the optical microscope, these sections revealed that the matrix was plastically deformed in a way similar to that due to a pure transverse compression. A subsection of the microscopic view of the deformed plane perpendicular to the fibre axis is shown in optical micrograph 6.3.3.

This finding strengthens the view that a unidirectional lamina fails in the same way whether it is under pure transverse compression ($-\sigma_2$) or biaxial stress involving σ_1 and $-\sigma_2$, provided the requirement

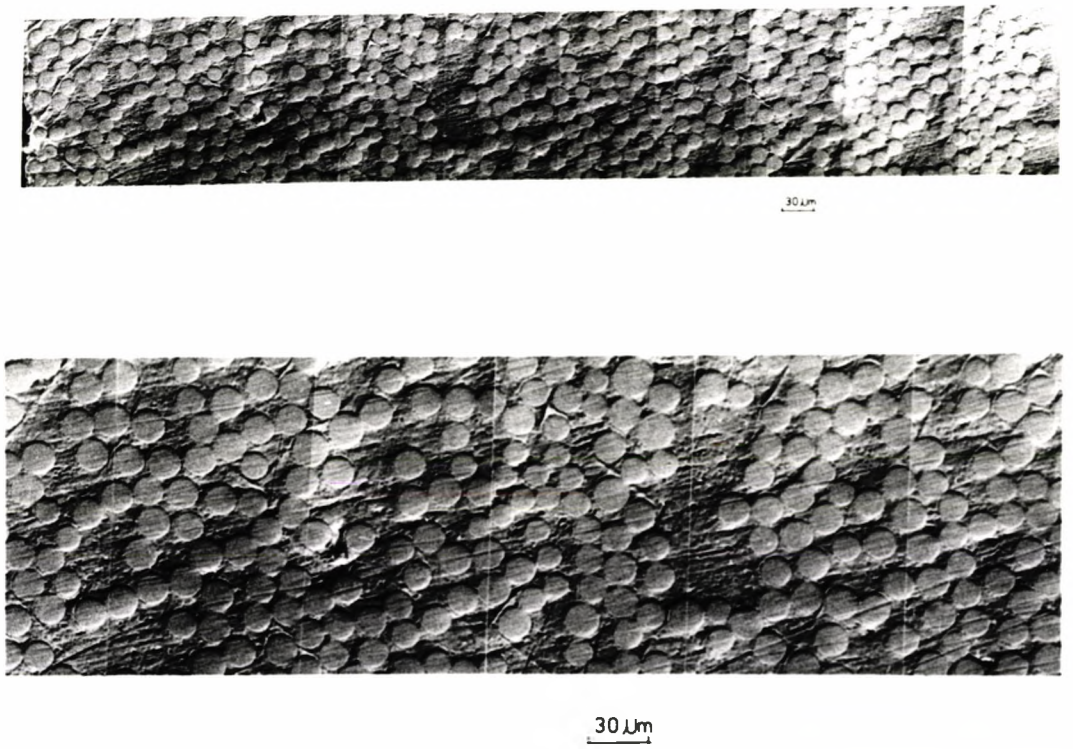

Optical Micrograph 6.3.3 Shear Deformation on the Matrix of a Hoop Wound Specimen Subjected to a State of Biaxial Stress Where the Stress Ratio K < 3 was satisfied.

$$\sigma_1 / |-\sigma_2| \leq 3 \qquad .....(6.3.1.3.5)$$

is met.

The model presented in this section suggest that the transverse compressive strength of hoop wound tubular specimen will increase indefinitely as the internal pressure increases. Unfortunately, this is not the case. As the hoop stress, which is induced by the internal pressure, reaches a level defined by the intrinsic properties of the constituent materials the unidirectional lamina starts to fail with a different fracture mode. The remainder of this section is devoted to the exploration of this 'new' fracture mode.

Laminae subjected to biaxial states of stress with stress ratio equal to 6 failed in a way similar to that shown in Plate 6.3.2. This indicated that fibre fracture was the controlling factor. It was assumed that for stress ratio greater than 3, laminae failed by fibre fracture. This view was confirmed later by testing laminae in the following conditions:

(i) stress ratio equal to 30/7,

(ii) stress ratio equal to 50.

The parameters σ_{1f}^{*} and $\sigma_{6'f}^{*}$ were used in the derivation of the failure criteria of laminae which failed by fibre fracture. The General Assumptions were used in the analysis. In the present context, the fibres in the lamina are assumed to be in an ideal condition. Figure 6.3.36 illustrates the state of stress an ideal fibre will be subjected to if a unidirectional lamina were to be

under a state of biaxial stress (σ_1 vs $-\sigma_2$). It is assumed that the failure of the fibre is initiated by the maximum shear stress present, due to the system of applied stresses.

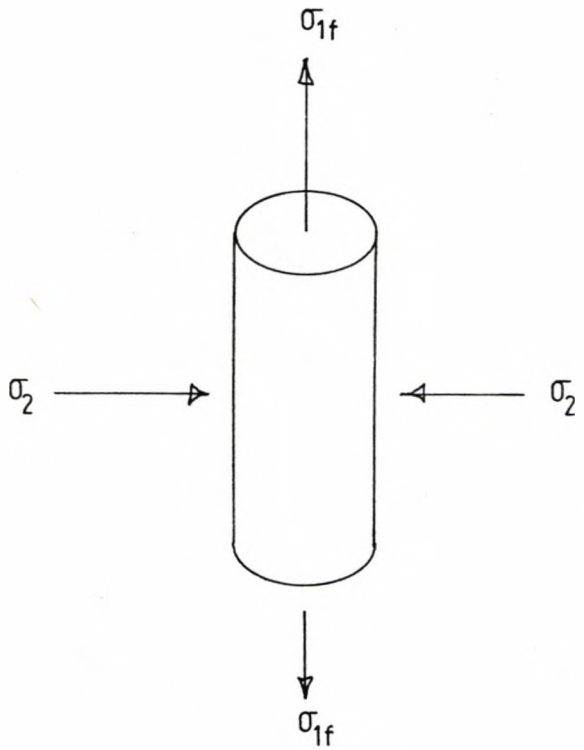

Fig 6.3.36 An Ideal Fibre under a System of Biaxial Stress.

Using equations (6.3.1.2.8b), (6.3.1.2.16) and (6.3.1.2.23) derived in Section 6.3.1.2, it is possible to make an approximation of the stress, due to the applied internal pressure, on the fibre along its axis. There are two ways to approach this problem

(i) using

$$\sigma_{1f} = S_{11} / (S_{11})_f \, \sigma_1 \qquad \text{.....(6.3.1.2.8b)}$$

(ii) using

$$\sigma_{1f} = (\sigma_1 - \sigma_1 (1 - v_f) (S_{11} / (S_{11})_m)) / v_f$$

i.e. $$\sigma_{1f} = (\sigma_1 / v_f) (1 - (S_{11} / (S_{11})_m) (1 - v_f)) \qquad \text{.....(6.3.1.3.32)}$$

Again, it is assumed that the fibre is experiencing the full effect of the transverse compressive stress ($-\sigma_2$). With σ_{1f} and $-\sigma_2$, a Mohr's circle of stress on the fibre can be constructed as sketched in fig 6.3.37.

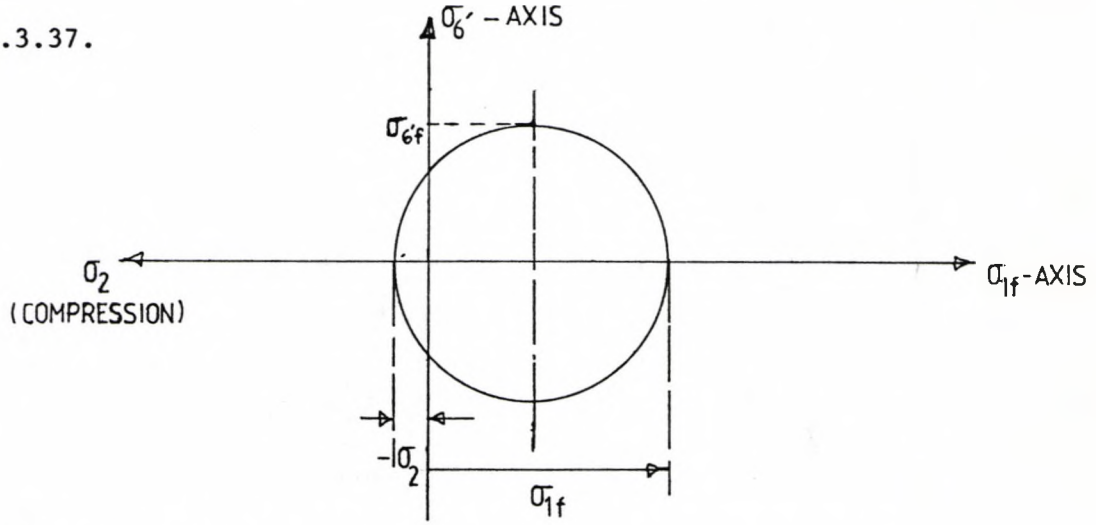

Fig 6.3.37 Mohr's Circle of a Biaxial State of Stress to which a Fibre is Being Subjected.

From geometry,

$$\sigma_{6'f} = (\sigma_{1f} + |-\sigma_2|)/2 \qquad .....(6.3.1.3.33)$$

Let the $\sigma^*_{6'f}$ be the fracture shear stress of the fibre determined from a pure internal pressure test on a hoop wound specimen.

$$\sigma^*_{6'f} = (1/2)\,(\sigma^*_{1f})_{\text{pure hoop}} \qquad .....(6.3.1.3.34)$$

$(\sigma^*_{1f})_{\text{pure hoop}}$ is computed from equation (6.3.1.2.8b). The following expression forms the failure criterion for shear fracture of a fibre.

$$\sigma_{6'f} \geq \sigma^*_{6'f} \qquad .....(6.3.1.3.35)$$

i.e

$$(\sigma_{1f} + |-\sigma_2|)/2 \geq \sigma_{6f}^{*}$$

.....(6.3.1.3.36)

When equations (6.3.1.2.8b) and (6.3.1.3.16) are substituted into equation (6.3.1.3.36) it is possible to show that

$$|(-\sigma_2/2)|\,(1 + (S_{11}/(S_{11})_m)K) \geq \sigma_{6f}^{*}$$

.....(6.3.1.3.37)

where

$$K = \sigma_1/|-\sigma_2|$$

.....(6.3.1.3.16)

However, if equation (6.3.1.3.32) were used in the substitution instead of (6.3.1.2.8b), then

$$\left|(-\sigma_2/2)\right|(1 + (K(1 - (S_{11}/(S_{11})_m)(1 - v_f))/v_f)) \geq \sigma_{6f}^{**}$$

.....(6.3.1.3.38)

Now

$$\sigma_{6f}^{**} = 1/2 \quad (\sigma_{1f}^{*})_{\text{pure hoop}}$$

.....(6.3.1.3.39)

with $(\sigma_{1f}^{*})_{\text{pure hoop}}$ determined from equation (6.3.1.3.32). Therefore, equations (6.3.1.3.29), (6.3.1.3.37), (6.3.1.3.38) and (6.3.1.3.16) were used to examine the failure behaviour of a unidirectional lamina under the biaxial stress (σ_1 vs $-\sigma_2$). It was found that for situations where

$$\sigma_1/|-\sigma_2| > 3$$

.....(6.3.1.3.31)

fibre fracture criteria [equations (6.3.1.3.37) and (6.3.1.3.38)]

were satisfied earlier than the matrix failure criterion [equation (6.3.1.3.29)]. Consequently, it was assumed that the fibre fracture was the critical failure mode for the lamina where the condition given in equation (6.3.1.3.31) was imposed. Figure 6.3.38 shows the performances of the fibre fracture criteria given by equations (6.3.1.3.37) & (6.3.1.3.38) against the experimental data. The existence of tensile stress normal to the plane of maximum shear stress could be a contributing factor towards the large experimental data scatter shown in fig 6.3.38. The small variation of volume fraction in the specimens prepared could be another reason. All the hoop wound specimens tested in the condition

$$|\sigma_1/+\sigma_2| > 3 \qquad .....(6.3.1.3.31)$$

fractured in a mode similar to that shown in Plate 6.3.2, i.e. fibre fracture that led to final failure of the lamina. The secondary fracture surface identical to those shown in scanning micrograph 6.3.6 were observed. No shiny white streaks were found on the tested specimen. Further optical microscopic examination did not reveal any of the features shown in optical micrograph 6.3.3. This suggested that there was no matrix plastic shear deformation on the weak planes (see fig 6.3.34).

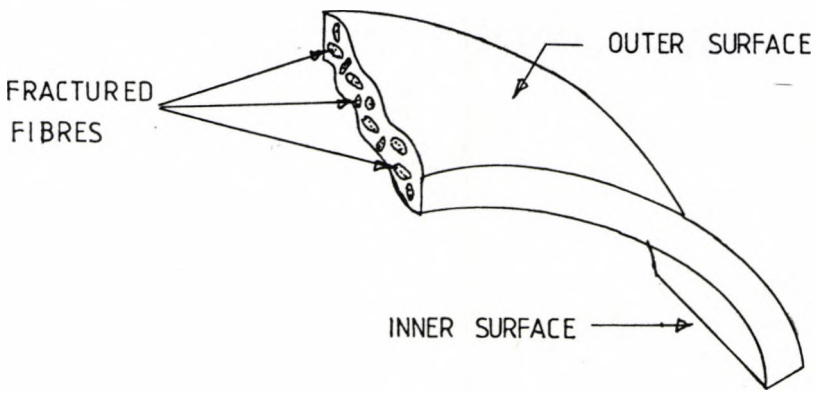

Fig 6.3.39 Section of the Specimen which Contains the Fractured Fibres.

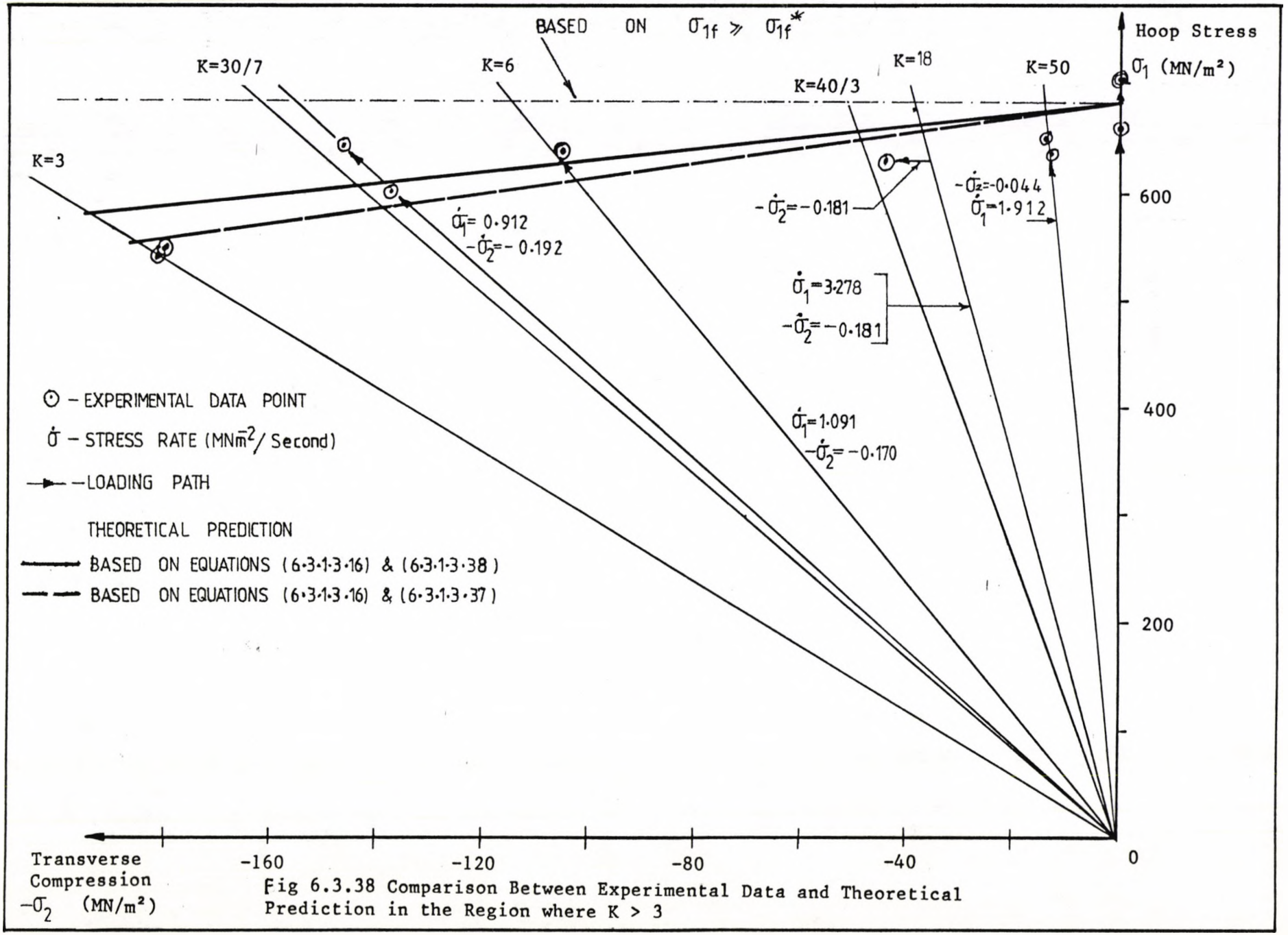

Fig 6.3.38 Comparison Between Experimental Data and Theoretical Prediction in the Region where K > 3

A section that contains complete fibre fracture (shown in fig 6.3.39) was obtained from each specimen which had been tested in condition

$$\sigma_1 / |-\sigma_2| > 3 \qquad .....(6.3.1.3.31)$$

These were examined using a scanning electron microscope. The general appearance of the fracture surfaces are similar to those shown in scanning micrographs 6.3.3, 6.3.4 and 6.3.6. They confirm that massive fibre fracture did take place. In addition, they also give evidence that the second phase of the failure of the lamina was identical to that due to pure hoop stress mentioned in Section 6.3.1.2.

The final form of the failure loci of a lamina was thought to resemble that shown in fig 6.3.40.

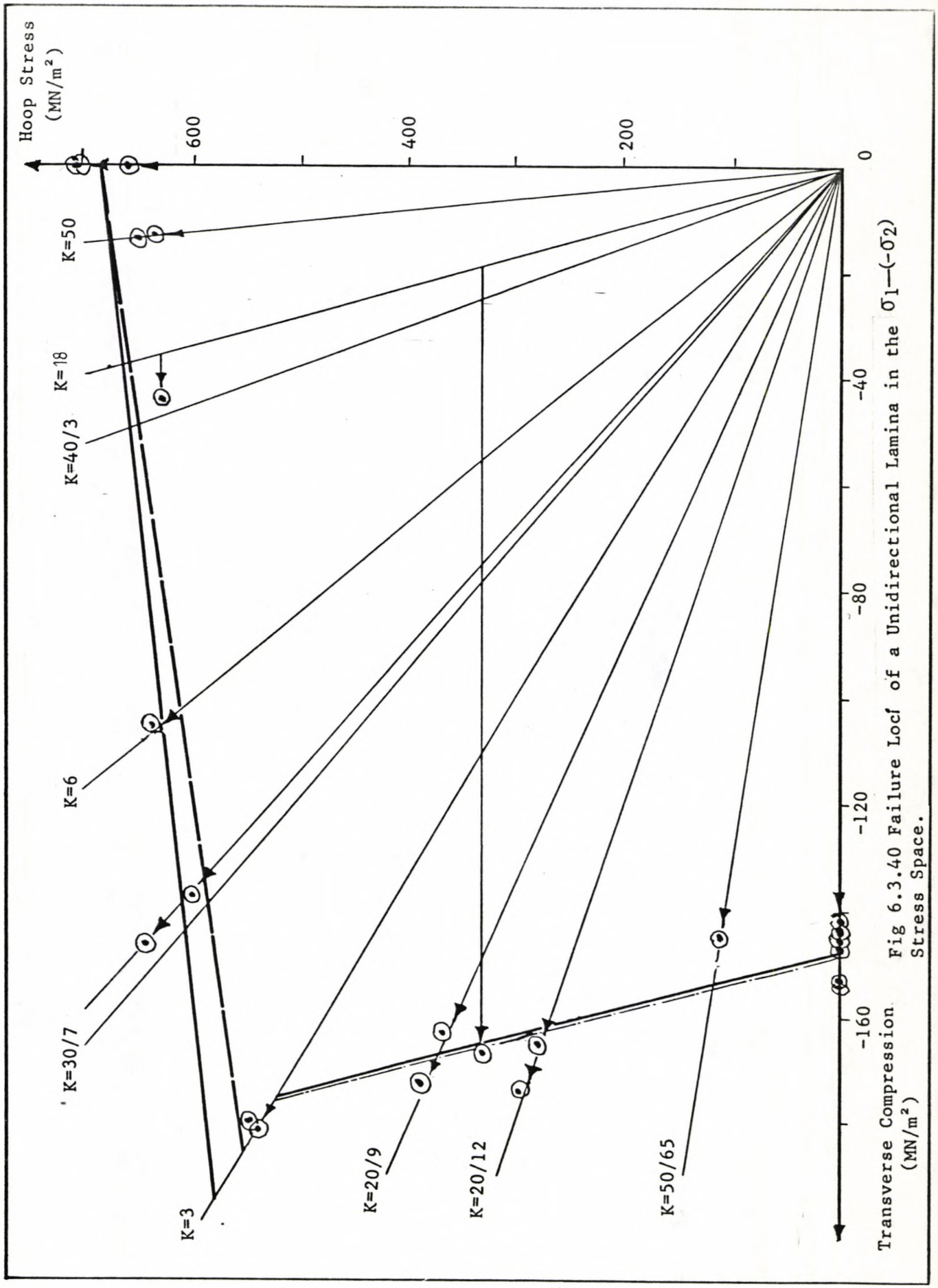

Fig 6.3.40 Failure Locf of a Unidirectional Lamina in the σ_1—($-\sigma_2$) Stress Space.

6.3.1.4 The Effect of Loading Path on the Failure Conditions of a Unidirectional Lamina:

The concept of the loading path effect on the failure conditions of unidirectional laminae is defined with the aid of fig 6.3.41.

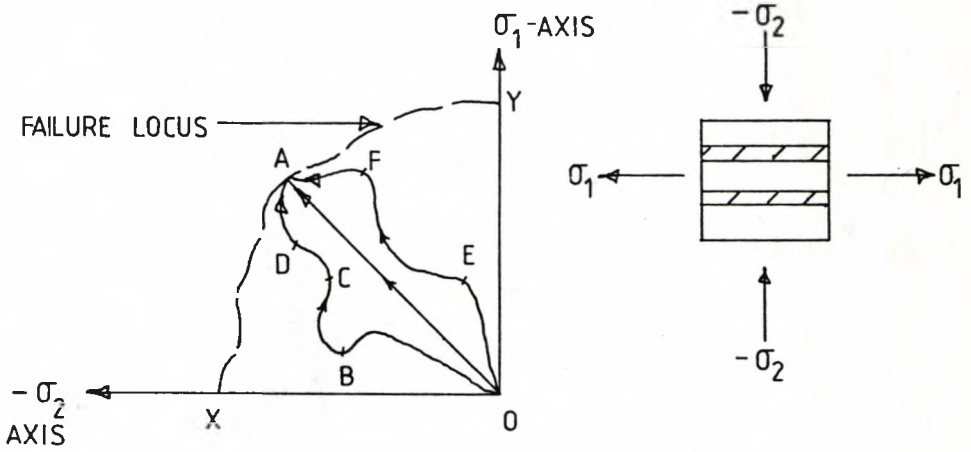

Fig 6.3.41 The Effect of Loading Path.

Assume that locus XAY is a failure locus of the unidirectional lamina. It is determined either experimentally or theoretically using straight-forward loading vectors such as OA. Point A is a failure point determined by loading a specimen along path OA. If the failure point A is independent of loading path, then identical specimens loaded along paths OEFA and OBCDA will also fail at point A. On the contrary, if the failure point A is dependent on the loading path, then identical specimens loaded along paths OA, OEFA and OBCDA will have different failure points.

As explained in Section 6.3 the failure locus shown in fig 6.3.40, which was established in Sections 6.3.1.1, 6.3.1.2 and 6.3.1.3, was employed for the planning of the loading paths. The

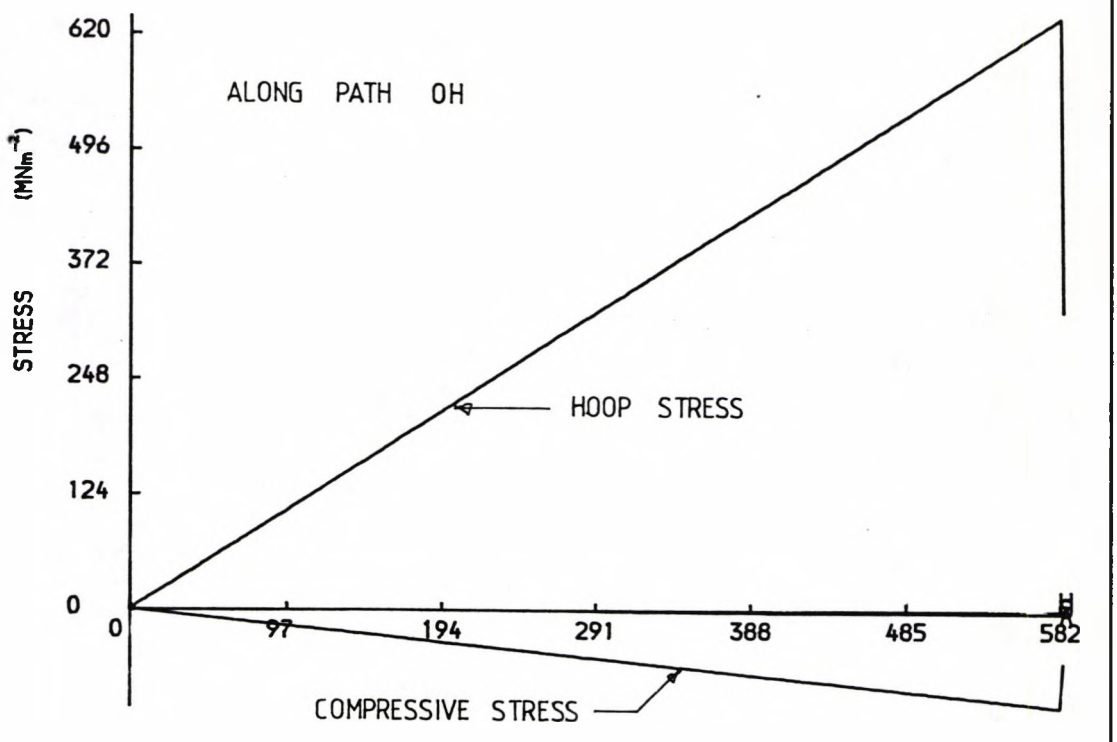

FIG 6.3.42a , STRESSES VS TIME

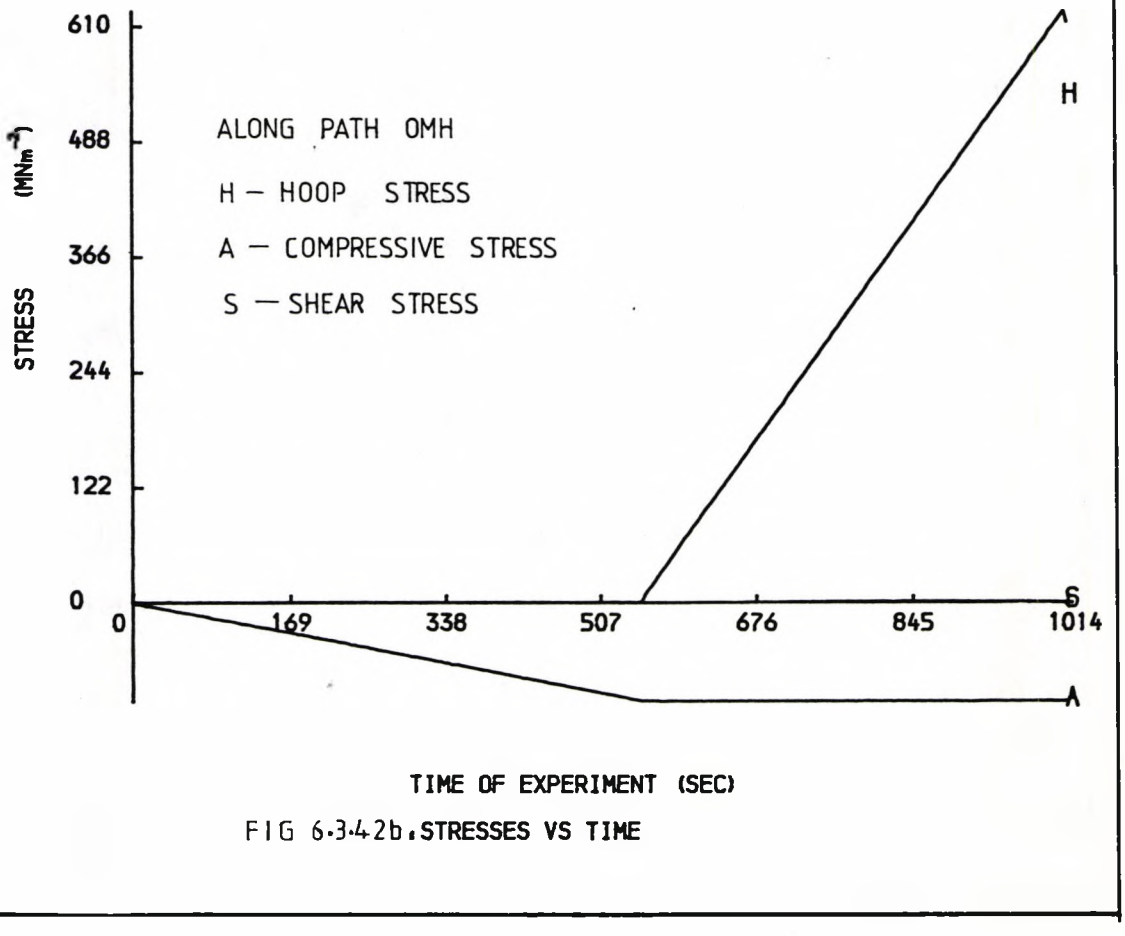

FIG 6.3.42b , STRESSES VS TIME

selected paths for the investigation of loading path effects were sketched in fig 6.3.4. For the ease of reference it is reproduced below.

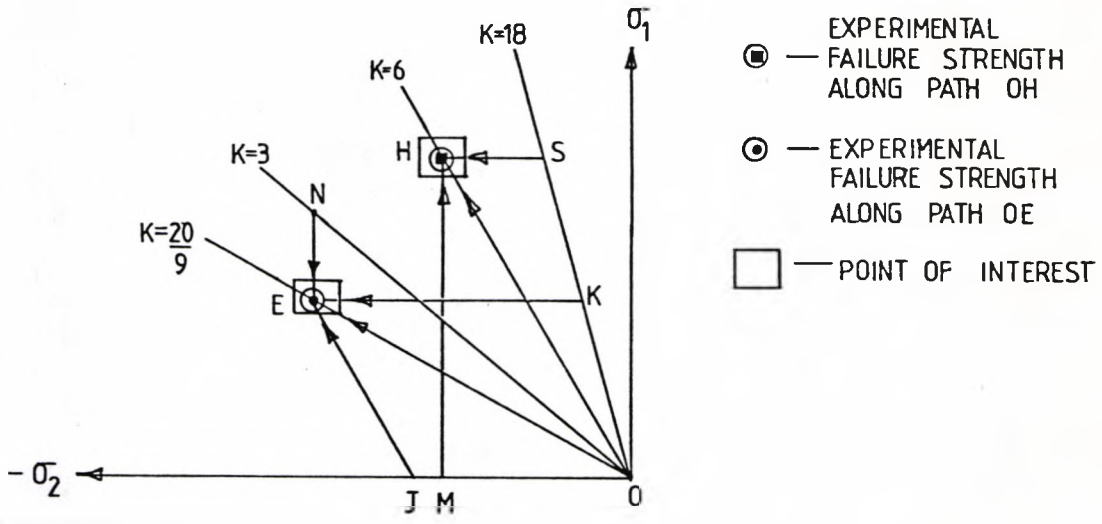

Fig 6.3.4 Experiments devised for the Examination of the Effect of Loading Paths.

The chosen regions of study, i.e. E & H, offer the opportunity to analyse the effects of loading path on two entirely different failure modes. Point E is in the domain where shear matrix failure is critical, whereas point H is in an area where fibre fracture is the dominant factor.

The loading histories of laminae along paths OH and OMH are given in fig 6.3.42. Due to time constraints, no strain responses were measured in the tests.

At point M, the transverse compressive stress was 103 MN/m^2. From fig 6.3.43 it can be seen that plastic flow would have certainly started at point M. It was discussed in Sections 6.3.1.1 and 6.3.1.2 that the plastic deformation of the matrix as illustrated in the

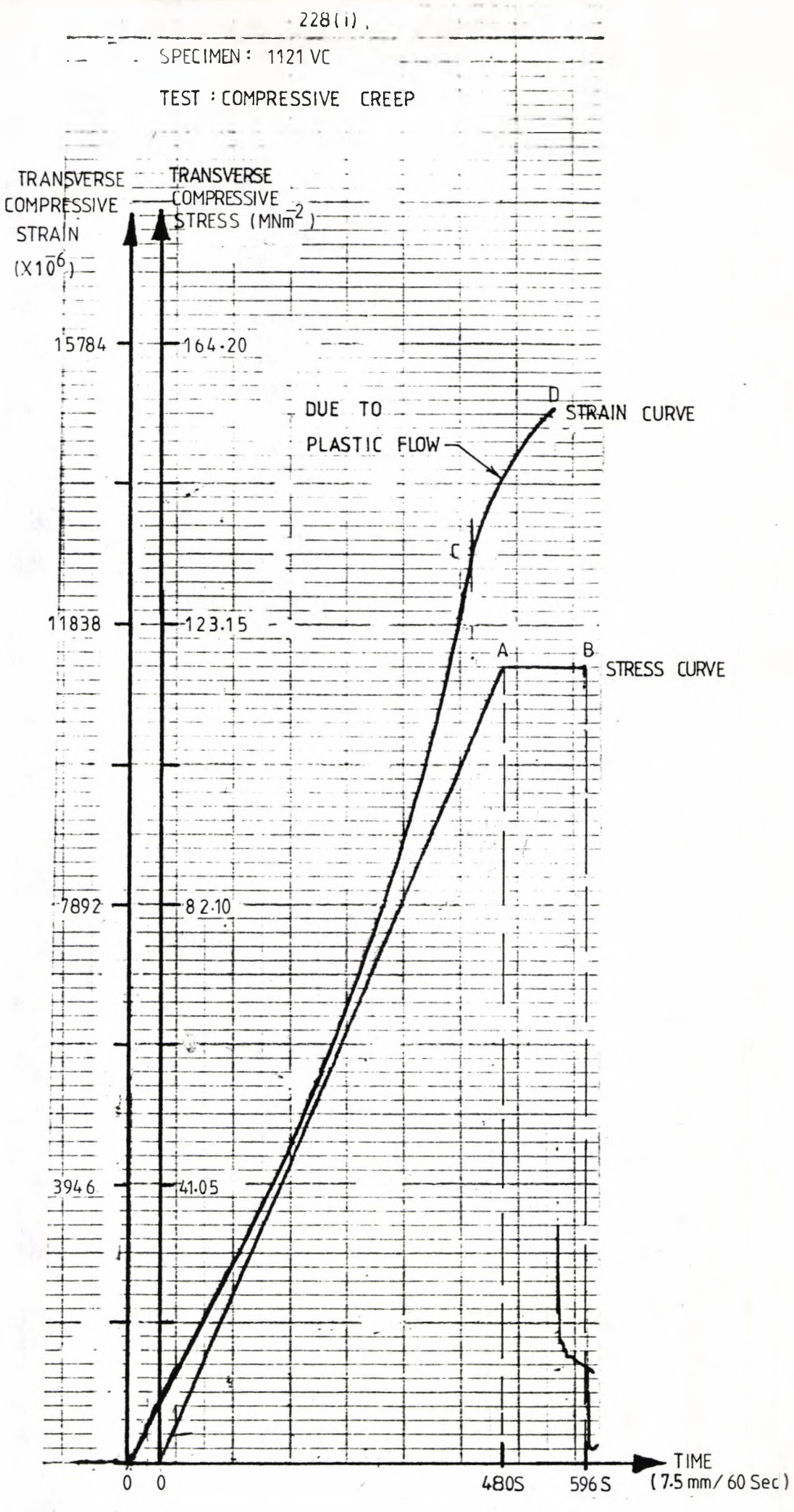

FIG 6.3.43 THE VISCOUS EFFECT (IN THE PLASTIC DOMAIN) ON A LAMINA UNDER A PURE TRANSVERSE COMPRESSIVE STRESS

diagram below does not lead to the total failure of the lamina because of the fibre.

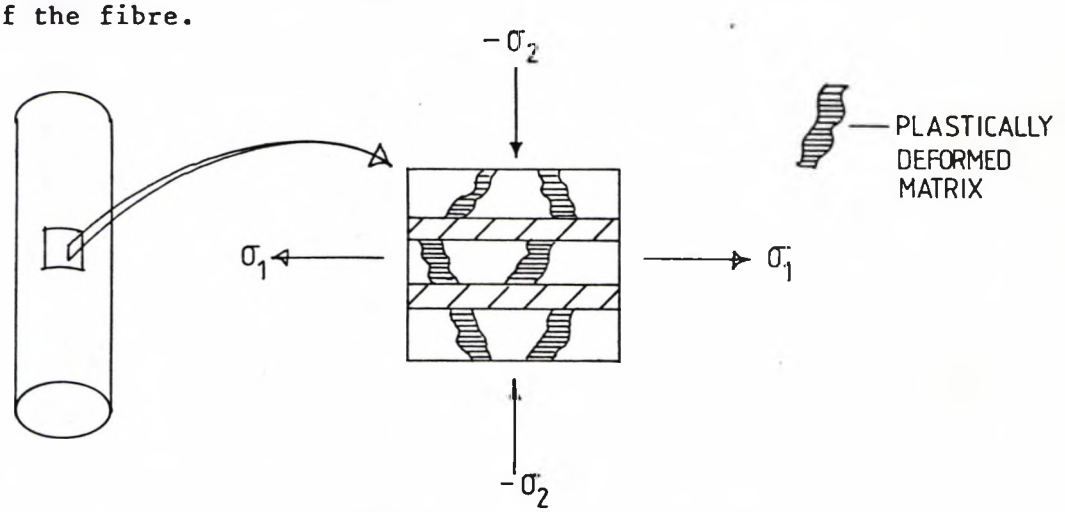

Fig 6.3.44 Element under Biaxial Stresses

Only when fibre fracture occurs will there be a complete lamina failure. In contrast, the viscous-plastic effect can influence the following weak planes profoundly.

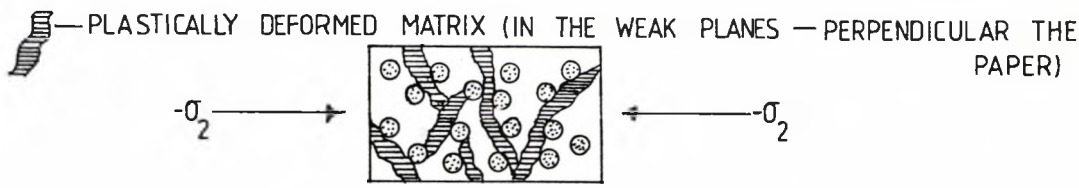

Fig 6.3.45 Element Under A System of Biaxial Stress (σ_1 vs $-\sigma_2$), σ_1 Is Perpendicular to Paper.

Indeed, as demonstrated in fig 6.3.43 the viscous-plastic effect on the weak planes shown in fig 6.3.45 can lead to complete failure of a lamina. Along path MH (fig 6.3.4) time becomes critical. Let the time required for the hoop stress (σ_1) to reach the level which precipitates fibre fracture be t_{ff}. Let the time required for the creep (in the plastic domain) from the point M to total failure of a lamina be t_{pc}.

If

$$t_{ff} > t_{pc}$$

.....(6.3.1.4.1)

creep failure (in the plastic domain) will take place. On the other hand, if

$$t_{pc} > t_{ff}$$

.....(6.3.1.4.2)

then failure of the lamina due to the fibre fracture will result. This phenomenon is one aspect of the loading path effect.

As discussed in Section 6.3.1.3, the internal pressure has an additional effect; it induces a compressive stress along the radial direction ($-\sigma_3$). The actual system of stress acting on the plane perpendicular to the fibre axis is shown in fig 6.3.46.

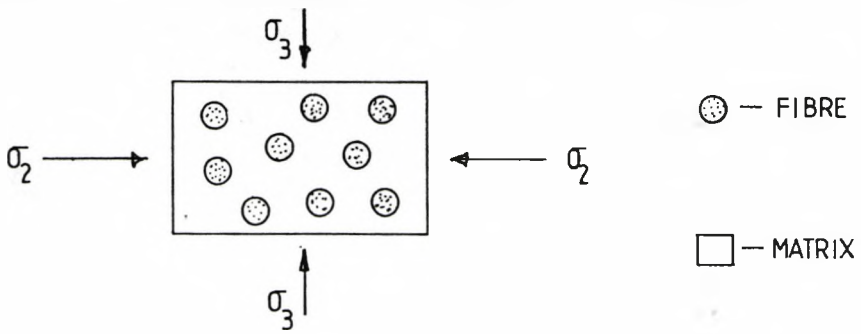

Fig 6.3.46 Element Under A System of Biaxial Stress

The addition of $-\sigma_3$ reduces the shear stress present in the matrix of the element shown in fig 6.3.46 (see Section 6.3.1.3). Therefore, along path MH (fig 6.3.4) this shear stress was decreasing with increasing internal pressure. As a result, the onset of the plastic flow was at least delayed and probably suppressed completely. In such a circumstance, fibre fracture becomes the only possible primary failure mode and hence the failure mode at point H was the same irrespective of whether the lamina was loaded along OH or OMH. The

limited experimental information indicates that this is so, i.e. the region considered might be independent of the loading path.

$-\sigma_3$ also plays a vital role at point E. In this case, the delay of plastic shear deformation on the matrix of the weak planes (see fig 6.3.46) does not lead to fibre fracture, since the level of σ'_{6f} at point E is far below σ'^{*}_{6f}. Such a delay merely increases the transverse compressive strength of the lamina for reasons that were explained earlier. The failure mode at point E is shear matrix failure in the weak planes. Therefore, it is expected that loading paths OE and OKE will produce the same failure conditions. Again by referring to fig 6.3.43 it becomes obvious that viscous-plastic behaviour of the lamina materialised at point J of fig 6.3.4 and that this behaviour will affect the failure conditions. The extent of this depends on the time taken for the application of $-\sigma_3$ along path JE. N is within the failure envelope. Therefore, at point N no failure will take place in normal circumstances. The case of internal pressure reduction along path NE can be explained tentatively in the following way:

Assume that at point N the Mohr's circle representation of the system of stress of an element shown in fig 6.3.47(a) has the appearance sketched in fig 6.3.47(b).

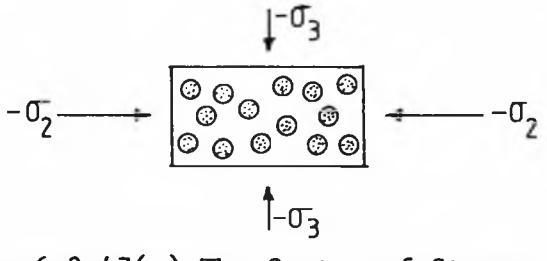

Fig 6.3.47(a) The System of Stress At Point N

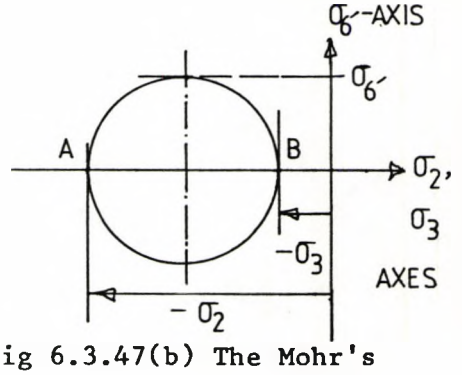

Fig 6.3.47(b) The Mohr's Circle Representation

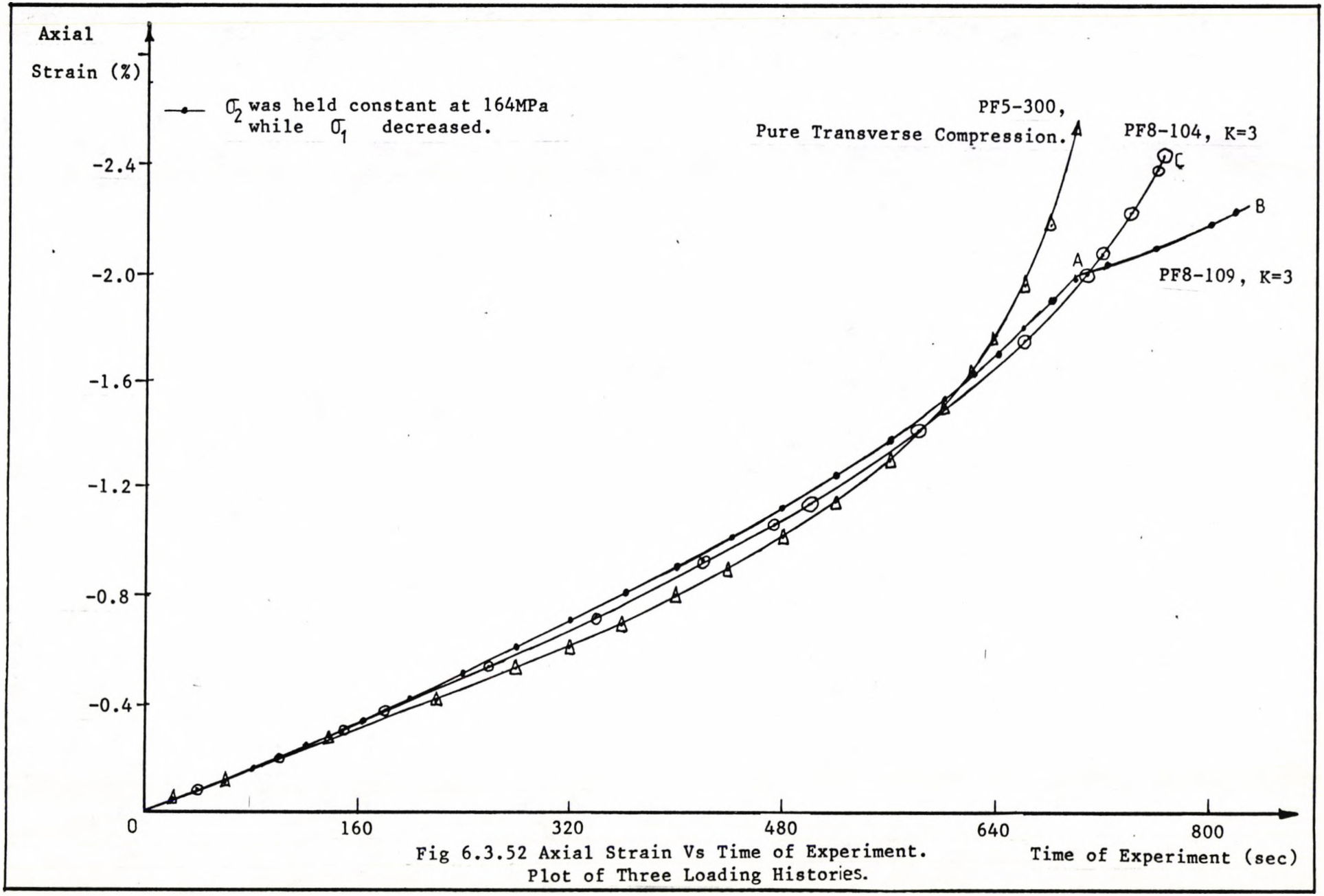

Fig 6.3.52 Axial Strain Vs Time of Experiment.
Plot of Three Loading Histories.

The magnitude of $\bar{\sigma}_{6'}$ is not high enough to cause matrix shear failure. Neither is the shear stress in the fibre large enough to cause fibre fracture. The transverse compression ($-\bar{\sigma}_2$) is held at a constant level along path NE. When the system of biaxial stress is changed from point N to E the Mohr's circle of stress alters in the manner shown in fig 6.3.47(c)

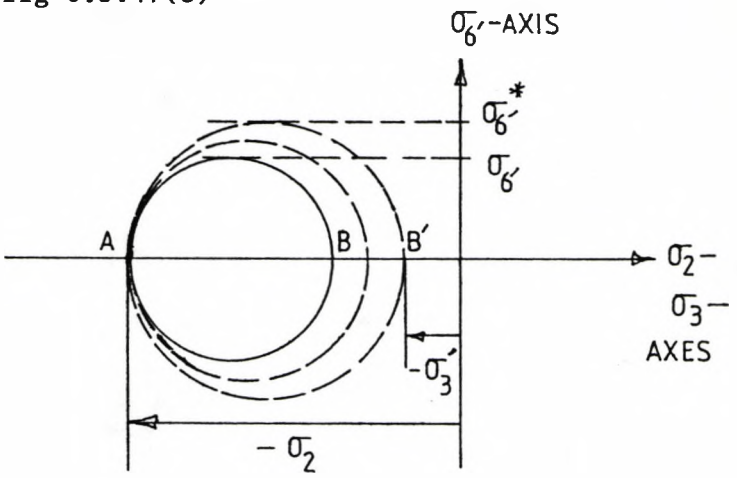

Fig 6.3.47(c) Alteration of the Mohr's Circle Along Path NE.

The effect of reducing the applied internal pressure is to shift point B towards the origin. This process undoubtedly increases the value of $\bar{\sigma}_{6'}$. When it reaches the level of $\bar{\sigma}_{6'}^*$ failure of the matrix takes place. As the value of $\bar{\sigma}_{6'}$ increases the transverse compressive strain would be expected to increase. This trend can be observed from fig 6.3.52. The drastic drop in the transverse compressive strain response from AC to AB is due to the Poisson effect of $\bar{\sigma}_1$. The increase of strain along AB is suspected to be partially due to the increase in $\bar{\sigma}_{6'}$ explained above.

Given below is a series of figures illustrating the loading and strain response histories of each loading path used for the investigation of its effect on the failure condition at point E shown in fig 6.3.4. The experimental data obtained from this study are

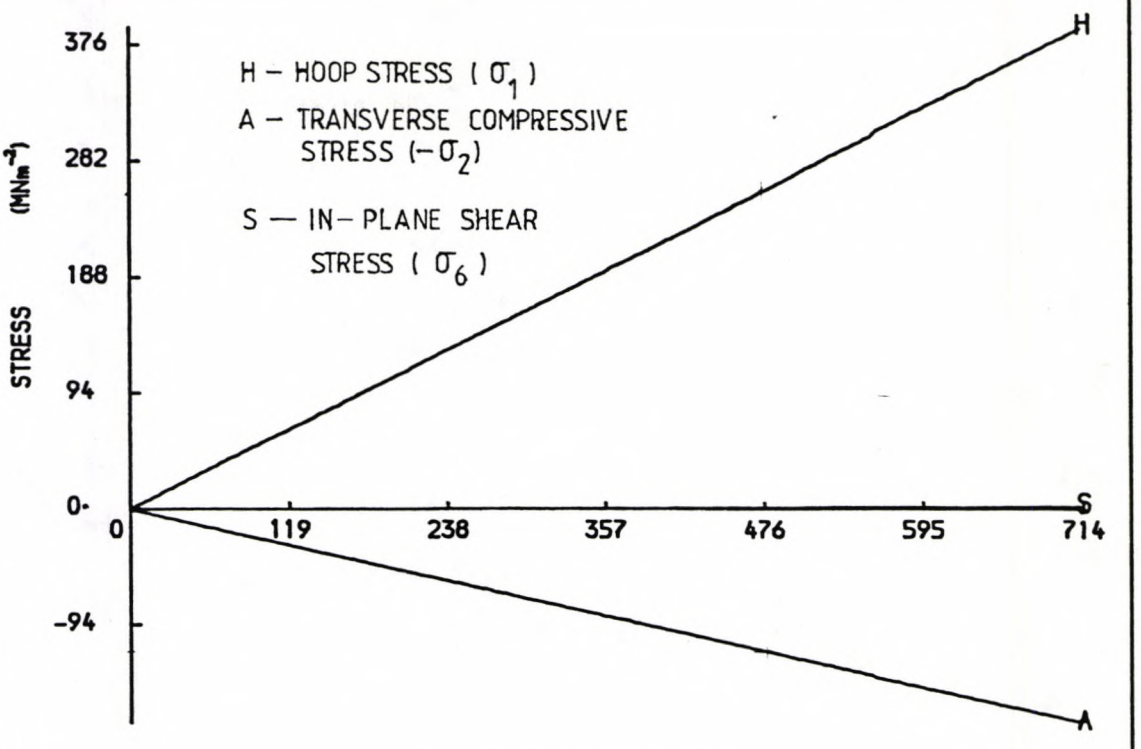

FIG 6·3·48a. STRESSES VS TIME FOR PATH OE

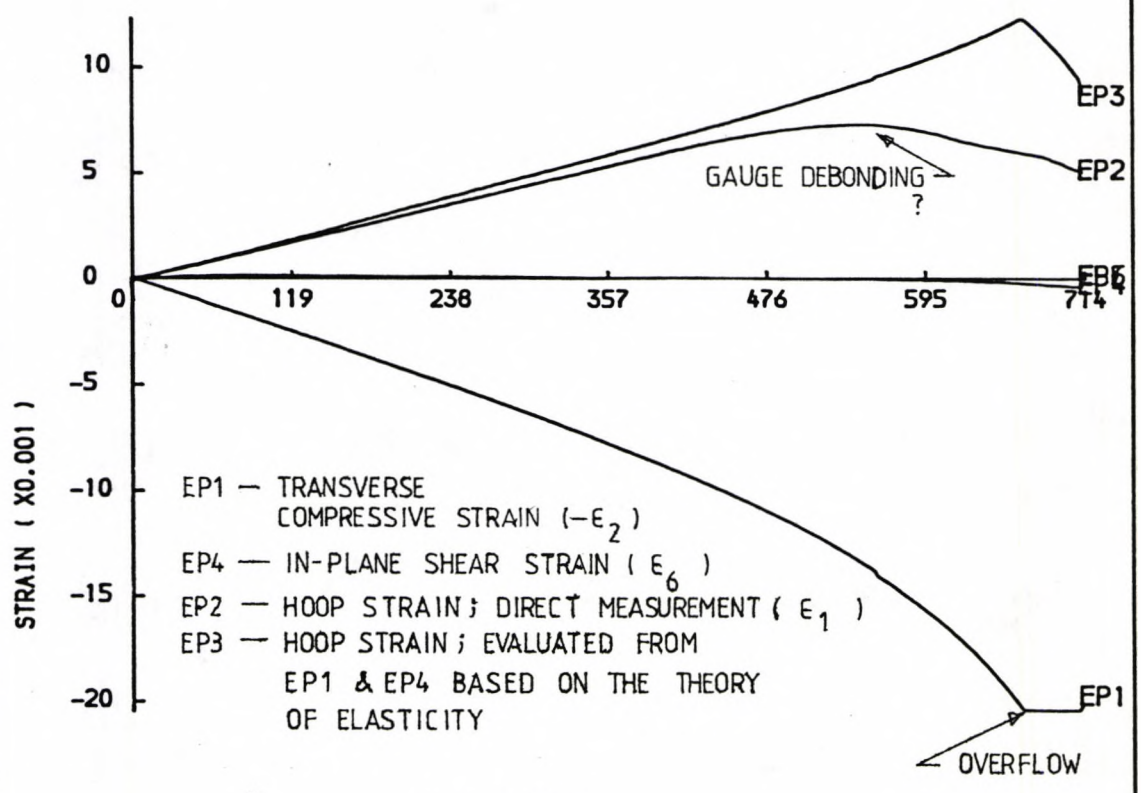

FIG 6·3·48b. STRAIN VS TIME

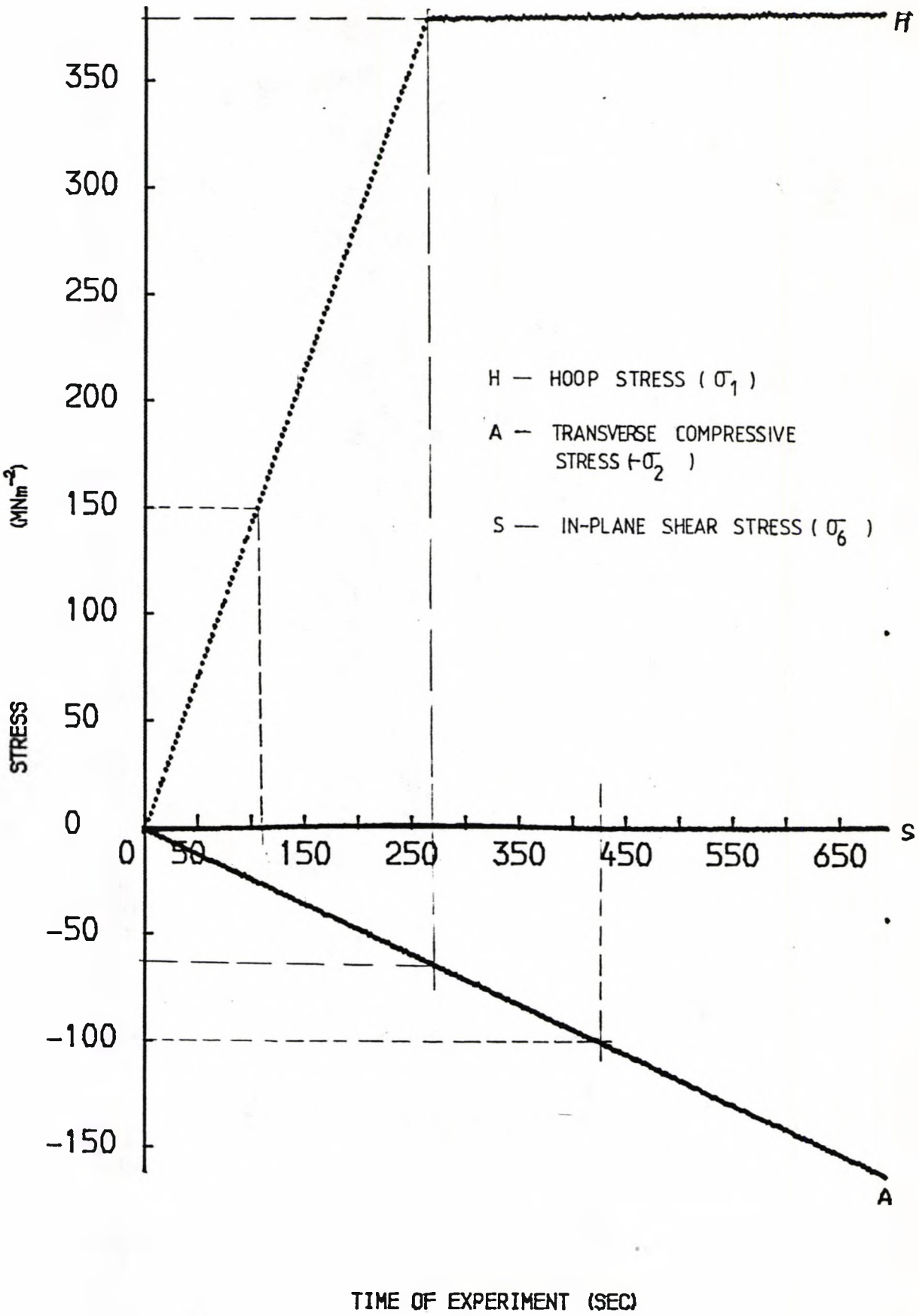

FIG 6.3.49a STRESSES VS TIME FOR PATH OKE

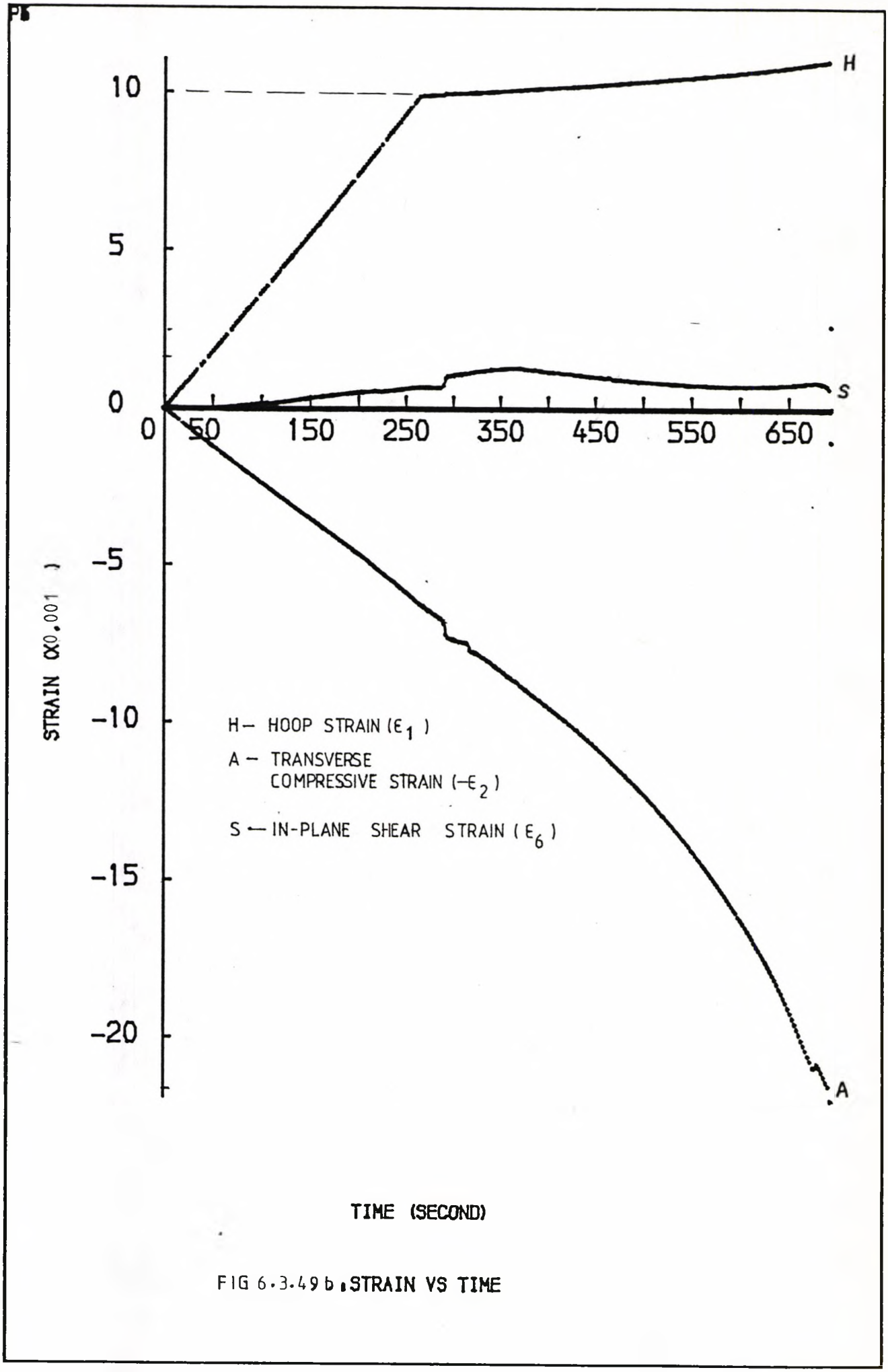

FIG 6.3.49 b : STRAIN VS TIME

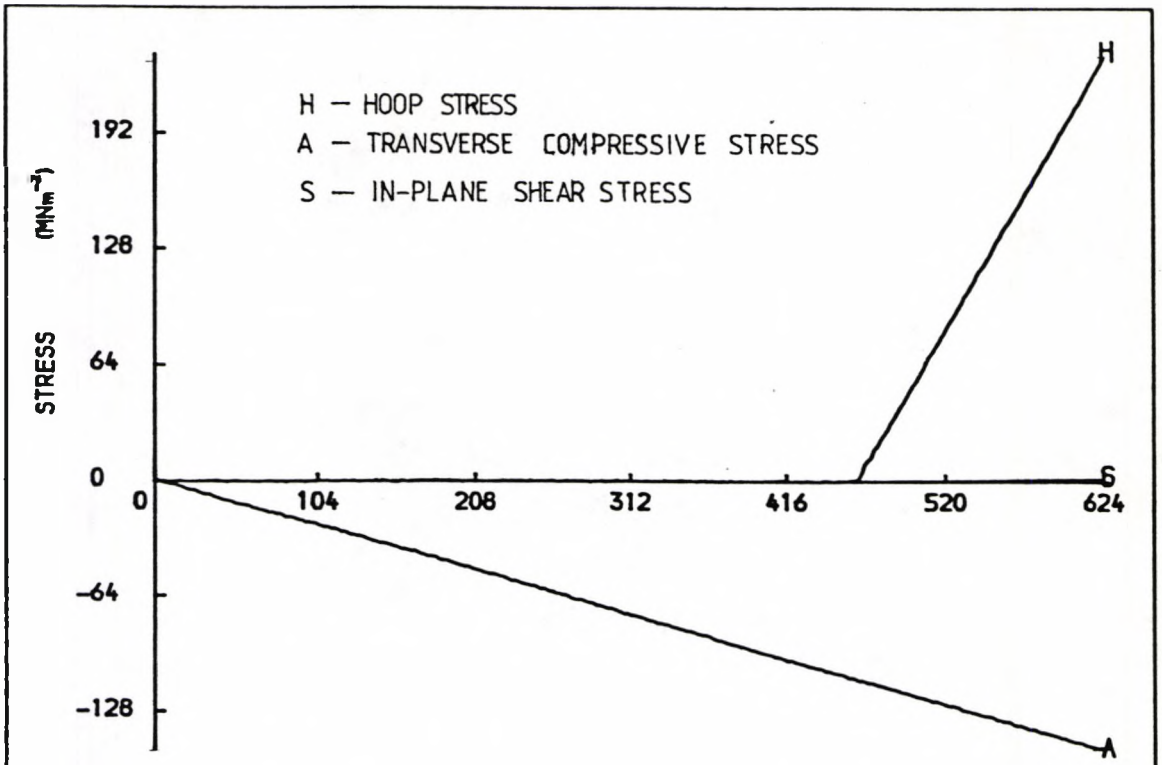

FIG 6.3.50a **STRESSES VS TIME**
FOR PATH OMJE

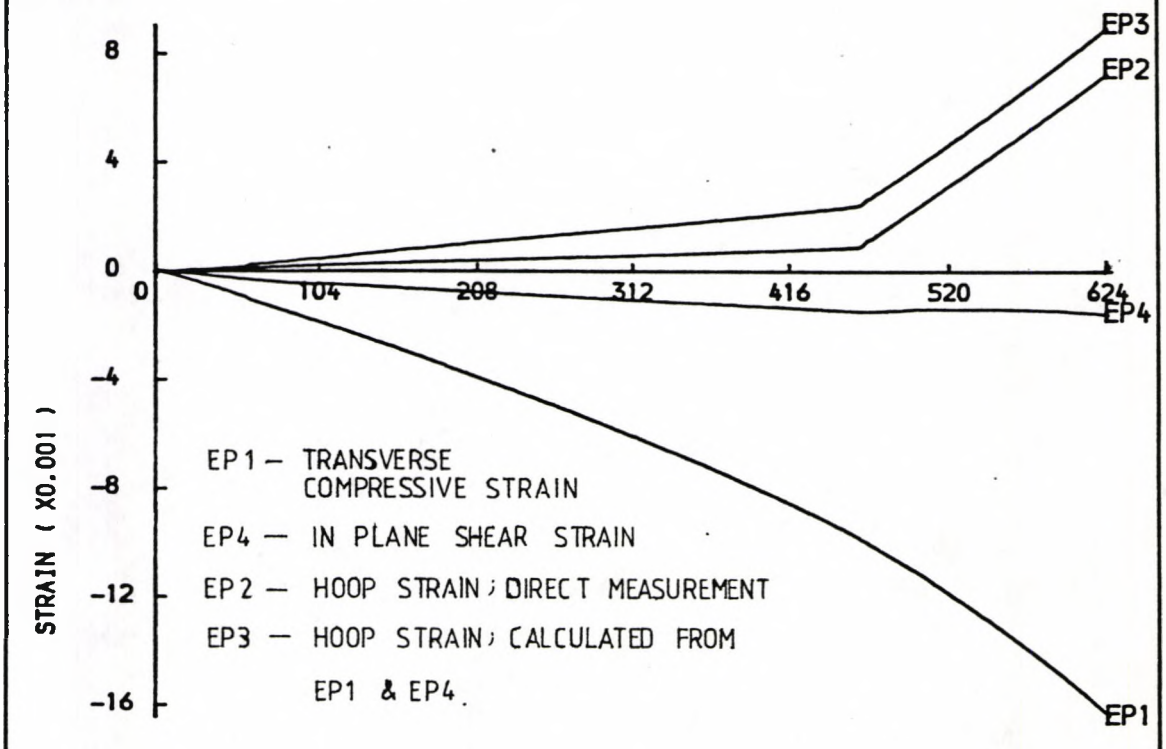

FIG 6.3.50b **STRAIN VS TIME**

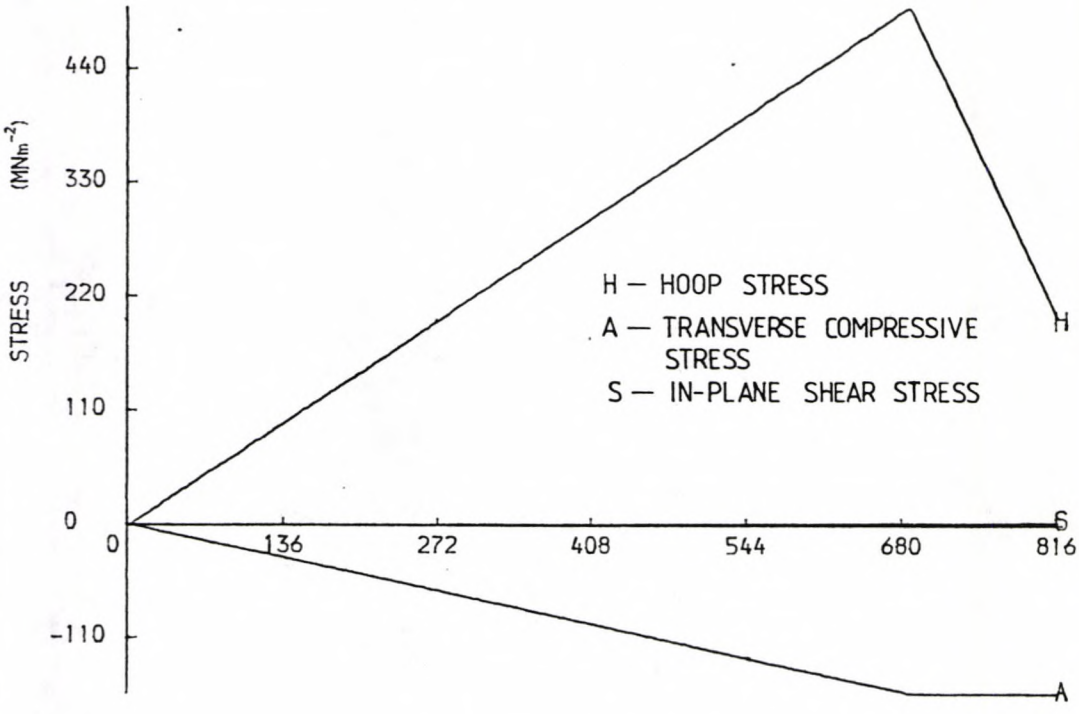

FIG 6.3.51a , STRESSES VS TIME FOR PATH ONE

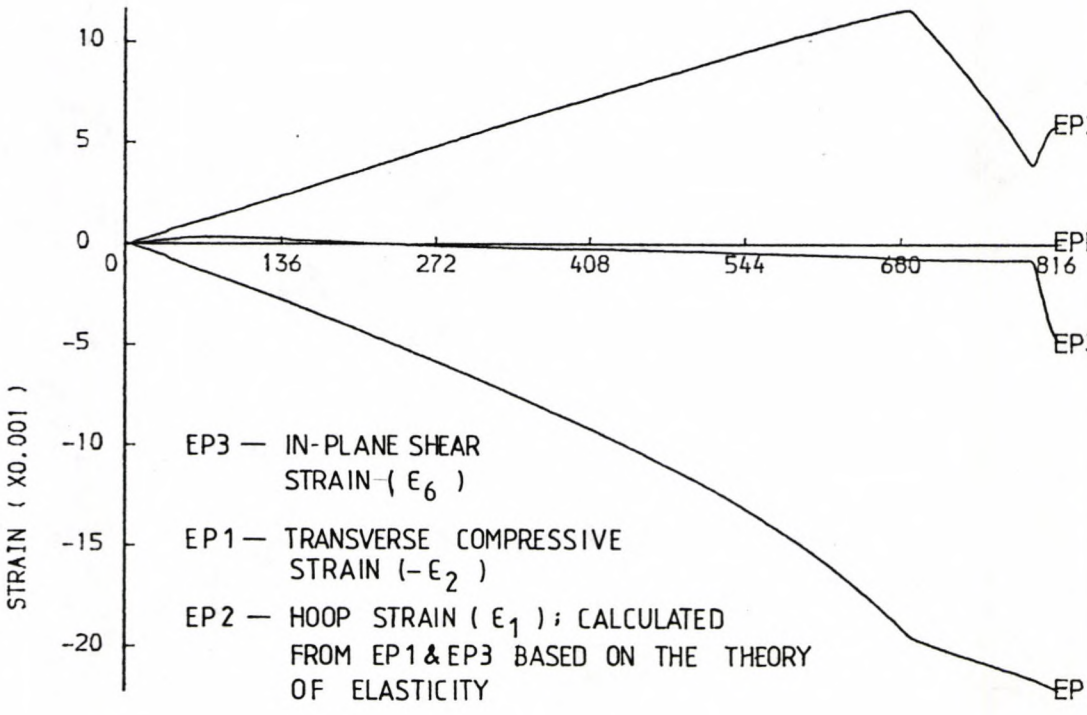

FIG 6.3.51b , STRAIN VS TIME

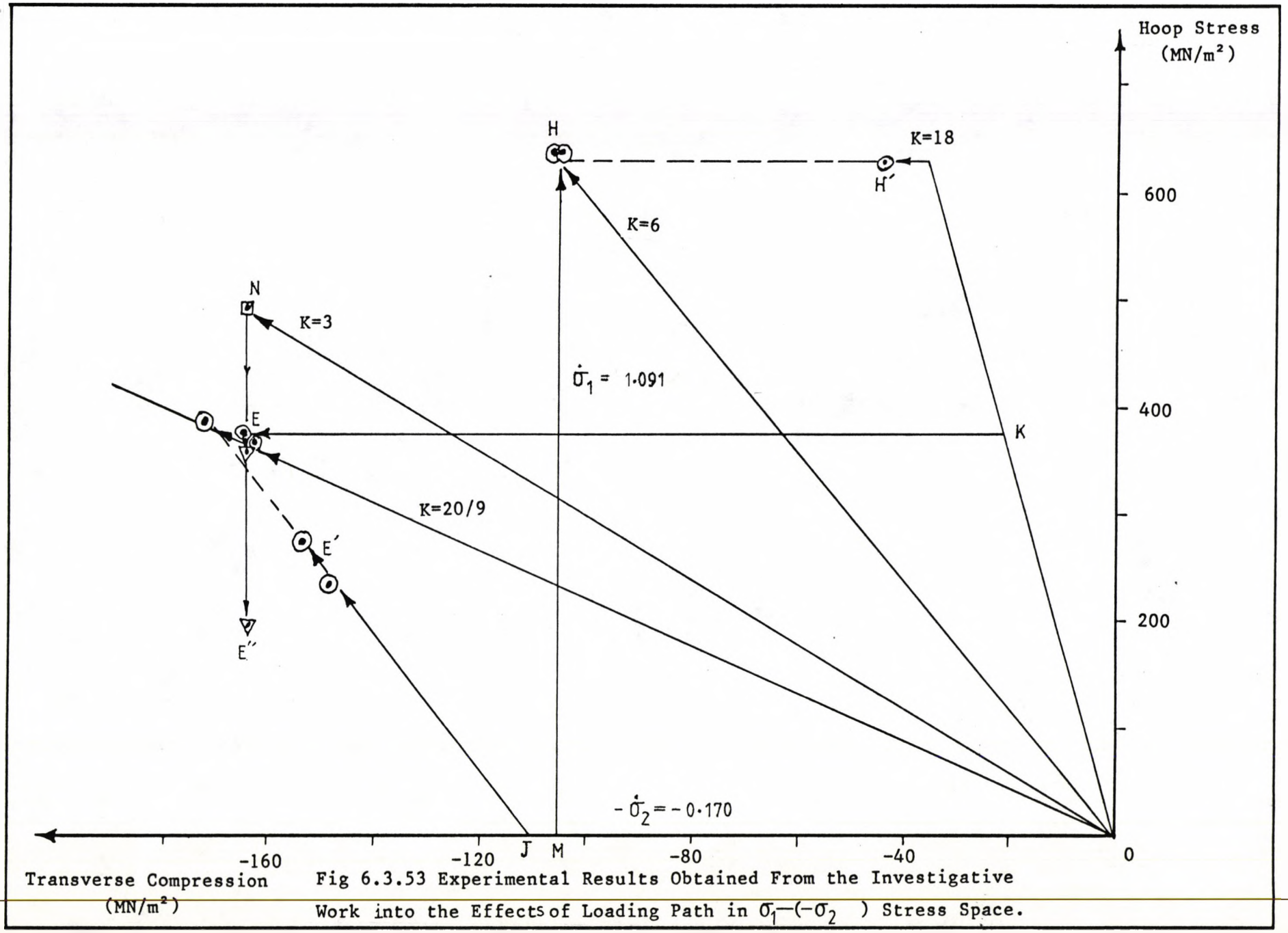

Fig 6.3.53 Experimental Results Obtained From the Investigative Work into the Effects of Loading Path in σ_1—($-\sigma_2$) Stress Space.

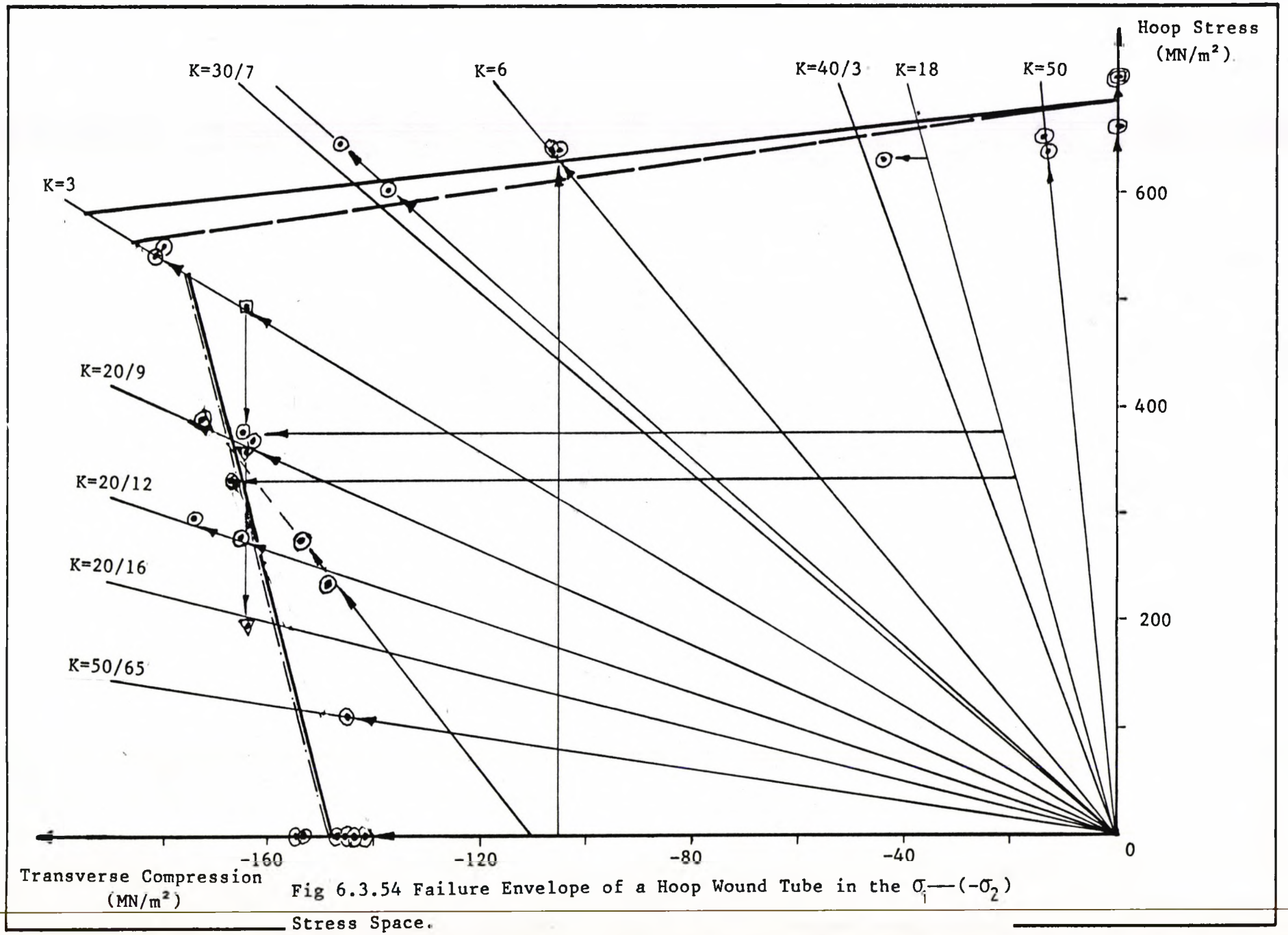

Fig 6.3.54 Failure Envelope of a Hoop Wound Tube in the σ_1—$(-\sigma_2)$ Stress Space.

presented in fig 6.3.53. The experimental data give an impression that the failure behaviour of the laminae subjected to biaxial stresses (σ_1 / $-\sigma_2$) is dependent on the loading path. The viscous-plastic effect was probably experienced by the laminae under stress along path MJE'. When fig 6.3.53 was superimposed onto fig 6.3.40 region E' was found to be very near to the failure locus as illustrated in fig 6.3.54. Owing to the scatter of the experimental data it was doubtful if the failure condition at region E' was solely due to the viscous-plastic effect and not the scatter of dimensions of the specimens.

Within the experimental error, it can be stated that the failure condition of a lamina is independent of the loading path in the σ_1 —— $-\sigma_2$ stress space. From the argument put forward above and the experimental information obtained, there are indications that in a true biaxial stress situation, i.e.

$$\begin{aligned} \sigma_1 &\neq 0 \\ -\sigma_2 &\neq 0 \\ \sigma_3 &= 0 \end{aligned} \qquad \text{.....(6.3.1.4.3)}$$

the failure condition of a lamina will be loading path dependent.

As a comparison, the numerical results based on the models presented in this section and the Tsai-Wu (1971) model were plotted alongside the experimental data as shown in fig 6.3.55. The strength values for the Tsai-Wu (1971) model are listed in Table 6.3. No experimental iteration was carried out to evaluated F_{12} for the Tsai-

TABLE 6.3. STRENGTH PARAMETERS FOR THE TSAI-WU(1971) MODEL

STRENGTH DATA	MNm^{-2}
X'_1	-950.0
X_1	675.0
X_2	30.7
X'_2	-140.0
STRENGTH TENSORS	$/Nm^{-2}$
F_1	4.288×10^{-10}
F_2	2.54517×10^{-8}
	$/(Nm^{-2})^2$
F_{11}	1.5594×10^{-18}
F_{22}	2.328×10^{-16}

	K		
F_{12} $/(Nm^{-2})^2$	20/9	3	30/7
	1.4844×10^{-17}	1.3623×10^{-17}	5.9902×10^{-18}

	K	
F_{12} $/(Nm^{-2})^2$	6	
	-1.6367×10^{-18}	

$\sqrt{F_{11}\ F_{22}}$ $\pm 1.9054 \times 10^{-17}$ $/(Nm^{-2})^2$

$$K = \sigma_1 \Big/ |-\sigma_2|$$

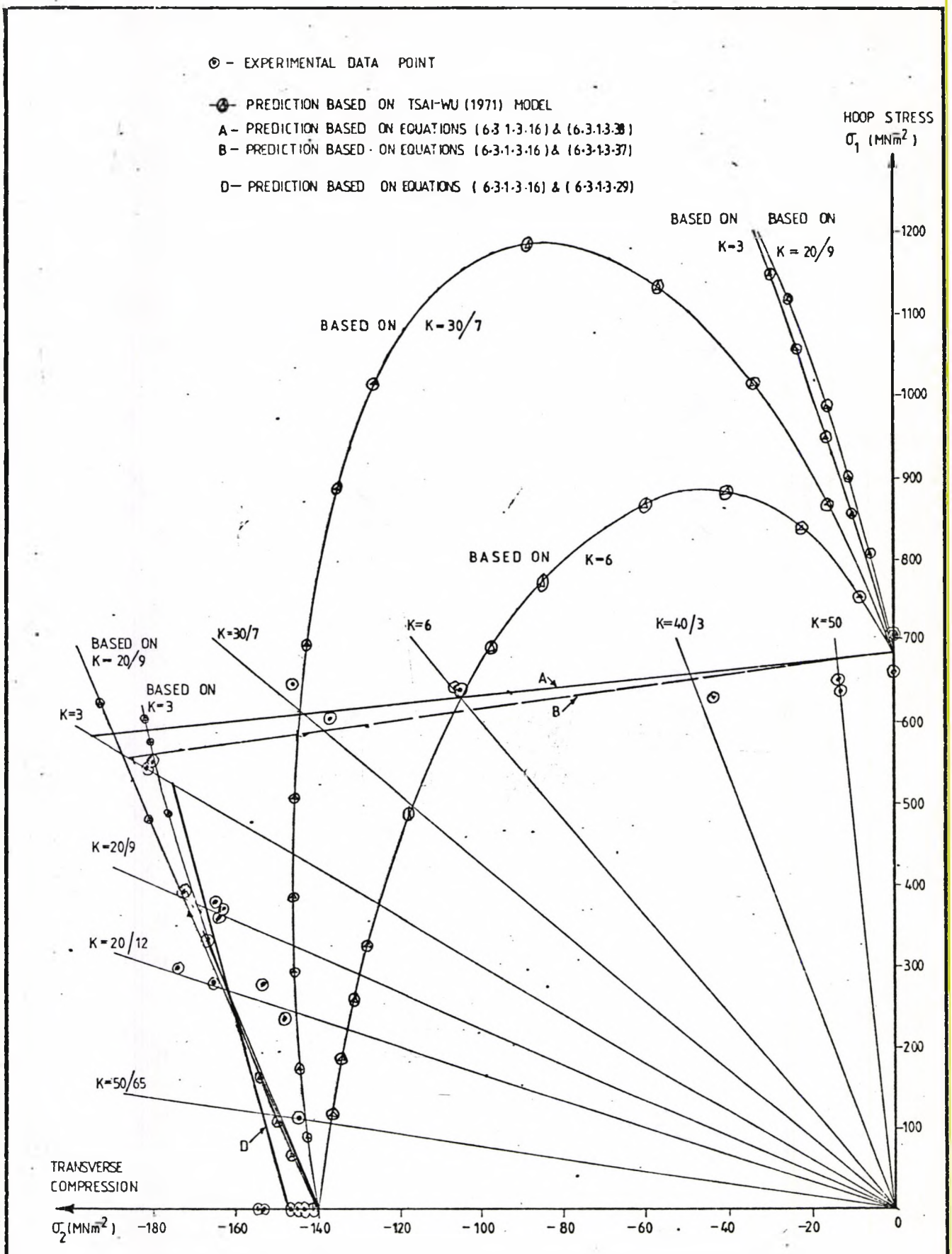

FIG 6·3·55 COMPARISON AMONG THE SIMPLE MODELS PROPOSED IN THIS CHAPTER AND THE TSAI-WU (1971) MODEL

Wu (1971) model. F_{12} was determined from biaxial test data where the stress ratios were

$$\bar{\sigma}_1 / |-\bar{\sigma}_2| = 20/9\ ,\ 3\ ,\ 30/7 \quad \& \quad 6$$

.....(6.3.1.4.4)

Perhaps,this is the main factor that causes the Tsai-Wu (1971) model to give such a poor prediction on the failure conditions of a lamina in the $\bar{\sigma}_1 - (-\bar{\sigma}_2)$ stress space.

It might be that as a theoretical failure criterion becomes more and more generalised, the effort required for the determination of the optimum strength parameters also increases. This is a major drawback of the general theoretical failure criterion.

6.4 The Effect of Loading Path on the Failure Conditions of a Lamina in the $-\bar{\sigma}_2 - \bar{\sigma}_6$ Stress Space

In this stress space, the dominant effects of a state of biaxial stress on a lamina can be simplified and represented as in fig 6.4.1. It was established in Section 6.3.1.1 that a shear zone due to the transverse compression (see fig 6.4.1 (c)) extends along the length of the fibre too. The matrix can be assumed to be isotropic and homogeneous without introducing excessive error into the failure behaviour analysis of the unidirectional lamina. Therefore, shear deformations on the matrix induced by $\bar{\sigma}_6$ and $-\bar{\sigma}_2$ probably complement each other. Consequently, the viscous-plastic behaviour has a very

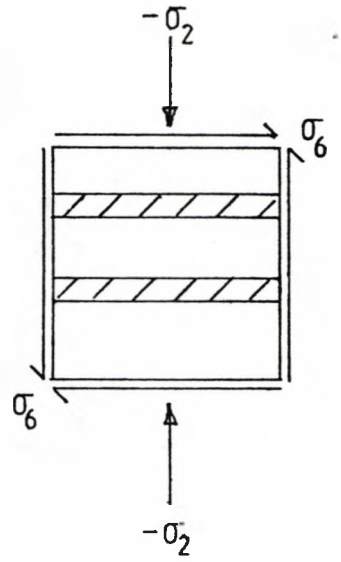

(a)

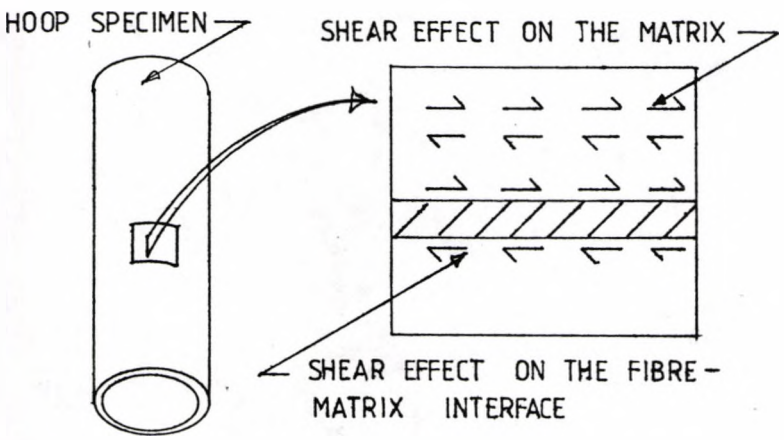

(b) SHEAR EFFECT ON THE MATRIX AND THE FIBRE-MATRIX INTERFACE DUE TO THE SHEAR STRESS σ_6.

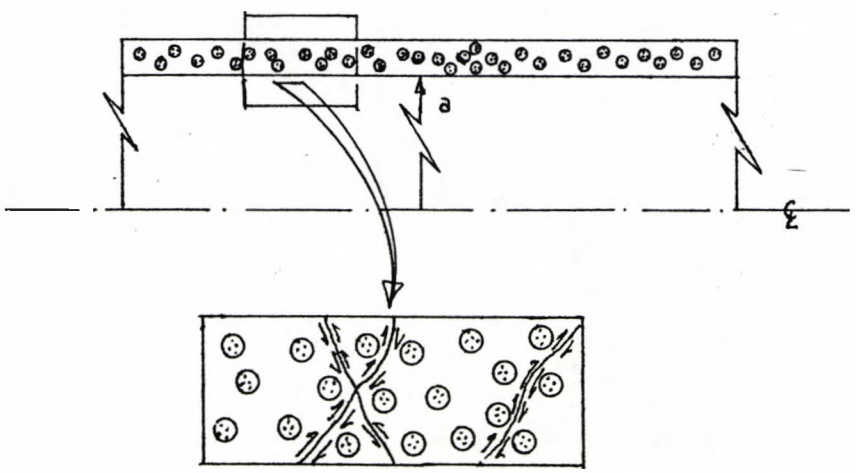

(c) SHEAR EFFECT ON THE MATRIX DUE TO THE TRANSVERSE COMPRESSION

FIG 6.4.1 A LAMINA IN A STATE OF BIAXIAL STRESS

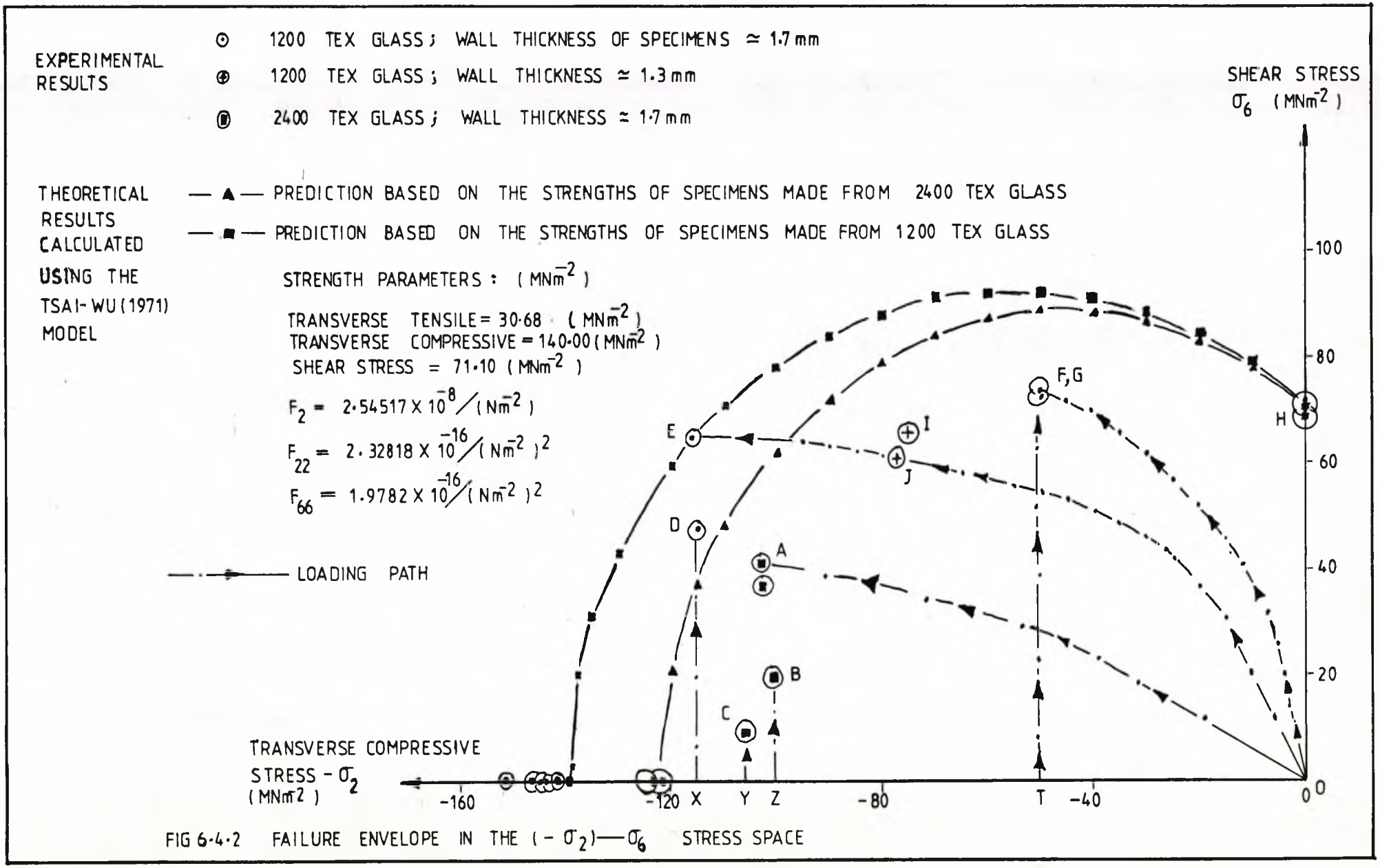

FIG 6·4·2 FAILURE ENVELOPE IN THE (- σ_2)— σ_6 STRESS SPACE

significant effect on the subsequent failure of the lamina, provided that the critical failure mode is matrix failure as observed experimentally. At the viscous-plastic phase of the shear deformation, the time factor becomes important. This is shown in fig 6.4.2. The plastic flow took place at the transverse compression level greater than 60 MN/m^2. The time taken along loading path OA and OZ were the same. The time required to arrive at point Y was longer than that at point Z.

But

$$(d\sigma_2/dt)_{\text{along loading path OZ}} = (d\sigma_2/dt)_{\text{along loading path OY}} \qquad .....(6.4.1)$$

Where t is time

$-\sigma_2$ is the transverse compression.

Similarly, experimental times along path OE and OX were identical. It can be seen that the failure stress was dependent on loading path (point E & D; point A & B). This principle can be applied to the case where viscous-plastic deformation is induced along a pure shear loading path first. The transverse compression was applied subsequently.

6.5 Conclusion

From the analysis presented in Sections 6.3 and 6.4 it seems that the failure condition of a unidirectional lamina is dependent on the loading path in the stress spaces tested. Therefore, it is erroneous to assume that the failure condition of a lamina is independent of loading paths. Apparently, for a given stress ratio

the failure behaviour of a lamina tested in the σ_1 —— $(-\sigma_2)$ stress space was independent of loading path. This was believed to be due to the presence of $-\sigma_3$ (radial stress). Such influence was pronounced in stress space where matrix failure dominated, i.e. in regions which satisfied the condition

$$\sigma_1 / -\sigma_2 | \leq 3 \qquad .....(6.3.1.3.5)$$

In view of the effect of $-\sigma_3$, the suitability of using pressurised thin wall tubular specimens for the induction of plane stress conditions is in doubt in the circumstances discussed above. Perhaps, it will be of relevance to investigate the influence of $-\sigma_3$ on laminated tubular specimen which has so far been ignored.

Chapter 7: CONCLUSIONS

A powerful and versatile feedback controlled servo-hydraulic multiaxial test rig has been developed. It can provide axial force, internal pressure and torque to a thin-walled tubular specimen. The applied axial force can be tensile or compressive. The applied torque can be either clockwise or counter-clockwise. The internal pressure generates only hoop stress in the specimen. The axial stress (parallel to the axis of the specimen) is produced by the applied axial force. The applied torque is responsible for the introduction of in-plane shear stress to the specimen. These three loads can be applied to a tubular specimen in any desired combination to produce the required combined states of stress. Although fibre reinforced composite tubular specimens were used in this work specimens made from other materials can also be tested using this machine.

The flexibility of the test rig is enhanced by the variability of the control software. By supplying the test rig with different control software it can be instructed to perform different experiments on tubular specimens. Its capabilities increase as more control software packages are developed.

The present specimen gripping system requires more than 2 hours to mount a specimen and dismantle it after testing. A better system would therefore be desirable, and can be added later to increase the efficiency of the test rig.

Automatic data logging facilities are available. At the time of the experimental work only the loads, strains and linear displacement of the end-grip signals were recorded automatically. Expansion can be carried out to enable the test rig to read up to 32 data channels.

Electrical filters can be included to filter noise from the feedback signals before they are used for the control purposes. This will make the test rig less susceptible to electrical noise. There is only one external hydraulic filter in the hydraulic power-pack. Two more such filters must be fitted to the hydraulic power input line, one next to each of the Moog servo-valves. This is to ensure that most of the debris in the hydraulic system is removed before the hydraulic fluid enters the servo-valves. The main objective of this modification is to improve the reliability of the servo-valves.

48 kilo bytes of **RAM** can still be added to the microcomputer of the control unit. This additional core memory space, together with two extra disc drive systems, will increase further the computing power of the microcomputer.

Initially the objective of this project was to conduct a study into the failure behaviour of unidirectional laminae and the effect of loading path on failure in the following stress spaces:

(i) combined transverse tensile and in-plane shear stresses (σ_2 —— σ_6)

(ii) combined parallel tensile and transverse compressive stresses (σ_1—$(-\sigma_2)$)

(iii) combined transverse compressive and in-plane shear stresses ($(-\sigma_2)$ —σ_6)

The degree of data scatter in the σ_2 - σ_6 stress space was high due to the presence of transverse tensile stresses. Many tests would be necessary before a meaningful conclusion could be drawn from the experimental results. The lack of time effectively ruled out this course of action. Effort was concentrated on the (σ_1—$(-\sigma_2)$) and the $(-\sigma_2)$—σ_6 stress spaces.

In the (σ_1—$(-\sigma_2)$) stress space there were two major modes of failure for the unidirectional laminae. Under pure transverse compression massive plastic shear deformation occurred in the matrix and led to the final failure

of the laminae. The plastic shear deformation took place in planes which were parallel to the fibre axis but at oblique angles to the applied transverse compressive stress. This produced white shiny streaks on the specimen tested. When laminae were subjected to pure tensile stress parallel to the fibre axis, fibre fracture was the critical event that precipitated the catastrophic failure of the laminae. The failure behaviour of the laminae subjected to combined transverse compressive stress and parallel tensile stress was as follow:

(i) for $K \leqslant 3$, the laminae failed in a similar manner to those under pure transverse compression (plastic shear deformation of the matrix),

(ii) for $K > 3$, fibre fracture was the dominant mode. The laminae behaved in an identical way to those which failed under pure parallel tensile stress.

The experimental data obtained agree with predictions made using the three tentative theoretical models. The performance of these models was compared with the Tsai & Wu (1971) model. The limited experimental results suggest that a better theoretical prediction on the failure behaviour of a fibre reinforced composite material can be achieved by using separate simple models for different stress spaces rather than by using a general and complex model which encompases all the stress spaces.

The radial stress component $(-\sigma_3)$ generated by the applied internal pressure was found to have a significant effect on the failure behaviour of the unidirectional laminae. In the $(\sigma_1 - (-\sigma_2))$ stress space $-\sigma_3$ was believed to have delayed and sometimes even suppressed the plastic shear deformation in the matrix caused by the transverse compression. The intensity of such effects increased with the increment of the applied internal pressure. As a result, in the domain where $K \leqslant 3$ transverse compressive

strength apparently improved as the level of radial stress increased. For a given state of combined stress in the region where $K \geq 3$ the magnitude of $(-\sigma_3)$ was higher than for $K \leq 3$. The plastic shear deformation in the matrix was suppressed to such an extent that its influence on the failure behaviour of the laminae was insignificant. Therefore, in the subsequent failure processes fibre fracture played the prime role.

In the plastic domain the matrix of the unidirectional laminae behaves in a viscous-plastic manner. Time becomes an important factor in the loading history of the laminae. This implies that the loading path has a strong influence on the failure strengths of the laminae. Such a phenomenon was demonstrated tentatively in the $((-\sigma_2)-\sigma_6)$ stress space. However, it was observed that the failure strengths of the laminae tested in the $(\sigma_1-(-\sigma_2))$ were independent of loading path. Such unexpected behaviour was due to the presence of the radial stress $(-\sigma_3)$ since it could delay or suppress plastic shear deformation in the matrix. Furthermore, the glass fibre reinforcement does not behave in a viscous-plastic way when subjected to a quasi-static stress environment. Therefore, if fibre fracture is the primary failure mode of a lamina due to the suppression of pastic shear deformation in the matrix, then the failure strength of the lamina becomes independent of loading path for a given stress ratio, K.

The unavoidable presence of the radial stress $(-\sigma_3)$ makes a thin-walled hoop wound tube behave differently from a flat unidirectional lamina in a state of plane stress involving σ_1 and $-\sigma_2$. This casts doubt on the suitability of using tubular hoop wound specimens to study the behaviour of laminae under plane stress when internal pressure is involved. Perhaps it would also be worthwhile to conduct an investigation into the effect of the radial stress $(-\sigma_3)$ on laminated tubes.

The analyses presented in Chapter 6 were over-simplified. Refined analytical work was not possible because of the time constraint. However, there are signs of agreement between the experimental data and the predictions based on the theoretical models proposed. This indicates that a more accurate prediction on the failure behaviour of a hoop wound tube might be achieved by improving these models.

BIBLIOGRAPHY

Altman, L. ((ed) 1975) 'Microprocessors' New York: McGraw-Hill (Electronic Book Series.)

Ashkenazi, E. K. (1965) 'Problems of the Anisotropy of Strength.' Mekhanika Polimerov, vol. 1, No. 2, pp 79 - 92.

Ashkenazi, E. K. and Pekker, F. P. (1970) 'Experimental testing of the Applicability of a Fourth Degree Polynomial in describing Surfaces of Equicritical Planar Stress Distributions in Glass-reinforced Plastics.' MEKH. POLIM (English Translated Version) vol. 6, No. 2, pp 251 - 258

Ashton, J. E., Halpin, J. C. and Petit, P. H. (1969) 'Primer on Composite Materials: Analysis.' Progress in Materials Science Series: vol III. Technomic Publication.

Azzi, V. D. and Tsai, S. W. (1965) Experimental Mechanics. pp 283 -

Boulaye, G. G. (1975) 'Microprogramming' Edited by Beaven, P. A., London Macmillan.

Chamis, C. C. (1969) 'Failure Criteria for Filamentary Composites.' NASA TN D - 5367. pp 1 - 30, August.

Cheng, S. & Ho. B. P. C. (1963) 'Stability of Heterogeneous Aeolotropic Cylindrical Shells Under Combined Loading.' AIAA Journal, vol. 1, No. 4, April, pp 892 - 898.

Choo, Vincent K. S. (1982) 'Control Software Manual for the Servo-hydraulic Closed-loop Controlled Multiaxial Test Rig.' (Not Published)

Daniel, I. M., Liber, T., Vanderby. R., and Koller, G. M. (1980) 'Analysis of Tubular Specimen for Biaxial Testing of Composite Laminates.' Proc. of the 1980 International Conference on Composite Materials. pp 840 - 855.

Dove, R. C. and Adams, P. H. (1964) 'Experimental Stress Analysis and Motion Measurement.' Charles E. Mervill Books Inc., Columbus, Ohio, U.S.A. p 515

Duggan, M. F., and Bailie, J. A. (1980) 'A New Test Specimen Geometry for Achieving Uniform Biaxial Stress Distributions in Laminated Composite Cylinders.' Proc. of the 1980 International Conference on Composite Materials. pp 900 - 913.

Eckold, G. C., Leadbetter, D., Soden, P. D. and Griggs, P. R. (1978) 'Lamination theory in the Prediction of failure envelopes for filament wound materials subjected to biaxial loading.' Composites. October. pp 243 - 246.

Findlay, W. and David, A. W. (1978) 'PASCAL - An Introduction to methodical Programming.' Pitman Publishing Limited. pp 306.

Flugge, W. (1973) 'Stresses in Shells' Springer - Verlag New York Heidelberg Berlin. pp 525.

Found, M. S. (1972) Nottingham University Ph. D. Thesis.

Franklin, H.G. (1968) Fibre Sci. Tech. 1 pp 137 - 150

Gatwood, C. H. (1982) Liverpool University Ph.D. Thesis. (To be published)

Greenwood, J. H. (1977) 'German work on grp design.' Composite. July. pp 175 - 184.

Gol'denblat, I. I., and Kopnov, V. A. (1965) 'Strength of glass-reinforced plastics in the Complex Stress State.' Polymer Mechanics, vol. 1, No. 2. pp 54 - 59.

Guess, T. R., and Haizlip, Jr. C. B. (1980) 'End-grip Configurations for Axial Loading of Composite Tubes.' Experimental Mechanics, vol. 20, No. 1, January. pp 31 -36.

Guillon, M (1961) - Translated by Griffiths, R. T. (1969) 'Hydraulic Servo System Analysis and Design.' Butterworth & Co. (Publishers) Ltd.

Halpin, J. C., Pagano, N. J., Whitney, J. M. and Wu, E. M. (1969) 'Characterization of Anisotropic Composite Materials.' Composite Materials: Testing and Design, ASTM STP 460, American Society for Testing and Materials. pp 37 - 47.

Harris, A. and Orringer, O. (1978) 'Investigation of Angle-Ply Delamination Specimen for Interlaminar Strength Test.' J. Composite Materials, vol. 12, July. pp 285 - 299.

Hill, R. (1948) Proc. Roy. Soc. A 193, pp 281 - 297.

Ho, B. P. C. and Cheng, S. (1963) 'Some Problems in Stability of Heterogeneous Aeolotropic Cylindrical Shells under Combined Loading.' AIAA Journal, vol. 1, No.7, July. pp 1603 - 1607.

Hogg, P. J. (1981) Liverpool University Ph. D. Thesis.

Hull, D., Legg, M. J. and Spencer, B. (1978) 'Failure of glass/polyester filament wound pipe.' Composites, January. pp 17 - 24.

Hütter, U., Schelling, H., and Krauss, H. (1974) 'An Experimental Study to Determine Failure Envelope of Composite Materials with Tubular Specimens under Combined Loads and Comparison Between Classical Criteria.' AGARD Conference Proceeding. No. 163, October. pp 3-1 to 3-11.

Intel Corporation (1977) SBC 724 Analogue Output Board Hardware Reference Manual.

Intel Corporation (1980) Component Data Catalog.

Intel Corporation (1976) SBC 104/108 Combination Memory and I/O Expansion Boards Hardware Reference Manual.

Intel Corporation (1978) System 80/20-4 Microcomputer Hardware Reference Manual.

Johnson, W. and Mellor, P. B. (1973) 'Engineering Plasticity.' Van Nostrand Reinhold Company. pp 646.

Jones, M. L. C. (1981) Liverpool University Ph.D. Thesis.

Kaminski, B. E. and Lantz, R. B. (1969) 'Strength Theories of Failure for Anisotropic Materials.' Composite Materials: Testing and Design, ASTM STP 460, American Society for Testing and Materials. pp 160 - 169.

Legg, M. J. (1980) Liverpool University Ph. D. Thesis.

Mullard LTD. (1977) Mullard technical handbook. Book one, Part seven B.

McGlynn, D. R. (1976) Microprocessors technology. Architecture and applications. New York: Wiley - Interscience.

Marlowe, D. E., Sushinsky, G. F. & Dexter, H. B. (1974) Elastic Torsion Buckling of Thin-walled Composite Cylinders.' Composite Materials: Testing and Design (Third Conference) ASTM STP 546, American Society of Testing and Materials. pp 84 - 108.

National semiconductor corporation (1978) BLC 711/732 Analogue Input and I/O Boards Hardware Reference Manual.

Norris, C. B. (1946) Forest Products Laboratory, U.S.A. Report No. 1328, January.

Norris, C. B. (1950) Forest Products Laboratory, U.S.A. Report No. 1816, July.

Owen, M. J. and Rice, D. J. (1981) 'Biaxial Strength Behaviour of glass fabric-reinforced polyester resins.' Composites. January. pp 13 - 25.

Owen, M. J. and Griffiths, J. R. (1978) 'Evaluation of Biaxial Stress Failure Surfaces for A Glass-Reinforce Polyester Resin under Static and Fatigue Loading.' Journal of Materials Science 13 pp 1521 - 1537.

Pagano, N. J., Halpin, J. C. and Whitney, J. M. (1968) 'Tension Buckling of Anisotropic Cylinders.' Journal of Composite Materials, vol. 2., No. 2., pp 154 - 167.

Pagano, N. J. and Whitney, J. M. (1970) 'Geometric Design of Composite Cylindrical Characterization Specimens.' J. Composite Materials, vol. 4., July. pp 360 - 378.

Pagano, N. J. and Halpin, J. C. (1968) 'Influence of End Constraint in the Testing of Anisotropic Bodies.' J. Composite Materials, vol. 2., No. 1., January pp 18 - 31.

Perex LTD (1978) Perex Perifile 6041 Mk III Users Manual.

Piggott, M. R., and Harris, B. (1980) 'Compression Strength of Carbon, glass and Kevlar -49 fibre reinforced polyester resins.' Journal of Materials Science. 15. pp 2523 - 2538.

Pipes, R. B. and Pagano, N. J. (1970) 'Interlaminar Stresses in Composite Laminates under Uniform Axial Extension.' J. Composite Materials, vol. 4, October. pp 538 - 548.

Pipes, R. B. (1971) 'Moire' Analysis of the Interlaminar Shear Edge Effect in Laminated Composites.' J. Composite Materials, vol. 5, April. pp 255 - 259.

Pipes, R. Byron (1980) 'Boundary Layer Effects in Composite Laminates.' Fibre Science Technology. 13. pp 49 - 71.

Polakowski, N. H. and Ripling, E. J. (1966) 'Strength and Structure of Engineering Materials.' Prentice - Hall, Inc. Englewood Cliffs, New Jersey. pp 235 - 241.

Protasov, V. D. and Kopnov, V. A. (1965) 'Study of the Strength of Glass-reinforced Plastics in Plane Stress State.' Mekhanika Polimerov, vol. 1, No. 5, pp 39 - 44. UDC 678: 539.4.011.

Puck, A. (1969) Kunststoffe 59.

Puck, A. (1967) 'The Stresses and Strains in GRP Multi-layer Composite Components.' Kunststoffe, vol. 57, April. pp 284 - 293.

Puck, A. and Schneider, W. (1969) 'On Failure Mechanisms and Failure Criteria of filament-wound glass fibre/resin Composites.' Plastics and Polymers, February. pp 33 - 44.

Puppo, A. H., and Evensen, H. A. (1972) 'Strength of Anisotropic Materials under Combined Stresses.' AIAA. Journal. vol. 10, No. 4, pp 468 - 474.

Puppo, A. H. and Evensen, H. A. (1970) 'Interlaminar Shear in Laminated Composites under Generalized Plane Stress.' J. Composite Materials, vol. 4, April. pp 204 - 220.

Rowlands, R. E. (1975) 'Flow and Failure of Biaxially loaded Composites: Experimental and Theoretical correlation.' Inelastic Behaviour of Composite Materials. AMD. vol. 13. pp 97 - 125. Presented at 1975 ASME Winter Annual Meeting, Houston, Texas. Nov 30 - Dec 5 1975 edited by Carl t. Herakovich

Schneider, W. and Bardenheier, R. (1975) 'Versagenskriterien fur Kunststoffe.' J. Mater. Technol. 6. pp 269 - 280.

Schwarzenbach, J. and Gill, K. F. (1979) System Modelling and Control' Edward Arnold (Publishers) Ltd. pp 229.

Soden, P. D., Leadbetter, D., Griggs, P. R. and Eckold, G. C.(1978) 'The Strength of a Filament Wound Composite under Biaxial Loading.' Composites. October. pp 247 - 250.

Sokolnikoff, I. S. and Specht, R. D. (1946) 'Mathematical Theory of Elasticity.' First Edition, McGraw-Hill Book Company, New York.

Suh, N. P., and Turner, A. L. (1975) 'Elements of the Mechanical Behaviour of Solids.' Scripta Book Company. Washington, D.C. pp 141 - 152.

Tennyson, R. C., MacDonald, D. and Nanyaro, A. P. (1978) 'Evaluation of the Tensor Polynomial Failure Criterion for Composite Materials.' J. Composite Materials, vol. 12, January. pp 63 -75.

Texas Instrument Inc (1976) The Memory and Microprocessors data Book for design engineers.

Texas Instruments (1981) The TTL Data Book for Design Engineers. (issued by) Texas Instruments. 5th edition.

Texas Instruments Incorporated (1975) 'Model 990 Computer: TMS 9900 Microprocessor: assembly language programmers' guide.' Rev. ed. Texas Instruments Ltd., Educations and Commuications Centre.

The GHOST Graphical Output System NWD 26. (OBTAINABLE FROM LIVERPOOL UNIVERSITY COMPUTOR LABORATORY)

The Superior Electric Company. Instructions for SLO - SYN Translator Type TM 600. pp 1 -15

Timoshenko, S. P. & Young, D. H. (1968) 'Elements of Strength of Materials.' D. VAN NOSTRAND COMPANY, INC. pp 377.

Tsai, S. W. (1964) 'Structural Behaviour of Composite Materials.' NASA Contractor Report. NASA CR -71.

Tsai, S. W. (1965) 'Strength Characteristics of Composite Materials.' NASA Contractor Report, NASA CR - 224.

Tsai, S. W. and Azzi, V. D. (1966) 'Strength of Laminated Composite Materials.' AIAA Journal. February. vol. 4, No. 2, pp 296 - 301.

Tsai, S. W., and Wu, E. M. (1971) 'A General Theory of Strength for Anisotropic Materials.' J. Composite Materials, vol. 5, January. pp 58 - 80.

Wang, J. T. S. and Dickson, J. N. (1978) 'Interlaminar Stresses in Symmetric Composite Laminates.' J. Composite Materials, vol. 12, October. pp 390 - 403.

Ward, I. M. (1971) 'Review: The Yield Behaviour of Polymers.' Journal of Materials Science. 6. pp 1397 - 1417.

Weston, P. M. (1979) Private Communication.

Whitney, J. M. and Browning, C. E. (1972) 'Free-Edge Delamination of Tensile Coupons.' J. Composite Materials, vol. 6, April. pp 300 - 303.

Whitney, J. M. and Halpin, J. C. (1968) 'Analysis of Laminated Tubes under Combined Loading.' J. Composite Materials, vol. 2, pp 360 - 367.

Whitney, J. M. and Sun, C. T. (1975) 'Buckling of Composite Cylindrical Characterization Specimens.' J. Composite Materials, vol. 9, April. pp 138 - 148.

Wu, E. M. and Jerina, K. L. (1972) 'Computer - Aided Mechanical Testing of Composites.' Materials Research and Standards, MTRSA, vol. 12, No. 2, February. pp 13 - 18.

Wu, E. M. (1972) 'Optimal Experimental Measurements of Anisotropic Failure Tensors.' J. Composite Materials, 6. pp 473 - 489.

Wu, E. M. and Scheublein, J. K. (1974) Composite Materials: Testing and Design (Third Conference), ASTM STP 546, American Society for Testing and Materials. pp 188 - 206.

Wu, E. M., Jerina, K. L. and Lavengood, R. E. (1973) 'Data Averaging of Anisotropic Composite Material Constants.' Analysis of Test Methods for High Modulus Fibres and Composites, ASTM STP 521, American Society for Testing and Materials. pp 229 - 252.

Wu, E. M.(1974) 'Phenomenological Anisotropic Failure Criterion.' Mechanics of Composite Materials, Edited by Sendeckyj, G. P., vol. 2. pp 353 -431.

Zakharov, K. V. (1961) Plastickeskie Massy, 8.

Appendix 2

$$\Phi_{\mu 22} = (1/(1 + p(A=1))) (1 + p(\upsilon_{f12} - \upsilon_{m12}A) ((E_{L22}\,\sigma_{L11} - \upsilon_{L21}\,E_{L11}\,\sigma_{L22}) / (E_{L11}\,\sigma_{L22} - \upsilon_{L12}\,E_{L22}\,\sigma_{L11})) \quad \text{-- (A2.1)}$$

$$\text{If} \quad E_{L11}\,\sigma_{L22} - \upsilon_{L12}\,E_{L22}\,\sigma_{L11} = 0 \quad \text{-- (A2.2)}$$

$$\Phi_{\mu 12} = 1/(1 - p(1 - G_{m12}/G_{f12})) \quad \text{-- (A2.3)}$$

$$p = (4k_f/\Pi)^{1/2} \quad \text{-- (A2.4)}$$

$$A = ((1 - \upsilon_{f12}\,\upsilon_{f21})/(1 - \upsilon_{m12}\,\upsilon_{m21}))\,E_{m22}/E_{f22} \quad \text{-- (A2.5)}$$

APPENDIX 3

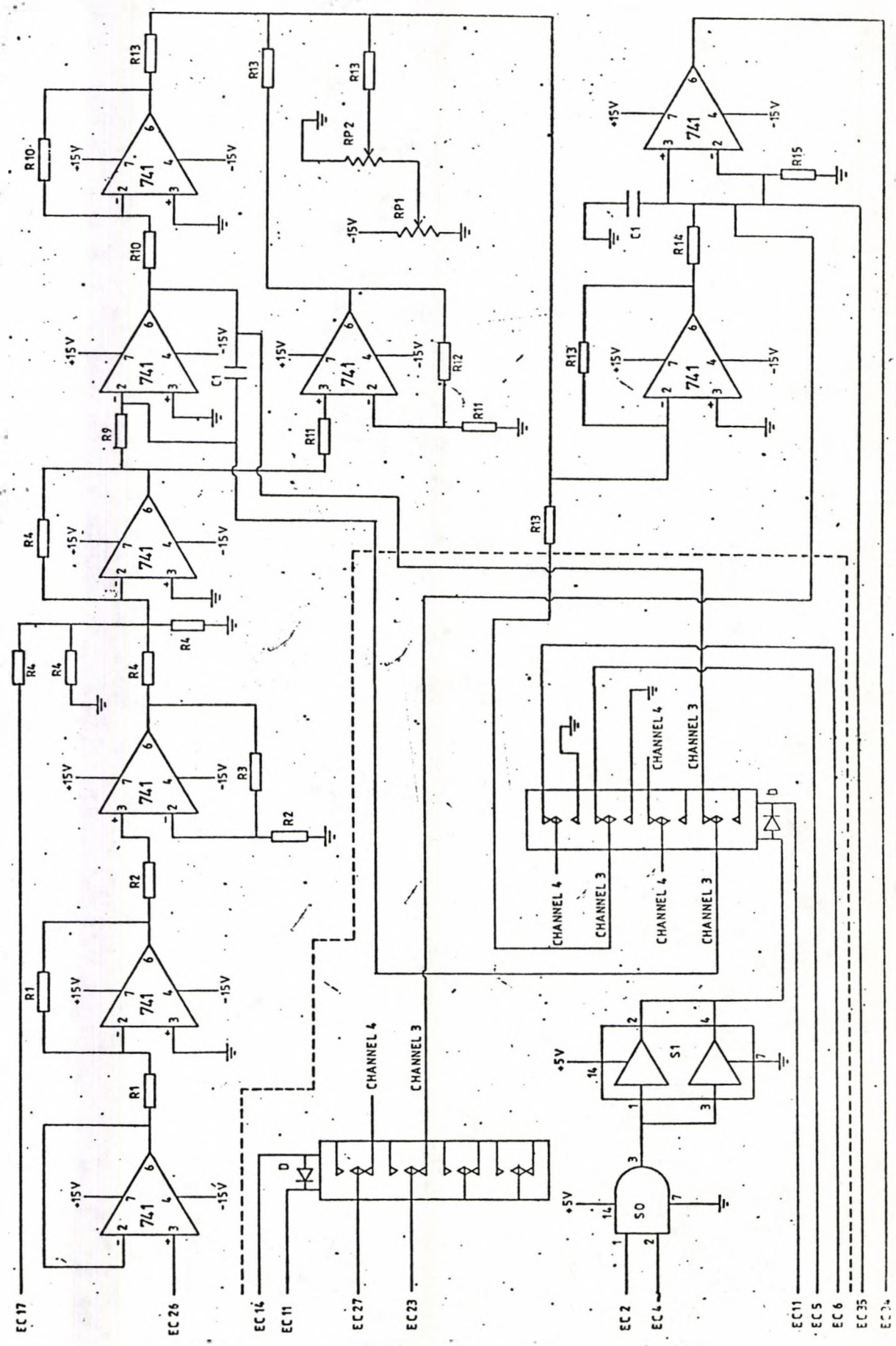

ANALOGUE DRIVER FOR INT. PRESSURE OR AXIAL FORCE

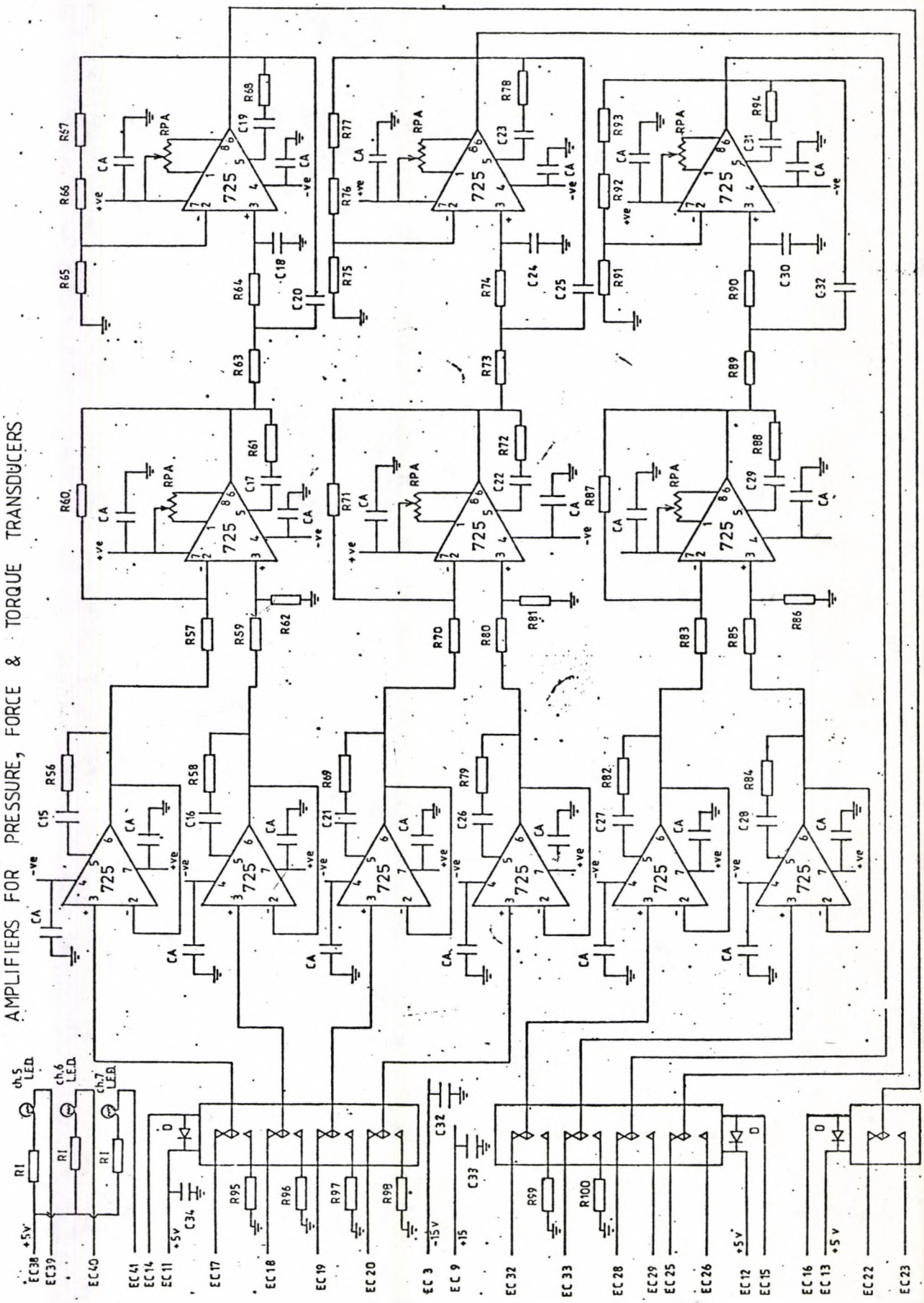
AMPLIFIERS FOR PRESSURE, FORCE & TORQUE TRANSDUCERS
725
RPA
CA
+ve
-ve
R1
ch.5 LED
ch.6 LED
ch.7 LED
+5v
-15v
+15
EC38
EC39
EC40
EC41
EC14
EC11
EC17
EC18
EC19
EC20
EC 3
EC 9
EC32
EC33
EC28
EC29
EC25
EC26
EC12
EC15
EC16
EC13
EC22
EC23

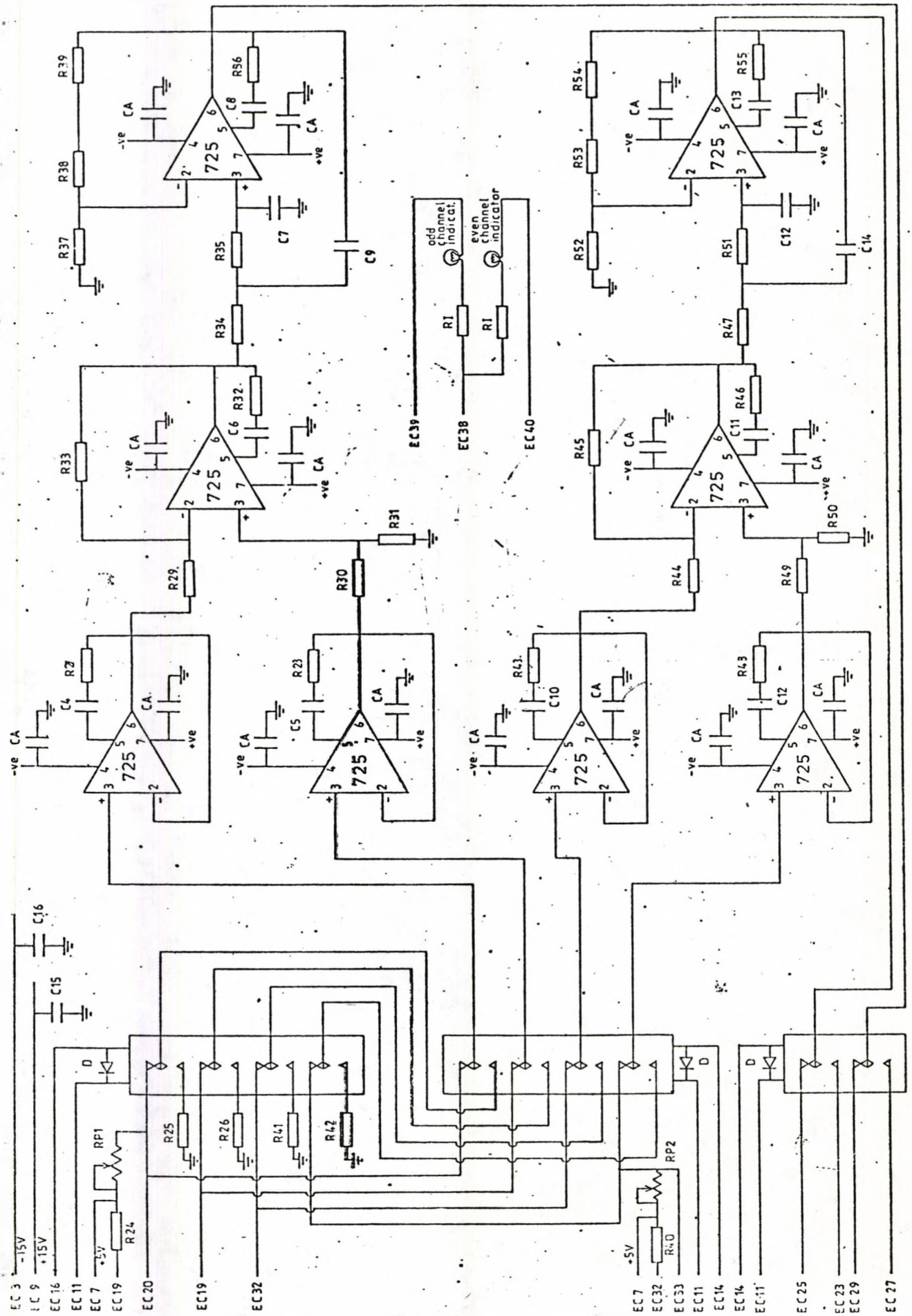

AMPLIFIERS FOR 2 STRAIN CHANNELS

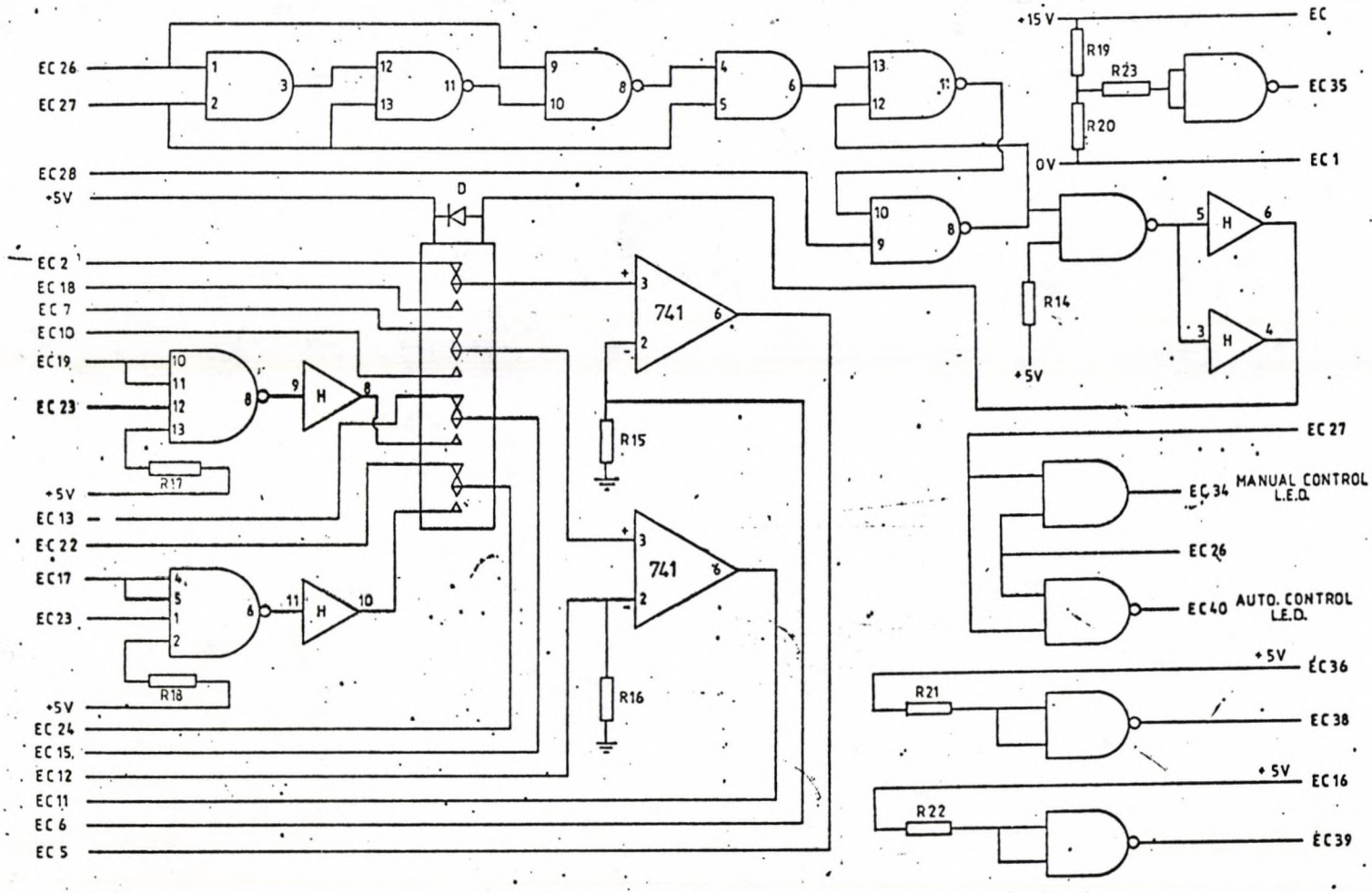

FOR FURTHER DETAILS ON THE DRAWINGS IN APPENDIX 3 REFER TO THE HARDWARE MANUAL OF THE RIG

APPENDIX 4

Appendix 4.1

Commands	Description
AGx	Amplifier Gain. This instructs the **User Monitor, SUZI,** to change the amplifier gain of the programmable amplifier. x is the gain parameter. It can be 1, 2, 4, or 8 times.
FCx	First Channel Number. **SUZI** assumes channel specified by x to be the first channel.
LCy	Last Channel Number. **SUZI** assumes channel specified by y to be the last channel. The microcomputer will sample from channel x to y continuously during the data sampling process.
FLPx	Tensile Force Limit. x is the amplified voltage, from the axial force load cell corresponding to the required force value. Range of x is from 0 to 32752 which is equivalent to the (0 to 10 volts) range.
FLNx	Compressive Force Limit. The range of x is from 0 to -32752
PLPx	Internal Pressure Limit. x ranges from 0 to 32752
PLNx	External Pressure Limit. x ranges from 0 to -32752
TLPx	Clock-wise Torque Limit. x ranges from 0 to 32752.
TLNx	Counter Clock-wise Torque Limit. x ranges from 0 to -32752.
PWTHx	Pipe Wall Thickness Input Command. x is the parameter value in millimeter.

Commands	Description
PDx	Pipe Internal Diameter Input Command. x is the parameter value in millimeter.
WAx	Winding Angle Input Command. x is in degree.
LXzee	**Read** and **Load** a **cross-assembled** program from a **perex file** call zee. z is the track name. It ranges from 0 to 3. ee is the file name. It ranges from 00 to 99.
LPzee	**Read** and **Load** a **Compiled PASCAL** program from a **perex file** call zee.
WFzee	Set up an empty **perex file** call zee for data collecting.
RSM	Return to the **System Monitor.** This passes control from **SUZI** to the **System Monitor.**
LRx	Loading Rate Factor. x is an integer that ranges from 0 to 255. The loading interval is 50x milliseconds.
SRx	Sampling Rate Factor. x is an integer that ranges from 0 to 255. The sampling interval is 50x milliseconds.

Appendix 4.2

Parameter	Default value
Amplifier	
Strain Channel 1	x1
Strain channel 2	x1
Strain Channel 3	x1
Strain Channel 4	x1
Pressure Channel 5	x1
Force Channel 6	x1
Torque Channel 7	x1
Last channel Number	32
First Channel Number	1
Loading Interval	12.5 seconds
Data Sampling Interval	4 seconds
*Force Limit:	
Tensile	3.787 volts
Compressive	-3.787 volts
*Torque Limit:	
Clock-wise	3.787 volts
Counter Clock-wise	-3.787 volts
*Pressure Limit:	
Internal Pressure	3.787 volts

*Note: The load limits are expressed in terms of electrical output signals from the load cells through the corresponding fixed gain amplifier.

The following steps must be taken in the course of overwriting the default load limits.

(i) For each new load limit required determine the equivalent signal level in volt after it has been amplified by the corresponding fixed gain differential amplifier. For the sake of argument let this be x.

(ii) Perform the following calculation:
$z = (x/10)(32752)$.

(iii) Type the new load limits z and – z using the appropriate commands given in Appendix 4.1.

(iv) IF the positive and negative load limits were different, then step (ii) would have to be repeated for these two values separately.

Appendix 6

The relation between the applied Torque and the associated applied Shear Stress in the wall of a Tube.

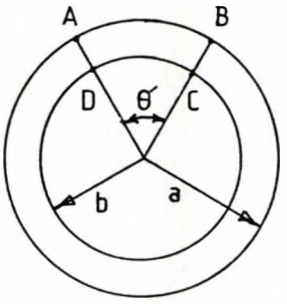

Let γ_a be the shear strain on the outside wall of the hollow cylinder.

$$\gamma_a = a\theta'/l \qquad \text{.....(A6.1)}$$

Where l is the total length of the cylinder.

Let $$\theta = \theta'/l \qquad \text{.....(A6.2)}$$

$$\therefore \quad \gamma_a = a\theta \qquad \text{-- (A6.3)}$$

Similarly,

$$\gamma_b = b\theta \qquad \text{.....(A6.4)}$$

where γ_b the shear strain on the inside wall of the hollow cylinder.

Therefore, the shear strain at distance r from the centre is

$$\gamma = r\theta \qquad \text{.....(A6.4a)}$$

Let T_i the sum of the internal torsional moments.

$$\therefore \quad T_i = 2\pi \int_b^a \tau r^2 \, dr \qquad \text{.....(A6.5)}$$

Let T be the applied external torque.

At equilibrium condition

$$T_i = T \qquad \text{.....(A6.6)}$$

Substituting (A6.4a) into (A6.5) one obtains

$$T = (2\Pi/\theta^3)\int_{b\theta}^{a\theta} \tau\gamma^2 \, d\gamma \qquad \text{.....(A6.7)}$$

$$\therefore \quad T\theta^3 = 2\Pi \int_{b\theta}^{a\theta} \tau \, \gamma^2 \, d\gamma \qquad \text{.....(A6.8)}$$

if $a \gg (a-b)$

$\tau_a \simeq \tau_b \simeq \tau_m$ see assumption (ii)

Therefore, equation (A6.8) can be simplified to

$$T\theta^3 = 2\Pi\tau_m\int_{b\theta}^{a\theta}\gamma^2 d\gamma$$

$$T\theta^3 = (2\Pi/3)\,\tau_m\,((a\theta)^3 - (b\theta)^3)$$

$$T = (2\Pi\tau_m/3)\,(a^3 - b^3)$$

$$T = (2\Pi\tau_m a^3/3)\,(1 - (b/a)^3)$$

$$\tau_m = 3T/(2\Pi a^3(1 - c^3))$$

$$c = b/a$$

$$\tau_m = 3T/(2\Pi a^3(1 - c^3)) \qquad \text{.....(A6.9)}$$

τ_m - mean shear stress

There are two alternative assumptions which can be used to produce the same equation (A6.9). They are as follow:

(i) the shell becomes completely plastic and there is no strain hardening.

(ii) the shell is very thin and represents the average shear stress across the thickness of the shell.

If b/a = 25 is consider to be a large value, then the shell with wall thickness t is classified as a thin shell. In such a situation

$$\tau_m = 3T \Big/ (2\pi a^3 (1 - c^3)) \qquad \text{.....(A6.9)}$$

holds.